THE UNIVERSITY
of EDINBURGH

SCHOOL OF CHEMISTRY

THE UNIVERSITY OF EDINBURGH

Elemental and supramolecular diversity of nanoporous phthalocyanine crystals

Thesis submitted for the degree of Doctor of Philosophy by:

Nikolaos – Angelos Stamos

Supervisor: Neil B. McKeown

2019

Acknowledgements

First and foremost, I would like to thank my supervisor and friend, Professor Neil B. McKeown, for not only giving me the chance to join his research group but also for his continual guidance and support over the past four years. Furthermore, I would like to thank all the post-docs: Lino, Grazia, Rich, Bibi, Kadhum and John for their help and support that guided me through my various projects. I would also like to thank everyone I had chance to work alongside in the lab during my PhD: Luke, Mike, Ian, Rhodri, Rich, Sandy, Hannah, Panos, Jie, ChunChun, Sarah, Ali, Sadiq, Travis, Emily, Mariagiulia, HongChun and Khairul who have made the lab a thoroughly enjoyable place to work in and given their support whenever I needed it. Without all of these people I don't think I would have been able to make it through the past few years to finish my PhD and so I can only wish them all the best of luck in their futures.

A special thanks go to my first (Elise Wolters, Isabel He, Jack Hemingway and Johnny Walmsley), second (Bella Chen, Jinling Wang, Lucinda Wilson and Scarlett Brown) and third (Igor Zamorski, Charlie Nason, Toria Twiddy and Iona Ivalo) 4P students who I had the pleasure of supervising during their time in their project, they were keen students who I enjoyed working with. They have made contributions to some of the work discussed in this thesis and I would like to not only acknowledge this but to thank them for their hard work and dedication to their projects.

A big thanks is also needed for the many collaborators that have made some of the work in this thesis possible. First, is to Stephen Moggach and Charlie McMonagle and Mark Warren for their crystallographic expertise and time dedicated to long trips to Diamond. Second is to Floriana Tuna and Eduardo Guimarães Vieira as well as the EPSRC UK National EPR Facility at Manchester for the EPR measurements of our complexes. I would also like to thank all the technical staff for their expertise and commitment to helping those when they need it. I would like to make a special thank you to the crystallography service, in particular Gary Nichol, who has not only facilitated us in our crystallographic endeavours, but also for his passion to help guide those such as myself in the art of crystallography.

I would like to thank my family, Andreas, Athanasia, Valeria and Marianna for their ever-enduring support in all my endeavours, because of their dedication and love I have made it to where I am today. I, of course, cannot forget to thank my friends as well, especially: Moutas, Antonis, Polydoros, Myrto, Stephan, Ingo and every single one of my friends in Edinburgh, Munich, Sydney and Athens. They have always been there for me and I have always been able to count on their friendship through thick and thin. Furthermore, I would like to thank both Nick and Karen for the support. They have been true, dedicated friends who help me unwind from the stresses of academia and work, even if it is in an unconventional way.

Lay summary

Phthalocyanines (Pcs) are a large, aromatic organic conjugated compound that is composed of four isoindole units that are linked through nitrogen atoms. The unsubstituted phthalocyanines are completely planar and have a ring system of 18 π-electrons. Due to the extensive delocalization of the π-electrons the molecule affords useful properties, such as being used as pigment and dyes. Furthermore, the macrocycle can host a large variety of elements, which can be useful in catalysis, organic solar cells and photodynamic therapy. There has been extensive research in nanobiotechnology and photodiagnosis, but the system that will be described in this thesis, was created in the McKeown group and the aggregation issues of the phthalocyanines were overcome, forming a nanoporous molecular crystal.

Abstract

Phthalocyanines (Pcs) have a wide variety of applications as colorants, photodynamic therapeutics, photovoltaic materials, catalysts etc. Pcs tend to co-facially aggregate due to the π – π interactions between their aromatic macrocycles, which may hinder certain applications. The insertion of 2,6-di-iso-propylphenoxy substituents at the peripheral sites of the Pc [$(dipPhO)_8Pc$] proved successful in preventing aggregation between the macrocycles while the bulky substituents created accessible voids towards the active metal centre. Upon crystallisation of various metal $(dipPhO)_8Pc$ derivatives, clathrates with an interesting cubic structure, where the volume occupied by the crystallisation solvent amounts to around 40% of the unit cell, were obtained. Suitably sized bidentate ligands act as wall-ties to stabilise the crystal structure upon removal of the solvents that otherwise would cause loss of crystallinity. We have found that there is an astonishing range of metal cations, axial ligands and molecular wall-ties that are compatible with the formation of the porous crystal. Preliminary data using a gas cell for the in-situ analysis of O_2, NO and CO binding to the metal cation will be reported. In addition, the co-crystallisation of $(dipPhO)_8Pc$ with tetraphenyl porphyrin (H_2TPP) and the in-situ incorporation of bidentate ligands and of metals in the macrocycle of the TPP will be demonstrated.

Abbreviations

Abbreviation	
Å	Angstrom
ADOR	Assembly-dissassemblyorganisation-reassembly
BET	Brunauer-Emmett-Teller
BiPy	4,4'-Bipyridine
CCD	Cambridge crystallographic database
COF	Covalent organic framework
COSY	Correlation Spectroscopy
CSD	Crystal Structure Database
D	Doublet
DBN	1,5-Diazabicyclo[4.3.0]non-5-ene
DBU	1,8-Diazabicyclo[5.4.0]undec-7-ene
DCC	Dynamic Covalent Chemistry
DCM	Dichloromethane
DDQ	2,3-Dichloro-5,6-dicyano-1,4-benzoquinone
DFT	Density funcional theory
DIPP	2,6-Di-*iso*-propylphenol
DMF	Dimethylformamide
EPR	Electron Paramagnetic Resonance
G	Gauss
G	Grams
Gpa	Gigapascals
H	Hour/s
HCCA	alpha-Cyano-4-hydroxycinnamic acid
Hz	Hertz
*i*PMC	Intrinsically Porous Molecular Crystal

IR	Infrared
J	Coupling constant (in Hz)
K	Kelvin
m	Meters
M.p.	Melting point
MALDI-TOF-TOF	Matrix-assisted laser desorption ionisation tandem time of flight
MOF	Metal organic framework
NBS	N-bromosuccinimide
nm	Nano meters
NMR	Nuclear Magnetic Resonance
***o*-DCB**	*Ortho*-dichlorobenzene
Pc	Phthalocyanine
$(dipPhO)_8Pc$	2,3,9,10,16,17,23,24-octa(2',6'-di-iso-propylphenoxy)phthalocyanine
PNC	Phthalocyanine Nanoporous Crystal
PnDIPP	4,5-bis(2',6'-di-iso-propylphenoxy)phthalonitrile
Q	Quartet
S	Singlet
SA	Surface Area
SCSC	Single-crystal to single-crystal transformation
SMM	Single Molecule Magnet
T	Triplet
TGA	Thermogravimetric Analysis
THF	Tetrahydrofuran
TLC	Thin layer chromatography
UV	Ultraviolet
UV-Vis	Ultraviolet-visible spectroscopy
XRD	X-ray diffraction

Contents

Chapter I:

Introduction

1.1 The history of phthalocyanines

Phthalocyanines (Pc) were named by Reginald Linstead (Imperial College, London) from the combination of the prefix phthal, from the Greek word naphtha (νάφθα) which means rock oil and the Greek cyano (κυανό) which means blue. They are 18-π electron aromatic macrocycles, formed by four isoindole units and can form complexes with over sixty different metal ions. Their structure is closely related to that of porphyrins with the main difference being the fused benzene rings and the addition of nitrogen atoms in the meso positions the benzene fused rings and the nitrogens in the meso positions (**Figure 1.1**).[1,2]

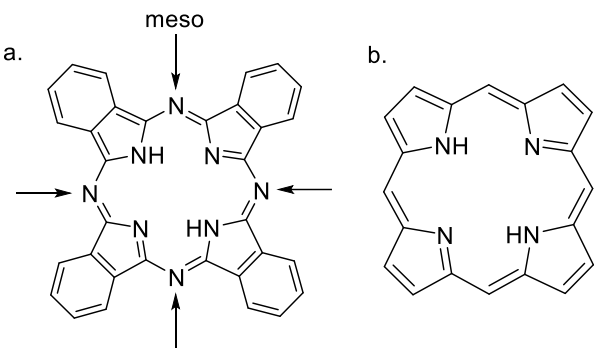

Figure 1.1. a. Structure of phthalocyanine, b. Structure of porphine

An accident led to the identification of the structure of the phthalocyanines. In 1928, during the course of the industrial production of phthalimide from phthalic anhydride and ammonia in the Grangemouth works of Scottish Dyes Ltd, the glass-lined reaction vessel had cracked, exposing the outer steel casing to the reaction resulting in the formation of a blue-green material. Preliminary studies revealed that this material contained iron and was stable, insoluble and could be used as pigment. In 1928, Imperial Chemical Industries (ICI) acquired Scottish Dyes Ltd. and sent a sample of this by-product to Thorp and Linstead at Imperial Collage London for further investigation. Papers from this collaboration describe the structure of Pc and the synthesis of

some metal derivatives.[3–8] In 1934, Robertson obtained the structure of phthalocyanine by X-ray structure determination, making it one of the first organic compounds to have its structure confirmed by crystallography.[9–13] From the 1930s to the 1950s, solubility and polymorphism, absorption spectra,[14] magnetic and catalytic properties,[15] oxidation and reduction potentials[16] were investigated.

1.2 Applications of phthalocyanines

To date phthalocyanines have been used as blue-green colorants. Further to that, phthalocyanines have found many more applications in different fields, such as photodynamic therapy (e.g. PcP), catalysis (e.g. PcM, M=Fe, Co, Mn, Ru), as photoconductors in copying machines and printers and as light absorbents of recordable compact disks (CD-R),[17] nonlinear optical materials, sensing agents,[18], photovoltaic (e.g. PcGe), semiconductors,[19] etc.[20,21]

1.3 Methods of phthalocyanine synthesis

Metal-free and metallated phthalocyanines can be synthesized via several methods (**Figure 1.2** a, b) each involving the cyclotetramerisation of an aromatic precursor. The main difference between these methods is how mild or forcing the conditions are. Alternatively, the synthesis of metallated Pcs, by deprotonating and inserting the metal into metal-free macrocycle, is considerably milder than coordination of phthalonitrile with metal salt in the presence of high boiling solvents. The methods described below, in the subchapters 1.3.1 and 1.3.2, are the ones that were used to synthesize the metal-free and metallated phthalocyanine of the derivative used in the current project.

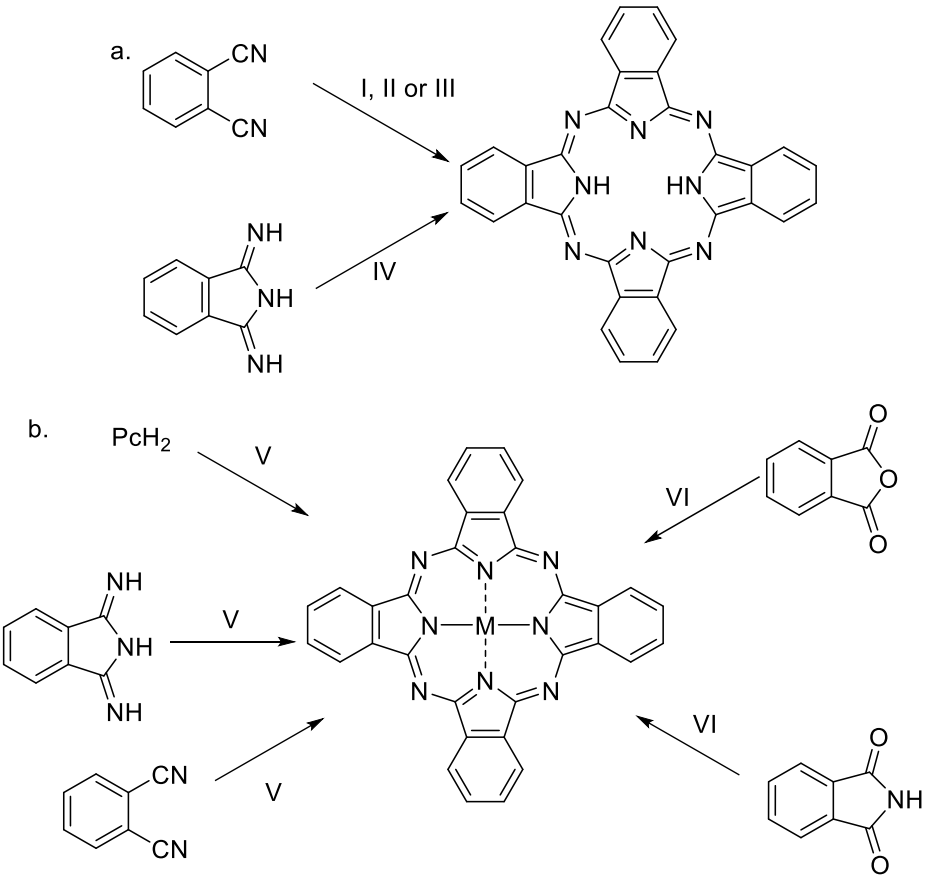

Figure 1.2. a. The synthesis of metal-free phthalocyanine. Reagents and conditions: Method I: lithium, refluxing pentanol, aqueous hydrolysis. Method II: Heat with DBU or DBN or NH_3 in refluxing pentanol or heat in DMAE. Method III: Fuse with hydroquinone. Method IV: Reflux in a high-boiling-point alcohol. b. The synthesis of metallated phthalocyanine. Reagents and conditions: Method V: Heat in a high-boiling-point solvent (e.g. quinoline) with metal salt. Method VI: Heat in a high-boiling-point solvent with metal salt and urea.

1.3.1 Metal-free phthalocyanine

Method I: Metal-Free Phthalocyanine from Phthalonitrile by Subsequent Removal of Metal Ions

Lithium, sodium, or magnesium alkoxides, formed *in-situ* with the addition of the metal to a primary alcohol (usually *n*-pentan-1-ol), are used for the cyclotetramerisation of phthalonitrile. The metal ions (e.g. Li^+, Na^+, K^+, Mg^{2+}) can be removed from phthalocyanine with acid, therefore when the cyclotetramerisation is complete, the metal ions are removed to give PcH_2 with an acidic or aqueous work-up (**Figure 1.3**).[22,23]

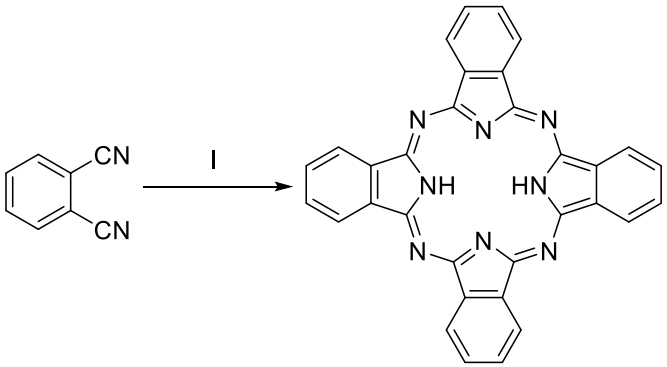

Figure 1.3. The synthesis of metal-free phthalocyanine (PcH_2). Method I: Lithium, sodium, or magnesium in n-pentan-1-ol.

1.3.2 The synthesis of metal phthalocyanine

Metal containing phthalocyanine can be synthesized from phthalonitrile with four different methods.

Method II: Metal Phthalocyanine from Phthalonitrile in Bulk Reaction

Heating phthalonitrile with a metal salt in a bulk reaction (without solvent) is a direct and convenient method of preparing phthalocyanines (**Figure 1.4**). The melting point of the phthalonitrile is above 180 °C so the cyclotetramerisation is taking place at temperatures above 200 °C. Typical method is using microwave irradiation.

Method III: Metal Phthalocyanine from Phthalonitrile in Solvent

In addition, the cyclotetramerisation of phthalonitrile with suitable metal compounds can be achieved in solution. Useful solvents for this method are high-boiling solvents such as quinoline, DMF, DMAE, and 1-chloronaphthalene (**Figure 1.4**).[24]

Method IV: Metal Phthalocyanine from Phthalonitrile and Base

Furthermore, heating phthalonitrile with a metal salt in a solvent and DBU or DBN is an efficient method for the cyclotetramerisation of phthalonitrile providing metal-containing phthalocyanines (**Figure 1.4**).[25]

Method V: Metal Phthalocyanine from Metal-Free Phthalocyanine

Complexing PcH_2 with metal ions is one of the most basic methods to introduce a metal into the cavity of the phthalocyanine and can be achieved under mild conditions. In order for this reaction to be successful, the metal-free Pc needs to be soluble in common organic solvents (e.g. *n*-pentan-1-ol, *o*-dichlorobenzene).[22] A small amount of DBU is added to the solution to deprotonate the PcH_2 and then the metal salt is added (**Figure 1.4**).

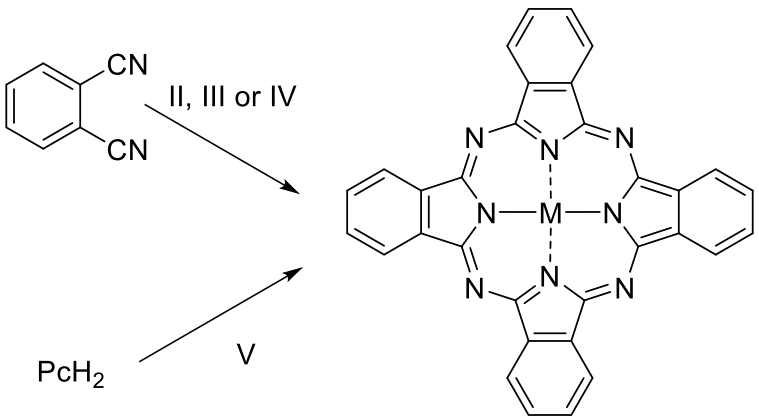

Figure 1.4. The synthesis of metal phthalocyanine (PcM).

1.4 Substitution sites on phthalocyanines

The phthalocyanine macrocycle has sixteen possible sites for substitution. When a metal ion is coordinated to the Pc, it can provide axial binding sites for further ligand incorporation. The ring sites on the benzene ring can be distinguished as peripheral and non-peripheral (B and A sites respectively in **Figure 1.5**). Incorporating axial ligands or ring substituents can improve the solubility or change the physical properties[26,27] of the phthalocyanine and inhibit the phthalocyanines tendency to co-facial aggregate due to the strong π-π interaction.

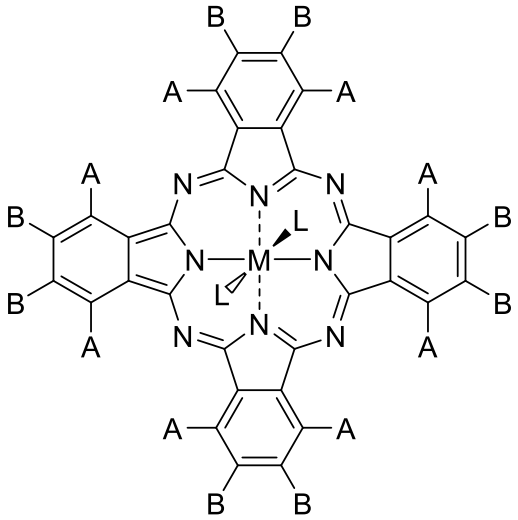

Figure 1.5. Possible sites for substitution of the phtalocyanines. L indicates axial ligands on the metal ion, B peripheral and A non-peripheral sites.

1.5 Nanoporous molecular crystals (NMCs)

Nanoporous materials are solids that contain interconnected pores and are used for catalysis, adsorption, separation and many other different applications.[28,29] By the definition of the International Union of Pure and Applied Chemistry (IUPAC), porous materials can be divided into three separate categories based on the predominant pore size: microporous materials contain pore diameters larger than 50 nm, mesoporous materials have diameters between 2 – 50 nm and microporous materials possess pore diameters smaller than 2 nm.[30] These porous materials can be either organic, inorganic or a combination of both and can be either man made or natural occurring and have attracted attention for the potential applications. Nanoporous is a non-systematic term that is often used for materials whose pores straddle the boundary between micro- and meso-porous.

By the definition of the International Union of Pure and Applied Chemistry (IUPAC), clathrates and inclusion compounds are all nomenclature closely related to each other. A complex in which one component (the host) forms a cavity or, in a case of a crystal, a crystal lattice containing spaces in the shape of long tunnels or channels in which molecular entities of a second chemical species (the guest) are located. There is no covalent bonding between guest and host, the attraction being generally due to van der Waals forces. If the spaces in the host lattice are

enclosed on all sides so that the guest species is 'trapped' as in a cage, such compounds are known as clathrates or 'cage compounds'. Nassimbeni, over 15 years ago, categorised into two generalised types of host molecules, those that form molecular complexes by fitting guests (e.g. solvents, anti-solvents) into the concave cavity or void of the host, and those that form lattice inclusion compounds by packing in such a manner as to leave cavities, channels, or layers in the crystal structure so as to accommodate various guest molecules.[31]

The porosity of NMCs can be generated from one or a combination of two strategies (**Figure 1.6**); in intrinsically porous molecular crystals (*i*NMCs), such as cage-like compounds, the porosity arises from the pre-fabricated internal cavities within the molecules themselves; in extrinsically porous molecular crystals (*e*NMC) the porosity arises as a result of inefficient packing of the molecules in the solid state, thus they are consequently more difficult to design and predict;[32] and finally a combination of the two strategies can result in both an intrinsically and extrinsically based porous material.[33]

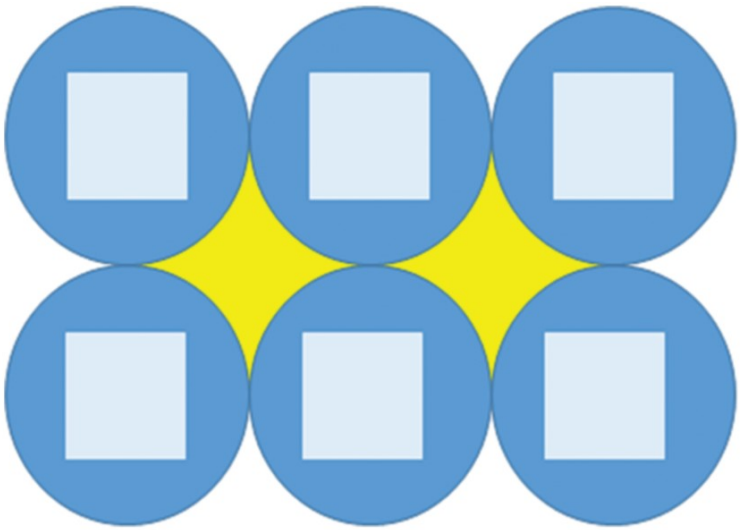

Figure 1.6. Intrinsic (light blue square) and extrinsic (yellow space between spherical molecules) pore spaces formed by molecular species in a periodic assembly.[34]

Conventional porous materials consist of crystalline inorganic frameworks (e.g. zeolites) or amorphous structures (e.g. silica and activated carbon). There have been major advances in the synthesis of new nanoporous materials using molecular components, for example, the crystalline organic–inorganic hybrid materials, such as the Metal Organic Frameworks (MOFs) or the Covalent Organic Frameworks (COFs) (**Figure 1.7**).

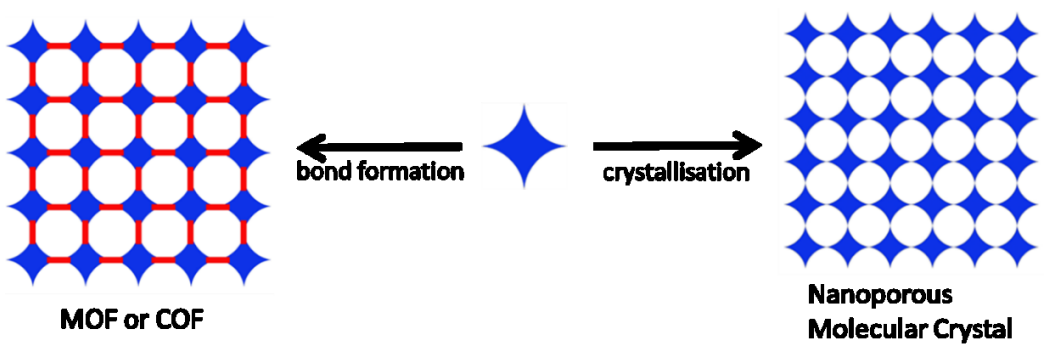

Figure 1.7. Schematic representation of formation of conventional nanoporous materials (e.g. MOFs and COFs) and of Nanoporous Molecular Crystals (NMCs).[35]

Nanoporous Molecular Crystals (NMCs)[35] are materials that are composed of discrete molecules (e.g. molecules with awkward shape that have concave faces) between which there are only weak interactions (e.g. hydrogen bonding or van der Waals interactions). Such materials combine nanoporosity with the ability to be dissolved and then reassembled. They are formed by simple crystallisation and subsequent removal of the included solvent of crystallisation. Solvent removal from clathrates usually results in the collapse of the structure and loss of crystallinity or causes a phase change leading to denser non-nanoporous crystals. Instead, in the NMCs the packing is retained and nanoporosity is gained (**Figure 1.8**). A notable family of nanoporous molecular materials are cages, which can be considered as prefabricated pores. In particular the work of the Cooper group has demonstrated that cages can form predictable crystal structures[36] with applications in molecular separations.[37]

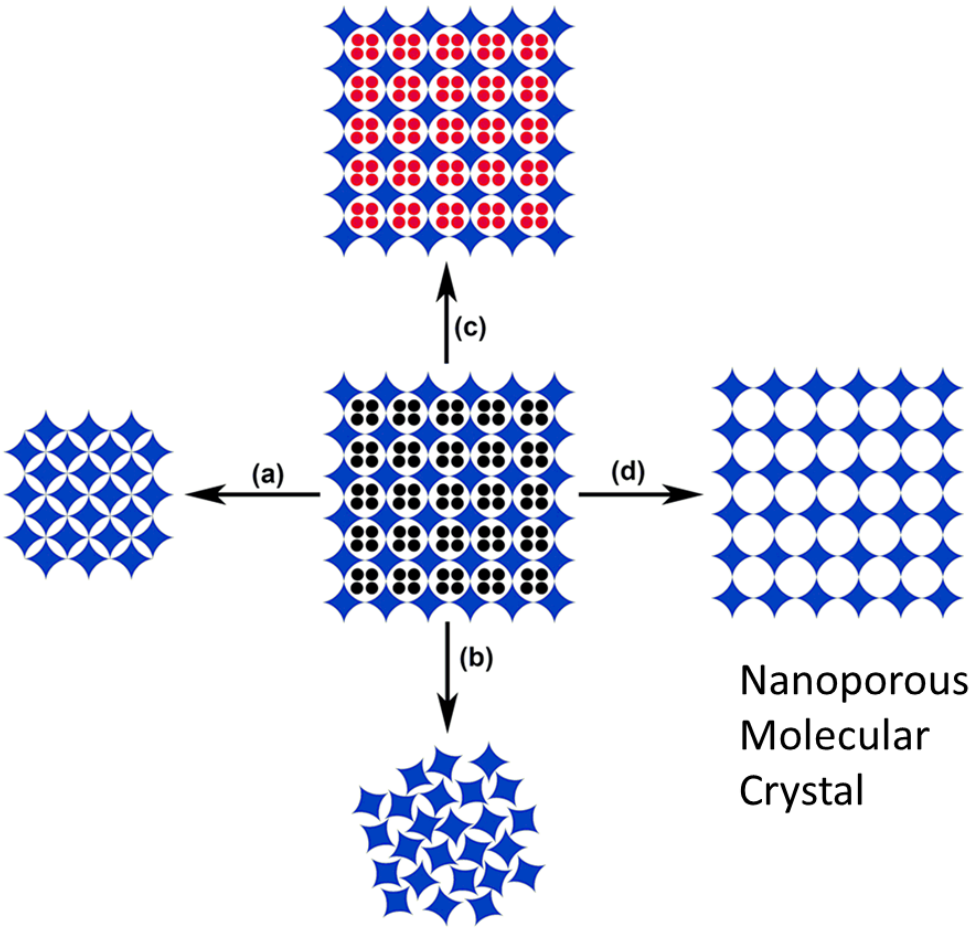

Figure 1.8. Possible outcomes following removal of solvents from a clathrate: (a) collapse to a non-nanoporous denser crystal, (b) collapse to an amorphous mass, (c) exchange with another solvent, (d) formation of a NMC.[38]

More specifically, as Nassimbeni,[31] and then Green and Lloyd[34] described, the production of a potentially porous crystalline material from a molecular building component required some form of crystallisation process (**Figure 1.9**). In most cases, when a crystallisation is performed, the host prefers to occupy most of the space in the unit cell without leaving any free space, but if the packing is not optimal for there are concaves then this results in the inclusion of guest molecules, such as solvent or anti-solvent, resulting in a multicomponent material. The densely packed solid form is described as the apohost, where apo comes from the Greek word από, meaning furthest point from, and the host which is the host structure. Since it is densely packed it exhibits the most stable lattice energy and will be referred as the α phase. Since the structure is concave, a

recrystallisation of the apohost, from the dissolved molecules in a solution that may contain potential guest molecules (anti-solvent in a vapour diffusion recrystallisation), can result in an inclusion complex (β phase). When materials are obtained with the same structure with different guest species, then these forms are all the same β phase. If the guest : host ratio decreases (e.g. temperature rises) and there is an expulsion of guest, then there is a new lattice compound (γ phase). A complete evacuation of the guest molecules from the structure leaving the host empty but retaining the host lattice structure results in a β_o phase. If the host lattice structure collapses then the result could be either a reformation of the α phase (apohost) or a close-packed polymorph of the α phase. The guest molecule can be exchanged with another guest molecule when the host lattice structure has already formed, resulting in a δ phase. This transformation must occure through a single crystal to single crystal mechanism and the δ phase may show its own versions of the γ and β_o phases.

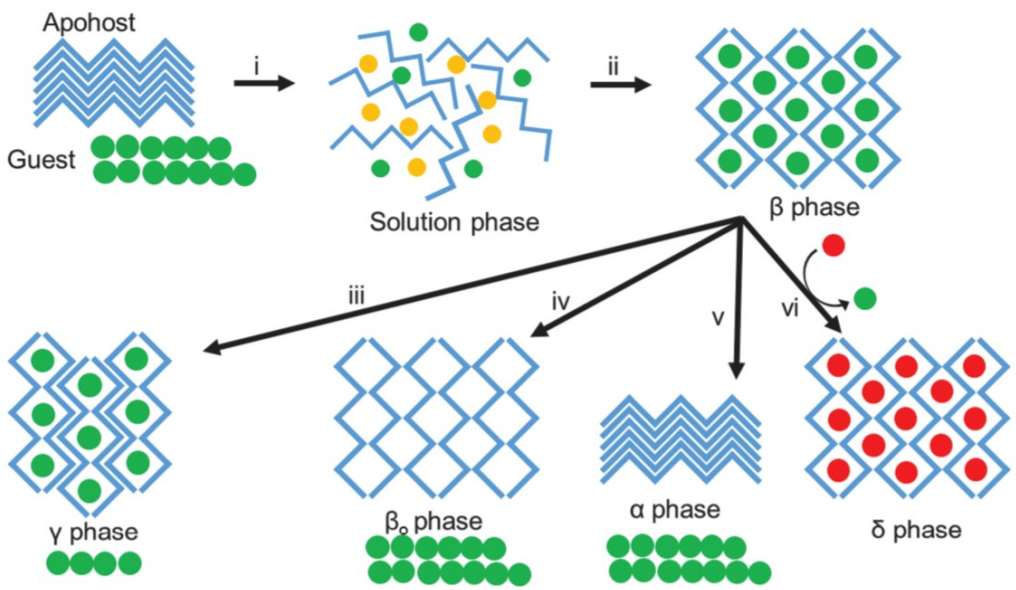

Figure 1.9. Schematic of the formation and decomposition of inclusion compounds. (i) The ''close-packed'' apohost lattice α phase is dissolved into a solution that may contain potential guest molecules (green dots), (ii) Recrystallisation results in an inclusion complex (β phase) with guests. (iii) Partial decomplexation can occur, resulting in a new lattice (γ phase). There can be a number of γ phases, e.g. stepped decomplexation. (iv) Complete decomplexation but retention of the host lattice structure (β_o phase). (v) Collapse of the host lattice reforming the α phase. (vi) Post-assembly modification through guest exchange resulting in a δ phase.[34]

1.6 Phthalocyanine Nanoporous Crystals (PNCs)[39–41]

Until 2005, there were few reports of inclusion compounds formed by phthalocyanines, since their tendency to co-facially aggregate because of their planarity and π-π interactions.[42–47] In order to form a NMC, the cofacial aggregation that characterizes Pc crystals needed to be overcome. This can be achieved by inserting bulky substituents at the periphery of the macrocycle to cause severe steric crowding or by placing large atomic radius metal ions within the central cavity to disrupt aggregation.

In 2005, McKeown et al.[39] reported a phthalocyanine derivative clathrate of cubic symmetry containing interconnected solvent-filled nanometres size voids. The synthesis of zinc complex of 2,3,9,10,16,17,23,24-octa(2',6'-di-*iso*-propylphenoxy) phthalocyanine (PNC[Zn]) was achieved via metal template cyclotetramerisation of 4,5-di(2',6'-di-*iso*-propylphenoxy) phthalonitrile which had been previously obtained by nucleophilic aromatic substitution of 2,6-di-*iso*-propylphenol on 4,5-dichlorophthalonitrile (**Scheme. 1.1**).[48] The recrystallisation by slow diffusion of acetone into a solution of the $(dipPhO)_8PcZn$ in $CHCl_3$ afforded large crystals with cubic symmetry, as the same cubic structure was obtained for the PNC[M] (for M = red coloured elements in **Figure 1.10**).

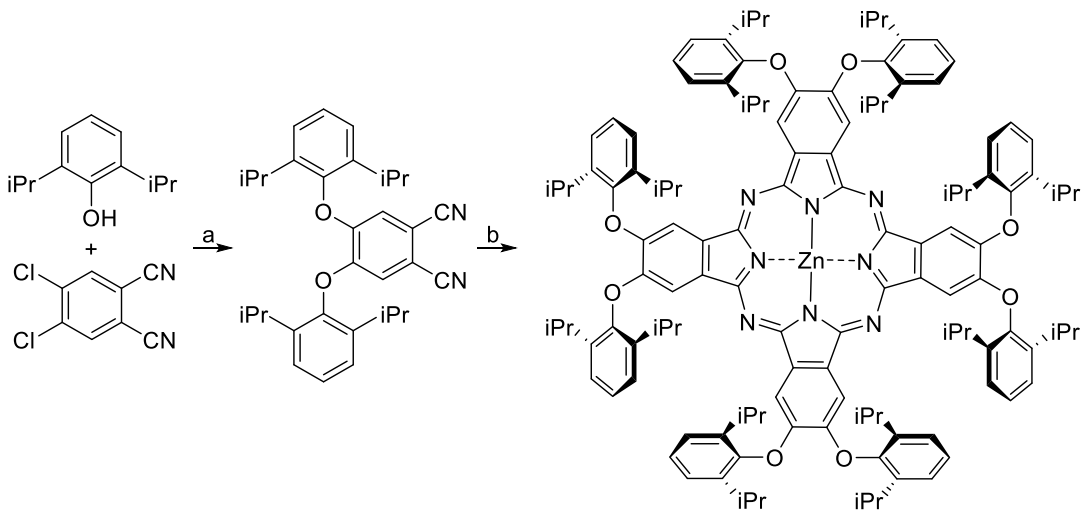

Scheme 1.1. Synthesis of zinc phthalocyanine derivative. Conditions: a. K_2CO_3, DMF, 60 °C, b. $Zn(OAc)_2$, NMP, 150 °C.

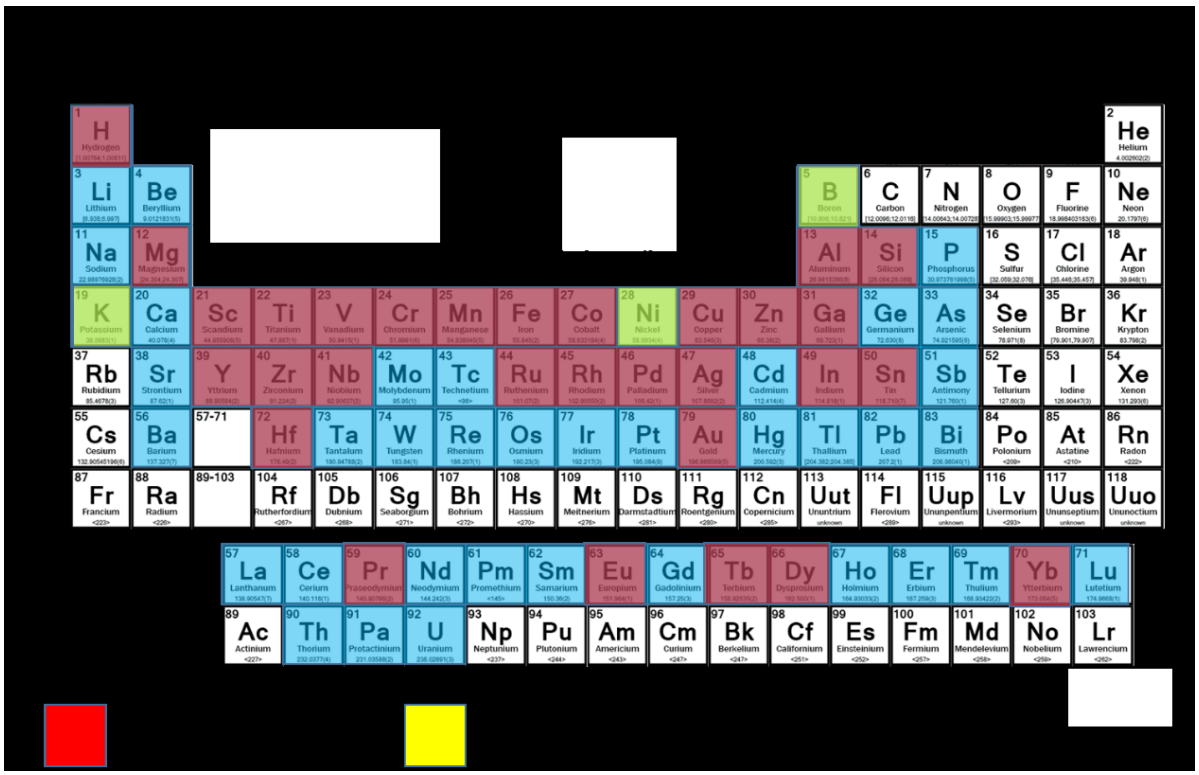

Figure 1.10. Periodic table depicting the state of play at the start of the PhD program with blue shading for elements that form complexes with phthalocyanines, red shading for the elements that form cubic nanoporous complexes with $(dipPhO)_8Pc$, called (PNC[M]), and with yellow shading for the elements that do not form cubic structure as characterised by sc-XRD analysis, called $(dipPhO)_8PcM$.

The XRD analysis revealed a remarkable structure (**Figure 1.11**) which belongs to the exceptionally rare space group $Pn\bar{3}n$ with only 171 structures published in CCDC and contains 12 $(dipPhO)_8PcZn$ molecules per unit cell (a = 3.77 nm). The phthalocyanine is distorted from planarity and assumes a cone-shape with the oxygen atom of the water ligand on the axial position, facing the cubic void and protruding from the molecular plane. The bulky substituents, 2,6-di-*iso*-propylphenoxy, lie perpendicular to the plane of the phthalocyanine inhibiting aggregation. The unit cell contains two solvent filled voids with six phthalocyanine molecules constituting the sides of each void and the distance between the metal centres of two phthalocyanines across the void being approximately 2.33 nm.

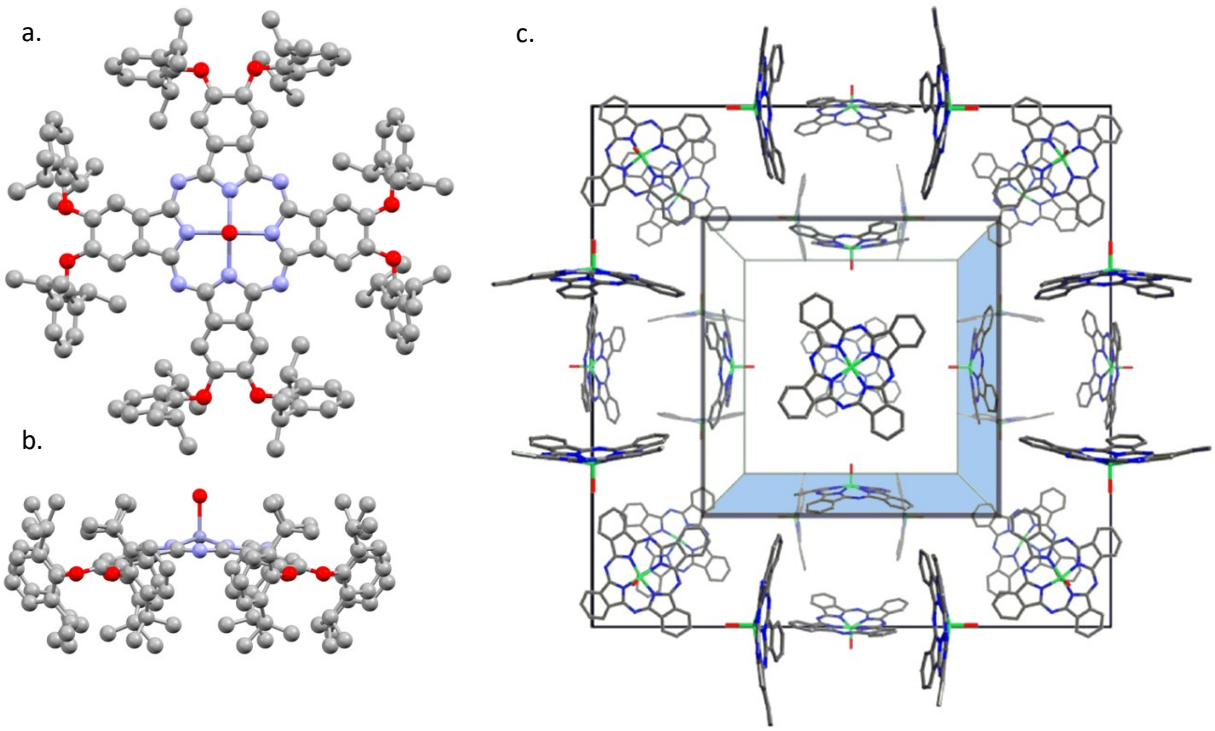

Figure 1.11. Molecular crystal structure of PNC[Zn] a. Face-on, b. Edge-on, c. The cubic packing arrangement of PNC[Zn] shown without the phenoxy substituents. The outer cube is the unit cell, with dimensions of 3.77 nm, which contains 12 molecules of PNC[Zn]. The inner cube represents one of the two voids of volume 8 nm^3. The second void is divided in four parts, each quarter of the void positioned at each of the four corners of the unit cell and when added up they have a volume of 8 nm^3.[40]

The solvent-occupied volume of the nanoporous structure of the PNCs is divided into two non-intersecting channels. The larger channels are named as the void, while the smaller channel as the cavity. The metal ions that are incorporated to the macrocycle have two different axial positions where a ligand can bind; one facing towards the cavity, and the other towards the void (**Figure 1.12**).

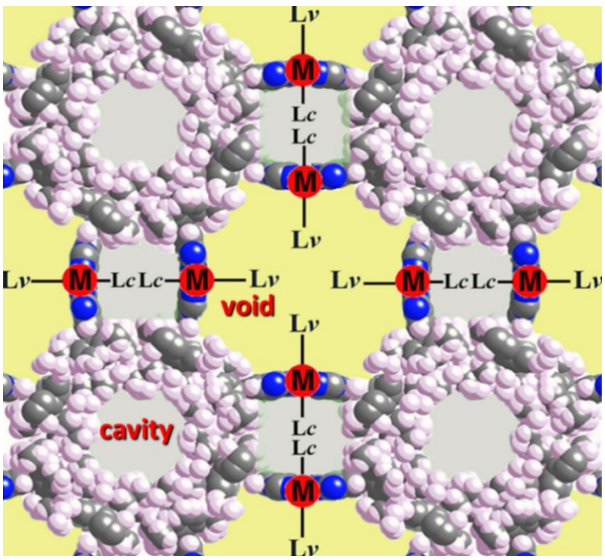

Figure 1.12. Space-filling model of the crystal structure composed of the phthalocyanine derivative where M is the metal cation, L*v* is the ligand facing towards the void, and L*c* is the ligand facing towards the cavity. The void is shaded yellow and the cavity is shaded gray.

Apart from the axial water ligand on PNC[Zn], another 24 water molecules per unit cell associated through hydrogen-bonding interactions to the meso nitrogen atoms of the phthalocyanine ring, were found. The calculated density of the PNC[Zn] was 0.75 g mL^{-3}, and the solvent-accessible void volume was 20.5 nm^3 per unit cell, about 38% of the total volume. The water refined by XRD analysis accounts for 1.6% of the crystallography determined total mass, while thermogravimetric analysis (TGA) showed a mass loss of 25.5% on heating up to 120 °C. This additional mass loss can be attributed to the disordered solvent of recrystallisation which is estimated to be a molar ratio of 1/11 of PNC[Zn]/acetone, which was confirmed by ^{1}H NMR spectroscopic analysis by redissolving the crystals and integrating the peak. Exchange of solvent revealed the interconnectivity of the void and that each unit cell can host 132 molecules of acetone or 360 H_2O or 240 methanol or 96 hexane molecules in the channels (determined by ^{1}H NMR). The clathrate is not stable upon removal of the included solvent, although the macroscopic appearance remains unchanged.

Apart from solvent exchange, axial ligands could be exchanged in single-crystal to single-crystal transformation (**Figure 1.13**). This exchange, which shows the accessibility of the metal center in the crystals, takes place either because the concentration of the new ligand is higher, or because there is higher affinity of the ligand with the metal ion.

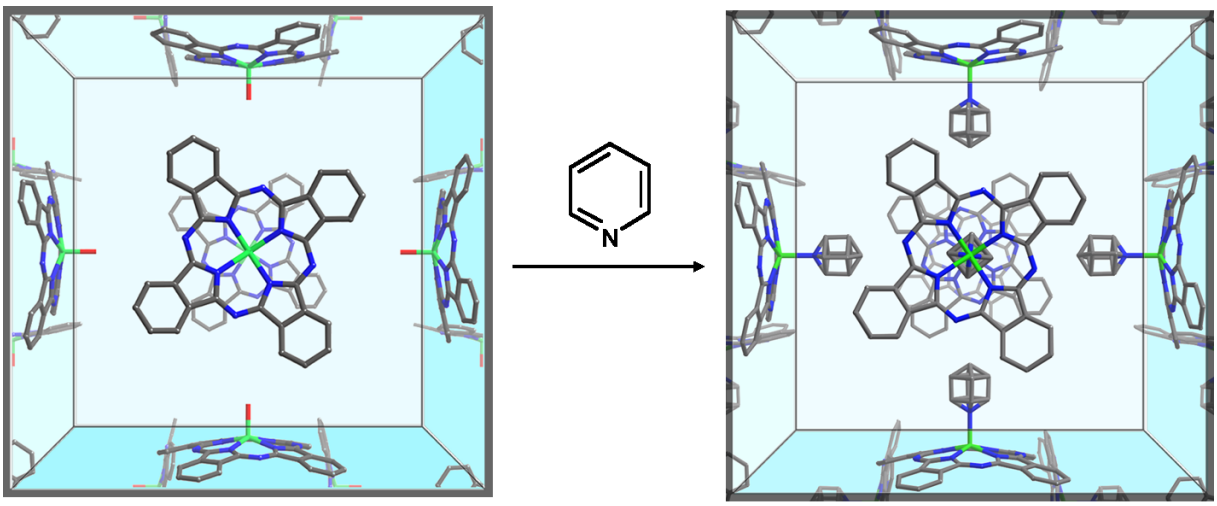

Figure 1.13. Single-crystal to single-crystal transformation. The PNC[Zn] has a water molecule on the axial position facing towards the void that is coordinated and by insertion of pyridine excess the pyridine takes the place of the water. Note the di-*iso*-propylphenoxy substituents are removed for clarity.

1.7 Stabilization of PNC with Bidentate ligands (Wall-ties)[40,41]

As has been stated, upon removal of the contained solvent from the inclusion compound, the crystal structure collapses. This problem could be overcome by inserting bidentate ligands such as 4,4-bipyridyl (bipy) (for the PNCs from $(dipPhO)_8PcFe$ or $(dipPhO)_8PcCo$) or, in the case of the PNC from $(dipPhO)_8PcFe$, 1,4-phenylenedi-iso-cyanide (pdic) within the cavity to stabilise the structure (**Figure 1.14**). Removal of the solvent by exposing the crystals to a stream of N_2 was confirmed by TGA, and the crystal stability by XRD analysis. As suggested by Barbour,[49] the permanent microporosity of the crystals was confirmed by N_2 adsorption, with Brunauer Emmett Teller (BET) surface areas ranging from 850-1000 $m^2\,g^{-1}$.

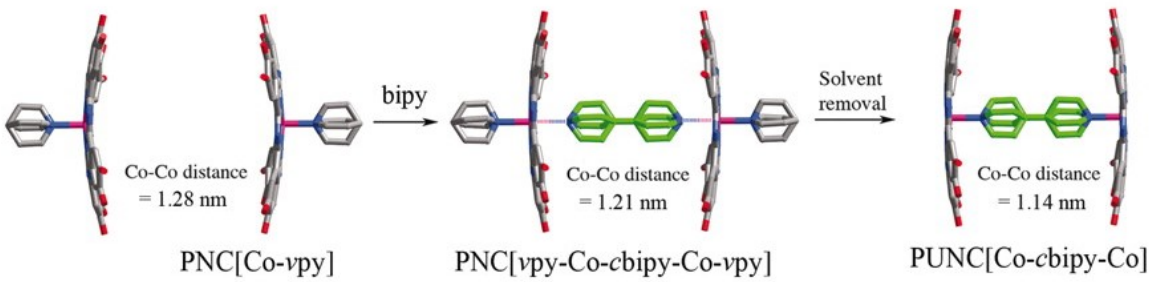

Figure 1.14. Bipyridine (bipy) acting as a bidentate ligand (wall-tie). When a bidentate ligand is incorporated there is a reduction of the distance between the phthalocyanines and also it provides stabilization of the crystal structure upon solvent removal.[40]

1.8 Aims and objectives

Even at the start of the PhD research programme, which forms the basis for this thesis, it was clear that the PNC nanoporous crystal system offers considerable choice of metal cation contained in the central cavity of the $(dipPhO)_8Pc$ macrocycle and axial ligand contained within both the voids and cavities of the PNC. During the early part of the research programme, further structural diversity was found by co-workers in the McKeown Group including lanthanide sandwich complexes (Luke Burt, unpublished) and the incorporation of fullerenes (Grazia Bezzu) (**Figure 1.15**).[50] Hence, it was anticipated that even further structural diversity could be uncovered. The initial aim was to further expand and analyse the range of metals that can be incorporated into the PNC, by comparing the curvature in relation with the extrusion of the metal and with the metal ion radii as well as categorising into cubic and non-cubic space groups either with or without axial ligands – this work forms the basis for Chapter 2. In addition, the range of wall-tie ligands and sandwich compounds was also to be expanded, with the same analysis as the Chapter 2 as well as gas cell XRD in Diamond Light Source (DLS) and gas cell EPR spectroscopy in Manchester University, as discussed in Chapter 3. Chapter 3 also describes the unexpected discovery that the commonly studied tetraphenylporphyrin ligand could also be incorporated within the PNC structure, forming the new series of PNC, which will be named as PNC[*v*H_2TPP / H_2], denoting that the metal-free porphyrin is on the side of the void and the phthalocyanine is metal-free.

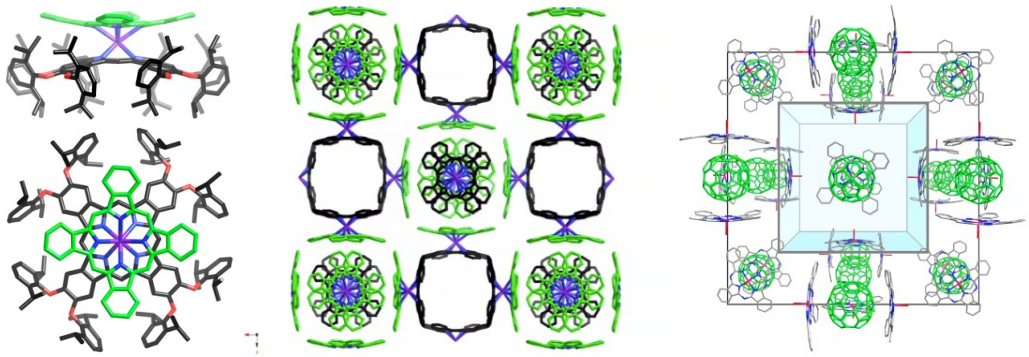

Figure 1.15. The PNC formed by a lanthanide sandwich complex (left) and stabilised by a fullerene (right).

Chapter II.

Elemental diversity in nanoporous molecular crystals

2.1 Introduction

In previous work within the McKeown group many metal derivatives (H_2, Mg, Al, Si, K, Sc, Ti, V, Cr, Mn, Fe, Co, Ni, Cu, Zn, Ga, Y, Zr, Nb, Ru, Rh, Pd, Ag, In, Sn, Au) of 2,3,9,10,16,17,23,24-octa(2',6'-di-iso-propylphenoxy)phthalocyanine [$(dipPhO)_8PcM$] were prepared and provided cubic crystals belonging to the $Pn\bar{3}n$ space group that contained pores greater than 8 nm^3.[40] Remarkably, the same crystal structure has also been obtained for some double decker lanthanide $(dipPhO)_8PcMPc$ complexes (M = Tb, Y, Dy, Pr and Yb) in which case the smaller Pc ligands face into the voids (unpublished results, Luke Burt PhD, 2018). Since phthalocyanines can form complexes with ~70 metal ions (**Figure 2.1**), the partial objective of the PhD programme was to prepare new metal derivatives of $(dipPhO)_8PcM$ (M = Fe, P, Ge, Mo, W, Re, Ir, Pt, Cd, Sb, Pb, Bi), to investigate further the occurrence of the cubic nanoporous structure. The metals that were selected for the incorporation in the macrocycle are metals that have various applications. For example porphyrin derivatives containing phosphorus is known to act as photosensitizer[51,52] and in photodynamic therapy of cancer.[53] Iron has previously been employed in phthalocyanines due to a number of interesting catalytic properties. They are used for synthesis of sulfones,[54] oxidation of phenol,[55] oxidation-aromatization of ketones,[56] making them potentially interesting to be employed within our nanoporous crystal system. Molybdenum containing porphyrins have been extensively studied for potential applications such as oxidation,[57] epoxidation[58] and nanotubes[59], while molybdenum phthalocyanines are used for the preparation of formaldehyde by oxidation of methanol.[60] Other applications for the remaining metals that were not mentioned above would be photocatalysts for the antimony,[61,62] photosensitizers[63] and oxygen reduction[64] for the iridium, as electrocatalysts for hydrogen evolution and oxygen reduction,[65] or used as batteries with replaceable metal anodes,[66] or as triplet sensitizers[67] for the platinum, phototransistors,[68] and photocatalytic material[69] for the lead and catalysts,[70] sandwich complexes of Bi – Li,[71] and radiotherapy[72] for the bismuth. Note that the legends shaded in red

indicate structures obtained during the PhD programme. This chapter summarises existing crystal data (including unpublished data) and new structure from crystals that were prepared during the PhD research programme.

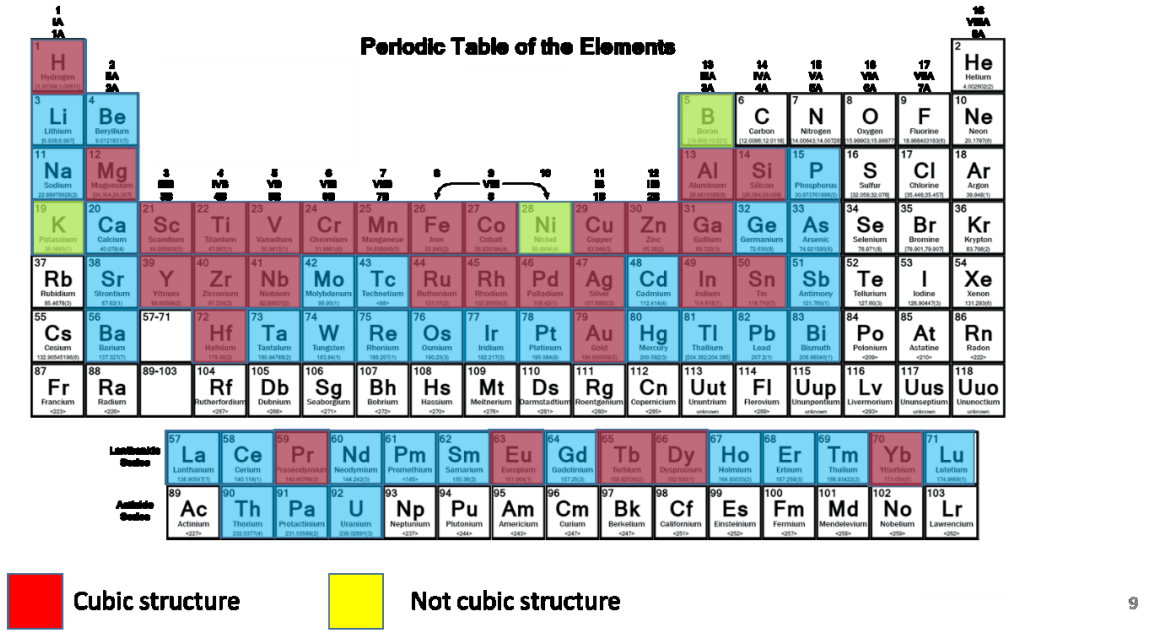

Figure 2.1. Periodic table depicting the state of play at the start of the PhD program with blue shading for elements that form complexes with phthalocyanines, red shading for the elements that form cubic nanoporous complexes with $(dipPhO)_8Pc$, denoted PNC[M], and with yellow shading for the elements that do not form cubic structure as characterised by sc-XRD analysis, denoted $(dipPhO)_8PcM$.

2.2 Synthesis of $(dipPhO)_8PcM$

For the synthesis of many $(dipPhO)_8PcM$ derivatives it was necessary to first prepare the key precursor 4,5-di(2',6'-di-*iso*-propylphenoxy)phthalonitrile, which can be made by nucleophilic aromatic substitution of the 2,6-di-*iso*-propylphenol on 4,5-dichlorophthalonitrile, as described in detail in the experimental section (**Scheme 2.1**).[48,39]

2.2.1 Synthesis of metal-free $(dipPhO)_8PcH_2$

The cyclotetramerisation of 4,5-di(2',6'-di-*iso*-propylphenoxy)phthalonitrile using lithium dissolved in pentanol followed by acidic work-up gives $(dipPhO)_8PcH_2$ (**Scheme 2.1**).

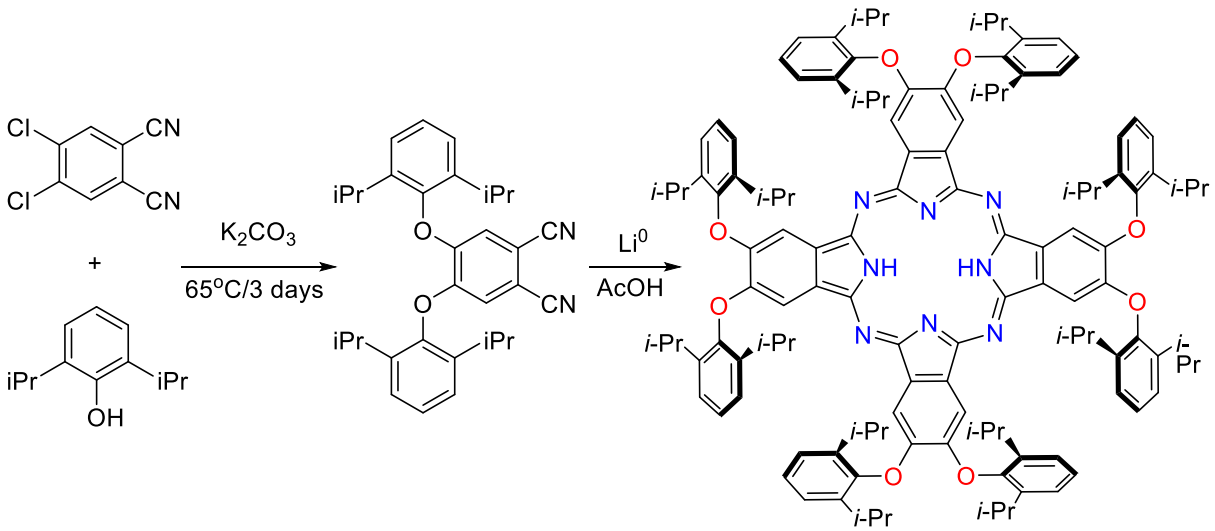

Scheme 2.1. a. Synthesis of 4,5-di(2',6'-di-*iso*-propylphenoxy) phthalonitrile. Conditions: K_2CO_3, DMF at 65 °C for 3 days. b. Synthesis of 2,3,9,10,16,17,23,24-octa(2',6'-di-*iso*-propylphenoxy)phthalocyanine. Reagents and conditions: i. Li, pentanol, reflux, 3 h, ii. Dilute AcOH, room temperature, overnight.

2.2.2 Synthesis of metal derivatives (dipPhO)$_8$PcM

Metal derivatives of (dipPhO)$_8$Pc can be prepared using various synthetic techniques as described below (**Scheme 2.2**). The results were gathered in **Table 2.1**.

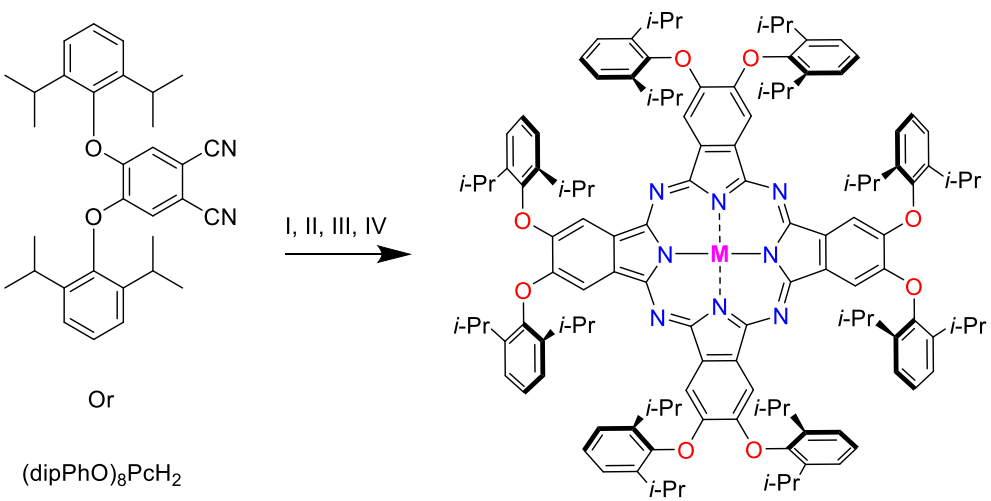

Scheme 2.2. Synthesis of metallated 2,3,9,10,16,17,23,24-octa(2',6'-di-*iso*-propylphenoxy) phthalocyanine. Reagents and conditions: Method I: Mw 200 °C, metal salt. Method II: High boiling solvent (quinoline, DMF, DMAE), metal salt. Method III: DBU/DBN, metal salt. Method IV: Deprotonation with DBU, o-dichlorobenzene/*n*-pentan-1-ol, metal salt.

- **Method I**: Metal Phthalocyanine from Phthalonitrile in Bulk Reaction

Heating the phthalonitrile with a metal salt in a bulk reaction (without solvent) proved a direct and convenient method of preparing $(dipPhO)_8PcM$ (**Scheme 2.2**). The melting point of the phthalonitrile is above 180 °C so the cyclotetramerisation is taking place at temperatures above 200 °C. Typically microwave irradiation was used.

- **Method II**: Metal Phthalocyanine from Phthalonitrile in Solvent

The cyclotetramerisation of phthalonitrile with a suitable metal compound can be achieved in solution. Useful solvents for this method proved to be high-boiling solvents such as quinoline, DMF, DMAE, and 1-chloronaphthalene (**Scheme 2.2**).

- **Method III**: Metal Phthalocyanine from Phthalonitrile and Base

Heating phthalonitrile with a metal salt in a solvent and DBU or DBN proved an efficient method for the cyclotetramerisation of phthalonitrile providing metal-containing phthalocyanines (**Scheme 2.2**).

- **Method IV**: Metal Phthalocyanine from Metal-Free Phthalocyanine

Complexing metal-free $(dipPhO)_8Pc$ with metal-ions is a straightforward method to introduce a metal into the cavity of the phthalocyanine and can be achieved under mild conditions. This approach proved successful as $(dipPhO)_8PcH_2$ is soluble in common organic solvents (e.g. *n*-pentan-1-ol, *o*-dichlorobenzene). A small amount of DBU was added to the solution to deprotonate the PcH_2 prior to the addition of the metal salt (**Scheme 2.2**).

Metal Phthalocyanines														
Acronym	Name	Chemical formula	Tried methods	Synthesis method	Solvent	Reaction time (min)	Reaction temperature (°C)	Yield	m.p. (°C)	FT-IT	UV-Vis	NMR	Mass Spectrometry	scXRD
$(dipPhO)_8PcBi$	$(dipPhO)_8PcBi$	$C_{128}H_{144}N_8O_8Bi$	I, II, III, IV	I	None	120	220	10%	> 300	Done	Done	Done	Done	No
$(dipPhO)_8PcPt$	$(dipPhO)_8PcPt$	$C_{128}H_{144}N_8O_8Pt$	I, II, III, IV	I	None	60	220	38%	> 300	Done	Done	Done	Done	No
$(dipPhO)_8PcW$	$(dipPhO)_8PcW$	$C_{128}H_{144}N_8O_8W$	I, II, III, IV	I	None	20	220	10%	> 300	Done	Done	No	Done	No
$(dipPhO)_8PcGe$	$(dipPhO)_8PcGe$	$C_{128}H_{144}N_8O_8Ge$	I, II, III, IV	IV	Quinoline	240	240	60%	> 300	Done	Done	No	Done	Done
$(dipPhO)_8PcHf$	$(dipPhO)_8PcHf$	$C_{128}H_{144}N_8O_8Hf$	I, II, III, IV	I	None	30	250	60%	> 300	Done	Done	No	Done	Done
PNC[P]	$(dipPhO)_8PcP$	$C_{128}H_{144}N_8O_8P$	I, II, III, IV	IV	Pyridine	60	118	50%	> 300	Done	Done	No	Done	Done
PNC[Fe-*v* Cl]	$(dipPhO)_8PcFe$	$C_{128}H_{144}N_8O_8Fe$	I, II, III, IV	IV	Quinoline	240	180	50%	> 300	Done	Done	No	Done	Done
PNC[Ge]	$(dipPhO)_8PcGe$	$C_{128}H_{144}N_8O_8Ge$	I, II, III, IV	IV	Quinoline	240	240	60%	> 300	Done	Done	No	Done	Done
PNC[Mo]	$(dipPhO)_8PcMo$	$C_{128}H_{144}N_8O_8Mo$	I, II, III, IV	I	None	90	250	35%	> 300	Done	Done	Done	Done	Done
PNC[Cd]	$(dipPhO)_8PcCd$	$C_{128}H_{144}N_8O_8Cd$	I, II, III, IV	IV	n-pentanol	45	140	10%	> 300	Done	Done	No	Done	Done
PNC[Sb]	$(dipPhO)_8PcSb$	$C_{128}H_{144}N_8O_8Sb$	I, II, III, IV	IV	n-pentanol / dichlorobenzene	960	120	49%	> 300	Done	Done	No	Done	Done
PNC[Re]	$(dipPhO)_8PcRe$	$C_{128}H_{144}N_8O_8Re$	I, II, III, IV	I	None	45	290	10%	> 300	Done	Done	Done	Done	Done
PNC[Ir]	$(dipPhO)_8PcIr$	$C_{128}H_{144}N_8O_8Ir$	I, II, III, IV	I	None	120	220	15%	> 300	Done	Done	No	Done	Done
PNC[Pb]	$(dipPhO)_8PcPb$	$C_{128}H_{144}N_8O_8Pb$	I, II, III, IV	IV	n-pentanol	480	140	40%	> 300	Done	Done	No	Done	Done

Table 2.1. Synthesis method, data and characterisation methods used for each new complex of the current PhD programme

2.3 Characterisation of $(dipPhO)_8PcH_2$/$(dipPhO)_8PcM$

The characterisation methods that were used for the molecular characterisation of $(dipPhO)_8PcM$ and $(dipPhO)_8PcH_2$ were Fourier-Transform Infra-red spectroscopy (FT-IR), UV-visible adsorption spectroscopy (UV-Vis), Nuclear Magnetic Resonance spectroscopy (NMR, where applicable), Matrix Assisted Laser Desorption Ionisation/Time of Flight/Time of Flight Mass Spectrometry (MALDI–TOF–TOF MS), Electron-Spray Ionisation Mass Spectrometry ESI-MS (in labile metallated samples). Only typical examples of spectra are shown below to illustrate use, however, details are reported in the experimental chapter. FT-IR gave near-identical spectra for all samples due to the dominance of the bonding in the Pc ligand.

There is a clear difference between the UV-Vis spectra of $(dipPhO)_8PcH_2$ and its metallated derivatives $(dipPhO)_8PcM$ in the Q-band region (600 to 750 nm). A double peak is observed for for $(dipPhO)_8PcH_2$ whereas for $(dipPhO)_8PcM$ a single Q-band peak is observed. This difference is symmetry related and is useful for the determination of successful metalation (**Figure 2.2**).

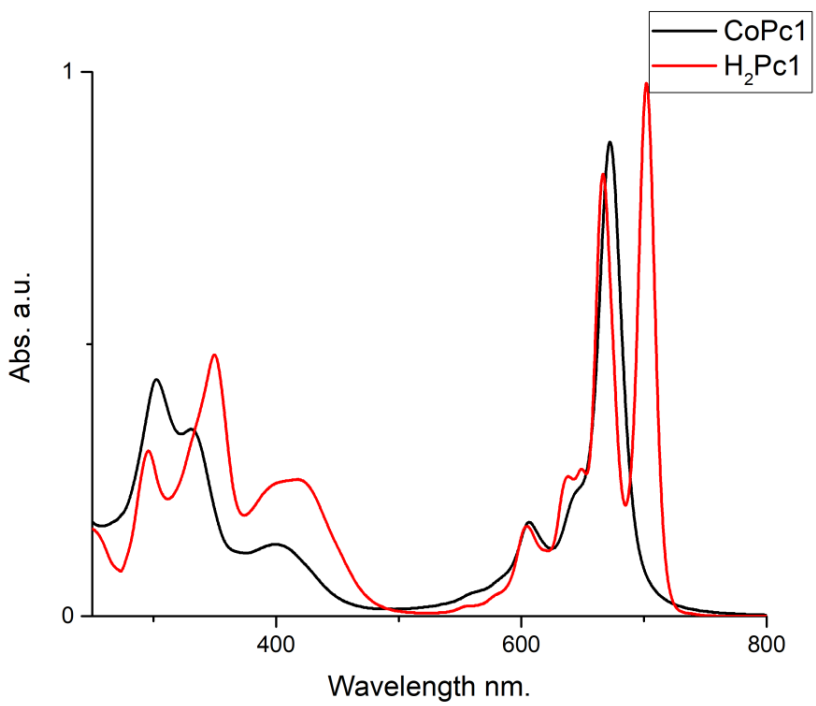

Figure 2.2. Overlapped UV-Vis spectra of $(dipPhO)_8PcCo$ and $(dipPhO)_8PcH_2$ showing the difference in Q-band structure.

Both ^{1}H and ^{13}C NMR were used for characterisation and representative examples of ^{1}H spectra for $(dipPhO)_8PcH_2$ and a diamagnetic $(dipPhO)_8PcM$ ($M = Zn^{2+}$) are provided in **Figure 2.3** and **2.4**, respectively.

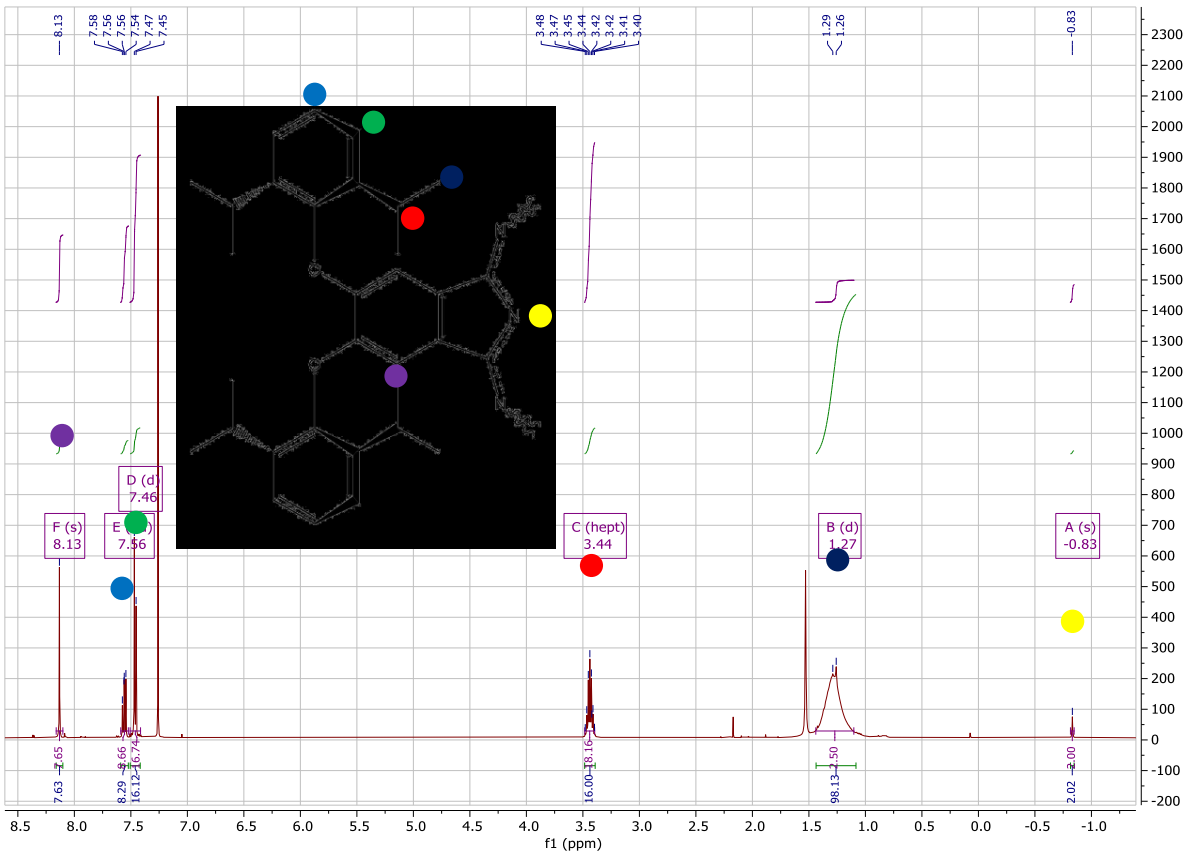

Figure 2.3. ^{1}H NMR spectrum of $(dipPhO)_8PcH_2$ with a quadrant of the phthalocyanine of D_4 symmetry depicted.

At 8.2 ppm there are 8 protons that correlate to those directly attached to the benzo unit of the macrocycle. At around 7.5 ppm there are two peaks corresponding to 8 (triplet) and 16 (doublet) protons that correspond to those on the benzene rings of the phenoxy group. At 3.5 ppm there is a septet that correlates to the 16 protons of the C-H of the di-*iso*-propyl groups and at 1.25 ppm there is a broad peak corresponding to the 96 protons of the $-CH_3$ groups. In the highly shielded position (-0.75 ppm) due to the Pc ring current are 2 protons bound on the nitrogen atoms that indicative of $(dipPhO)_8PcH_2$ (**Figure 2.3**). The spectrum of $(dipPhO)_8PcZn$ is similar except for the lack of internal protons at -0.75 ppm (**Figure 2.4**).

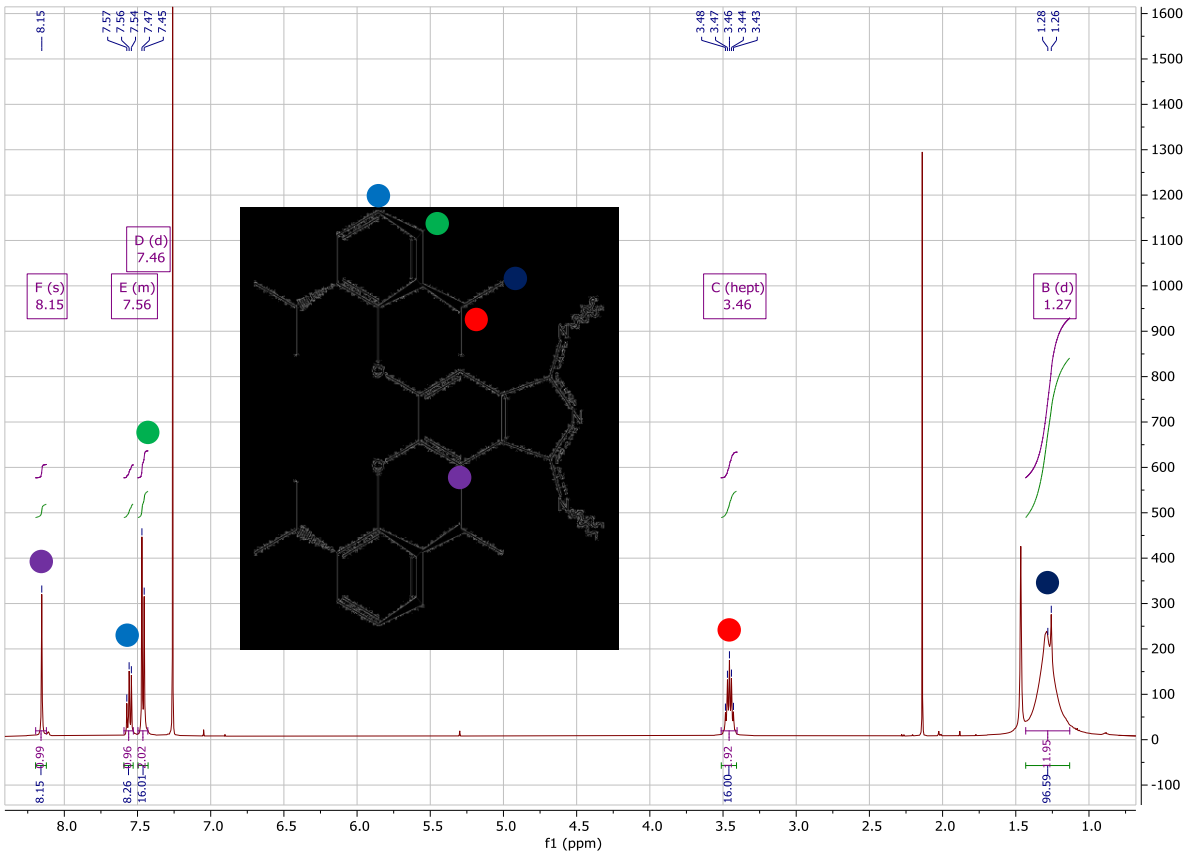

Figure 2.4. ^{1}H NMR spectrum of $(dipPhO)_8PcZn$ with a quadrant of the phthalocyanine of D_4 symmetry depicted.

All new $(dipPhO)_8PcM$ complexes provided MALDI–TOF–TOF MS spectra corresponding to their structure. A typical example of a spectrum is given below for $(dipPhO)_8PcPb$ (**Figure 2.5**). In each case the experimental spectrum can be compared to one calculated on the basis of the ideal molecular formula. Differences can occur due to protonation or axial complexation to the metal cation.

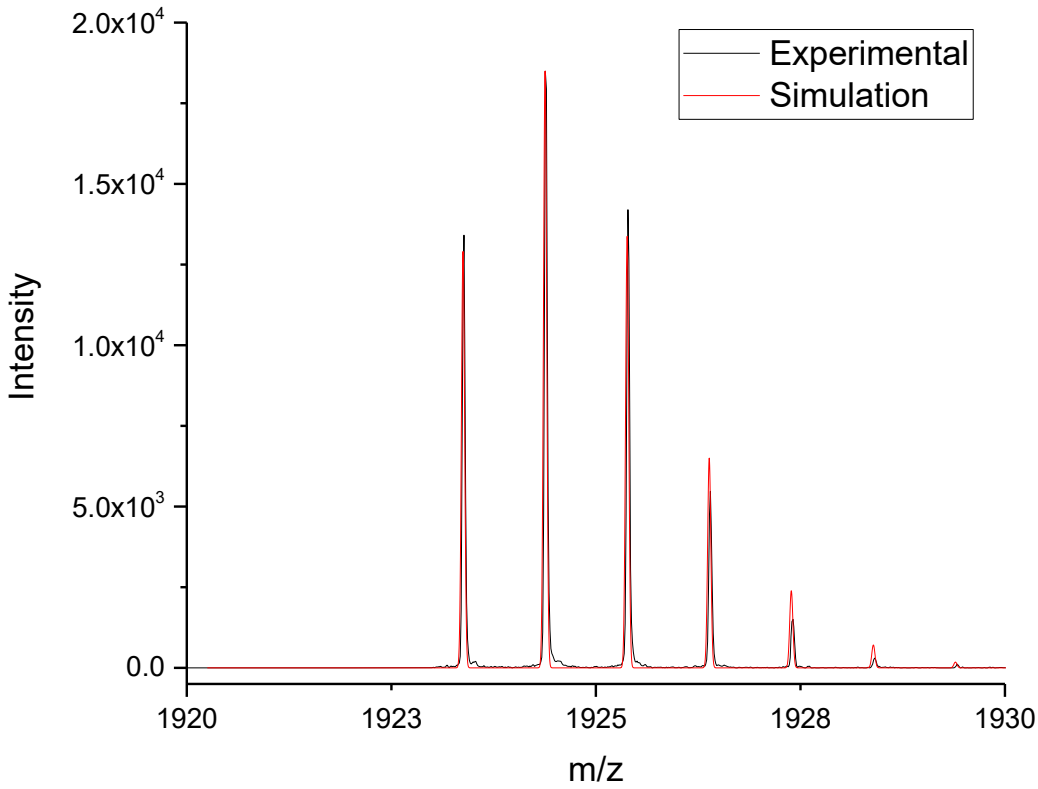

Figure 2.5. MALDI–TOF–TOF spectrum of $(dipPhO)_8PcH_2$.

2.4 Analysis of the molecular structures of $(dipPhO)_8PcM$ from single crystal XRD

In this section the molecular structure, as determined by single crystal XRD, of all $(dipPhO)_8PcM$ complexes prepared to date, including the new complexes prepared during the PhD programme are analysed with Mercury (version 4.0, 2019). Effect of the atomic radius of the metal cation, atomic number and charge on the extrusion of the metal from the plane of the macrocycle will be investigated. Also, the effect of the axial ligands binding on the metal extrusion will be noted.

Initially, the chosen method of defining the distance of the metal extrusion from the plane defined by the four inner nitrogen atoms of the phthalocyanine and the curvature of the macrocycle will be described. The four nitrogen atoms that were selected for the creation of a centroid at the middle of the macrocycle are shown in **Figure 2.6**.

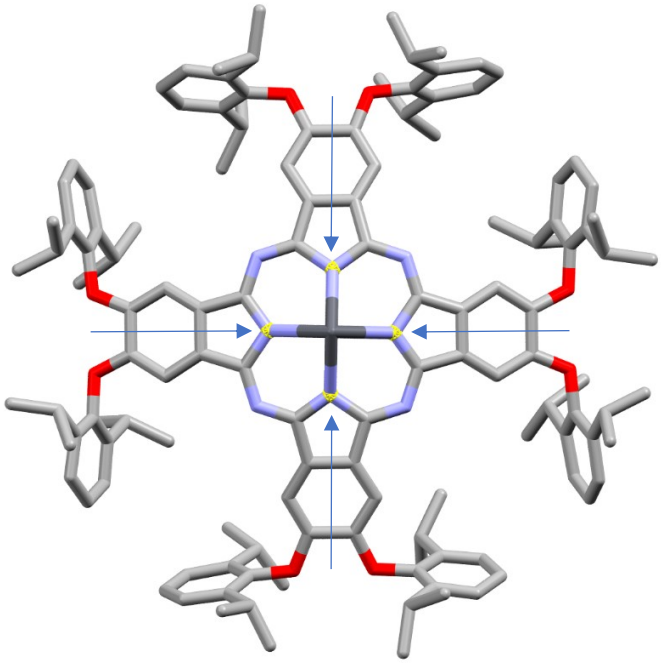

Figure 2.6. Selected nitrogen atoms (yellow net) used to create a centroid in the macrocycle.

The distance measured between the metal cation from the virtual centroid is shown in **Figure 2.7**. This distance was evaluated for all structures formed by $(dipPhO)_8PcM$ complexes (cubic or non-cubic) including those with from the same metal but with different axial ligands.

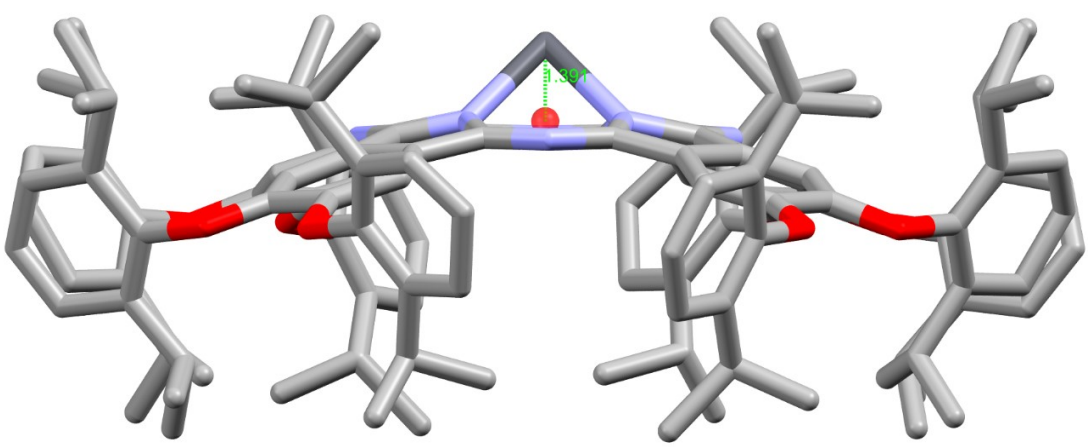

Figure 2.7. Measured distance between the metal and the virtual centroid of the macrocycle.

Similarly, the curvature of the complexes was determining for all $(dipPhO)_8PcM$ complexes by defining the positions of the carbon atoms from the substituted benzene rings of two opposing

isoindole units (**Figure 2.8**). Then by creating the two planes, the angle was measured to determine the deviation from planarity (**Figure 2.9**).

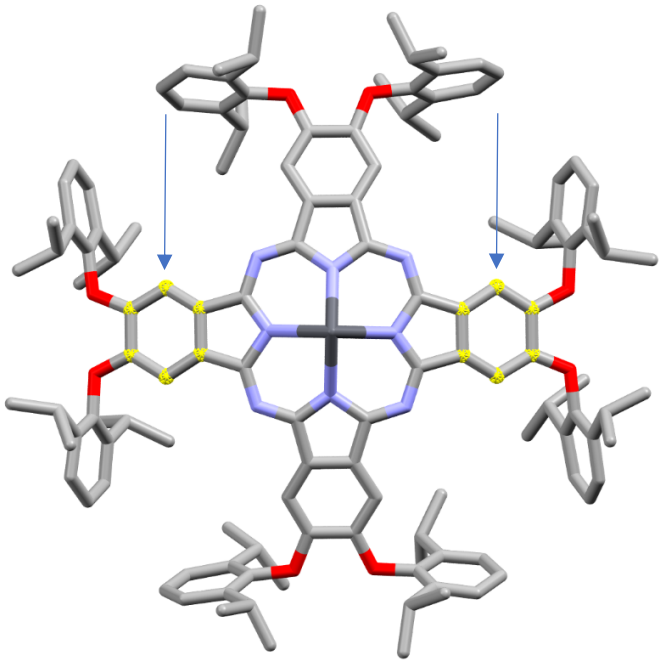

Figure 2.8. Carbon atoms (yellow net), which help to calculate the two intersecting planes.

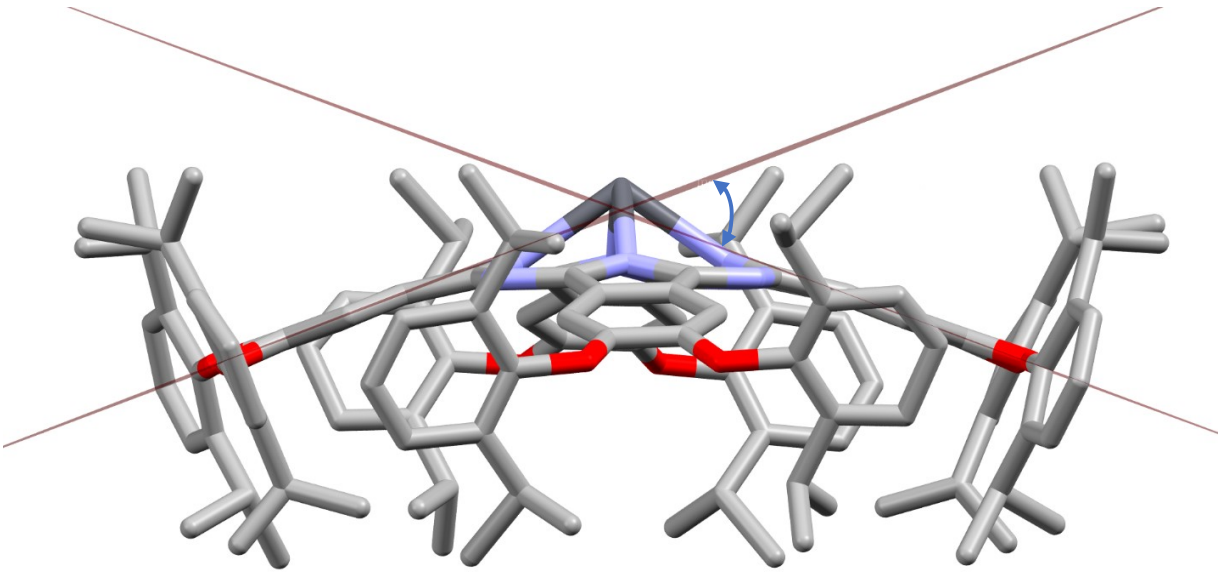

Figure 2.9. Intersecting planes, which indicate the deviation from planarity.

2.5 Molecular structure analysis of $(dipPhO)_8PcM$ within non-cubic crystals

Most of the complexes crystallised in the cubic nanoporous structure, but several $(dipPhO)_8PcM$ complexes provide crystals of different space groups (**Figure 2.10 – 2.23**; **Table 2.2**). Boron incorporation gives subphthalocyanines $(dipPhO)_6PcB$ containing only three benzoiminodoline ring rather than four for the standard phthalocyanine macrocycle.[73] It is unsurprising that these complexes do not form the nanoporous cubic crystals. For the other examples of non-cubic structure from $(dipPhO)_8PcM$ complexes, it appears that planar complexes either with no axial ligands (i.e. M = H_2, Ni, Cu, Ag) or only small water ligands (i.e. M = Fe) are favoured. In addition, dimeric complexes with bridging axial ligands do not form cubic crystals (**Figure 2.22** and **2.23**).

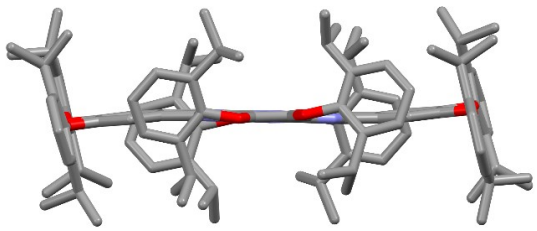

Figure 2.10. $(dipPhO)_8PcH_2$, monoclinic, *$P2_1/c$*

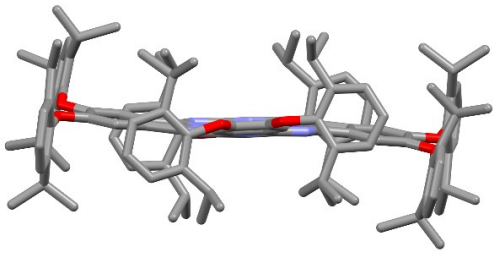

Figure 2.11. $(dipPhO)_8PcH_2$, orthorhombic, *Pbca*

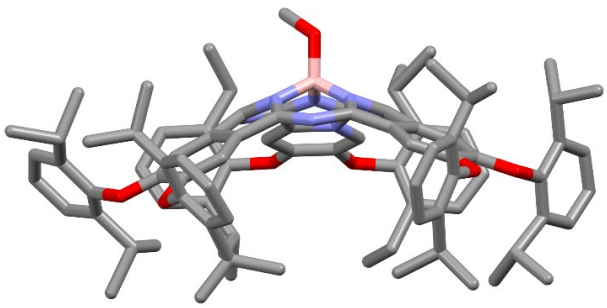

Figure 2.12. $(dipPhO)_6subPcB$, triclinic, $P\bar{1}$

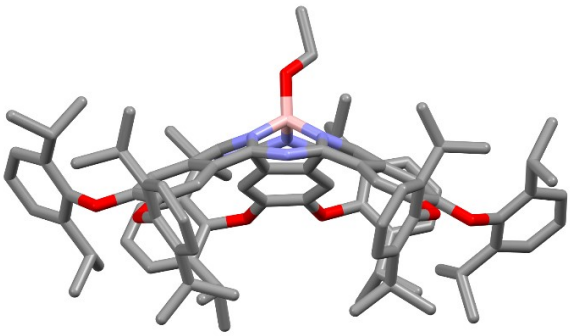

Figure 2.13. $(dipPhO)_6subPcB$, orthorhombic, *$Pna2_1$*

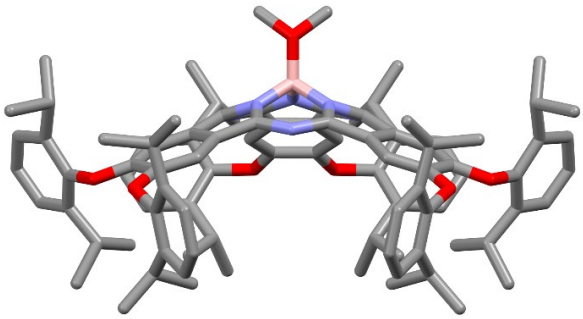

Figure 2.14. (dipPhO)$_6$subPcB, monoclinic, *P2$_1$/m*

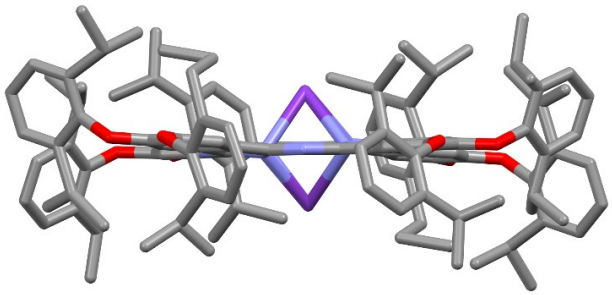

Figure 2.15. (dipPhO)$_8$PcK, monoclinic, *P2$_1$/c*

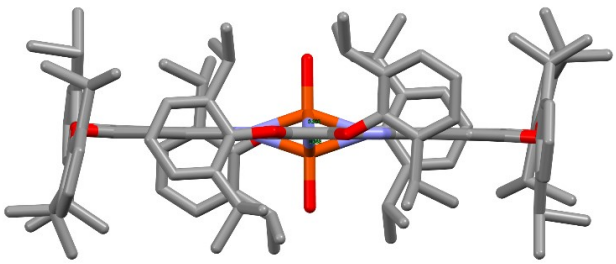

Figure 2.16. (dipPhO)$_8$PcFe, monoclinic, *P2$_1$/c*

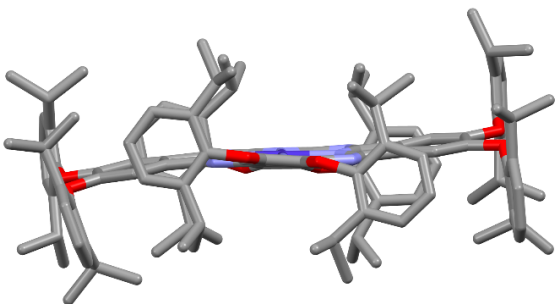

Figure 2.17. (dipPhO)$_8$PcCo, monoclinic, *P2$_1$/c*

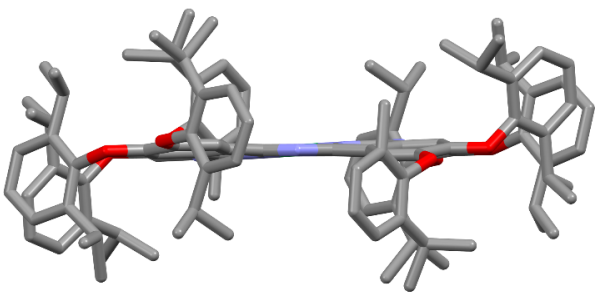

Figure 2.18. (dipPhO)$_8$PcNi, monoclinic, *P2$_1$/c*

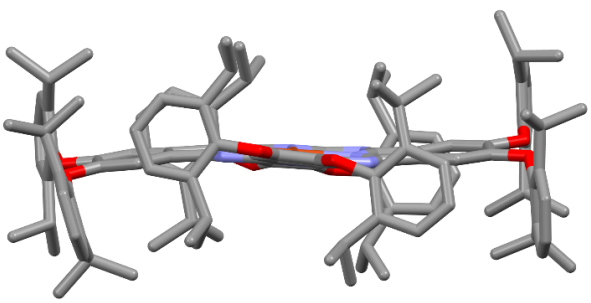

Figure 2.19. (dipPhO)$_8$PcCu, monoclinic, *P2$_1$/c*

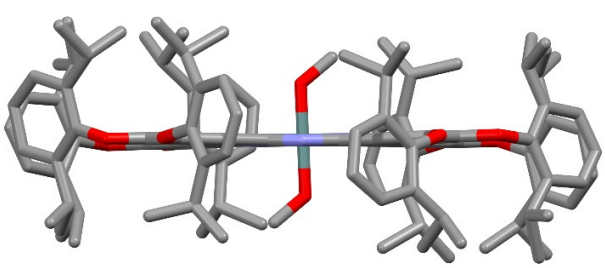

Figure 2.20. (dipPhO)$_8$PcGe, triclinic, $P\bar{1}$

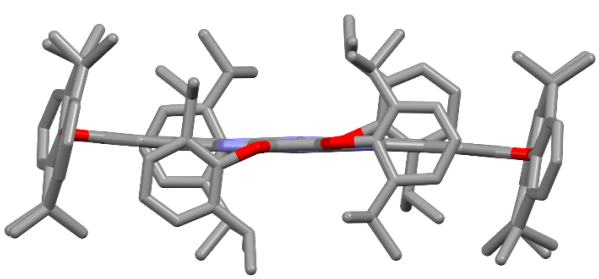

Figure 2.21. (dipPhO)$_8$PcAg, monoclinic, *P2$_1$/c*

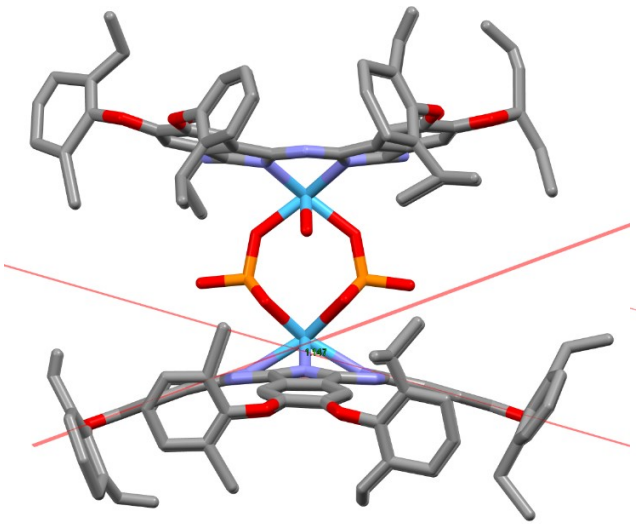

Figure 2.22. (dipPhO)$_8$PcHf, orthorhombic, Pnma

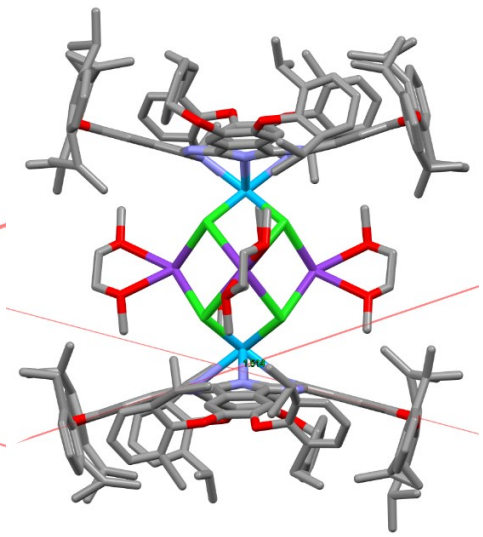

Figure 2.23. (dipPhO)$_8$PcTh, triclinic, $P\bar{1}$

(Note that the legends shaded in red indicate structures obtained during the PhD programme.)

A trend was observed when the macrocycle was not crystallising in the cubic structure. Firstly, in most cases the phthalocyanine was completely planar, which indicates that the metal is exactly at the middle of the macrocycle without extruding from the plane. Also, the di-*iso*-propylphenoxy groups orientate themselves perpendicular to the phthalocyanine, but one of them being above of the plane the other below, while in the cubic structure all the bulky substituents were aligned below the plane of the macrocycle (**Figure 2.9**). As can be observed, if the metal was substituted with two axial ligands, the metal has no extrusion from the plane of the macrocycle. Mostly probably the charge of the metal ion and the preferred geometry of the metal could have an impact on the space group chosen by the phthalocyanine. In the case of hafnium and thorium, there was strong curvature observed, but the whole molecule was crystallised in a more compact way, due to their dimeric structure, and the system was not nanoporous. The versatility of this system enables the formation of cubic nanoporous structures even from (dipPhO)$_8$PcM with M = H_2, Cu, Co, Ni, Fe, Pt by using an additive, which could be a an axial ligand, a bidentate ligand, a fullerene or porphyrin as will be described later. The metal complexes investigated in the current project, which did not form cubic structure were germanium and hafnium (**Table 2.2**).

Metal Phthalocyanines											
Acronym	Name	Chemical formula	M_r	Crystal system, space group	*a* (Å)	*b* (Å)	*c* (Å)	*V* (Å^3)	*Z*	Phthalocyanine curvature (degrees)	Metal to macrocycle distance (Å)	CCDC
$(dipPhO)_8PcH_2$	$(dipPhO)_8PcH_2$	$C_{128}H_{144}N_8O_8H_2$	1925.710	monoclinic, *P2 $_1$/c*	21.293(7)	16.896(5)	18.283(6)	59778(7)	2	0	0	
$(dipPhO)_8PcH_2$	$(dipPhO)_8PcH_2$	$C_{128}H_{144}N_8O_8H_2$	1925.710	orthorhombic, *Pbca*	19.4927(4)	16.2918(10)	38.420(2)	12201(1)	4	0	0	
$(dipPhO)_6subPcB$	$(dipPhO)_6subPcB$	$C_{96}H_{108}N_6O_6B$	1452.735	orthorhombic, *Pna2 $_1$*	17.0589(7)	18.9511(7)	29.1287(10)	9416.76	4	0	0	1446195
$(dipPhO)_6subPcB$	$(dipPhO)_6subPcB$	$C_{96}H_{108}N_6O_6B$	1452.735	monoclinic, *P2 $_1$/m*	12.3733(11)	27.376(2)	15.3281(13)	5173.84	2	0	0	1446196
$(dipPhO)_6subPcB$	$(dipPhO)_6subPcB$	$C_{96}H_{108}N_6O_6B$	1452.735	triclinic, $P\bar{1}$	17.9938(5)	18.7702(6)	21.3568(6)	5856.358	2	0	0	1446197
$(dipPhO)_8PcK$	$(dipPhO)_8PcK$	$C_{128}H_{144}N_8O_8K$	1961.664	monoclinic, *P2 $_1$/c*	21.7346(8)	17.2849(6)	17.0779(7)	6306.22	3	0	0	
$(dipPhO)_8PcFe$	$(dipPhO)_8PcFe$	$C_{128}H_{144}N_8O_8Fe$	1978.411	monoclinic, *P2 $_1$/c*	18.943(2)	18.658(2)	33.270(4)	11744.5	4	0	0.666	
$(dipPhO)_8PcCo$	$(dipPhO)_8PcCo$	$C_{128}H_{144}N_8O_8Co$	1981.499	monoclinic, *P2 $_1$/c*	38.714(3)	16.8469(12)	18.2104(13)	11876.1(15)	4	0	0	900380
$(dipPhO)_8PcNi$	$(dipPhO)_8PcNi$	$C_{128}H_{144}N_8O_8Ni$	1981.259	monoclinic, *P2 $_1$/c*	21.370(2)	16.88255(18)	18.726(2)	6098.7(11)	2	0	0	
$(dipPhO)_8PcCu$	$(dipPhO)_8PcCu$	$C_{128}H_{144}N_8O_8Cu$	1986.112	monoclinic, *P2 $_1$/c*	38.607(2)	16.8676(10)	18.4282(11)	11997	4	0	0	
$(dipPhO)_8PcGe$	**$(dipPhO)_8PcGe$**	**$C_{128}H_{144}N_8O_8Ge$**	2031.415	triclinic, $P\bar{1}$	13.6357(12)	13.9372(14)	17.1525(15)	3115.85	1	0	0	
$(dipPhO)_8PcAg$	$(dipPhO)_8PcAg$	$C_{128}H_{144}N_8O_8Ag$	2034.434	monoclinic, *P2 $_1$/c*	20.9390(17)	15.8950(10)	19.2421(15)	6102.42	2	0	0	
$(dipPhO)_8PcHf$	**$(dipPhO)_8PcHf$**	**$C_{128}H_{144}N_8O_8Hf$**	2101.051	orthorhombic, Pnma	63.9973(8)	25.2396(5)	20.3123(6)	32809.8	2	36.34	1.147	
$(dipPhO)_8PcTh$	$(dipPhO)_8PcTh$	$C_{128}H_{144}N_8O_8Th$	2154.604	triclinic, $P\bar{1}$	21.0441(9)	23.3749(12)	40.9956(19)	18387.3	2	33.52	1.514	

Table 2.2. $(dipPhO)_8M$ that do not crystallise in the cubic nanoporous structure. Red coloured were synthesized for the current PhD programme, while black were from past group members

2.6 Analysis of $(dipPhO)_8PcM$ molecules within the cubic crystals

Most $(dipPhO)_8PcM$ complexes form cubic nanoporous crystals especially if an axial ligand other than water is present. In each case there is distinct phthalocyanine curvature and metal extrusion from the plane of the macrocycle. The distance of the metal from the centre of the macrocycle deviates from 0.009 Å to 1.611 Å, while the angle of the two intersecting planes could deviate from 41.07 ^{o} for the lead phthalocyanine to 19.60 ^{o} for the chromium phthalocyanine (**Table 2.3**).

Metal Phthalocyanines												
Acronym	Name	Chemical formula	M_r	Crystal system, space group	*a* (Å)	*b* (Å)	*c* (Å)	*V* (Å^3)	*Z*	Phthalocyanine curvature (degrees)	Metal to macrocycle distance (Å)	CCDC
PNC[Mg]	$(dipPhO)_8PcMg$	$C_{128}H_{144}N_8O_8Mg$	1946.871	cubic, $Pn\bar{3}n$	37.3320(5)	37.3320(5)	37.3320(5)	52028.8(12)	12	30.89	0.170	
PNC[Al]	$(dipPhO)_8PcAl$	$C_{128}H_{144}N_8O_8Al$	1949.548	cubic, $Pn\bar{3}n$	37.4064(4)	37.4064(4)	37.4064(4)	52340.5(10)	12	26.48	0.062	
PNC[Si]	$(dipPhO)_8PcSi$	$C_{128}H_{144}N_8O_8Si$	1950.652	cubic, $Pn\bar{3}n$	37.612(7)	37.612(7)	37.612(7)	53208.3	12	20.17	0.023	
PNC[P]	**$(dipPhO)_8PcP$**	**$C_{128}H_{144}N_8O_8P$**	1968.858	cubic, $Pn\bar{3}n$	37.6935(3)	37.6935(3)	37.6935(3)	53554.9	12	20.80	0.015	
PNC[Sc]	$(dipPhO)_8PcSc$	$C_{128}H_{144}N_8O_8Sc$	1967.522	cubic, $Pn\bar{3}n$	37.1225(8)	37.1225(8)	37.1225(8)	51157.8	12	36.94	1.072	
PNC[Ti]	$(dipPhO)_8PcTi$	$C_{128}H_{144}N_8O_8Ti$	1970.433	cubic, $Pn\bar{3}n$	37.5117(9)	37.5117(9)	37.5117(9)	52784(2)	12	25.90	0.745	
PNC[Cr]	$(dipPhO)_8PcCr$	$C_{128}H_{144}N_8O_8Cr$	1974.562	cubic, $Pn\bar{3}n$	37.7555(3)	37.7555(3)	37.7555(3)	53819.6	12	19.60	0.003	
PNC[Mn]	$(dipPhO)_8PcMn$	$C_{128}H_{144}N_8O_8Mn$	1977.504	cubic, $Pn\bar{3}n$	37.2511(5)	37.2511(5)	37.2511(5)	51691.3(12)	12	26.69	0.059	761412
PNC[Fe]	$(dipPhO)_8PcFe$	$C_{128}H_{144}N_8O_8Fe$	1978.411	cubic, $Pn\bar{3}n$	37.4562(14)	37.4562(14)	37.4562(14)	52549.8	12	25.90	0.040	
PNC[Fe-*v*Cl]	**$(dipPhO)_8PcFe$**	**$C_{128}H_{144}N_8O_8Fe$**	2013.385	cubic, $Pn\bar{3}n$	37.4365(2)	37.4365(2)	37.4365(2)	52466.9	12	24.90	0.056	
PNC[Zn]	$(dipPhO)_8PcZn$	$C_{128}H_{144}N_8O_8Zn$	1987.975	cubic, $Pn\bar{3}n$	37.6973(2)	37.6973(2)	37.6973(2)	53571.1	12	26.74	0.419	279644
PNC[Ga]	$(dipPhO)_8PcGa$	$C_{128}H_{144}N_8O_8Ga$	1992.289	cubic, $Pn\bar{3}n$	37.6003(2)	37.6003(2)	37.6003(2)	53158.9(6)	12	28.30	0.119	
PNC[Ge]	**$(dipPhO)_8PcGe$**	**$C_{128}H_{144}N_8O_8Ge$**	2031.415	cubic, $Pn\bar{3}n$	37.650(4)	37.650(4)	37.650(4)	53370	12	27.66	0.173	
PNC[Y]	$(dipPhO)_8PcY$	$C_{128}H_{144}N_8O_8Y$	2011.472	cubic, $Pn\bar{3}n$	37.1526	37.1526	37.1526	51282	12	37.23	1.353	
PNC[Zr]	$(dipPhO)_8PcZr$	$C_{128}H_{144}N_8O_8Zr$	2103.790	cubic, $Pn\bar{3}n$	37.2617(3)	37.2617(3)	37.2617(3)	51735.4	12	37.35	1.186	
PNC[Mo]	**$(dipPhO)_8PcMo$**	**$C_{128}H_{144}N_8O_8Mo$**	2034.128	cubic, $Pn\bar{3}n$	37.5869(5)	37.5869(5)	37.5869(5)	53101.8(2)	12	32.50	0.613	
PNC[Ru]	$(dipPhO)_8PcRu$	$C_{128}H_{144}N_8O_8Ru$	2023.631	cubic, $Pn\bar{3}n$	37.700(7)	37.700(7)	37.700(7)	53584(17)	12	24.72	0.028	761414
PNC[Rh]	$(dipPhO)_8PcRh$	$C_{128}H_{144}N_8O_8Rh$	2025.472	cubic, $Pn\bar{3}n$	37.396(2)	37.396(2)	37.396(2)	52296.8	12	16.58	0.040	
PNC[Cd]	**$(dipPhO)_8PcCd$**	**$C_{128}H_{144}N_8O_8Cd$**	2035.208	cubic, $Pn\bar{3}n$	37.3224(3)	37.3224(3)	37.3224(3)	51988.7	12	36.47	1.007	
PNC[In]	$(dipPhO)_8PcIn$	$C_{128}H_{144}N_8O_8In$	2037.384	cubic, $Pn\bar{3}n$	37.4428(8)	37.4428(8)	37.4428(8)	52493.4(19)	12	33.92	0.995	
PNC[Sn]	$(dipPhO)_8PcSn$	$C_{128}H_{144}N_8O_8Sn$	2041.276	cubic, $Pn\bar{3}n$	37.776(9)	37.776(9)	37.776(9)	53906(23)	12	24.71	0.153	
PNC[Sb]	**$(dipPhO)_8PcSb$**	**$C_{128}H_{144}N_8O_8Sb$**	2044.146	cubic, $Pn\bar{3}n$	37.3901(4)	37.3901(4)	37.3901(4)	52272.1	12	29.32	1.119	
PNC[Pr]	$(dipPhO)_8PcPr$	$C_{128}H_{144}N_8O_8Pr$	2063.474	cubic, $Pn\bar{3}n$	37.2220(12)	37.2220(12)	37.2220(12)	51570(3)	12	37.37	1.611	
PNC[Eu]	$(dipPhO)_8PcEu$	$C_{128}H_{144}N_8O_8Eu$	2074.530	cubic, $Pn\bar{3}n$	37.034(3)	37.034(3)	37.034(3)	50792(8)	12	35.55	1.428	
PNC[Tb]	$(dipPhO)_8PcTb$	$C_{128}H_{144}N_8O_8Tb$	2081.491	cubic, $Pn\bar{3}n$	37.3171(3)	37.3171(3)	37.3171(3)	51966.5	12	38.11	1.465	
PNC[Dy]	$(dipPhO)_8PcDy$	$C_{128}H_{144}N_8O_8Dy$	2085.065	cubic, $Pn\bar{3}n$	37.25810(10)	37.25810(10)	37.25810(10)	51720.4	12	38.23	1.343	
PNC[Yb]	$(dipPhO)_8PcYb$	$C_{128}H_{144}N_8O_8Yb$	2095.604	cubic, $Pn\bar{3}n$	36.9702(8)	36.9702(8)	36.9702(8)	50530(19)	12	39.56	1.315	
PNC[Re]	**$(dipPhO)_8PcRe$**	**$C_{128}H_{144}N_8O_8Re$**	2124.315	cubic, $Pn\bar{3}n$	37.6052(2)	37.6052(2)	37.6052(2)	53179.4	12	27.81	0.598	
PNC[Ir]	**$(dipPhO)_8PcIr$**	**$C_{128}H_{144}N_8O_8Ir$**	2114.340	cubic, $Pn\bar{3}n$	37.4658(2)	37.4658(2)	37.4658(2)	52590.2	12	24.77	0.052	
PNC[Au]	$(dipPhO)_8PcAu$	$C_{128}H_{144}N_8O_8Au$	2119.533	cubic, $Pn\bar{3}n$	37.667(4)	37.667(4)	37.667(4)	53442	12	24.80	0.009	
PNC[Pb]	**$(dipPhO)_8PcPb$**	**$C_{128}H_{144}N_8O_8Pb$**	2129.009	cubic, $Pn\bar{3}n$	37.1115(2)	37.1115(2)	37.1115(2)	51112.3	12	41.07	1.391	

Table 2.3. $(dipPhO)_8M$ that crystallise in the cubic nanoporous structure. Red coloured were synthesized for the current PhD programme, while black were from past group members.

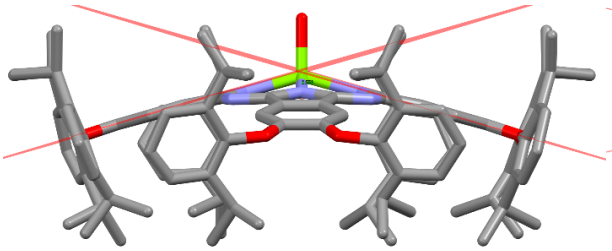

Figure 2.24. PNC[Mg], cubic, $Pn\bar{3}n$ **(9a)**

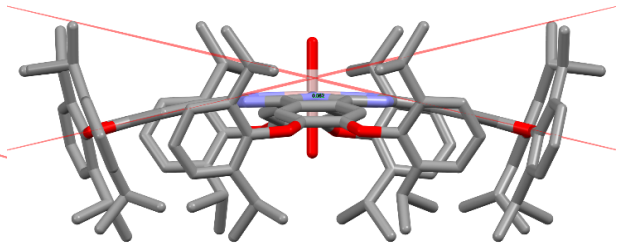

Figure 2.25. PNC[Al], cubic, $Pn\bar{3}n$ **(9b)**

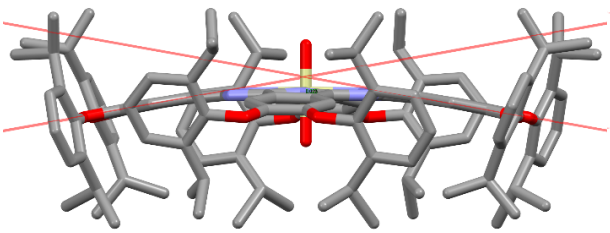

Figure 2.26. PNC[Si], cubic, $Pn\bar{3}n$ **(9c)**

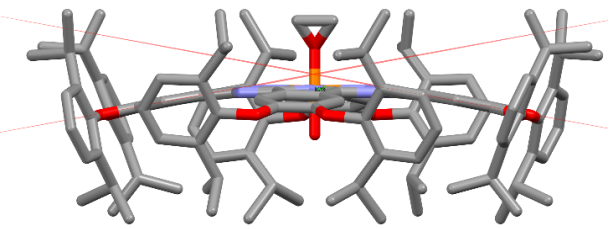

Figure 2.27. PNC[P], cubic, $Pn\bar{3}n$ **(9d)**

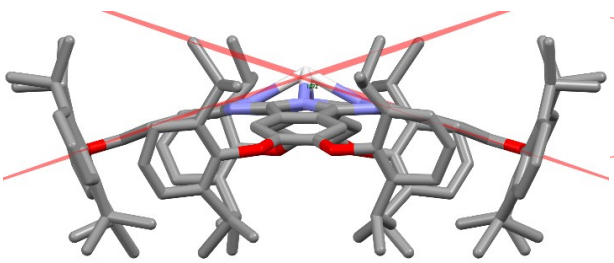

Figure 2.28. PNC[Sc], cubic, $Pn\bar{3}n$ **(9e)**

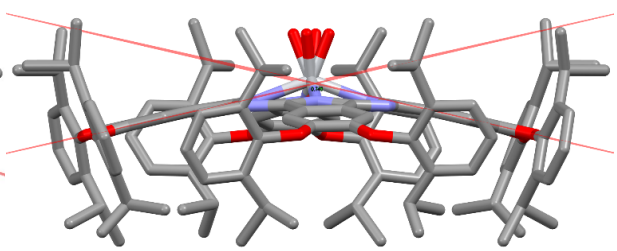

Figure 2.29. PNC[Ti], cubic, $Pn\bar{3}n$ **(9f)**

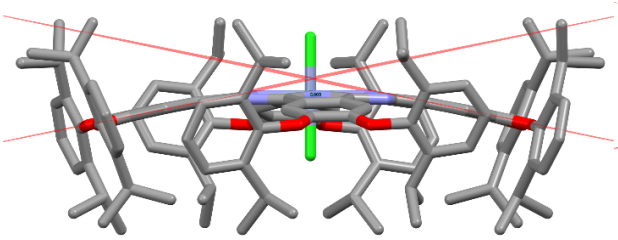

Figure 2.30. PNC[Cr], cubic, $Pn\bar{3}n$ **(9g)**

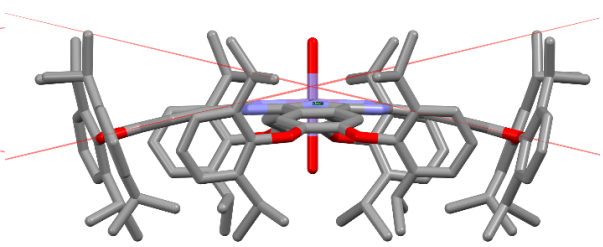

Figure 2.31. PNC[Mn], cubic, $Pn\bar{3}n$ **(9h)**

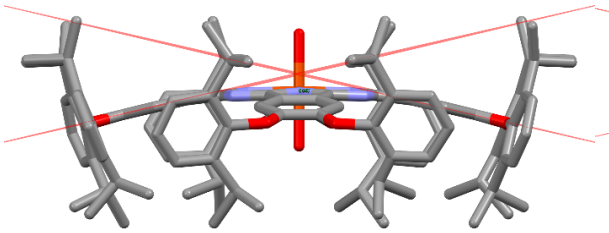

Figure 2.32. PNC[Fe], cubic, $Pn\bar{3}n$ **(9i)**

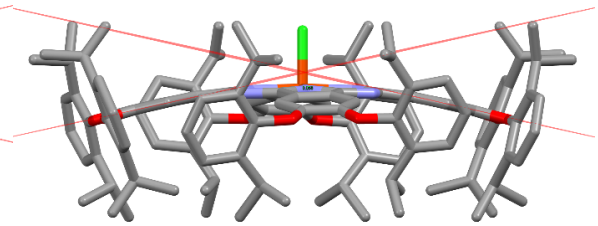

Figure 2.33. PNC[*v*Cl-Fe], cubic, $Pn\bar{3}n$ **(9j)**

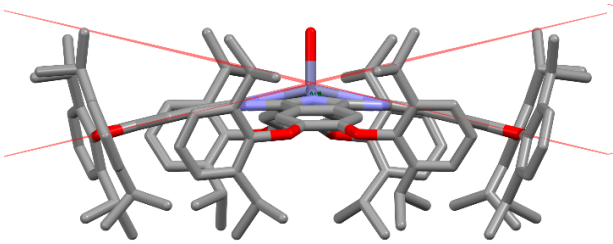

Figure 2.34. PNC[Zn], cubic, $Pn\bar{3}n$ **(9k)**

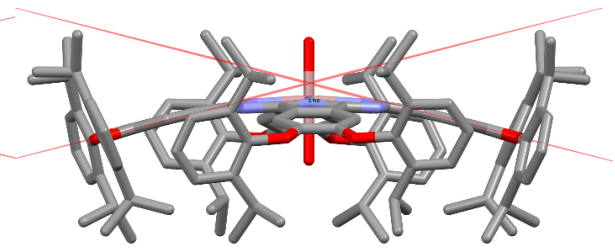

Figure 2.35. PNC[Ga], cubic, $Pn\bar{3}n$ **(9l)**

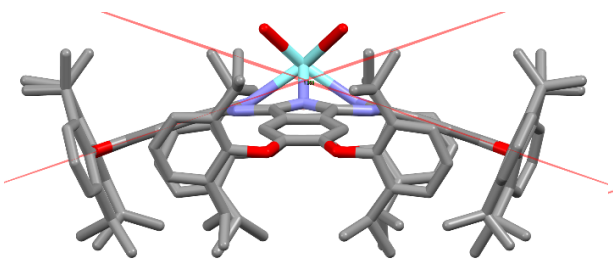

Figure 2.36. PNC[Y], cubic, $Pn\bar{3}n$ **(9n)**

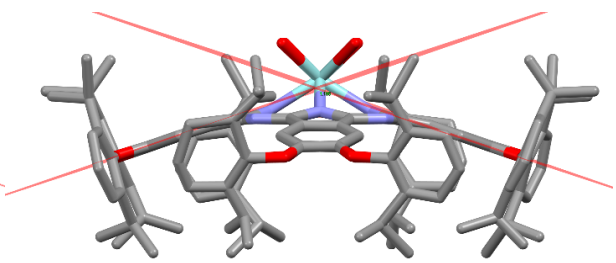

Figure 2.37. PNC[Zr], cubic, $Pn\bar{3}n$ **(9o)**

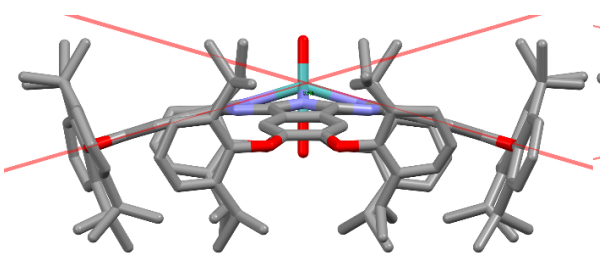

Figure 2.38. PNC[Mo], cubic, $Pn\bar{3}n$ **(9p)**

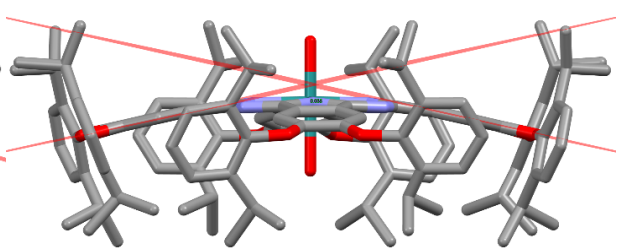

Figure 2.39. PNC[Ru], cubic, $Pn\bar{3}n$ **(9q)**

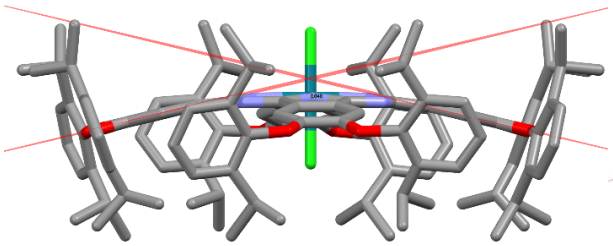

Figure 2.40. PNC[Rh], cubic, $Pn\bar{3}n$ **(9r)**

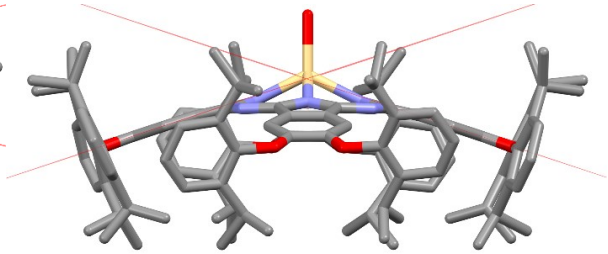

Figure 2.41. PNC[Cd], cubic, $Pn\bar{3}n$ **(9s)**

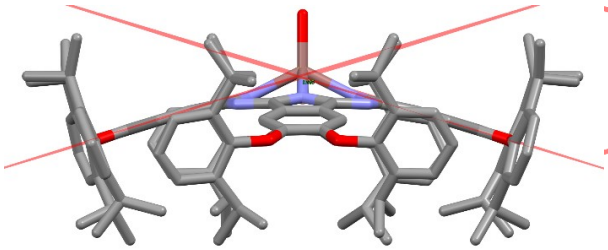

Figure 2.42. PNC[In], cubic, $Pn\bar{3}n$ **(9t)**

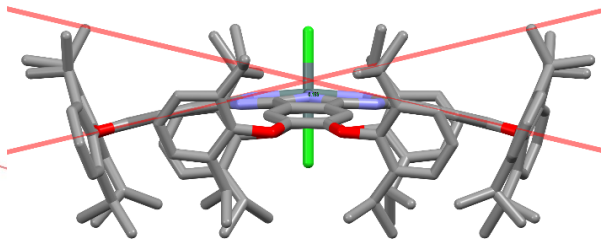

Figure 2.43. PNC[Sn], cubic, $Pn\bar{3}n$ **(9u)**

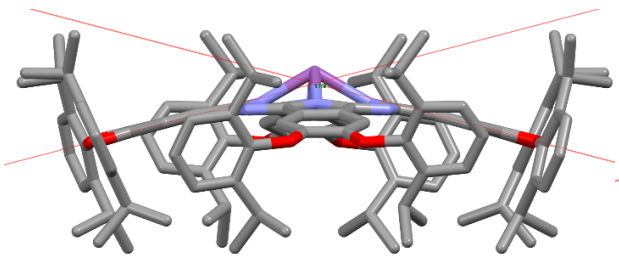

Figure 2.44. PNC[Sb], cubic, $Pn\bar{3}n$ **(9v)**

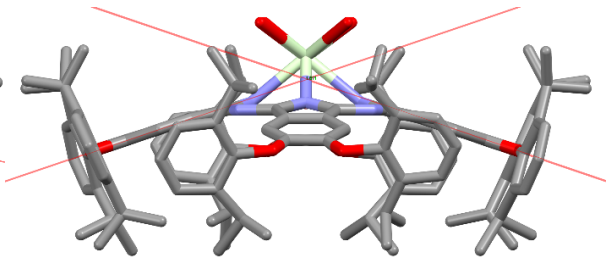

Figure 2.45. PNC[Pr], cubic, $Pn\bar{3}n$ **(9w)**

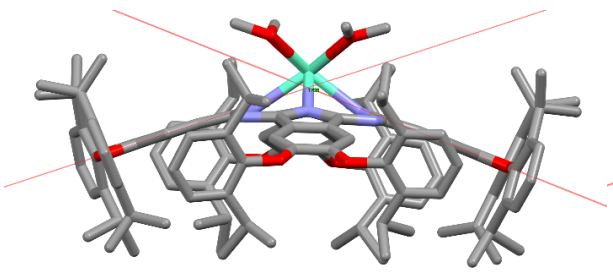

Figure 2.46. PNC[Eu], cubic, $Pn\bar{3}n$ **(9x)**

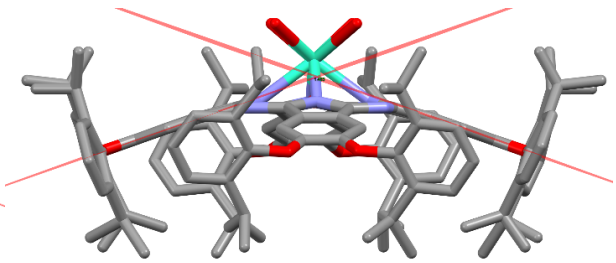

Figure 2.47. PNC[Tb], cubic, $Pn\bar{3}n$ **(9y)**

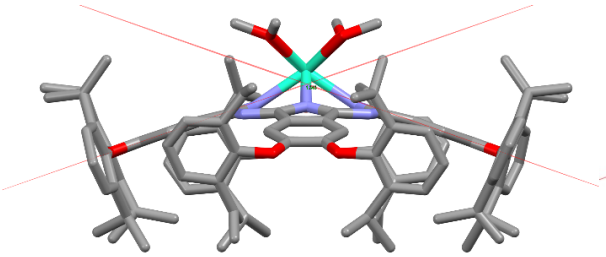

Figure 2.48. PNC[Dy], cubic, $Pn\bar{3}n$ **(9z)**

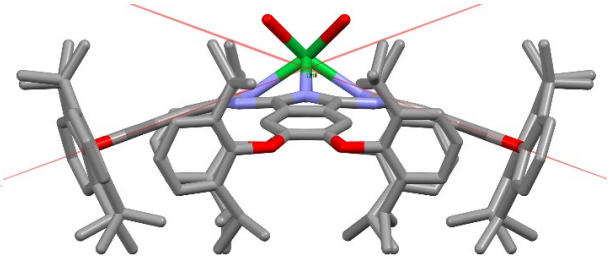

Figure 2.49. PNC[Yb], cubic, $Pn\bar{3}n$ **(9aa)**

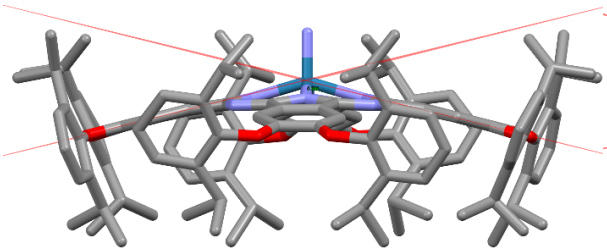

Figure 2.50. PNC[Re], cubic, $Pn\bar{3}n$ **(9ab)**

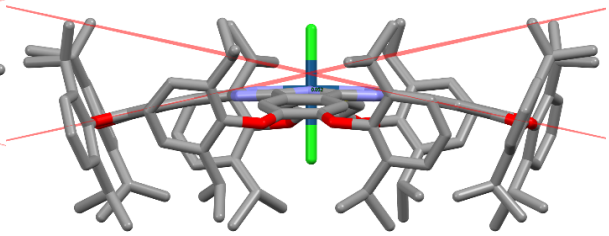

Figure 2.51. PNC[Ir], cubic, $Pn\bar{3}n$ **(9ac)**

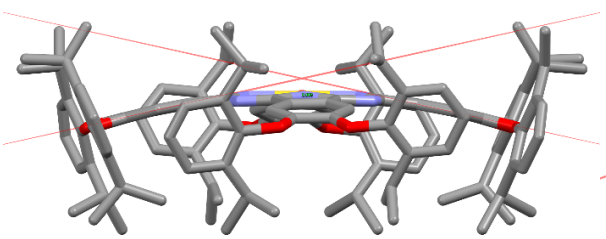

Figure 2.52. PNC[Au], cubic, $Pn\bar{3}n$ **(9ad)**

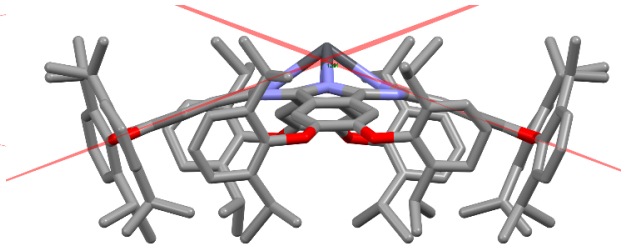

Figure 2.53. PNC[Pb], cubic, $Pn\bar{3}n$ **(9ae)**

(Note that the legends shaded in red indicate structures obtained during the PhD programme.)

2.7 Single-crystal to single-crystal transformation, axial ligand substitution of (dipPhO)$_8$PcM

The effect on the (dipPhO)$_8$PcM molecular structure within the nanoporous cubic crystal of ligands incorporated via the addition of ligands to the crystallising solution or by subsequent SCSC transformation was also investigated.

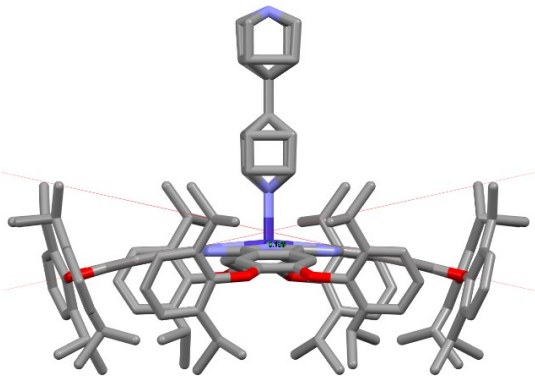

Figure 2.54. PNC[Co-*v*bipy], cubic, $Pn\bar{3}n$ **(6a)**

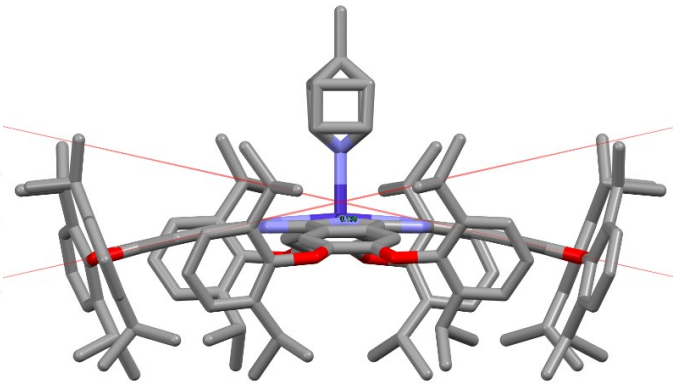

Figure 2.55. PNC[Co-*v*pic], cubic, $Pn\bar{3}n$ **(6b)**

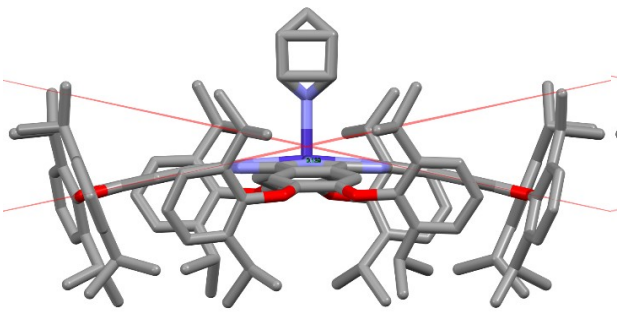

Figure 2.56. PNC[Co-*v*py], cubic, $Pn\bar{3}n$ **(6o)**

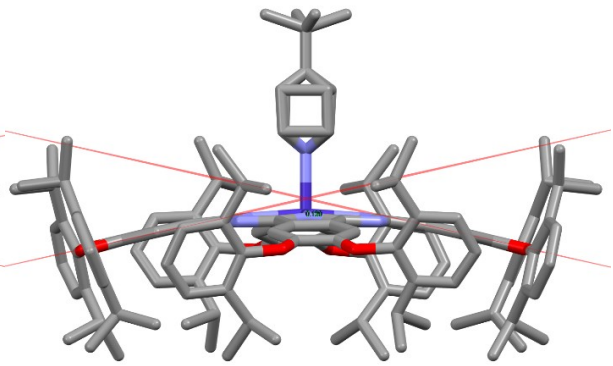

Figure 2.57. PNC[Co-*v*py0.82^{t}Bupy0.18], cubic, $Pn\bar{3}n$ **(6d)**

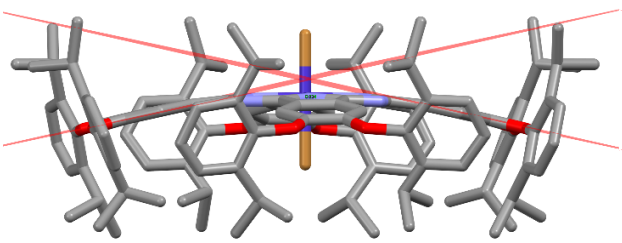

Figure 2.58. PNC[*v*Br0.36-Co-*c*Br0.51], cubic, $Pn\bar{3}n$ **(6f)**

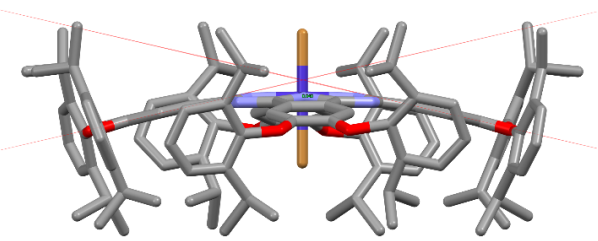

Figure 2.59. PNC[*v*Br0.47-Co-*c*Br0.85], cubic, $Pn\bar{3}n$ **(6g)**

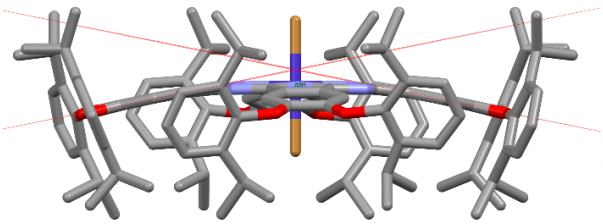

Figure 2.60. PNC[*v*Br-Co-*c*Br], cubic, $Pn\bar{3}n$ **(6e)**

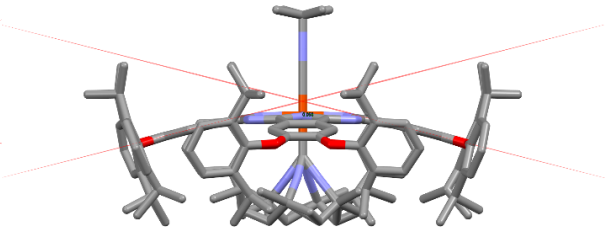

Figure 2.61. PNC[*v*BuNC-Fe-*c*BuNC], cubic, $Pn\bar{3}n$ **(10d)**

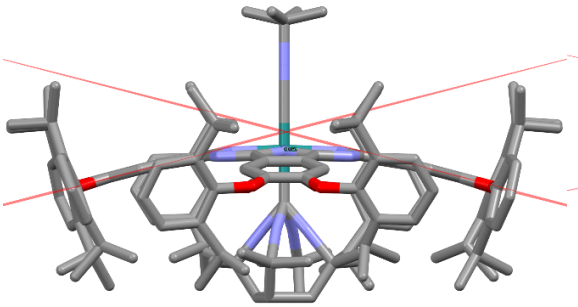

Figure 2.62. PNC[*v*BuNC-Ru-*c*BuNC], cubic, $Pn\bar{3}n$ **(10g)**

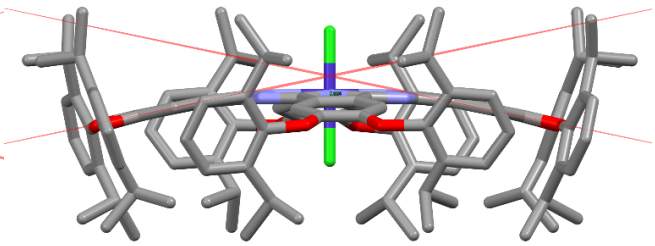

Figure 2.63. PNC[*v*Cl0.68-Co-*c*Cl0.67], cubic, $Pn\bar{3}n$ **(6j)**

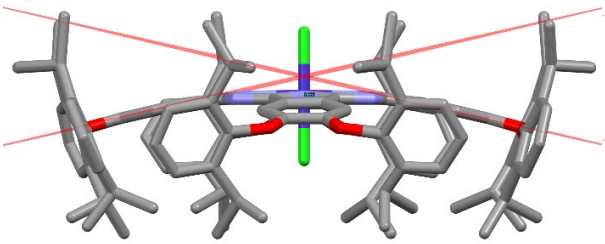

Figure 2.64. PNC[*v*Cl-Co-*c*Cl], cubic, $Pn\bar{3}n$ **(6i)**

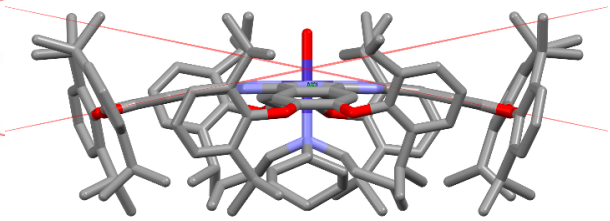

Figure 2.65. PNC[*v*H_2O-Co-*c*TBA], cubic, $Pn\bar{3}n$ **(6h)**

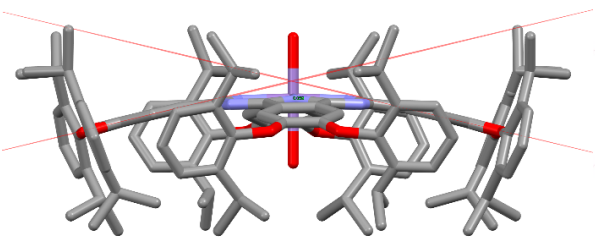

Figure 2.66. PNC[*v*H_2O-Mn-*c*H_2O], cubic, $Pn\bar{3}n$ **(9h)**

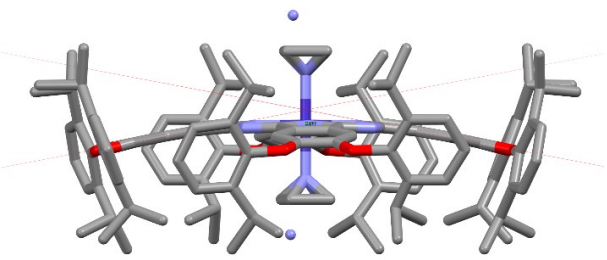

Figure 2.67. PNC[*v*Im-Co-*c*Im], cubic, $Pn\bar{3}n$ **(6l)**

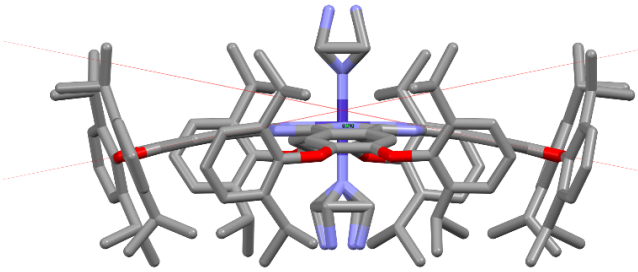

Figure 2.68. PNC[*v*Im-Co-*c*Im], cubic, $Pn\bar{3}n$ **(6m)**

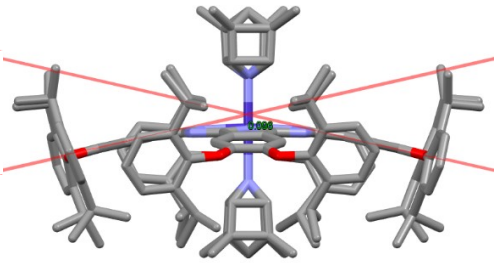

Figure 2.69. PNC[*v*Iu-Co-*c*Iu], cubic, $Pn\bar{3}n$ **(6n)**

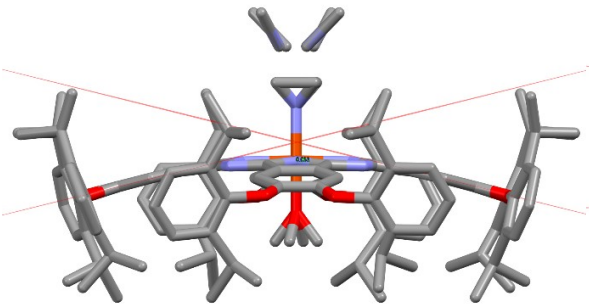

Figure 2.70. PNC[*v*Meim-Fe-*c*MeOH], cubic, $Pn\bar{3}n$ **(10c)**

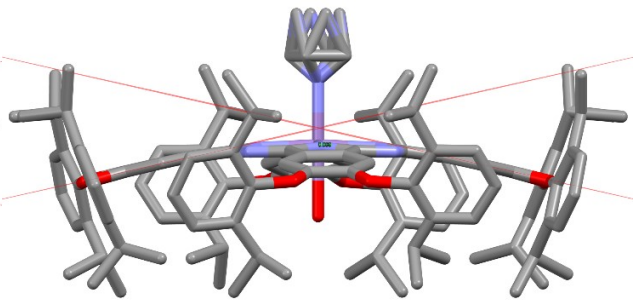

Figure 2.71. PNC[*v*Meim-Mn-*c*H_2O], cubic, $Pn\bar{3}n$ **(10f)**

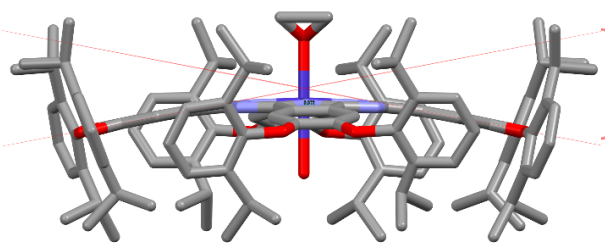

Figure 2.72. PNC[*v*MeOH-Co-*c*H_2O], cubic, $Pn\bar{3}n$ **(6k)**

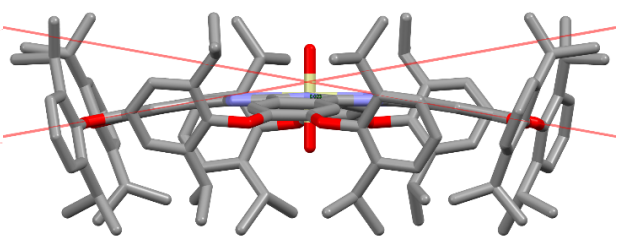

Figure 2.73. PNC[*v*OH-Si-*c*OH], cubic, $Pn\bar{3}n$ **(9c)**

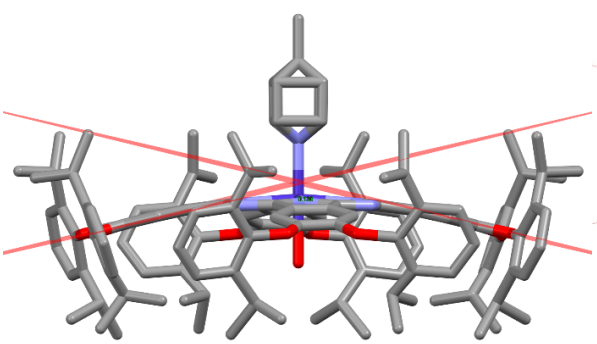

Figure 2.74. PNC[*v*pic-Co-*c*H_2O], cubic, $Pn\bar{3}n$ **(6c)**

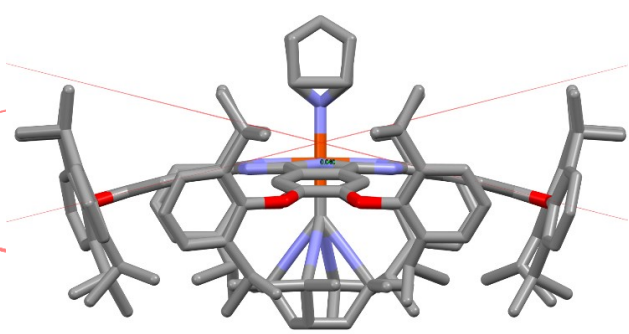

Figure 2.75. PNC[*v*py-Fe-*c*BuNC], cubic, $Pn\bar{3}n$ **(10e)**

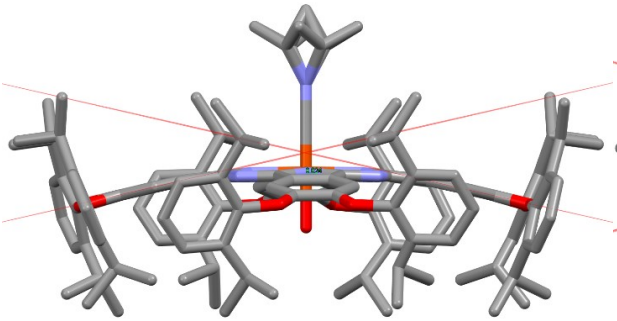

Figure 2.76. PNC[*v*py-Fe-*c*H_2O], cubic, $Pn\bar{3}n$ **(10a)**

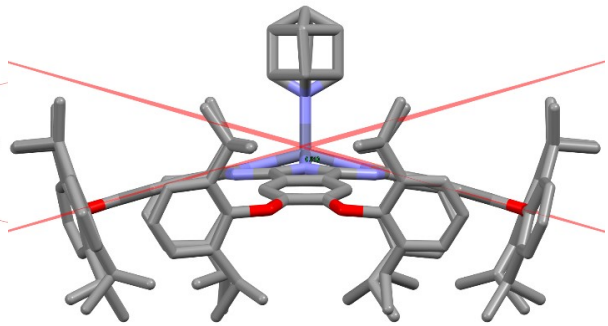

Figure 2.77. PNC[*v*py-Zn], cubic, $Pn\bar{3}n$ **(10a)**

(Note that the legends shaded in red indicate structures obtained during the PhD programme.)

An interesting aspect of the axial ligand exchange was that when the small water ligand on cobalt phthalocyanine was substituted by either pyridine or bipyridine, the crystal system changed from the non-porous monoclinic to the cubic nanoporous structure. It appears that blocking at least one face of the $(dipPhO)_8PcM$ complex encourages the cubic crystal formation (**Figure 2.56**). Furthermore, different ligands on the cobalt phthalocyanine have a different effect on the metal extrusion from the phthalocyanine plane and the phthalocyanine curvature (**Table 2.4**).

Metal with axial ligand phthalocyanines												
Acronym	Name	Chemical formula	M_r	Crystal system, space group	a (Å)	b (Å)	c (Å)	V (Å^3)	Z	Phthalocyanine curvature (degrees)	Metal to macrocycle distance (Å)	CCDC
PNC[*v* bipy-Co]	$(dipPhO)_8PcCo$ + bipy	$C_{128}H_{144}N_8O_8Co\ C_{10}H_8N_2$	2137.684	cubic, $Pn\bar{3}n$	37.4921(9)	37.4921(9)	37.4921(9)	52701(2)	12	24.93	0.159	900365
PNC[*v* pic-Co]	$(dipPhO)_8PcCo$ + pic	$C_{128}H_{144}N_8O_8Co\ C_6H_7N$	2074.626	cubic, $Pn\bar{3}n$	37.5208(2)	37.5208(2)	37.5208(2)	52822.2(5)	12	25.25	0.135	900366
PNC[*v* pic-Co-*c* H_2O]	$(dipPhO)_8PcCo$ + pic	$C_{128}H_{144}N_8O_8Co\ C_6H_7N$	2074.626	cubic, $Pn\bar{3}n$	37.1172(4)	37.1172(4)	37.1172(4)	51135.9(10)	12	26.85	0.136	900367
PNC[*v* py0.82tBupy0.18-Co]	$(dipPhO)_8PcCo$ + py/tBupy	$C_{128}H_{144}N_8O_8Co\ C_5H_5N$	2060.599	cubic, $Pn\bar{3}n$	37.5512(3)	37.5512(3)	37.5512(3)	52950.7(7)	12	25.37	0.139	900368
PNC[*v* Br-Co-*c* Br]	$(dipPhO)_8PcCo$	$C_{128}H_{144}N_8O_8Co$	1981.499	cubic, $Pn\bar{3}n$	37.627(4)	37.627(4)	37.627(4)	53272(10)	12	22.92	0.011	900369
PNC[*v* Br0.36-Co-*c* Br0.51]	$(dipPhO)_8PcCo$	$C_{128}H_{144}N_8O_8Co$	1981.499	cubic, $Pn\bar{3}n$	37.2791(3)	37.2791(3)	37.2791(3)	51807.9	12	24.78	0.024	900370
PNC[*v* Br0.47-Co-*c* Br0.85]	$(dipPhO)_8PcCo$	$C_{128}H_{144}N_8O_8Co$	1981.499	cubic, $Pn\bar{3}n$	37.017(4)	37.017(4)	37.017(4)	50722.9	12	26.08	0.040	900371
PNC[*v* H_2O-Co-*c* TBA]	$(dipPhO)_8PcCo$ + TBA	$C_{128}H_{144}N_8O_8Co\ C_{16}H_{36}N$	2223.964	cubic, $Pn\bar{3}n$	37.458(5)	37.458(5)	37.458(5)	52556(12)	12	23.24	0.001	900372
PNC[*v* Cl-Co-*c* Cl]	$(dipPhO)_8PcCo$	$C_{128}H_{144}N_8O_8Co$	1981.499	cubic, $Pn\bar{3}n$	37.230(4)	37.230(4)	37.230(4)	51605(10)	12	25.60	0.022	900373
PNC[*v* Cl0.68-Co-*c* Cl0.67]	$(dipPhO)_8PcCo$	$C_{128}H_{144}N_8O_8Co$	1981.499	cubic, $Pn\bar{3}n$	37.365(4)	37.365(4)	37.365(4)	52166.9	12	23.38	0.024	900374
PNC[*v* MeOH-Co-*c* H_2O]	$(dipPhO)_8PcCo$	$C_{128}H_{144}N_8O_8Co$	1981.499	cubic, $Pn\bar{3}n$	37.6395(3)	37.6395(3)	37.6395(3)	53325.1(7)	12	21.66	0.072	900375
PNC[*v* Im-Co-*c* Im]	$(dipPhO)_8PcCo$ + 2 x Im	$C_{128}H_{144}N_8O_8Co\ (C_3H_4N_2)_2$	2117.654	cubic, $Pn\bar{3}n$	37.5719(16)	37.5719(16)	37.5719(16)	53038.3	12	21.35	0.017	900376
PNC[*v* Im-Co-*c* Im]	$(dipPhO)_8PcCo$ + 2 x Im	$C_{128}H_{144}N_8O_8Co\ (C_3H_4N_2)_2$	2117.654	cubic, $Pn\bar{3}n$	37.603(3)	37.603(3)	37.603(3)	53170.1	12	22.99	0.010	900377
PNC[*v* Iu-Co-*c* Iu]	$(dipPhO)_8PcCo$ + 2 x Iu	$C_{128}H_{144}N_8O_8Co\ (C_7H_8N)_2$	2193.790	cubic, $Pn\bar{3}n$	37.3922(2)	37.3922(2)	37.3922(2)	52280.9(5)	12	25.48	0.096	900378
PNC[*v* py-Fe-*c* H_2O]	$(dipPhO)_8PcFe$ + py	$C_{128}H_{144}N_8O_8Fe\ C_5H_5N$	2057.511	cubic, $Pn\bar{3}n$	37.57680(10)	37.57680(10)	37.57680(10)	53059.0(2)	12	25.55	0.024	
PNC[*v* py-Zn]	$(dipPhO)_8PcZn$ + py	$C_{128}H_{144}N_8O_8Zn\ C_5H_5N$	2067.075	cubic, $Pn\bar{3}n$	37.4212(9)	37.4212(9)	37.4212(9)	52403(2)	12	31.61	0.510	761408
PNC[*v* py-Co]	$(dipPhO)_8PcCo$ + py	$C_{128}H_{144}N_8O_8Co\ C_5H_5N$	2060.599	cubic, $Pn\bar{3}n$	37.5596(4)	37.5596(4)	37.5596(4)	52986.2(10)	12	24.26	0.139	761407
PNC[*v* Meim-Fe-*c* MeOH]	$(dipPhO)_8PcFe$ + MeOH + Meim	$C_{128}H_{144}N_8O_8Fe\ CH_3OH\ C_4H_6N_2$	2092.557	cubic, $Pn\bar{3}n$	37.5202(5)	37.5202(5)	37.5202(5)	52819.6	12	27.85	0.033	761415
PNC[*v* BuNC-Fe-*c* BuNC]	$(dipPhO)_8PcFe$ + 2 x BuNC	$C_{128}H_{144}N_8O_8Fe\ (C_5H_9N)_2$	2144.675	cubic, $Pn\bar{3}n$	37.4083(3)	37.4083(3)	37.4083(3)	52348.5	12	28.40	0.058	761409
PNC[*v* py-Fe-*c* BuNC]	$(dipPhO)_8PcFe$ + BuNC + py	$C_{128}H_{144}N_8O_8Fe\ C_5H_9N\ C_5H_5N$	2140.643	cubic, $Pn\bar{3}n$	37.5004(9)	37.5004(9)	37.5004(9)	52736.1	12	28.28	0.040	761410
PNC[*v* Meim-Mn-*c* H_2O]	$(dipPhO)_8PcFe$ + Meim	$C_{128}H_{144}N_8O_8Fe\ C_4H_6N_2$	2059.608	cubic, $Pn\bar{3}n$	37.4581(15)	37.4581(15)	37.4581(15)	52557.8	12	25.29	0.089	761413
PNC[*v* BuNC-Ru-*c* BuNC]	$(dipPhO)_8PcRu$ + 2 x BuNC	$C_{128}H_{144}N_8O_8Ru\ (C_5H_9N)_2$	2189.895	cubic, $Pn\bar{3}n$	37.6390(4)	37.6390(4)	37.6390(4)	53323	12	28.90	0.063	761411
PNC[*v* TEP-Eu]	$(dipPhO)_8PcEu$ + TEP	$C_{128}H_{144}N_8O_8Eu\ C_{28}H_{34}N_4$	2501.128	cubic, $Pn\bar{3}n$	37.181(4)	37.181(4)	37.181(4)	51400	12	34.25	1.610	
PNC[*v* Pc-Tb]	$(dipPhO)_8PcTb$ + Pc	$C_{128}H_{144}N_8O_8Eu\ C_{32}H_{16}N_8$	2594.016	cubic, $Pn\bar{3}n$	37.852(4)	37.852(4)	37.852(4)	54233.4	12	32.81	1.405	
azaPNC[*v* H_2O-Co]	$(dipPhO)_8$azaPcCo	$C_{120}H_{136}N_{16}O_8Co$	1989.403	cubic, $Pn\bar{3}n$	37.3715(2)	37.3715(2)	37.3715(2)	52194.1	12	17.48	0.077	

Table 2.4. Different ligands that were incorporated with *in-situ* axial ligand exchange.

2.8 Incorporation of wall-ties in $(dipPhO)_8PcM$

In order to increase the stability of the crystal structure, even upon desolvation of the system and to avoid formation of an amorphous structure, SCSC transformation to incorporate a bidentate ligand or co-crystallisation to incorporate a fullerene gave crystals with wall-tie enhancement of stability (**Table 2.5**).

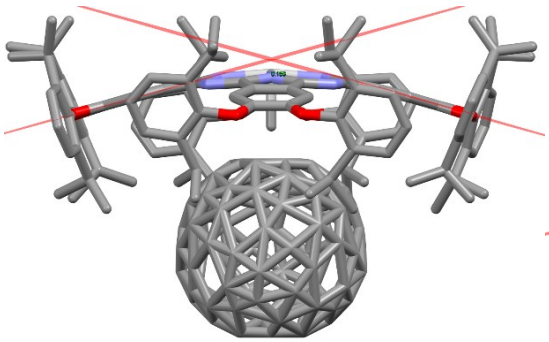

Figure 2.78. PNC[Ag/*c*C_{60}/Ag], cubic, $Pn\bar{3}n$ **(7l)**

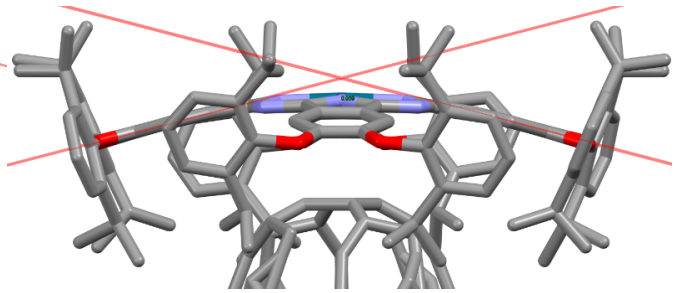

Figure 2.79. PNC[Pd/*c*C_{60}/Pd], cubic, $Pn\bar{3}n$ **(7j)**

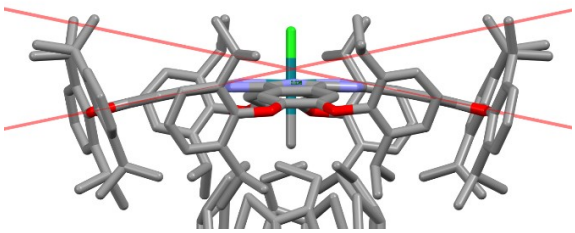

Figure 2.80. PNC[*v*Cl-Rh/*c*C_{60}/Rh-*v*Cl], cubic, $Pn\bar{3}n$ **(7k)**

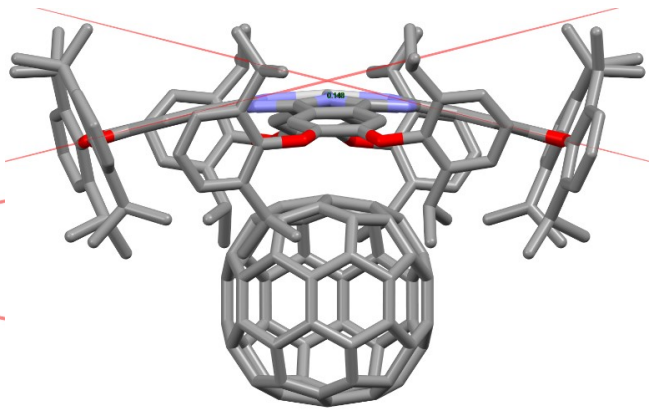

Figure 2.81. PNC[Ag/*c*C_{60}/Ag] vacuum, cubic, $Pn\bar{3}n$ **(7g)**

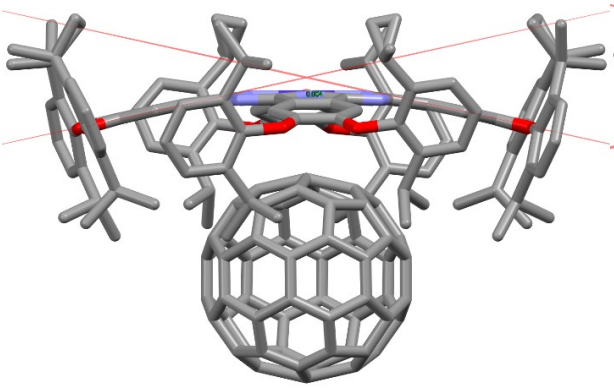

Figure 2.82. PNC[Co/*c*C_{60}/Co] desolv. N_2, cubic, $Pn\bar{3}n$ **(7b)**

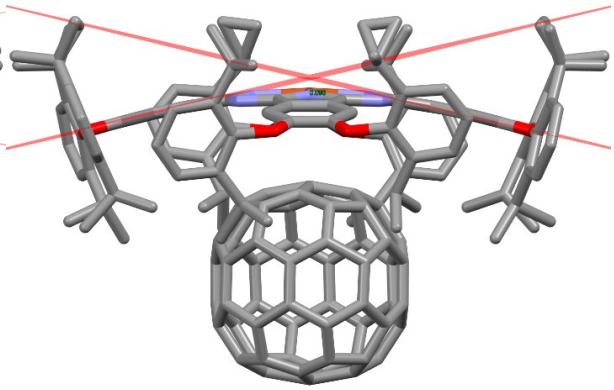

Figure 2.83. PNC[Cu/*c*C_{60}/Cu] vacuum, cubic, $Pn\bar{3}n$ **(7h)**

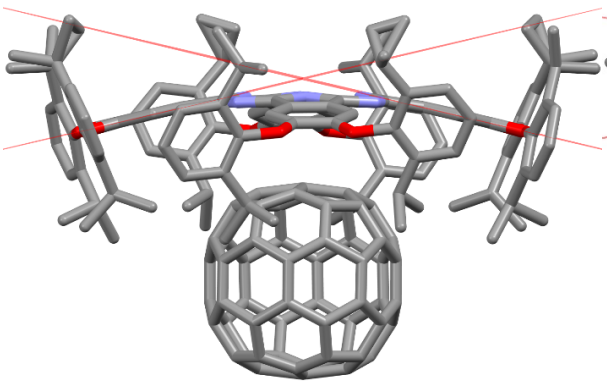

Figure 2.84. PNC[H_2/*c*C_{60}/ H_2] vacuum, cubic, $Pn\bar{3}n$ **(7i)**

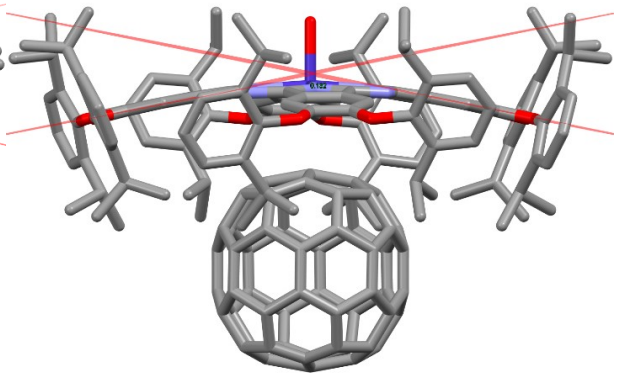

Figure 2.85. PNC[*v*H_2O-Co/*c*C_{60}/Co-*v*H_2O], cubic, $Pn\bar{3}n$ **(7c)**

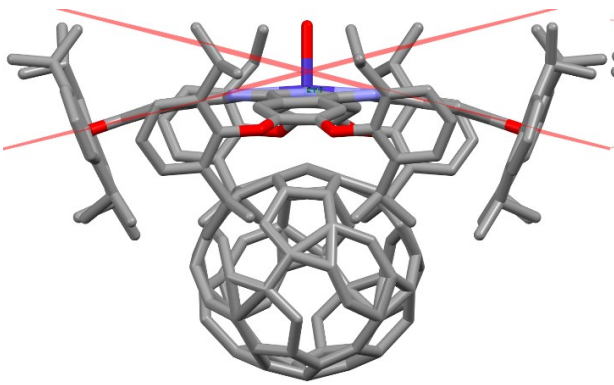

Figure 2.86. PNC[*v*H_2O-Co/*c*C_{70}/Co-*v*H_2O], cubic, $Pn\bar{3}n$ **(7d)**

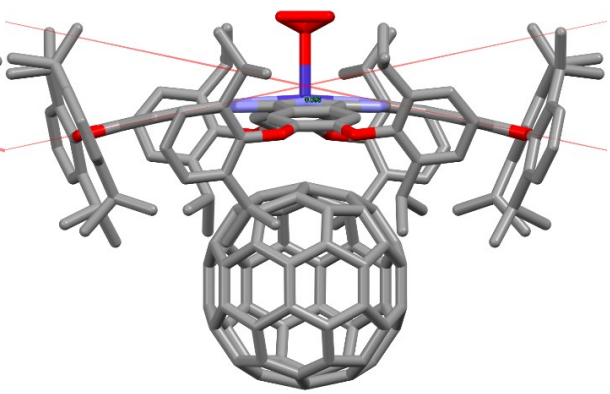

Figure 2.87. PNC[*v*O_2-Co/*c*C_{60}/Co-*v*O_2], cubic, $Pn\bar{3}n$ **(7f)**

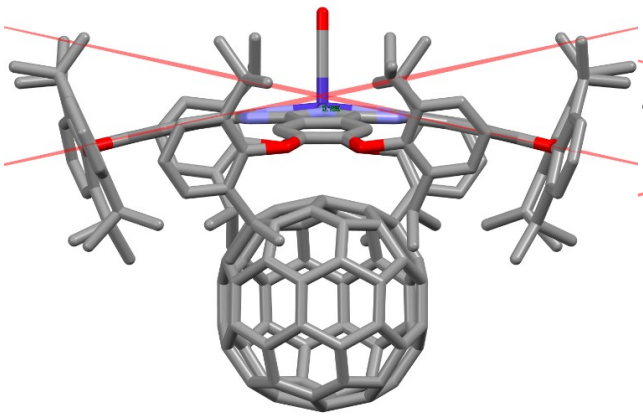

Figure 2.88. PNC[*v*CO-Co/*c*C_{60}/Co-*v*CO], cubic, $Pn\bar{3}n$ **(7e)**

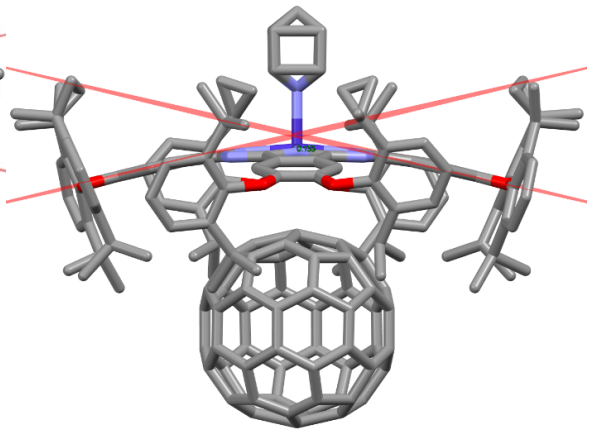

Figure 2.89. PNC[*v*py-Co/*c*C_{60}/Co-*v*py], cubic, $Pn\bar{3}n$ **(7a)**

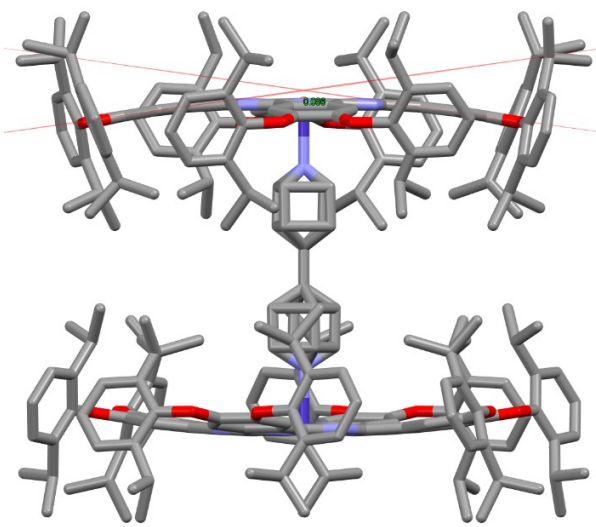

Figure 2.90. PNC[Co-*c*bipy-Co], cubic, $Pn\bar{3}n$ **(8a)**

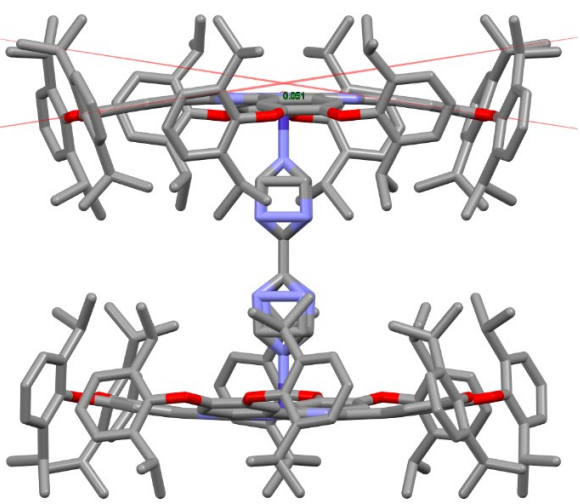

Figure 2.91. PNC[Co-*c*bpm-Co], cubic, $Pn\bar{3}n$ **(8g)**

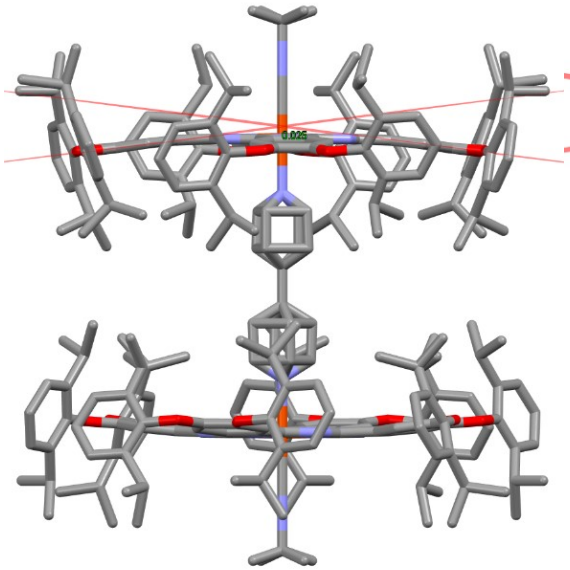

Figure 2.92. PNC[*v*BuNC-Fe-*c*bipy-Fe-*v*BuNC], cubic, $Pn\bar{3}n$ **(8e)**

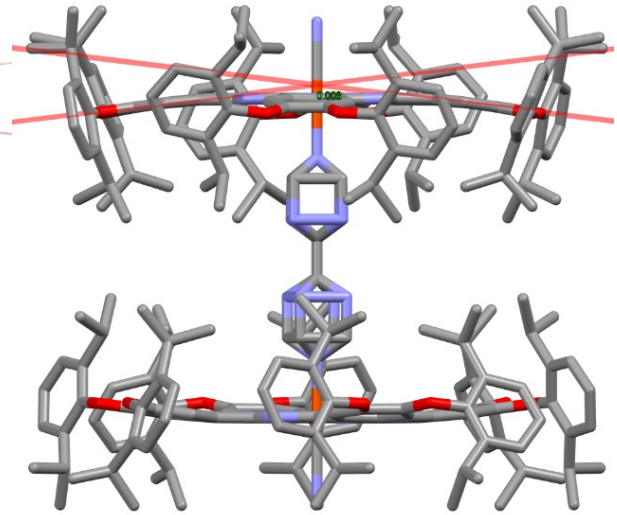

Figure 2.93. PNC[*v*BuNC-Fe-*c*bpm-Fe-*v*BuNC], cubic, $Pn\bar{3}n$ **(8h)**

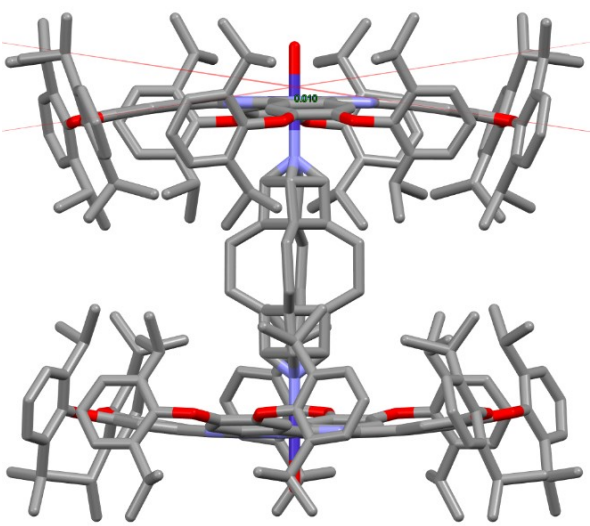

Figure 2.94. PNC[*v*H_2O-Co-*c*daa-Co-*v*H_2O], cubic, $Pn\bar{3}n$ **(8i)**

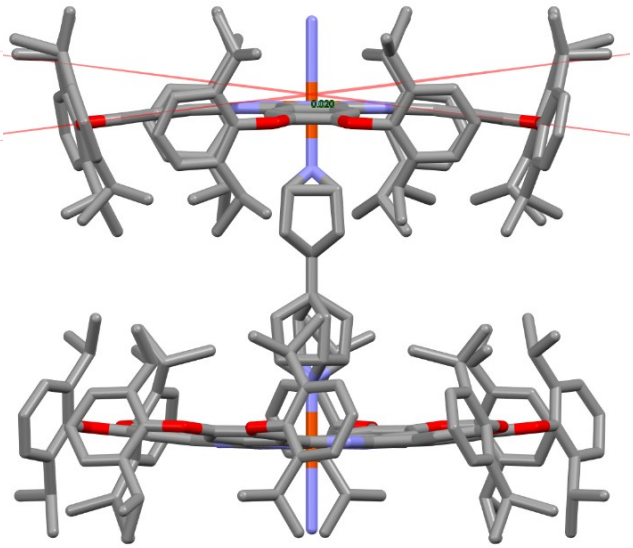

Figure 2.95. PNC[*v*N-Fe-*c*bipy-Fe-*v*N], cubic, $Pn\bar{3}n$ **(8c)**

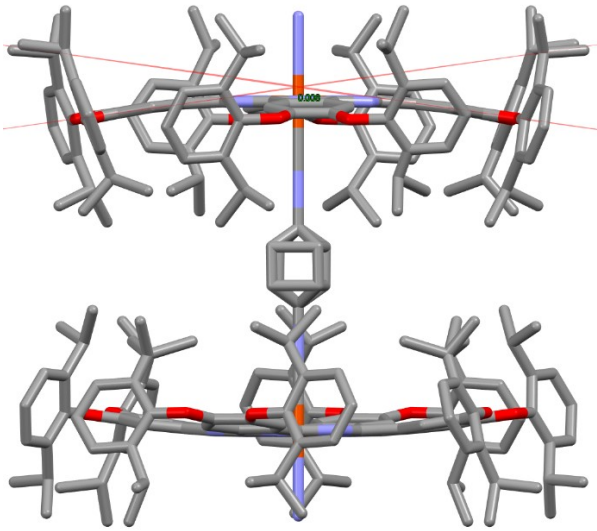

Figure 2.96. PNC[*v*N-Fe-*c*pidic-Fe-*v*N], cubic, $Pn\bar{3}n$ **(8f)**

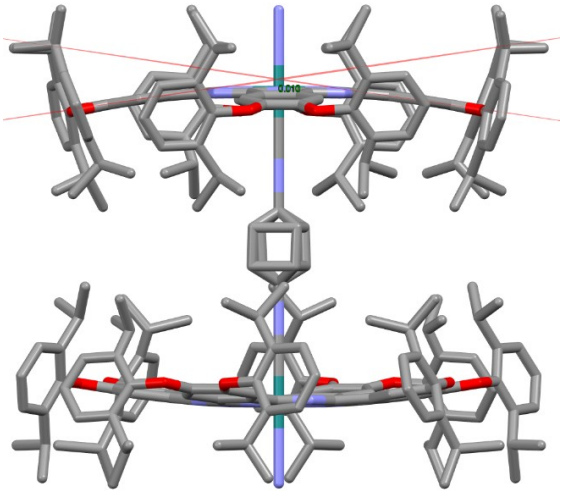

Figure 2.97. PNC[*v*N-Ru-*c*pidic-Ru-*v*N], cubic, $Pn\bar{3}n$ **(8d)**

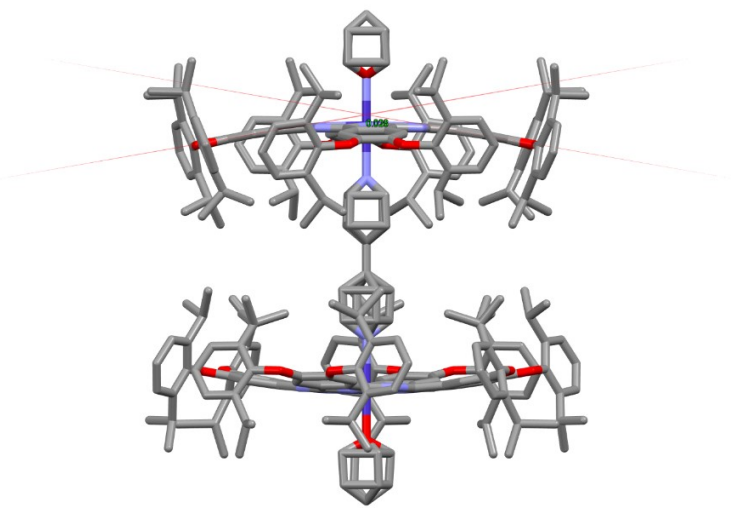

Figure 2.98. PNC[*v*py-Co-*c*bipy-Co-*v*py], cubic, $Pn\bar{3}n$ **(8b)**

(Note that the legends shaded in red indicate structures obtained during the PhD programme.)

The successful incorporation of different bidentate ligands in the cavity resulted in permanent nanoporosity upon desolvation. The nitrogen adsorption measurements provided approximate BET surface areas of ~1000 $m^2\ g^{-1}$.

Metal with axial and bidentate ligands phthalocyanines												
Acronym	Name	Chemical formula	M_r	Crystal system, space group	a (Å)	b (Å)	c (Å)	V (Å^3)	Z	Phthalocyanine curvature (degrees)	Metal to macrocycle distance (Å)	CCDC
PNC[Co-*c* bipy-Co]	$(dipPhO)_8PcCo$ + bipy	$(C_{128}H_{144}N_8O_8Co)_2\ C_{10}H_8N_2$	4119.183	cubic, $Pn\bar{3}n$	37.698(14)	37.698(14)	37.698(14)	53574(34)	12	15.98	0.086	761420
PNC[*v* py-Co-*c* bipy-Co-*v* py]	$(dipPhO)_8PcCo$ + py + bipy	$(C_{128}H_{144}N_8O_8Co)_2\ (C_5H_5N)_2\ C_{10}H_8N_2$	4277.383	cubic, $Pn\bar{3}n$	37.647(3)	37.647(3)	37.647(3)	53359(7)	12	19.70	0.028	761419
PNC[*v* N-Fe-*c* bipy-Fe-*v* N]	$(dipPhO)_8PcFe$ + bipy	$(C_{128}H_{144}N_8O_8Fe)_2\ C_{10}H_8N_2$	4113.007	cubic, $Pn\bar{3}n$	37.603(9)	37.603(9)	37.603(9)	53170(21)	12	14.46	0.020	761421
PNC[*v* N-Ru-*c* pidic-Ru-*v* N]	$(dipPhO)_8PcRu$ + pidic	$(C_{128}H_{144}N_8O_8Ru)_2\ C_8H_4N_2$	4175.394	cubic, $Pn\bar{3}n$	37.7453(4)	37.7453(4)	37.7453(4)	53776.0(10)	12	16.70	0.010	761418
PNC[*v* BuNC-Fe-*c* bipy-Fe-*v* BuNC]	$(dipPhO)_8PcFe$ + bipy + BuNC	$(C_{128}H_{144}N_8O_8Fe)_2\ (C_5H_9N)_2\ C_{10}H_8N_2$	4279.271	cubic, $Pn\bar{3}n$	37.8590(2)	37.8590(2)	37.8590(2)	54263.5	12	14.48	0.025	761416
PNC[*v* N-Fe-*c* pidic-Fe-*v* N]	$(dipPhO)_8PcFe$ + pidic	$(C_{128}H_{144}N_8O_8Fe)_2\ C_8H_4N_2$	4084.954	cubic, $Pn\bar{3}n$	37.560(12)	37.560(12)	37.560(12)	52987.9	12	16.31	0.005	761422
PNC[*v* py-Co-*c* bpm-Co-*v* py]	**$(dipPhO)_8PcCo$ + bpm**	**$(C_{128}H_{144}N_8O_8Co)_2\ C_8H_6N_4$**	4121.159	cubic, $Pn\bar{3}n$	37.6423(2)	37.6423(2)	37.6423(2)	53337	12	22.53	0.091	
PNC[*v* BuNC-Fe-*c* bpm-Co-vBuNC]	**$(dipPhO)_8PcCo$ + bpm +BuNC**	**$(C_{128}H_{144}N_8O_8Co)_2\ (C_5H_9N)_2\ C_8H_6N_4$**	4287.423	cubic, $Pn\bar{3}n$	37.8046(4)	37.8046(4)	37.8046(4)	54029.9	12	13.88	0.008	
PNC[*v* H_2O-Co-*c* daa-Co-*v* H_2O]	$(dipPhO)_8PcCo$ + daa	$(C_{128}H_{144}N_8O_8Co)_2\ C_{12}H_{12}N_2$	4147.236	cubic, $Pn\bar{3}n$	37.4908(2)	37.4908(2)	37.4908(2)	52695.6	12	17.21	0.010	
PNC[Pd/*c* C_{60}/Pd]	$(dipPhO)_8PcPd$ + C_{60}	$(C_{128}H_{144}N_8O_8Pd)_2\ C_{60}$	4778.607	cubic, $Pn\bar{3}n$	37.3727(12)	37.3727(12)	37.3727(12)	52199.1	12	29.05	0.069	
PNC[Rh/*c* C_{60}/Rh]	$(dipPhO)_8PcRh$ + C_{60}	$(C_{128}H_{144}N_8O_8Rh)_2\ C_{60}$	4771.588	cubic, $Pn\bar{3}n$	37.5844(7)	37.5844(7)	37.5844(7)	53091.2	12	23.61	0.026	
PNC[Ag/*c* C_{60}/Ag]	$(dipPhO)_8PcAg$ + C_{60}	$(C_{128}H_{144}N_8O_8Ag)_2\ C_{60}$	4781.513	cubic, $Pn\bar{3}n$	37.5946(3)	37.5946(3)	37.5946(3)	53134.5	12	30.97	0.158	
PNC[*v* py-Co/*c* C_{60}/Co-*v* py]	$(dipPhO)_8PcCo$ + C_{60} + py	$(C_{128}H_{144}N_8O_8Co)_2\ (C_5H_5N)_2\ C_{60}$	4841.843	cubic, $Pn\bar{3}n$	37.594(2)	37.594(2)	37.594(2)	53131.9	12	25.95	0.153	1853490
PNC[Co/*c* C_{60}/Co]	$(dipPhO)_8PcCo$ + C_{60}	$(C_{128}H_{144}N_8O_8Co)_2\ C_{60}$	4683.643	cubic, $Pn\bar{3}n$	37.610(10)	37.610(10)	37.610(10)	53199.8	12	24.70	0.004	1857087
PNC[*v* H_2O-Co/*c* C_{60}/Co-*v* H_2O]	$(dipPhO)_8PcCo$ + C_{60} + H_2O	$(C_{128}H_{144}N_8O_8Co)_2\ (H_2O)_2\ C_{60}$	4719.674	cubic, $Pn\bar{3}n$	37.8101(13)	37.8101(13)	37.8101(13)	54053.5	12	22.48	0.132	1851749
PNC[*v* H_2O-Co/*c* C_{70}/Co-*v* H_2O]	$(dipPhO)_8PcCo$ + C_{70} + H_2O	$(C_{128}H_{144}N_8O_8Co)_2\ (H_2O)_2\ C_{70}$	4839.781	cubic, $Pn\bar{3}n$	36.6188(17)	36.6188(17)	36.6188(17)	49103.5	12	28.58	0.117	1851730
PNC[*v* CO-Co/*c* C_{60}/Co-*v* CO]	$(dipPhO)_8PcCo$ + C_{60} + CO	$(C_{128}H_{144}N_8O_8Co)_2\ (CO)_2\ C_{60}$	4739.663	cubic, $Pn\bar{3}n$	37.7788(3)	37.7788(3)	37.7788(3)	53919.3	12	24.35	0.189	1851741
PNC[*v* O_2-Co/*c* C_{60}/Co-*v* O_2]	$(dipPhO)_8PcCo$ + C_{60} + O_2	$(C_{128}H_{144}N_8O_8Co)_2\ (O)_2\ C_{60}$	4747.641	cubic, $Pn\bar{3}n$	37.8616(2)	37.8616(2)	37.8616(2)	54274.6	12	24.06	0.098	1851419
PNC[Ag/*c* C_{60}/Ag]	$(dipPhO)_8PcAg$ + C_{60}	$(C_{128}H_{144}N_8O_8Ag)_2\ C_{60}$	4781.513	cubic, $Pn\bar{3}n$	37.7144(2)	37.7144(2)	37.7144(2)	53644.1	12	28.08	0.148	1851746
PNC[Cu/*c* C_{60}/Cu]	$(dipPhO)_8PcCu$ + C_{60}	$(C_{128}H_{144}N_8O_8Cu)_2\ C_{60}$	4692.869	cubic, $Pn\bar{3}n$	37.55590(16)	37.55590(16)	37.55590(16)	52970.6	12	26.39	0.096	1851747
PNC[H_2/*c* C_{60}/H_2]	$(dipPhO)_8PcH_2$ + C_{60}	$(C_{128}H_{144}N_8O_8H_2)_2\ C_{60}$	4569.808	cubic, $Pn\bar{3}n$	37.7340(3)	37.7340(3)	37.7340(3)	53727.7	12	26.48	N.A.	1851748

Table 2.5. Metal phthalocyanine with axial and bidentate ligands. Red coloured were synthesized for the current PhD programme, while black were from past group members.

2.9 Analysis of the Pc curvature and metal extrusion in $(dipPhO)_8PcM$

It can be deduced from comparing the ionic radii and extrusion of the metal from the $(dipPhO)_8PcCo$ macrocyclic plane that those metal cations which are a good fit with the diameter of the phthalocyanine internal cavity (~0.55 Å) do not extrude greatly from the macrocycle. In contrast those metal cations that are larger than the cavity extrude significantly.

However, the correlation between cation size and extrusion is weak presumably because of the difference in valency of the metal ion, its coordination chemistry, the preferred geometry of the metal, the hardness or softness of the ligand, and the errors from estimation of the cationic radius.

The analysis will be presented in three different kind of plots, which will be: (i) the cationic radii versus the extrusion of the metal; (ii) the cationic radii versus the curvature of the phthalocyanine and (iii) the extrusion of the metal versus the curvature.

The most investigated phthalocyanine was $(dipPhO)_8PcCo$ in which different axial ligands, fullerenes and the bidentate ligands were incorporated. Initial analysis is of the $(dipPhO)_8PcCo$ complexes with different axial ligands and “wall-ties” acting as bidentate ligands as indicated in the **Tables 2.6, 2.7** and **2.8** (**Figure 2.99**).[41,50]

	Cobalt phthalocyanine with axial ligands													
	Acronym	Name	Chemical formula	M_r	Crystal system, space group	a (Å)	b (Å)	c (Å)	V (Å^3)	Z	Phthalocyanine curvature (degrees)	Metal to macrocycle distance (Å)	CCDC
6a	PNC[*v* bipy-Co]	$(dipPhO)_8PcCo$ + bipy	$C_{128}H_{144}N_8O_8Co\ C_{10}H_8N_2$	2137.684	cubic, $Pn\bar{3}n$	37.4921(9)	37.4921(9)	37.4921(9)	52701(2)	12	24.93	0.159	900365
6b	PNC[*v* pic-Co]	$(dipPhO)_8PcCo$ + pic	$C_{128}H_{144}N_8O_8Co\ C_6H_7N$	2074.626	cubic, $Pn\bar{3}n$	37.5208(2)	37.5208(2)	37.5208(2)	52822.2(5)	12	25.25	0.135	900366
6c	PNC[*v* pic-Co-*c* H_2O]	$(dipPhO)_8PcCo$ + pic	$C_{128}H_{144}N_8O_8Co\ C_6H_7N$	2074.626	cubic, $Pn\bar{3}n$	37.1172(4)	37.1172(4)	37.1172(4)	51135.9(10)	12	26.85	0.136	900367
6d	PNC[*v* py0.82tBupy0.18-Co]	$(dipPhO)_8PcCo$ + py/tBupy	$C_{128}H_{144}N_8O_8Co\ C_5H_5N$	2060.599	cubic, $Pn\bar{3}n$	37.5512(3)	37.5512(3)	37.5512(3)	52950.7(7)	12	25.37	0.139	900368
6e	PNC[*v* Br-Co-*c* Br]	$(dipPhO)_8PcCo$	$C_{128}H_{144}N_8O_8Co$	1981.499	cubic, $Pn\bar{3}n$	37.627(4)	37.627(4)	37.627(4)	53272(10)	12	22.92	0.011	900369
6f	PNC[*v* Br0.36-Co-*c* Br0.51]	$(dipPhO)_8PcCo$	$C_{128}H_{144}N_8O_8Co$	1981.499	cubic, $Pn\bar{3}n$	37.2791(3)	37.2791(3)	37.2791(3)	51807.9	12	24.78	0.024	900370
6g	PNC[*v* Br0.47-Co-*c* Br0.85]	$(dipPhO)_8PcCo$	$C_{128}H_{144}N_8O_8Co$	1981.499	cubic, $Pn\bar{3}n$	37.017(4)	37.017(4)	37.017(4)	50722.9	12	26.08	0.040	900371
6h	PNC[*v* H_2O-Co-*c* TBA]	$(dipPhO)_8PcCo$ + TBA	$C_{128}H_{144}N_8O_8Co\ C_{16}H_{36}N$	2223.964	cubic, $Pn\bar{3}n$	37.458(5)	37.458(5)	37.458(5)	52556(12)	12	23.24	0.001	900372
6i	PNC[*v* Cl-Co-*c* Cl]	$(dipPhO)_8PcCo$	$C_{128}H_{144}N_8O_8Co$	1981.499	cubic, $Pn\bar{3}n$	37.230(4)	37.230(4)	37.230(4)	51605(10)	12	25.60	0.022	900373
6j	PNC[*v* Cl0.68-Co-*c* Cl0.67]	$(dipPhO)_8PcCo$	$C_{128}H_{144}N_8O_8Co$	1981.499	cubic, $Pn\bar{3}n$	37.365(4)	37.365(4)	37.365(4)	52166.9	12	23.38	0.024	900374
6k	PNC[*v* MeOH-Co-*c* H_2O]	$(dipPhO)_8PcCo$	$C_{128}H_{144}N_8O_8Co$	1981.499	cubic, $Pn\bar{3}n$	37.6395(3)	37.6395(3)	37.6395(3)	53325.1(7)	12	21.66	0.072	900375
6l	PNC[*v* Im-Co-*c* Im]	$(dipPhO)_8PcCo$ + 2 x Im	$C_{128}H_{144}N_8O_8Co\ (C_3H_4N_2)_2$	2117.654	cubic, $Pn\bar{3}n$	37.5719(16)	37.5719(16)	37.5719(16)	53038.3	12	21.35	0.017	900376
6m	PNC[*v* Im-Co-*c* Im]	$(dipPhO)_8PcCo$ + 2 x Im	$C_{128}H_{144}N_8O_8Co\ (C_3H_4N_2)_2$	2117.654	cubic, $Pn\bar{3}n$	37.603(3)	37.603(3)	37.603(3)	53170.1	12	22.99	0.010	900377
6n	PNC[*v* Iu-Co-*c* Iu]	$(dipPhO)_8PcCo$ + 2 x Iu	$C_{128}H_{144}N_8O_8Co\ (C_7H_8N)_2$	2193.790	cubic, $Pn\bar{3}n$	37.3922(2)	37.3922(2)	37.3922(2)	52280.9(5)	12	25.48	0.096	900378
6o	PNC[*v* py-Co]	$(dipPhO)_8PcCo$ + py	$C_{128}H_{144}N_8O_8Co\ C_5H_5N$	2060.599	cubic, $Pn\bar{3}n$	37.5596(4)	37.5596(4)	37.5596(4)	52986.2(10)	12	24.26	0.139	761407
6p	azaPNC[*v* H_2O-Co]	$(dipPhO)_8$azaPcCo	$C_{120}H_{136}N_{16}O_8Co$	1989.403	cubic, $Pn\bar{3}n$	37.3715(2)	37.3715(2)	37.3715(2)	52194.1	12	17.48	0.077	

Table 2.6. Different ligands that were incorporated with *in-situ* axial ligand exchange.

	Metal phthalocyanines with axial and fullerenes acting as "wall-ties"												
	Acronym	Name	Chemical formula	M_r	Crystal system, space group	a (Å)	b (Å)	c (Å)	V (Å^3)	Z	Phthalocyanine curvature (degrees)	Metal to macrocycle distance (Å)	CCDC
7a	PNC[*v* py-Co/*c* C_{60}/Co-*v* py]	$(dipPhO)_8PcCo + C_{60} + py$	$(C_{128}H_{144}N_8O_8Co)_2\,(C_5H_5N)_2\,C_{60}$	4841.843	cubic, $Pn\bar{3}n$	37.594(2)	37.594(2)	37.594(2)	53131.9	12	25.95	0.153	1853490
7b	PNC[Co/*c* C_{60}/Co]	$(dipPhO)_8PcCo + C_{60}$	$(C_{128}H_{144}N_8O_8Co)_2\,C_{60}$	4683.643	cubic, $Pn\bar{3}n$	37.610(10)	37.610(10)	37.610(10)	53199.8	12	24.70	0.004	1857087
7c	PNC[*v* H_2O-Co/*c* C_{60}/Co-*v* H_2O]	$(dipPhO)_8PcCo + C_{60} + H_2O$	$(C_{128}H_{144}N_8O_8Co)_2\,(H_2O)_2\,C_{60}$	4719.674	cubic, $Pn\bar{3}n$	37.8101(13)	37.8101(13)	37.8101(13)	54053.5	12	22.48	0.132	1851749
7d	PNC[*v* H_2O-Co/*c* C_{70}/Co-*v* H_2O]	$(dipPhO)_8PcCo + C_{70} + H_2O$	$(C_{128}H_{144}N_8O_8Co)_2\,(H_2O)_2\,C_{70}$	4839.781	cubic, $Pn\bar{3}n$	36.6188(17)	36.6188(17)	36.6188(17)	49103.5	12	28.58	0.117	1851730
7e	PNC[*v* CO-Co/*c* C_{60}/Co-*v* CO]	$(dipPhO)_8PcCo + C_{60} + CO$	$(C_{128}H_{144}N_8O_8Co)_2\,(CO)_2\,C_{60}$	4739.663	cubic, $Pn\bar{3}n$	37.7788(3)	37.7788(3)	37.7788(3)	53919.3	12	24.35	0.189	1851741
7f	PNC[*v* O_2-Co/*c* C_{60}/Co-*v* O_2]	$(dipPhO)_8PcCo + C_{60} + O_2$	$(C_{128}H_{144}N_8O_8Co)_2\,(O)_2\,C_{60}$	4747.641	cubic, $Pn\bar{3}n$	37.8616(2)	37.8616(2)	37.8616(2)	54274.6	12	24.06	0.098	1851419
7g	PNC[Ag/*c* C_{60}/Ag]	$(dipPhO)_8PcAg + C_{60}$	$(C_{128}H_{144}N_8O_8Ag)_2\,C_{60}$	4781.513	cubic, $Pn\bar{3}n$	37.7144(2)	37.7144(2)	37.7144(2)	53644.1	12	28.08	0.148	1851746
7h	PNC[Cu/*c* C_{60}/Cu]	$(dipPhO)_8PcCu + C_{60}$	$(C_{128}H_{144}N_8O_8Cu)_2\,C_{60}$	4692.869	cubic, $Pn\bar{3}n$	37.55590(16)	37.55590(16)	37.55590(16)	52970.6	12	26.39	0.096	1851747
7i	PNC[H_2/*c* C_{60}/H_2]	$(dipPhO)_8PcH_2 + C_{60}$	$(C_{128}H_{144}N_8O_8H_2)_2\,C_{60}$	4569.808	cubic, $Pn\bar{3}n$	37.7340(3)	37.7340(3)	37.7340(3)	53727.7	12	26.48	0	1851748
7j	PNC[Pd/*c* C_{60}/Pd]	$(dipPhO)_8PcPd + C_{60}$	$(C_{128}H_{144}N_8O_8Pd)_2\,C_{60}$	4778.607	cubic, $Pn\bar{3}n$	37.3727(12)	37.3727(12)	37.3727(12)	52199.1	12	29.05	0.069	
7k	PNC[Rh/*c* C_{60}/Rh]	$(dipPhO)_8PcRh + C_{60}$	$(C_{128}H_{144}N_8O_8Rh)_2\,C_{60}$	4771.588	cubic, $Pn\bar{3}n$	37.5844(7)	37.5844(7)	37.5844(7)	53091.2	12	23.61	0.026	
7l	PNC[Ag/*c* C_{60}/Ag]	$(dipPhO)_8PcAg + C_{60}$	$(C_{128}H_{144}N_8O_8Ag)_2\,C_{60}$	4781.513	cubic, $Pn\bar{3}n$	37.5946(3)	37.5946(3)	37.5946(3)	53134.5	12	30.97	0.158	

Table 2.7. Metal phthalocyanine with axial and fullerenes acting as "wall-ties" ligands.

	Metal phthalocyanines with axial and bidentate ligands												
	Acronym	Name	Chemical formula	M_r	Crystal system, space group	*a* (Å)	*b* (Å)	*c* (Å)	*V* (Å^3)	*Z*	Phthalocyanine curvature (degrees)	Metal to macrocycle distance (Å)	CCDC
8a	PNC[Co-*c* bipy-Co]	$(dipPhO)_8PcCo$ + bipy	$(C_{128}H_{144}N_8O_8Co)_2\ C_{10}H_8N_2$	4119.183	cubic, $Pn\bar{3}n$	37.698(14)	37.698(14)	37.698(14)	53574(34)	12	15.98	0.086	761420
8b	PNC[*v* py-Co-*c* bipy-Co-*v* py]	$(dipPhO)_8PcCo$ + py + bipy	$(C_{128}H_{144}N_8O_8Co)_2\ (C_5H_5N)_2\ C_{10}H_8N_2$	4277.383	cubic, $Pn\bar{3}n$	37.647(3)	37.647(3)	37.647(3)	53359(7)	12	19.70	0.028	761419
8c	PNC[*v* N-Fe-*c* bipy-Fe-*v* N]	$(dipPhO)_8PcFe$ + bipy	$(C_{128}H_{144}N_8O_8Fe)_2\ C_{10}H_8N_2$	4113.007	cubic, $Pn\bar{3}n$	37.603(9)	37.603(9)	37.603(9)	53170(21)	12	14.46	0.020	761421
8d	PNC[*v* N-Ru-*c* pidic-Ru-*v* N]	$(dipPhO)_8PcRu$ + pidic	$(C_{128}H_{144}N_8O_8Ru)_2\ C_8H_4N_2$	4175.394	cubic, $Pn\bar{3}n$	37.7453(4)	37.7453(4)	37.7453(4)	53776.0(10)	12	16.70	0.010	761418
8e	PNC[*v* BuNC-Fe-*c* bipy-Fe-*v* BuNC]	$(dipPhO)_8PcFe$ + bipy + BuNC	$(C_{128}H_{144}N_8O_8Fe)_2\ (C_5H_9N)_2\ C_{10}H_8N_2$	4279.271	cubic, $Pn\bar{3}n$	37.8590(2)	37.8590(2)	37.8590(2)	54263.5	12	14.48	0.025	761416
8f	PNC[*v* N-Fe-*c* pidic-Fe-*v* N]	$(dipPhO)_8PcFe$ + pidic	$(C_{128}H_{144}N_8O_8Fe)_2\ C_8H_4N_2$	4084.954	cubic, $Pn\bar{3}n$	37.560(12)	37.560(12)	37.560(12)	52987.9	12	16.31	0.005	761422
8g	**PNC[*v* py-Co-*c* bpm-Co-*v* py]**	**$(dipPhO)_8PcCo$ + bpm**	**$(C_{128}H_{144}N_8O_8Co)_2\ C_8H_6N_4$**	4121.159	cubic, $Pn\bar{3}n$	37.6423(2)	37.6423(2)	37.6423(2)	53337	12	22.53	0.091	
8h	**PNC[*v* BuNC-Fe-*c* bpm-Co-vBuNC]**	**$(dipPhO)_8PcCo$ + bpm +BuNC**	**$(C_{128}H_{144}N_8O_8Co)_2\ (C_5H_9N)_2\ C_8H_6N_4$**	4287.423	cubic, $Pn\bar{3}n$	37.8046(4)	37.8046(4)	37.8046(4)	54029.9	12	13.88	0.008	
8i	PNC[*v* H_2O-Co-*c* daa-Co-*v* H_2O]	$(dipPhO)_8PcCo$ + daa	$(C_{128}H_{144}N_8O_8Co)_2\ C_{12}H_{12}N_2$	4147.236	cubic, $Pn\bar{3}n$	37.4908(2)	37.4908(2)	37.4908(2)	52695.6	12	17.21	0.010	

Table 2.8. Metal phthalocyanine with axial and bidentate ligands. Red coloured were synthesized for the current PhD programme, while black were from past group members.

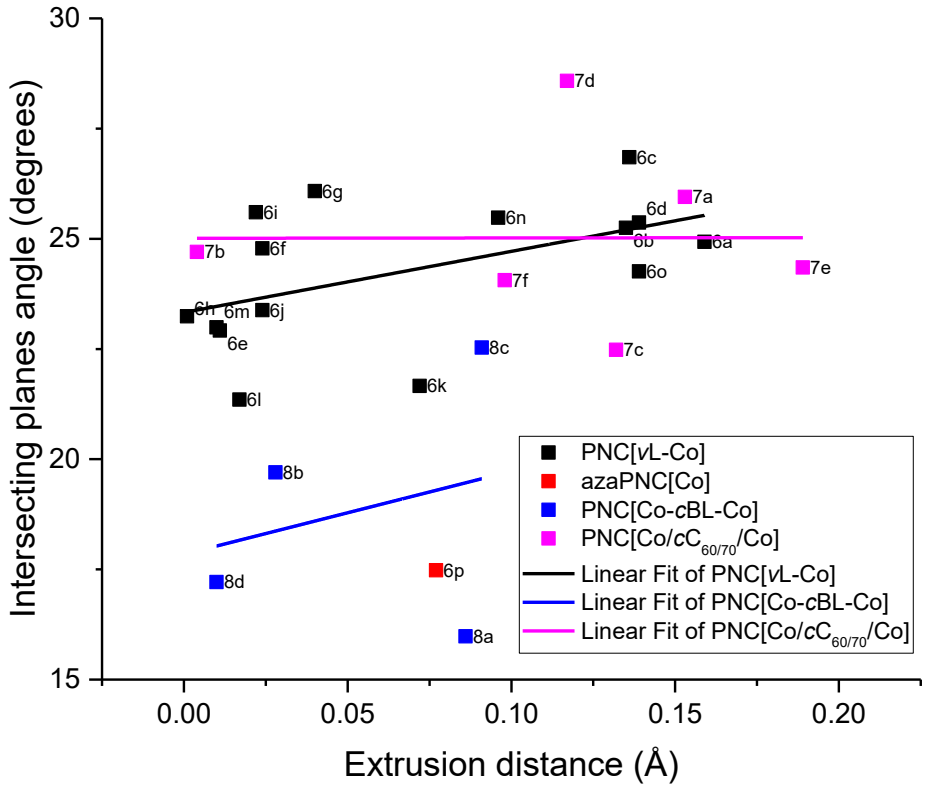

Figure 2.99. Plot of different axial ligands of PNC[*v*L-Co] as well as different "wall-ties" ligand and fullerenes indicating the trend of increasing the curvature of the macrocycle with the extrusion of the metal from the phthalocyanine.

The cationic radius for Co^{II} is 0.58 Å and as can be seen in **Figure 2.99**, there is a deviation of the extrusion distance from 0.001 Å (for PNC[*v*H_2O-Co-*c*TBA]) up to 0.159 Å (for PNC[*v*bipy-Co]) and the angle of curvature is in the range of 17.48 ° (for azaPNC[*v*H_2O-Co]) to 26.85° (for PNC[*v*pic-Co-*c*H_2O]). Thus, there is a weak positive correlation between the metal extrusion distance and $(dipPhO)_8PcCo$ curvature. The octaazaphthalocyanine (6p) appears less curved than the standard phthalocyanine. The same trend is followed for bidentate ligands that are acting as "wall-ties" although the curvature is significantly reduced. For the fullerene containing $(dipPhO)_8PcCo$ crystals there is no correlation between metal extrusion distance and curvature perhaps due to the curvature being dictated by the Pc-fullerene surface interactions.[41,50]

	Metal Phthalocyanines												
	Acronym	Name	Chemical formula	M_r	Crystal system, space group	a (Å)	b (Å)	c (Å)	V (Å^3)	Z	Phthalocyanine curvature (degrees)	Metal to macrocycle distance (Å)	CCDC
9a	PNC[Mg]	$(dipPhO)_8PcMg$	$C_{128}H_{144}N_8O_8Mg$	1946.871	cubic, $Pn\bar{3}n$	37.3320(5)	37.3320(5)	37.3320(5)	52028.8(12)	12	30.89	0.170	
9b	PNC[Al]	$(dipPhO)_8PcAl$	$C_{128}H_{144}N_8O_8Al$	1949.548	cubic, $Pn\bar{3}n$	37.4064(4)	37.4064(4)	37.4064(4)	52340.5(10)	12	26.48	0.062	
9c	PNC[Si]	$(dipPhO)_8PcSi$	$C_{128}H_{144}N_8O_8Si$	1950.652	cubic, $Pn\bar{3}n$	37.612(7)	37.612(7)	37.612(7)	53208.3	12	20.17	0.023	
9d	**PNC[P]**	**$(dipPhO)_8PcP$**	**$C_{128}H_{144}N_8O_8P$**	1968.858	cubic, $Pn\bar{3}n$	37.6935(3)	37.6935(3)	37.6935(3)	53554.9	12	20.80	0.015	
9e	PNC[Sc]	$(dipPhO)_8PcSc$	$C_{128}H_{144}N_8O_8Sc$	1967.522	cubic, $Pn\bar{3}n$	37.1225(8)	37.1225(8)	37.1225(8)	51157.8	12	36.94	1.072	
9f	PNC[Ti]	$(dipPhO)_8PcTi$	$C_{128}H_{144}N_8O_8Ti$	1970.433	cubic, $Pn\bar{3}n$	37.5117(9)	37.5117(9)	37.5117(9)	52784(2)	12	25.90	0.745	
9g	PNC[Cr]	$(dipPhO)_8PcCr$	$C_{128}H_{144}N_8O_8Cr$	1974.562	cubic, $Pn\bar{3}n$	37.7555(3)	37.7555(3)	37.7555(3)	53819.6	12	19.60	0.003	
9h	PNC[Mn]	$(dipPhO)_8PcMn$	$C_{128}H_{144}N_8O_8Mn$	1977.504	cubic, $Pn\bar{3}n$	37.2511(5)	37.2511(5)	37.2511(5)	51691.3(12)	12	26.69	0.059	761412
9i	PNC[Fe]	$(dipPhO)_8PcFe$	$C_{128}H_{144}N_8O_8Fe$	1978.411	cubic, $Pn\bar{3}n$	37.4562(14)	37.4562(14)	37.4562(14)	52549.8	12	25.90	0.040	
9j	**PNC[Fe-*v* Cl]**	**$(dipPhO)_8PcFe$**	**$C_{128}H_{144}N_8O_8Fe$**	2013.385	cubic, $Pn\bar{3}n$	37.4365(2)	37.4365(2)	37.4365(2)	52466.9	12	24.90	0.056	
9k	PNC[Zn]	$(dipPhO)_8PcZn$	$C_{128}H_{144}N_8O_8Zn$	1987.975	cubic, $Pn\bar{3}n$	37.6973(2)	37.6973(2)	37.6973(2)	53571.1	12	26.74	0.419	279644
9l	PNC[Ga]	$(dipPhO)_8PcGa$	$C_{128}H_{144}N_8O_8Ga$	1992.289	cubic, $Pn\bar{3}n$	37.6003(2)	37.6003(2)	37.6003(2)	53158.9(6)	12	28.30	0.119	
9m	**PNC[Ge]**	**$(dipPhO)_8PcGe$**	**$C_{128}H_{144}N_8O_8Ge$**	2031.415	cubic, $Pn\bar{3}n$	37.650(4)	37.650(4)	37.650(4)	53370	12	27.66	0.173	
9n	PNC[Y]	$(dipPhO)_8PcY$	$C_{128}H_{144}N_8O_8Y$	2011.472	cubic, $Pn\bar{3}n$	37.1526	37.1526	37.1526	51282	12	37.23	1.353	
9o	PNC[Zr]	$(dipPhO)_8PcZr$	$C_{128}H_{144}N_8O_8Zr$	2103.790	cubic, $Pn\bar{3}n$	37.2617(3)	37.2617(3)	37.2617(3)	51735.4	12	37.35	1.186	
9p	**PNC[Mo]**	**$(dipPhO)_8PcMo$**	**$C_{128}H_{144}N_8O_8Mo$**	2034.128	cubic, $Pn\bar{3}n$	37.5869(5)	37.5869(5)	37.5869(5)	53101.8(2)	12	32.50	0.613	
9q	PNC[Ru]	$(dipPhO)_8PcRu$	$C_{128}H_{144}N_8O_8Ru$	2023.631	cubic, $Pn\bar{3}n$	37.700(7)	37.700(7)	37.700(7)	53584(17)	12	24.72	0.028	761414
9r	PNC[Rh]	$(dipPhO)_8PcRh$	$C_{128}H_{144}N_8O_8Rh$	2025.472	cubic, $Pn\bar{3}n$	37.396(2)	37.396(2)	37.396(2)	52296.8	12	16.58	0.040	
9s	**PNC[Cd]**	**$(dipPhO)_8PcCd$**	**$C_{128}H_{144}N_8O_8Cd$**	2035.208	cubic, $Pn\bar{3}n$	37.3224(3)	37.3224(3)	37.3224(3)	51988.7	12	36.47	1.007	
9t	PNC[In]	$(dipPhO)_8PcIn$	$C_{128}H_{144}N_8O_8In$	2037.384	cubic, $Pn\bar{3}n$	37.4428(8)	37.4428(8)	37.4428(8)	52493.4(19)	12	33.92	0.995	
9u	PNC[Sn]	$(dipPhO)_8PcSn$	$C_{128}H_{144}N_8O_8Sn$	2041.276	cubic, $Pn\bar{3}n$	37.776(9)	37.776(9)	37.776(9)	53906(23)	12	24.71	0.153	
9v	**PNC[Sb]**	**$(dipPhO)_8PcSb$**	**$C_{128}H_{144}N_8O_8Sb$**	2044.146	cubic, $Pn\bar{3}n$	37.3901(4)	37.3901(4)	37.3901(4)	52272.1	12	29.32	1.119	
9w	PNC[Pr]	$(dipPhO)_8PcPr$	$C_{128}H_{144}N_8O_8Pr$	2063.474	cubic, $Pn\bar{3}n$	37.2220(12)	37.2220(12)	37.2220(12)	51570(3)	12	37.37	1.611	
9x	PNC[Eu]	$(dipPhO)_8PcEu$	$C_{128}H_{144}N_8O_8Eu$	2074.530	cubic, $Pn\bar{3}n$	37.034(3)	37.034(3)	37.034(3)	50792(8)	12	35.55	1.428	
9y	PNC[Tb]	$(dipPhO)_8PcTb$	$C_{128}H_{144}N_8O_8Tb$	2081.491	cubic, $Pn\bar{3}n$	37.3171(3)	37.3171(3)	37.3171(3)	51966.5	12	38.11	1.465	
9z	PNC[Dy]	$(dipPhO)_8PcDy$	$C_{128}H_{144}N_8O_8Dy$	2085.065	cubic, $Pn\bar{3}n$	37.25810(10)	37.25810(10)	37.25810(10)	51720.4	12	38.23	1.343	
9aa	PNC[Yb]	$(dipPhO)_8PcYb$	$C_{128}H_{144}N_8O_8Yb$	2095.604	cubic, $Pn\bar{3}n$	36.9702(8)	36.9702(8)	36.9702(8)	50530(19)	12	39.56	1.315	
9ab	**PNC[Re]**	**$(dipPhO)_8PcRe$**	**$C_{128}H_{144}N_8O_8Re$**	2124.315	cubic, $Pn\bar{3}n$	37.6052(2)	37.6052(2)	37.6052(2)	53179.4	12	27.81	0.598	
9ac	**PNC[Ir]**	**$(dipPhO)_8PcIr$**	**$C_{128}H_{144}N_8O_8Ir$**	2114.340	cubic, $Pn\bar{3}n$	37.4658(2)	37.4658(2)	37.4658(2)	52590.2	12	24.77	0.052	
9ad	**PNC[Pb]**	**$(dipPhO)_8PcPb$**	**$C_{128}H_{144}N_8O_8Pb$**	2129.009	cubic, $Pn\bar{3}n$	37.1115(2)	37.1115(2)	37.1115(2)	51112.3	12	41.07	1.391	

Table 2.9. $(dipPhO)_8M$ that crystallise in the cubic nanoporous structure. Red coloured were synthesized for the current PhD programme, while black were from past group members.

	Metal with axial ligand phthalocyanines												
	Acronym	Name	Chemical formula	M_r	Crystal system, space group	a (Å)	b (Å)	c (Å)	V (Å^3)	Z	Phthalocyanine curvature (degrees)	Metal to macrocycle distance (Å)	CCDC
10a	PNC[*v* py-Fe-*c* H_2O]	$(dipPhO)_8PcFe$ + py	$C_{128}H_{144}N_8O_8Fe\ C_5H_5N$	2057.511	cubic, $Pn\bar{3}n$	37.57680(10)	37.57680(10)	37.57680(10)	53059.0(2)	12	25.55	0.024	
10b	PNC[*v* py-Zn]	$(dipPhO)_8PcZn$ + py	$C_{128}H_{144}N_8O_8Zn\ C_5H_5N$	2067.075	cubic, $Pn\bar{3}n$	37.4212(9)	37.4212(9)	37.4212(9)	52403(2)	12	31.61	0.510	761408
10c	PNC[*v* Meim-Fe-*c* MeOH]	$(dipPhO)_8PcFe$ + MeOH + Mei	$C_{128}H_{144}N_8O_8Fe\ CH_3OH\ C_4H_6N_2$	2092.557	cubic, $Pn\bar{3}n$	37.5202(5)	37.5202(5)	37.5202(5)	52819.6	12	27.85	0.033	761415
10d	PNC[*v* BuNC-Fe-*c* BuNC]	$(dipPhO)_8PcFe$ + 2 x BuNC	$C_{128}H_{144}N_8O_8Fe\ (C_5H_9N)_2$	2144.675	cubic, $Pn\bar{3}n$	37.4083(3)	37.4083(3)	37.4083(3)	52348.5	12	28.40	0.058	761409
10e	PNC[*v* py-Fe-*c* BuNC]	$(dipPhO)_8PcFe$ + BuNC + py	$C_{128}H_{144}N_8O_8Fe\ C_5H_9N\ C_5H_5N$	2140.643	cubic, $Pn\bar{3}n$	37.5004(9)	37.5004(9)	37.5004(9)	52736.1	12	28.28	0.040	761410
10f	PNC[*v* Meim-Mn-*c* H_2O]	$(dipPhO)_8PcFe$ + Meim	$C_{128}H_{144}N_8O_8Fe\ C_4H_6N_2$	2059.608	cubic, $Pn\bar{3}n$	37.4581(15)	37.4581(15)	37.4581(15)	52557.8	12	25.29	0.089	761413
10g	PNC[*v* BuNC-Ru-*c* BuNC]	$(dipPhO)_8PcRu$ + 2 x BuNC	$C_{128}H_{144}N_8O_8Ru\ (C_5H_9N)_2$	2189.895	cubic, $Pn\bar{3}n$	37.6390(4)	37.6390(4)	37.6390(4)	53323	12	28.90	0.063	761411
10h	PNC[*v* TEP-Eu]	$(dipPhO)_8PcEu$ + TEP	$C_{128}H_{144}N_8O_8Eu\ C_{28}H_{34}N_4$	2501.128	cubic, $Pn\bar{3}n$	37.181(4)	37.181(4)	37.181(4)	51400	12	34.25	1.610	
10i	PNC[*v* Pc-Tb]	$(dipPhO)_8PcTb$ + Pc	$C_{128}H_{144}N_8O_8Eu\ C_{32}H_{16}N_8$	2594.016	cubic, $Pn\bar{3}n$	37.852(4)	37.852(4)	37.852(4)	54233.4	12	32.81	1.405	

Table 2.10. Different ligands that were incorporated with *in-situ* axial ligand exchange.

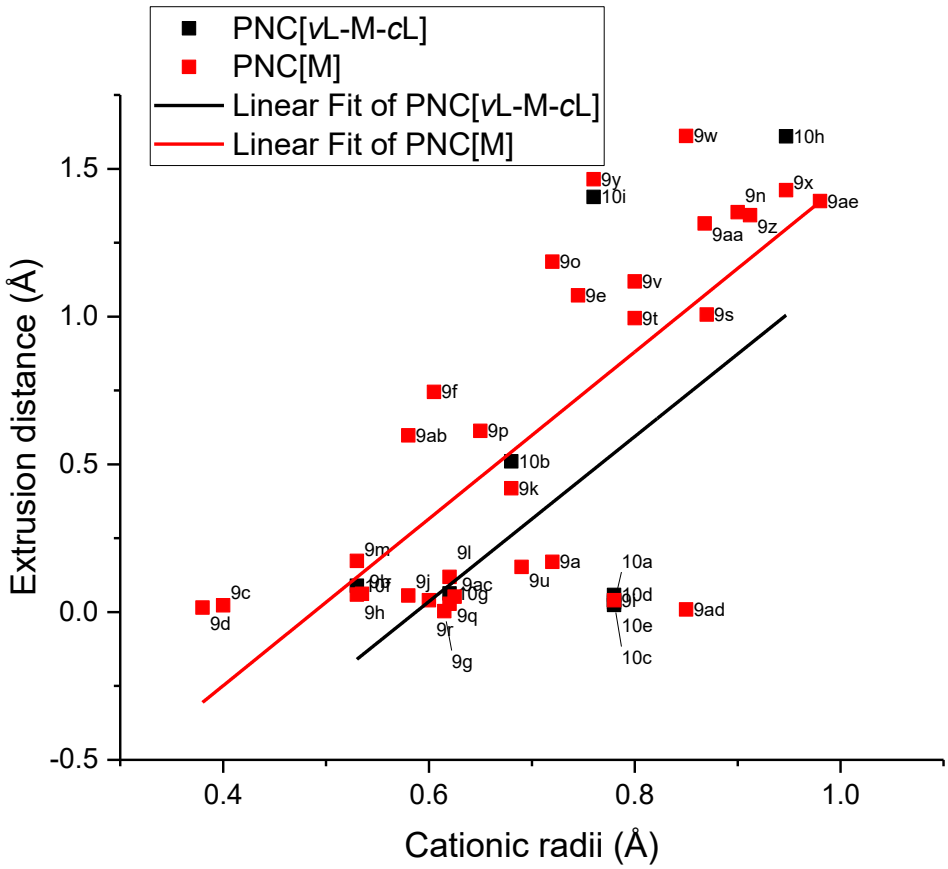

Figure 2.100. Plot of different PNC[M] with axial ligands indicating the flexibility of the extrusion of the metal in the cavity of the macrocycle.

Table 2.9 provides the data for 30 structures of $(dipPhO)_8PcM$ with various elements (M) in the central cavity of the macrocycle.[40,41] **Table 2.10** included further data with ligands that have been introduced by SCSC transformation or by further synthesis using $(dipPhO)_8PcM$. **Figure 2.100** indicates that there is a strong correlation between the cationic radius[74] (**Table 2.11**) and the metal cation extraction distance both for structure with a single axial ligand (void) and for those with both void and axial sites occupied. **Figure 2.101** shows a similarly strong correlation between cationic radius[74] and curvature of the Pc macrocycle. **Figure 2.102** show the strong positive correlation between metal extrusion and curvature.

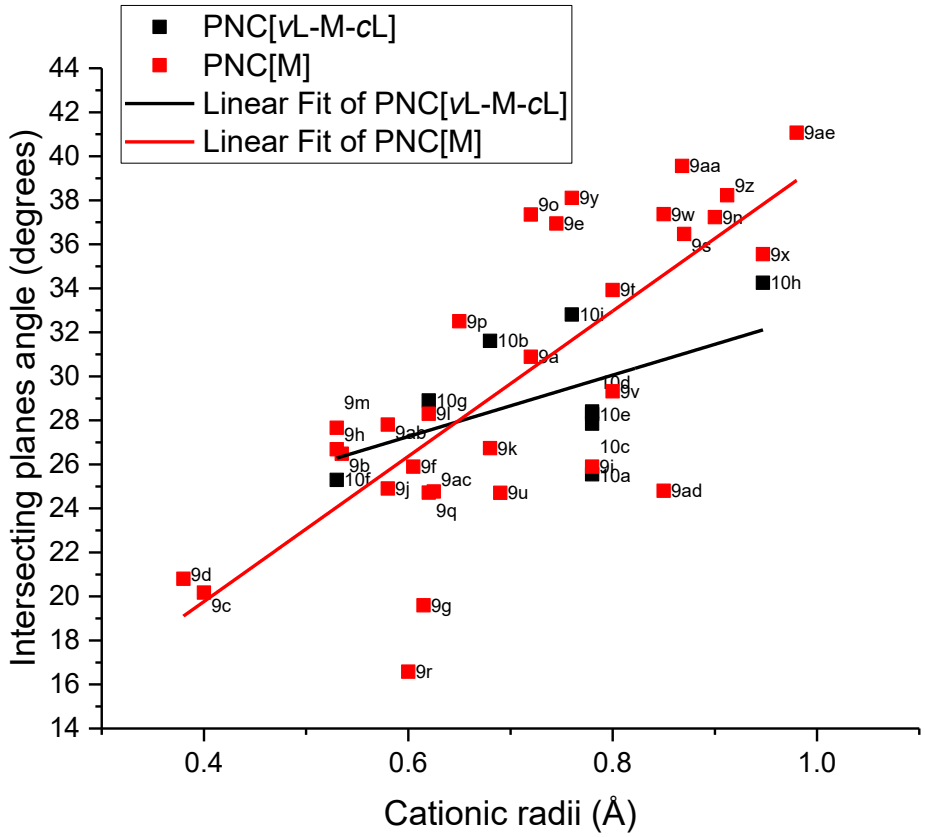

Figure 2.101. Plot of different PNC[M] with axial ligands indicating the flexibility of the phthalocyanine changing the axial ligand.

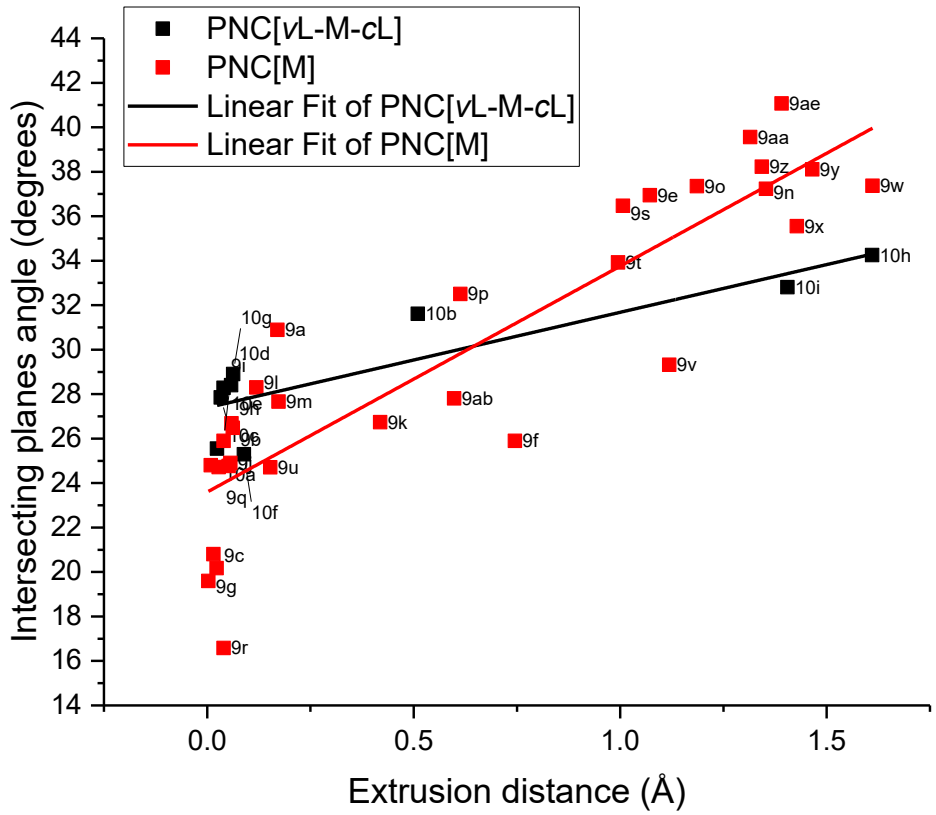

Figure 2.102. Plot of different axial and bidentate ligands of PNC[M] indicating the trend of increasing the curvature of the macrocycle with the extrusion of the metal from the phthalocyanine.

Acronym	Charge	Coordination	HS / LS	Crystal radius	Ionic radius	Phthalocyanine curvature (degrees)	Metal to macrocycle distance (Å)
$(dipPhO)_8PcH_2$	1	I		-0.24	-0.38	0	0
$(dipPhO)_8PcH_2$	1	I		-0.24	-0.38	0	0
$(dipPhO)_6subPcB$	3	IV		0.25	0.11	0	0
$(dipPhO)_6subPcB$	3	IV		0.25	0.11	0	0
$(dipPhO)_6subPcB$	3	IV		0.25	0.11	0	0
PNC[Mg]	2	VI		0.86	0.72	30.89	0.170
PNC[Al]	3	VI		0.675	0.535	26.48	0.062
PNC[Si]	4	VI		0.54	0.4	20.17	0.023
PNC[P]	5	VI		0.52	0.38	20.8	0.015
$(dipPhO)_8PcK$	1	IV		1.51	1.37	0	0
PNC[Sc]	3	VI		0.885	0.745	36.94	1.072
PNC[Ti]	4	VI		0.745	0.605	25.9	0.745
PNC[Cr]	3	VI		0.755	0.615	19.6	0.003
PNC[Mn]	4	VI		0.67	0.53	26.69	0.059
$(dipPhO)_8PcFe$	2	VI	HS	0.92	0.78	0	0.666
PNC[Fe]	2	VI	HS	0.92	0.78	25.9	0.040
PNC[Fe-*v* Cl]	3	V		0.72	0.58	24.9	0.056
$(dipPhO)_8PcCo$	2	IV	HS	0.72	0.58	0	0
$(dipPhO)_8PcNi$	2	IV		0.69	0.55	0	0
$(dipPhO)_8PcCu$	2	IV		0.71	0.57	0	0
PNC[Zn]	2	V		0.82	0.68	26.74	0.419
PNC[Ga]	3	VI		0.76	0.62	28.3	0.119
$(dipPhO)_8PcGe$	4	VI		0.67	0.53	0	0
PNC[Ge]	4	VI		0.67	0.53	27.66	0.173
PNC[Y]	3	VI		1.04	0.9	37.23	1.353
PNC[Zr]	4	VI		0.86	0.72	37.35	1.186
PNC[Mo]	4	VI		0.79	0.65	32.5	0.613
PNC[Ru]	4	VI		0.76	0.62	24.72	0.028
PNC[Rh]	4	VI		0.74	0.6	16.58	0.040
PNC[Pd]	2	IVSQ		0.78	0.64	29.05	0.069
$(dipPhO)_8PcAg$	2	IV		0.93	0.79	0	0
PNC[Cd]	2	V		1.01	0.87	36.47	1.007
PNC[In]	3	VI		0.94	0.8	33.92	0.995
PNC[Sn]	4	VI		0.83	0.69	24.71	0.153
PNC[Sb]	3	V		0.94	0.8	29.32	1.119
PNC[Pr]	4	VI		0.99	0.85	37.37	1.611
PNC[Eu]	3	VI		1.087	0.947	35.55	1.428
PNC[Tb]	4	VI		0.9	0.76	38.11	1.465
PNC[Dy]	3	VI		1.052	0.912	38.23	1.343
PNC[Yb]	3	VI		1.008	0.868	39.56	1.315
$(dipPhO)_8PcHf$	4	VI		0.85	0.71	36.34	1.147
PNC[Re]	5	VI		0.72	0.58	27.81	0.598
PNC[Ir]	4	VI		0.765	0.625	24.77	0.052
PNC[Au]	3	VI		0.99	0.85	24.8	0.009
PNC[Pb]	2	IV		1.12	0.98	41.07	1.391
$(dipPhO)_8PcTh$	4	VI		1.08	0.94	33.52	1.514

Table 2.11. Correlation of ionic radius of metals, extrusion distance and curvature of the phthalocyanines

2.10 Conclusions

Within this chapter, the synthesis of a variety of metal phthalocyanines was described, along with their crystallographic analysis, which further indicates the structural versatility of this cubic system. Each complex was found to crystallise in the cubic space group $Pn\bar{3}n$. In particular, interesting porous crystals were prepared from complex of $(dipPhO)_8PcM$ with large metal cations, where they displayed a significant effect on the curvature on the phthalocyanine macrocycle, and a large deviation of the metal from the plane of the pyrrolic nitrogen. Furthermore, detailed analysis was conducted on the extrusion distance and curvature versus the ionic radii of the metals. The updated PNC periodic able is shown in **Figure 2.103**.

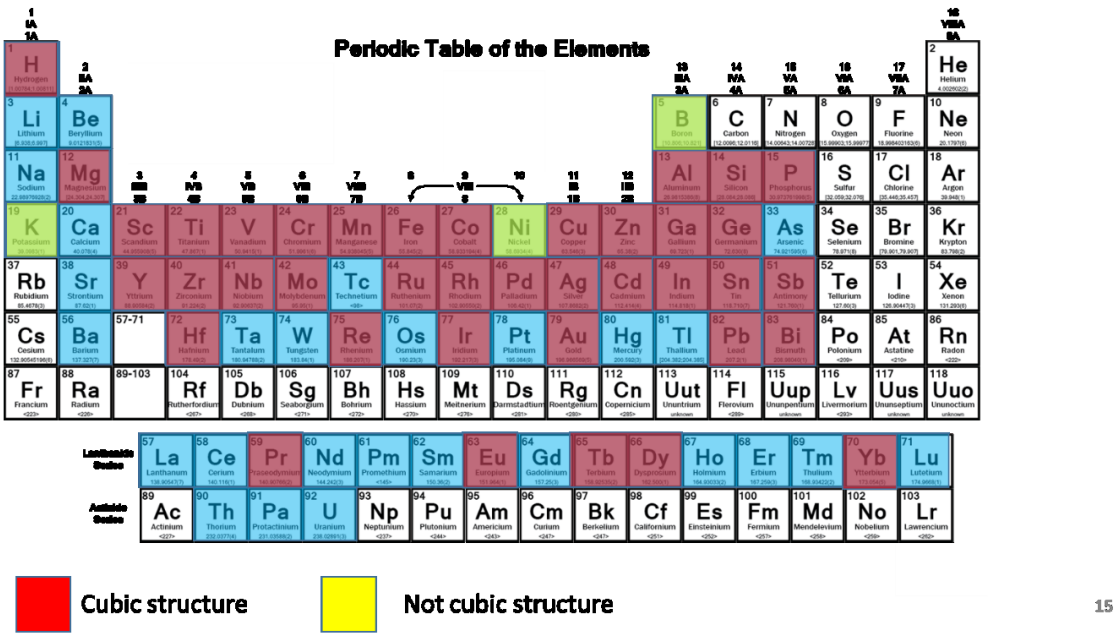

Figure 2.103. Periodic table depicting the state of play at the end of the PhD program with blue shading for elements that form complexes with phthalocyanines, red shading for the elements that form cubic nanoporous complexes with $(dipPhO)_2Pc$ and with yellow shading for the elements that do not form cubic structure as characterised by sc-XRD analysis.

Chapter III.

Phthalocyanine nanoporous co-crystals

3.1 Introduction

Previous work in the McKeown group showed that the formation of co-crystals by the insertion of bidentate ligands[40,41] or fullerenes,[50] such as C_{60} and C_{70}, proved to be successful in avoiding structural collapsing during solvent removal. In addition, fullerenes favoured the formation of cubic crystals for those phthalocyanine derivatives such as $(dipPhO)_8PcH_2$ and $(dipPhO)_8PcCu$ which previously formed crystals with different symmetry.[50] Suitable bidentate ligands were bipyridine (bipy) and 1,4-phenylene diisocyanide. These act as "wall-ties", preventing the collapse of the cubic nanoporous structure upon desolvation, but also because of their different electron configuration, they are likely to influence the properties of the metal in the phthalocyanine. Reported in this chapter is work on a new wall-tie, bipyrimidine (bpm), which was assumed to possess an additional metal binding site. The target by adding another metal on the bidentate ligand was to notice if there is any interaction between the macrocyclic metals with the bidentate ligand metal and analyse it with EPR or NMR and check the reactivity of the metal that would bind. In addition, co-crystallisations of $(dipPhO)_8PcM$ complexes with metal-free or metallated tetraphenylporphyrins was also found to form the cubic nanoporous structure, including co-crystals with $(dipPhO)_8PcH_2$, $(dipPhO)_8PcCu$ and $(dipPhO)_8PcNi$, which previously formed crystals with different nonporous structures. These concepts were combined by the *in-situ* and SCSC insertion of bidentate ligands within co-crystallised phthalocyanine and porphyrin components providing stability to the structure even upon desolvation. The exploration of metal to metal interactions through space was the primary target for the addition of the porphyrin through EPR spectroscopy, since it is of major interest, as well as to detect if the binding strength to gasses would change. The synthesis and crystallographic characterisation of these complexes will be discussed. As aforementioned, note that the legends shaded in red indicate structures obtained during the PhD programme.

3.2 Synthesis of 4,4'-bipyrimidine (bpm)

The synthesis of this bidentate ligand was achieved readily by performing a sodium metal mediated coupling of pyrimidine (**Scheme 3.1**).[75]

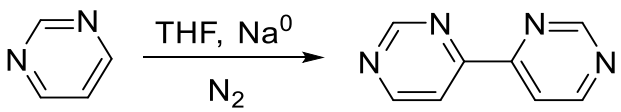

Scheme 3.1. Reaction scheme of bipyrimidine.

3.3 Preparation of PNC[M-*c*bipy-M] and PNC[M-*c*bpm-M] complexes

The stabilization of the phthalocyanine nanoporous crystal structure was successfully performed by the insertion of bipyridine (bipy) or bipyrimidine (bpm) bidentate ligands. The incorporation was achieved either by solubilising both the phthalocyanine and the bidentate ligand and then inducing co-crystallisation by the slow diffusion of a non-solvent or by introducing the bidentate ligand to the non-solvent in contact with premade phthalocyanine crystals to effect single crystal to single crystal transformation or *in-situ* coordination (**Figure 3.1**).

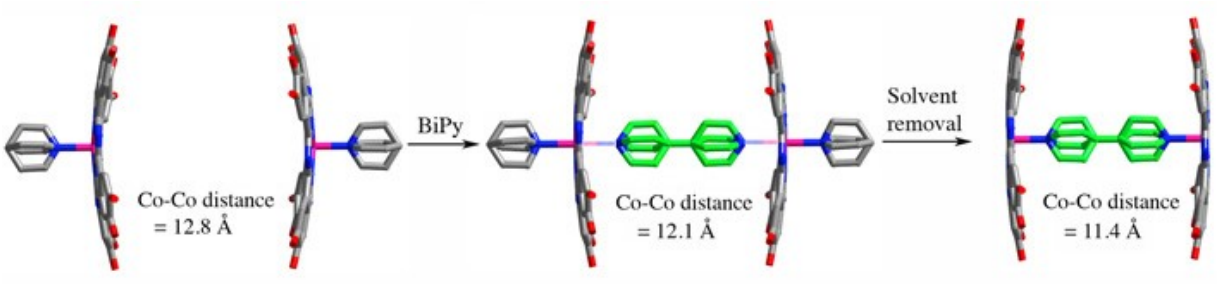

Figure 3.1. Single-crystal to single-crystal transformation by the insertion of bipy. First structure has a pyridine as axial ligand, while in the second structure a bidentate ligand was incorporated reducing the distance between two metals. In the third structure the removal of the solvent and axial ligand (pyridine) was performed, and further reduction of metal to metal distance was observed.[40]

3.4 Crystallographic analysis of PNC[M-*c*bpm-M]

XRD analysis was performed on the novel PNC[*v*py-Co-*c*bpm-Co-*v*py] (**Figure 3.2**) showing that the bpm was successfully incorporated by either co-crystallisation or SCSC transformation and it was coordinated to the two metal cations across the cavity. As previously observed for the bipy

ligand, the distance between the two phthalocyanines was reduced from 12.8 to 11.3 Å on bpm insertion. The bpm is disordered over 4 positions by symmetry. PNC[*v*H_2O-Co-*c*bpm-Co-*v*H_2O] was analysed at Beamline I19 of the Diamond Light Source (DLS) in a gas cell sc-XRD experiment (see below). When it was in ambient environment, water occupied the axial position with 100% occupancy. When high vacuum was applied to the system the water molecule was evacuated totally and crystal order was maintained.

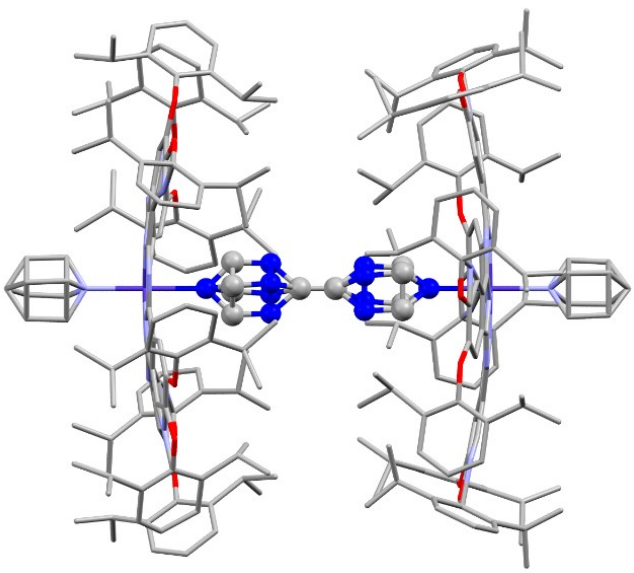

Figure 3.2. Molecular structure of PNC[*v*py-Co-*c*bpm-Co-*v*py] edge-on projection.

Similarly the bpm bidentate ligand was shown to be incorporated into PNC[*v*tBuNC-Fe-*c*bpm-Co-*v*tBuNC] XRD analysis (**Figure 3.3**) and caused a reduction of the distance between the two phthalocyanines.

For both complexes, an insufficient amount of material was prepared to prove permanent porosity using gas adsorption.

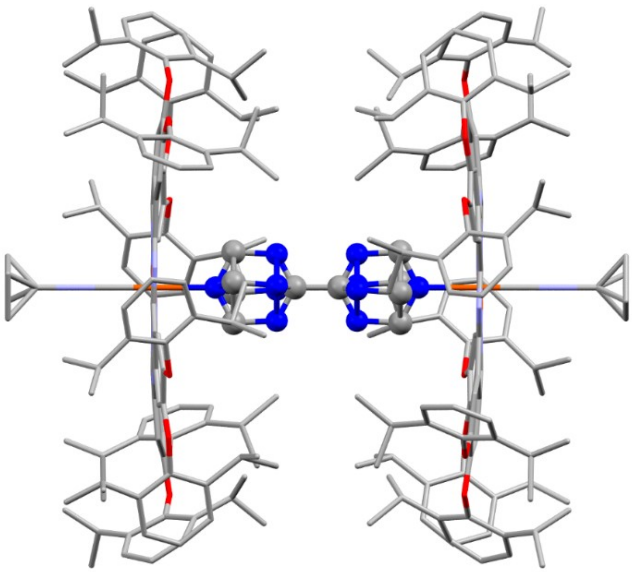

Figure 3.3. Molecular structure of PNC[*v*tBuNC-Fe-*c*bpm-Co-*v*tBuNC] edge-on projection.

3.5 PNC[Co-cbipy-Co] and PNC[Co-cbpm-Co] comparison with gas cell XRD experiment

The chemisorption of carbon monoxide (CO) and nitric oxide (NO) at the open Co^{2+} axial binding sites in two phthalocyanine nanoporous crystals (PNCs) with bipy (PNC[Co-*c*bipy-Co]) or bpm (PNC[Co-*c*bpm-Co]) wall ties was examined *in-situ* by synchrotron single crystal X-ray crystallography using a gas cell attached to Beamline I19 of the Diamond Light Source (DLS) in collaboration with Dr. Charlie McMonagle, Dr. Stephen Moggach (both UoE), Gemma Turner (UWA) and Dr. Mark Warren (DLS). Complete activation of the nanovoid binding sites was not observed after heating the crystals to 300 K under vacuum (10^{-6} mbar), so gas loading into the pores was carried out in the presence of a small quantity of residual crystallisation solvent or adsorbate. No chemisorbed solvent was found in the partially evacuated macrocycle by X-ray crystallography.

Crystallographic refinement and uptake data for PNC[Co-*c*bipy-Co] and PNC[Co-*c*bpm-Co] during gas loading and evacuation are given in **Table 3.1**. Dosing PNC[Co-*c*bipy-Co] and PNC[Co-*c*bpm-Co] with NO at 2.63 bar and 4.28 bar, respectively, led to the irreversible chemisorption of nitrosyl at the open Co^{2+} axial coordination sites in a single crystal to single crystal (SCSC) transformation.

The respective Co-NO bond distances of 1.882 Å and 1.935 Å and CoNO angles of 118.63° and 116.26° in PNC[Co-*c*bipy-Co] and PNC[Co-*c*bpm-Co] in the partially evacuated structures are close to the reported values in porphyrin[76] and cobalamin[77] complexes (Co-NO = 1.828 – 1.940 Å, CoNO = 121.23 – 123.73°).

The bent coordination geometry of the chemisorbed nitrosyl is unsurprising for cobalt phthalocyanine complexes, which may be expressed as $\{CoNO\}^8$ in Enemark-Feltham nomenclature.[78] The superscript refers to the number of π-electrons in metal-nitrosyl fragment. Metal-nitrosyl complexes rich in π-electrons (> 6) are characterised by anionic NO^- ligands that form a covalent bond with the metal instead of a dative coordination bond, as is formed by linear cationic nitrosyls, NO^+. The lone-pair on the nitrosyl N-atom distorts the nitrosyl π^*-anti-bonding LUMO out of the plane of the Co^{2+} d-orbitals leading to attenuation of the metal-to-ligand back-bonding and lessening of the *trans*-effect of the 4,4'-bipyridyl and 4,4'-bipyrimidyl ligands on the strength of the Co-NO binding. However, the *trans*-effect of the 4,4'-bipyridyl and 4,4'-bipyrimidyl wall ties in PNC[Co-*c*bipy-Co] and PNC[Co-*c*bpm-Co] is still considerable.

The comparison of the occupancy of the coordinated N-atom of the nitrosyl ligand during crystallographic refinement for the dosed phthalocyanines indicated a NO uptake of 0.40 mmol g^{-1} in PNC[Co-*c*bipy-Co] and an uptake of 0.33 mmol g^{-1} in PNC[Co-*c*bpm-Co] (*ca*. theoretical NO uptakes of 0.484 mmol g^{-1} and 0.485 mmol g^{-1}, respectively). These values are comparable to the ~0.8 mmol g^{-1} NO uptake reported in a Ca-based metal-organic framework, BioMIL-3 at 1 bar of loading pressure, which is a promising material for the controlled release of NO in biomedical applications.[79] Subsequent treatment of the crystals under vacuum resulted in a 17.9% loss of the chemisorbed NO from PNC[Co-*c*bipy-Co] and a 27.4% loss from PNC[Co-*c*bpm-Co], according to the decrease in the nitrosyl N-atom q-peak intensity.

The uptake behaviours of the macrocycles may reflect the electronic properties of the *trans*-ligands. Higher gas uptake and retention under vacuum for PNC[Co-*c*bipy-Co] over PNC[Co-*c*bpm-Co] is expected due to the lesser ability of the 4,4'-bipyridyl ligand to participate in back-bonding with the Co^{2+} centre compared with the 4,4'-bipyrimidyl ligand, which increases the strength of the metal-nitrosyl or metal-carbonyl bond. This effect is also seen in the increase of the CoNO

angle in the nitrosyl complexes by 2.37° from PNC[Co-*c*bpm-Co] to PNC[Co-*c*bipy-Co], which corroborates previously reported ^{15}N NMR studies where larger CoNO angles are observed in complexes with more shielding ligand sets.[80]

A considerably lower uptake of CO compared with NO was observed for both crystals when dosed with CO at 5 bar of loading pressure. The Co^{2+} binding sites in PNC[Co-*c*bipy-Co] remained vacant after gas loading, whilst a quarter of sites were occupied by CO in PNC[Co-*c*bpm-Co], corresponding to an uptake of 0.12 mmol g^{-1}. The measured Co-CO bond length of 1.644 Å is in agreement with bond distances reported in the literature (1.786 – 1.855 Å).[81,82] Uptake of CO in PNC[Co-*c*bpm-Co] is assumed to be fully reversible , owing to the short Co-CO bond measured in the evacuated structure (**Table 3.1**), the small q-peak corresponding to the carbonyl C-atom (< 1 e^-) and the instability of the structure model during crystallographic refinement. Counterintuitively, a larger uptake of CO is seen in the 4,4'-bipyrimidyl containing macrocycles where the Co^{2+} binding sites are less electrophilic than its 4,4'-bipyridyl counterpart. Further experiments are required to determine the cause of this discrepancy.

Whilst the capability of phthalocyanine nanoporous crystals to coordinate small molecular species at the open metal sites situated in the void has previously been recognised,[40,41] the electronic *trans*-effect of the ligands on the binding site adsorption properties is unreported. Demonstrably, modifications of the *trans*-ligand, which is achieved in a facile SCSC transformation, can change the NO and CO uptake capabilities of the open cobalt binding site, offering the possibility of the crystals with tuneable adsorption and desorption kinetics. The partially reversible chemisorption of NO in the voids of PNC[Co-*c*bipy-Co] and PNC[Co-*c*bpm-Co] is promising for the potential application of these materials as hosts for the controlled delivery of NO in biomedical settings, or as anti-thrombotic lining materials for catheters and stents.[83]

According to the review[84] and a publication by Jeffrey Long,[85] metal organic frameworks have been widely used for gas sorption studies, but the main difference between the present system and MOFs is that the first can be solubilized and reassemble to the nanoporous structure while the latter cannot. So, the next step after the insertion of the bpm in the cavity was to determine what changes are made on the metal between bipy and bpm. The two systems were examined

by gas cell XRD experiments to see the reactivity of the metal centre with different gases and to observe if there would be physisorption or chemisorption.

The procedure for both samples was performed at 180 K unless other specified. Initially, a data set of the crystal was obtained under ambient conditions, then high vacuum was applied for at least 10 minutes in order to determine if the samples' crystallinity is retained. The gas cell was then loaded with 5.00 bar of CO and the dataset collected to determine if there is binding of the CO at the metal. High vacuum was then applied in order to remove the CO and the system was purged with nitrogen and the high vacuum was reapplied for at least 20 minutes. After that the system was filled with 4.28 bar of NO gas and the dataset was collected. Lastly, sequential high vacuum and nitrogen purge was applied to attempt removal of the NO.

PNC[Co-*c*bipy-Co] was found to be stable under high vacuum. No change to the electron density around the axial metal site was observed on applying 5.00 bar of CO gas within the gas cell. Following a repeated evacuation at high pressure, the crystal was exposed to 4.28 bar of NO gas and crystallography showed that NO was successfully bound to the metal centre. The application of both high vacuum and heat did not result in the release of the NO.

For PNC[Co-*c*bpm-Co], following the same procedure, CO was reversibly bound to the metal suggesting that the electronic properties of the bpm wall-tie ligand provided a more active metal centre. NO was bound irreversibly at 2.63 bar.

Table 3.1. Uptake of NO and CO in PNC[Co-*c*bipy-Co] and PNC[Co-*c*bpm-Co] during gas loading and evacuation. Vacuum is at 10^{-6} mbar for 10 min after NO dosing and 43 min after CO dosing. Q1 is the unassigned donor nitrogen or carbon atom in the NO or CO ligand. Theoretical uptake values of NO and CO in PNC[Co-*c*bipy-Co] and PNC[Co-*c*bpm-Co], respectively, are 0.484 g $mmol^{-1}$ and 0.485 g $mmol^{-1}$.

	PNC[Co-*c*bipy-Co-*v*NO]		PNC[Co-*c*bpm-Co-*v*NO]		PNC[Co-*c*bpm-Co-*v*CO]	
	2.63 bar NO	Vacuum	4.28 bar NO	Vacuum	5 bar CO	Vacuum
T (K)	180	298	180	298	180	298
*q*1 (e^-)	5.78	4.74	4.68	3.40	1.71	0.93
Uptake (%)	82.6	67.7	66.9	48.6	24.4	13.3
Uptake (g mmol-*1*)	0.40	0.33	0.32	0.24	0.12	0.06
Co-L (Å)	1.880	1.904	1.859	1.936	1.644	1.193
CoNO (°)	122.2	118.3	120.4	116.2	180.0	180.0

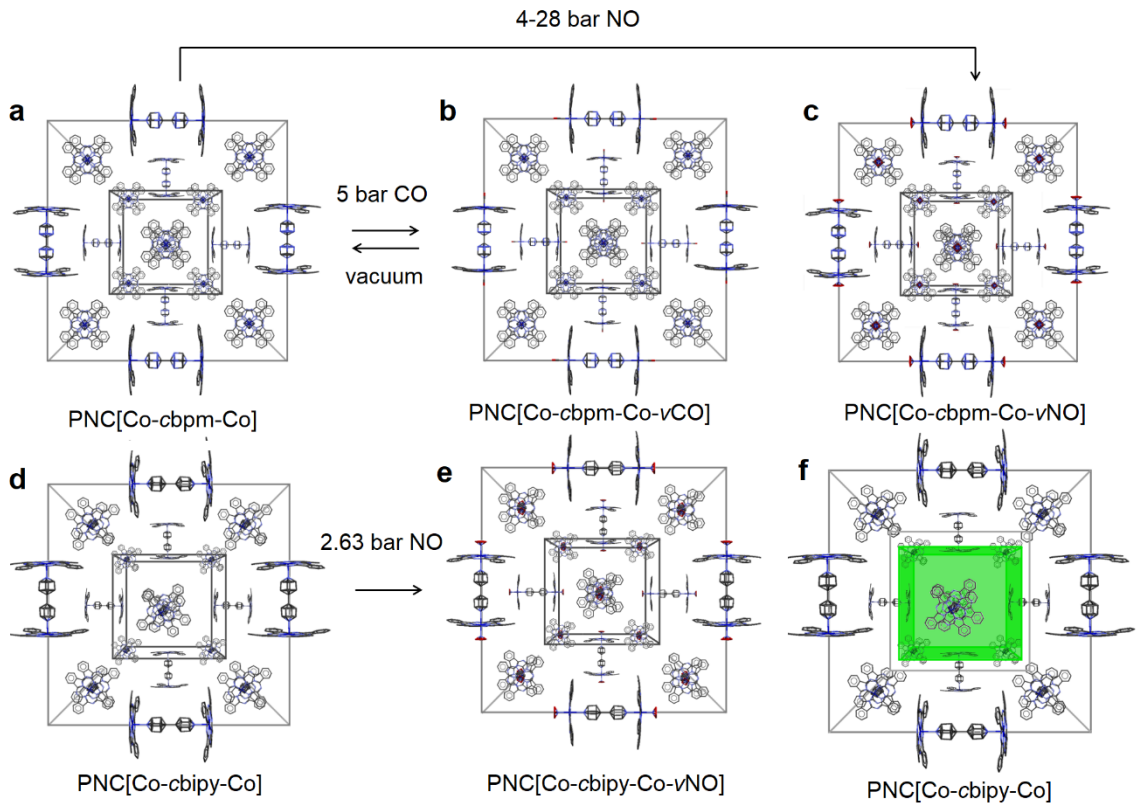

Figure 3.4. Crystal structure of a. PNC[Co-*c*bpm-Co] before gas loading, b. after loading with 5 bar CO showing reversibility under vacuum and c. after loading with 4.28 bar NO. Crystal structure of d. PNC[Co-*c*bipy-Co] before gas loading and e. after loading with 2.63 bar NO. f. Crystal structure of PNC[Co-*c*bipy-Co] with the void highlighted in green.

3.6 Brief introduction to cw-EPR[86]

The energy differences studied in EPR spectroscopy are due predominately to the interaction of an unpaired electron in the sample with a magnetic field, B_0, produced by a magnet in the apparatus. This effect is called the Zeeman effect. Because the electron has a magnetic moment, it acts like a compass or a bar magnet when it is placed in a magnetic field. Since energies are quantized, a single unpaired electron has only two allowed energy states. It has a state of lower energy when the moment of the electron, μ, is aligned with the magnetic field and a higher energy state when μ is aligned against the magnetic field (**Figure 3.5**). The difference between the energies of these two states, caused by the interaction between the electron spin and the magnetic field, is shown in:

$$\Delta E = g\mu_B B_0 \Delta m_s = g\mu_B B_0$$

where g is the g-factor, μ_B is the Bohr magneton, which is the natural unit of the electron's magnetic moment, and the change in spin state is $\Delta m_s = \pm 1$. The energy, $\Delta E = h\nu$, that is required to cause a transition between the two spin states is given by $\Delta E = h\nu = g\mu_B B_0$ and $\mu_B = g_e \beta / 2$.

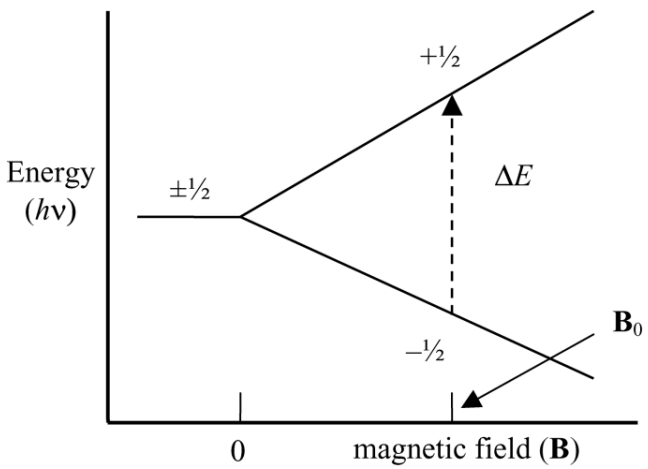

Figure 3.5. When the magnetic field is scanned, the energies of the two spin states of an unpaired electron diverge.

Because the energy difference between the two spin states can be varied by changing the magnetic field strength, there are two potential approaches to obtaining spectra. The magnetic field could be held constant while the frequency of the electromagnetic radiation is scanned,

which would be analogous to UV-VIS spectroscopy. Alternatively, the electromagnetic radiation frequency could be held constant while the magnetic field is scanned as shown in **Figure 3.5**. Absorption of energy occurs when the magnetic field "tunes" the two spin states such that the energy difference matches the energy of the applied radiation. This field is called the "field for resonance". Because of difficulties in scanning microwave frequencies and because of the use of a resonant cavity for signal detection, most EPR spectrometers operate at constant microwave frequency and scan the magnetic field.

The samples contain a large number of spins allocated in the continuous magnetic field between the two allowed states. The relative population of the two states is described with the Boltzmann distribution:

$N_+/N_- = \exp(\Delta E/kT)$

where k is the Boltzmann constant and T is the temperature of the sample. For the uncoupled electron with g_e = 2.0023, the ratio of spin population is around 1.0015 in a 3400 Gauss field. The magnetic field in the resonance frequency v_0 causes transitions with same probability.

The population of the lower energy state is bigger than that of the higher energy state, causing a large number of transitions towards the higher energy state, with distinctive absorption of energy from the sample. This phenomenon is the basis for the simple continuous wave EPR experiment. The sample has paramagnetic species, which gets excited with microwave radiation with constant frequency whilst the magnetic field is changing (scanning).

3.7 PNC[Co-*c*bpm-Co] single crystal, powder and frozen solution cw-EPR experiments

The chemisorption of oxygen (O_2) as a superoxide radical at the open Co^{2+} axial binding sites in two phthalocyanine nanoporous crystals (PNCs) with bipy (PNC[Co-cbipy-Co]) or bpm (PNC[Co-cbpm-Co]) wall ties was examined *in-situ* by continuous-wave (cw) electron paramagnetic resonance (EPR) using a Bruker X-band EPR spectrometer equipped with a goniometer that enables a 360^o crystal rotation around a chosen direction in collaboration with Dr. Floriana Tuna of the EPSRC National EPR facility.

Given the cubic symmetry of the crystal and existence of dimeric molecules that pack perpendicularly to one another, the single crystal was oriented such that the *z*-axis (which is along bpm) of one of such PNC[Co-*c*bpm-Co] dimers is perpendicular to the magnetic field of the EPR setup; by symmetry, same axis is also parallel to the *x,y* plane of the PNC-Co entities belonging to another dimer that packs perpendicularly to the first one. Thus, the crystal was rotated around this axis and collected spectra at room temperature at every 10 degrees, in order to identify an orientation that brings the *z*-axis of one of the dimers parallel with the magnetic field, while also placing the *x,y* plane of another dimer perpendicular to the magnetic field. Such orientation allows the extraction of both the g_z and $g_{x,y}$ values, as well as the ^{59}Co hyperfine coupling constants, A_z and $A_{x,y}$. Because of the high symmetry of the crystal, spectra recorded at every 90 degrees display identical spectral features (**Figures 3.6, 3.7**).

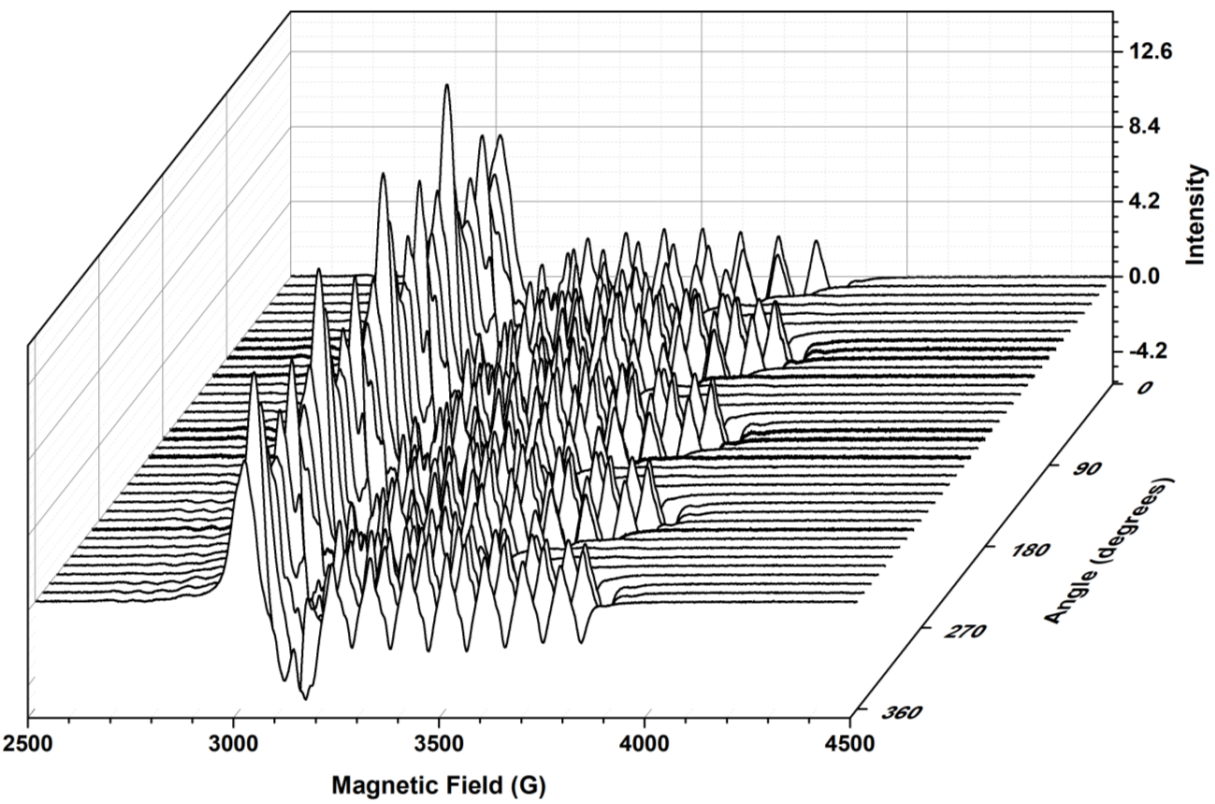

Figure 3.6. Waterfall representation of the X-band cw-EPR spectra of a single crystal of PNC[Co-*c*bpm-Co] that has followed rotation by 10 degrees around the z-axis of one of the dimers present in the structure.

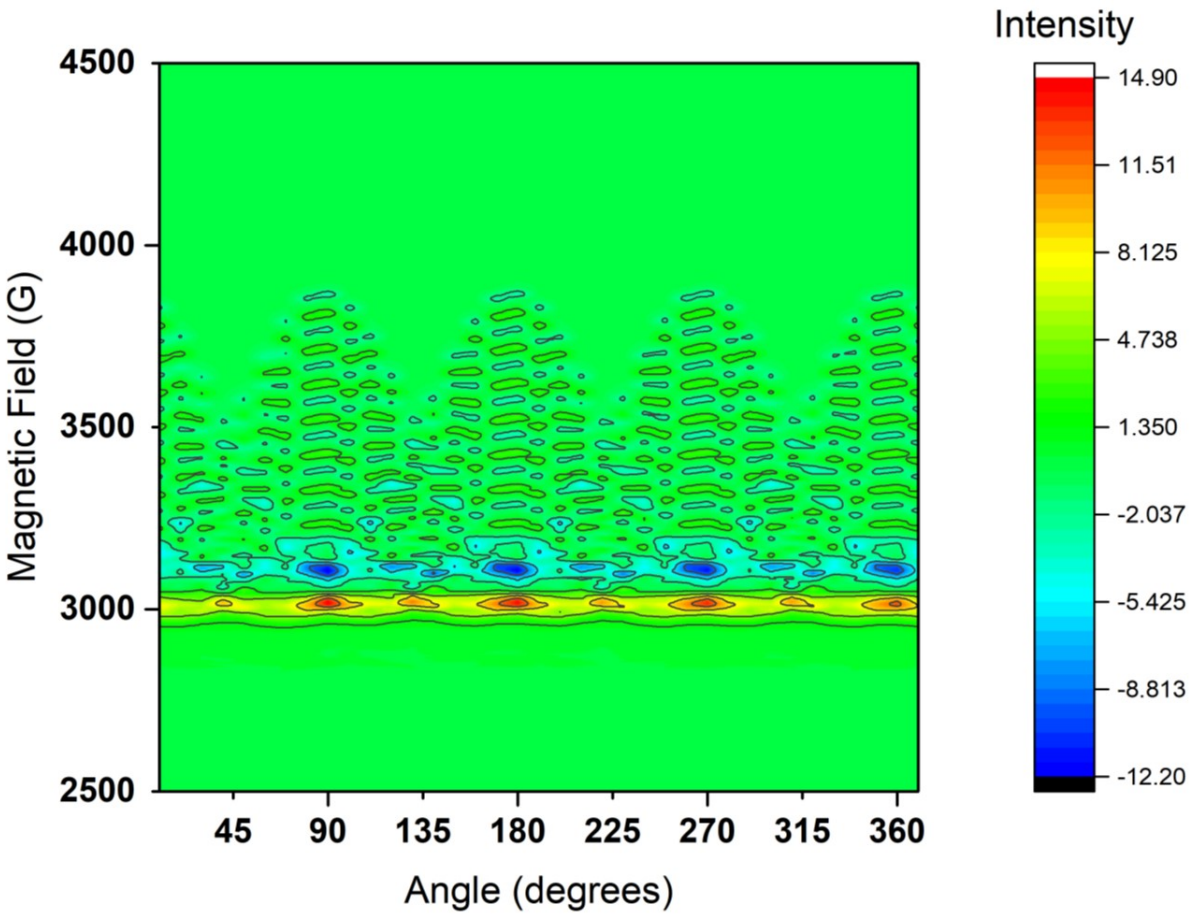

Figure 3.7. 2D representation of the X-band cw-EPR spectra of a single crystal of PNC[Co-*c*bpm-Co] that has undergone rotation in similar conditions as noted in **Figure 3.6**.

An EPR road map study of one well oriented PNC[Co-*c*bpm-Co] single crystal are presented in **Figure 3.6-3.8** and discussed below. Hyperfine coupling structure of Co^{2+} ion coordinated to a phthalocyanine $(dipPhO)_8PcCo$ was detected and analysed for angular dependence at room temperature. EPR spectra for PNC[Co-*c*bpm-Co] and its angular dependence exhibited the presence of five equivalent centres in the crystal at 80, 170, 260, 350 and 440 degrees (**Figure 3.8**) and the linewidths for all centres remain practically constant in the measured temperature range.

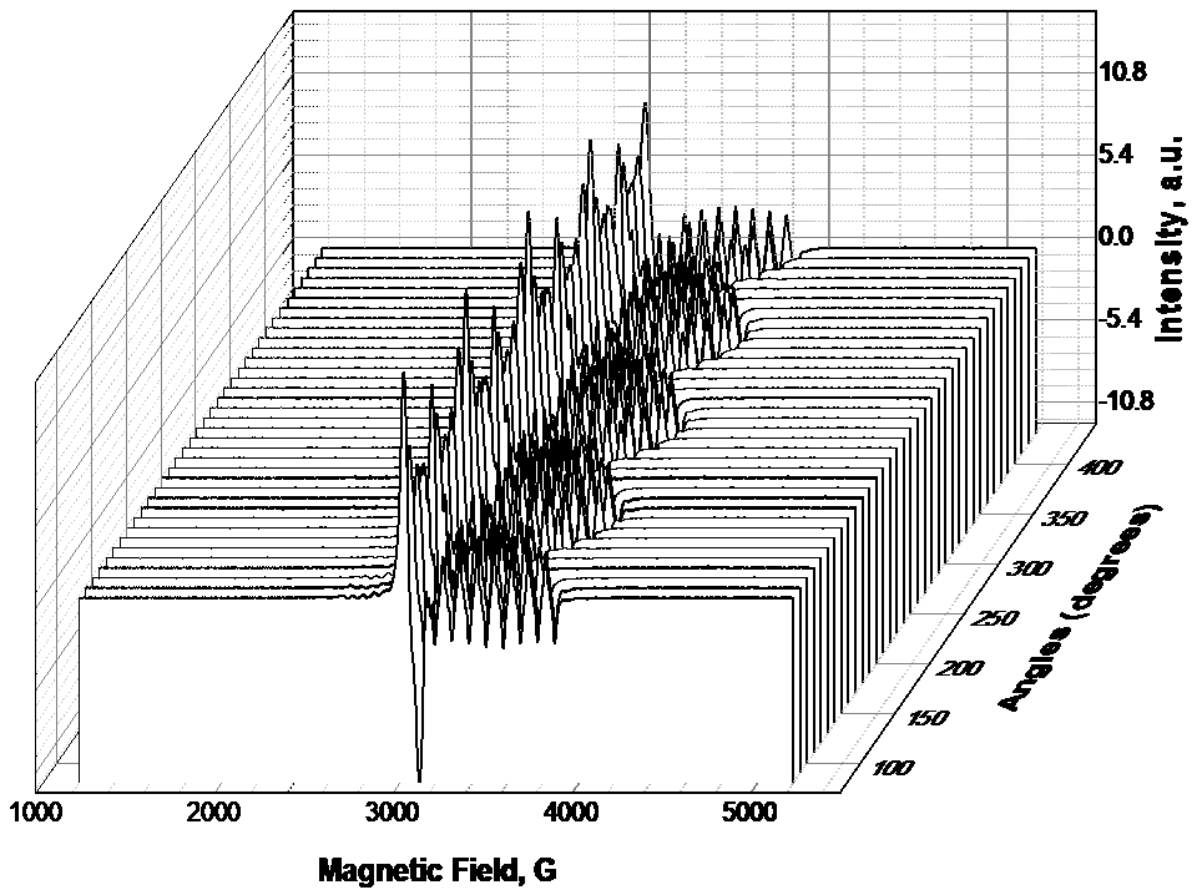

Figure 3.8. EPR road map of PNC[Co-*c*bpm-Co] single crystal.

Cobalt(II) has two isotopes ^{59}Co and ^{60}Co with natural abundance of 100 and 0% respectively. A characteristic of the EPR spectrum for PNC[Co-*c*bpm-Co] crystal is a strong central line from g_{xy} components and the eight lines (I = 7/2) splitting to the right side correspond to hyperfine transitions from g_z component.

Next, the most shifted spectrum (260 °) was chosen in order to obtain key parameters. As can be seen in **Figure 3.9**, the simulation of the most shifted single crystal spectrum displayed a g_z smaller than g_{xy} with g-factor values of 1.983 and 2.297, respectively, and hyperfine coupling interactions of 35 MHz for the A_{xy} component and 280 MHz for the zeta component (A_z). Moreover, the spectrum revealed nitrogen super hyperfine coupling splitting in the A_z component due to the interaction of the electronic spin of cobalt with the nitrogen nuclear spin (75 MHz).

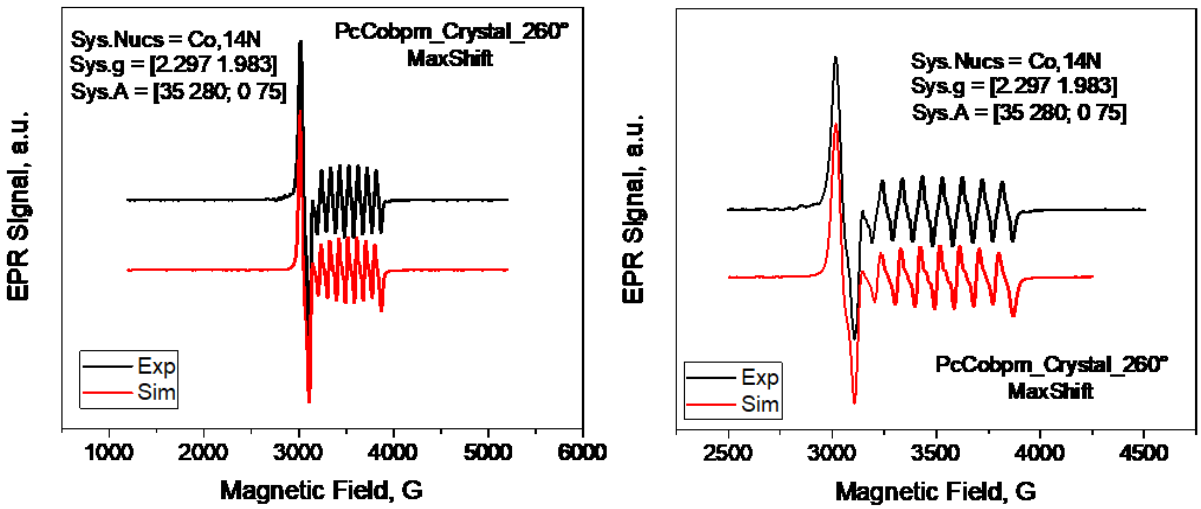

Figure 3.9. EPR spectrum of most shifted PNC[Co-*c*bpm-Co] single crystal.

In order to confirm these results, some measurements from the powder form of PNC[Co-*c*bpm-Co] were performed at room and low temperature. As shown in **Figure 3.10**, the simulation for powder at room temperature presented a g_z smaller than g_{xy} with g-factor values of 2.009 and 2.306, respectively, and hyperfine coupling interaction of 55 MHz for A_{xy} component and 290 MHz for zeta component (A_z). Similar parameters were recorded in cw Q-band.

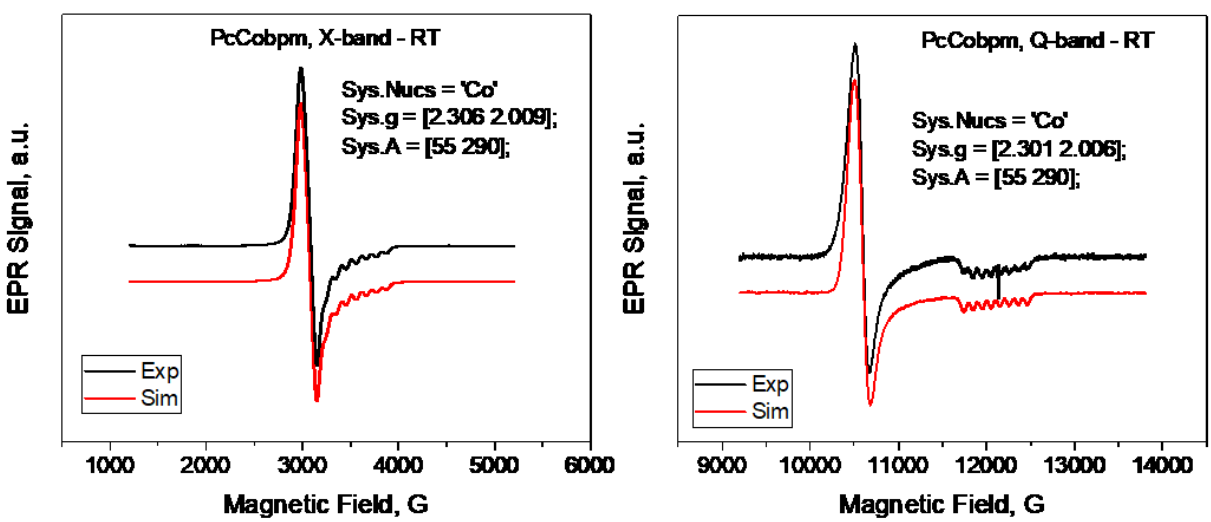

Figure 3.10. EPR spectra of PNC[Co-*c*bpm-Co] in powder obtained using X and Q bands at room temperature.

Thereafter, the temperature was cooled to 77 K and the predominant signal was identified as a strong isotropic superoxide radical with g-factor 2.0075 (**Figure 3.11A**) due to the high interaction of cobalt with the electron of the radical. The parameters found for g_{xy}, g_z, A_{xy} and A_z were 2.285, 2.004, 20 MHz and 295 MHz, respectively. Subsequently, the sample was kept under vacuum using a Schlenk flask tube in order to degas the sample, avoiding the interaction between the metal and paramagnetic oxygen, and a clearer spectrum was obtained (**Figure 3.11B**). However, the parameters found at the degassed sample at 77 K were the same as for the sample containing the superoxide radical signal, as well as of the regasified sample (**Figure 3.11C**) that confirmed its reversibility.

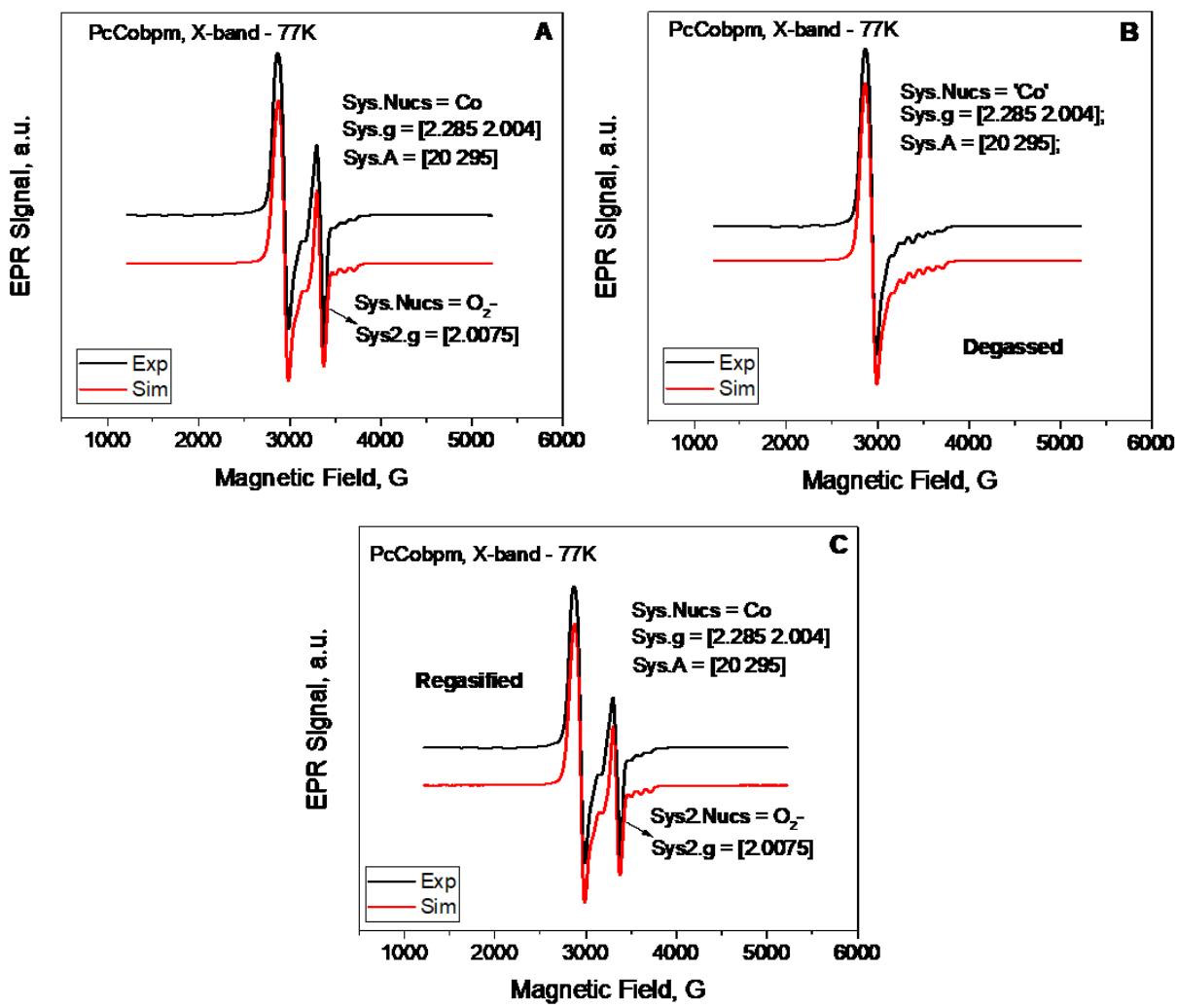

Figure 3.11. X-band powder EPR spectra of PNC[Co-*c*bpm-Co] at 77K.

The spectra of PNC[Co-*c*bpm-Co] in frozen solution (77 K) gave provided more information. As can be seen in **Figure 3.12A**, the spectrum showed the same superoxide radical signal with g-factor 2.0055. However, other features such as nitrogen splitting and at least two different species could be observed, one with $g_z < g_{xy}$ and nitrogen super hyperfine coupling splitting in the A_z and the other with $g_{xy} >> g_z$ without nitrogen splitting. The parameters found for the first species with $g_z < g_{xy}$ were g_{xy} = 2.273, g_z = 2.006, A_{xy} = 0 MHz, A_z = 290 MHz and A_{zN} = 50 MHz, respectively, whereas, the parameters for the second species $g_{xy} >> g_z$ were g_{xy} = 2.270, g_z = 2.849, A_{xy} = 0 MHz, and A_z = 650 MHz, respectively. The solution and a clearer spectrum was obtained (**Figure 3.12B**). However, the parameters found for the first $g_z < g_{xy}$ species in the degassed frozen solution were g_{xy} = 2.282, g_z = 2.018, A_{xy} = 0 MHz, A_z = 290 MHz and A_{zN} = 50 MHz, respectively. In contrast, the parameters for the $g_{xy} >> g_z$ second species were g_{xy} = 2.282, g_z = 2.840, A_{xy} = 0 MHz, and A_z = 650 MHz, respectively. The re-aerated frozen solution (**Figure 3.12C**) demonstrated the return of the superoxide radical signal with g-factor = 2.0055 and the parameters for $g_z < g_{xy}$ are the same as those for the frozen solution before degassing. Nevertheless, the parameters for $g_{xy} >> g_z$ (second species) show a slight shift.

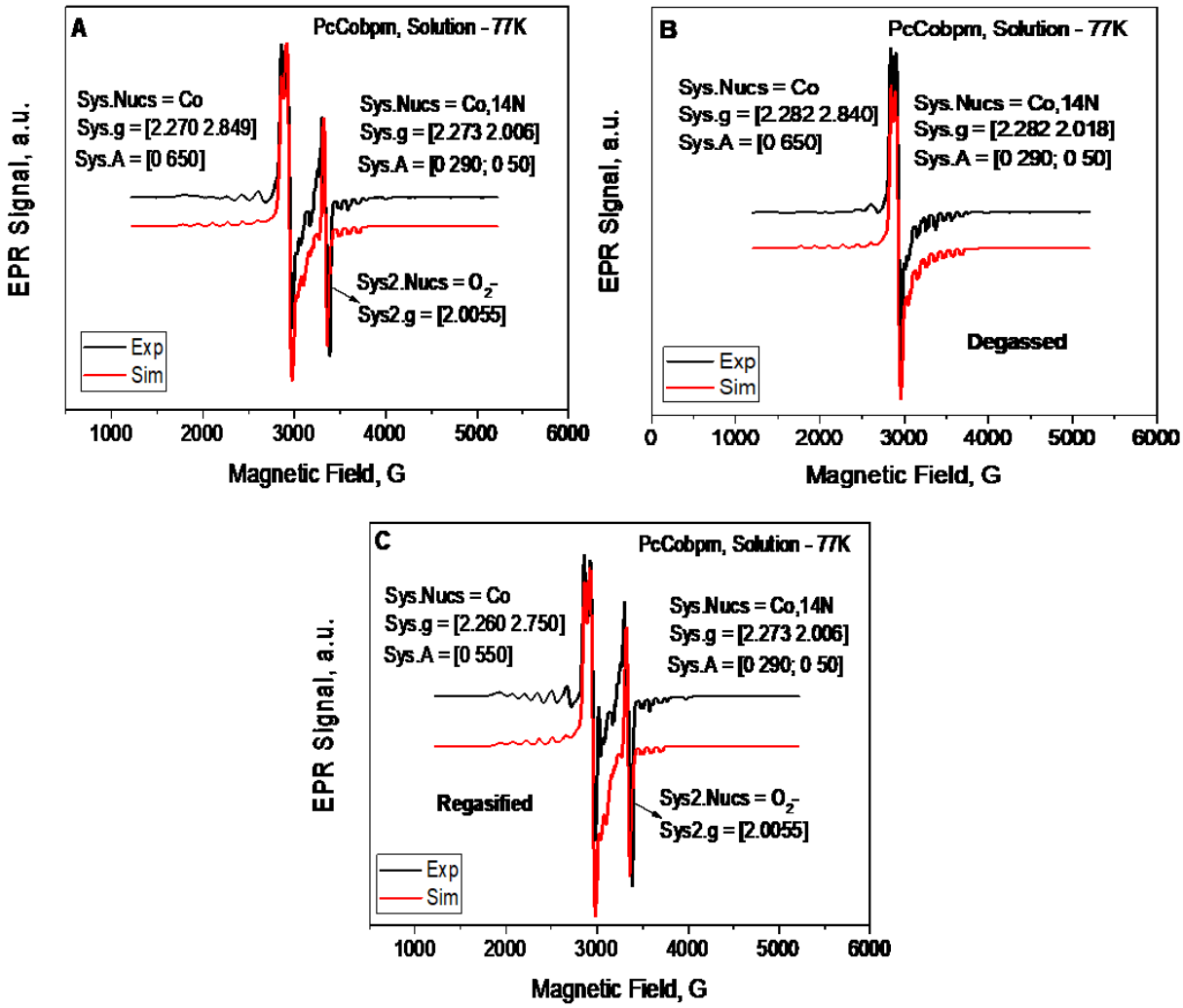

Figure 3.12. X-band frozen solution EPR spectra of PNC[Co-*c*bpm-Co] at 77K.

3.8 PNC[Co-*c*bipy-Co] single crystal, powder, and frozen solution cw-EPR experiments

Figure 3.13 show the spectrum and the simulation of most shifted single crystal spectrum (212 °) of PNC[Co-*c*bipy-Co] displayed a g_z smaller than g_{xy} with g-factor values of 1.948 and 2.353, respectively and hyperfine coupling interaction of 60 MHz for A_{xy} component and 160 MHz for zeta component (A_z). Moreover, the obtained spectrum revealed cobalt super hyperfine coupling splitting in both components due to the interaction of electron spin of cobalt with cobalt nuclear spin, at 60 and 160 MHz.

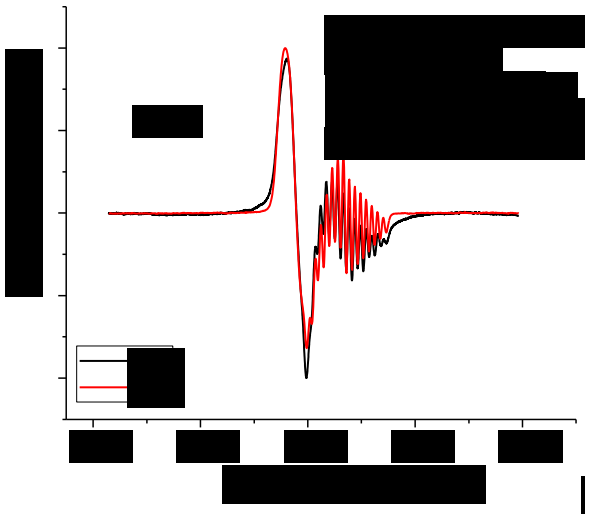

Figure 3.13. EPR spectrum of most shifted PNC[Co-*c*bipy-Co] single crystal.

These results were obtained from powder samples at room and low temperature. As shown in **Figure 3.14**, the simulation for powder at room temperature presented a g_z smaller than g_{xy} with g-factor values of 2.007 and 2.301, respectively and hyperfine coupling interaction of 60 MHz for A_{xy} component and 30 MHz for zeta component (A_z). Similar parameters were recorded in c.w. Q-band.

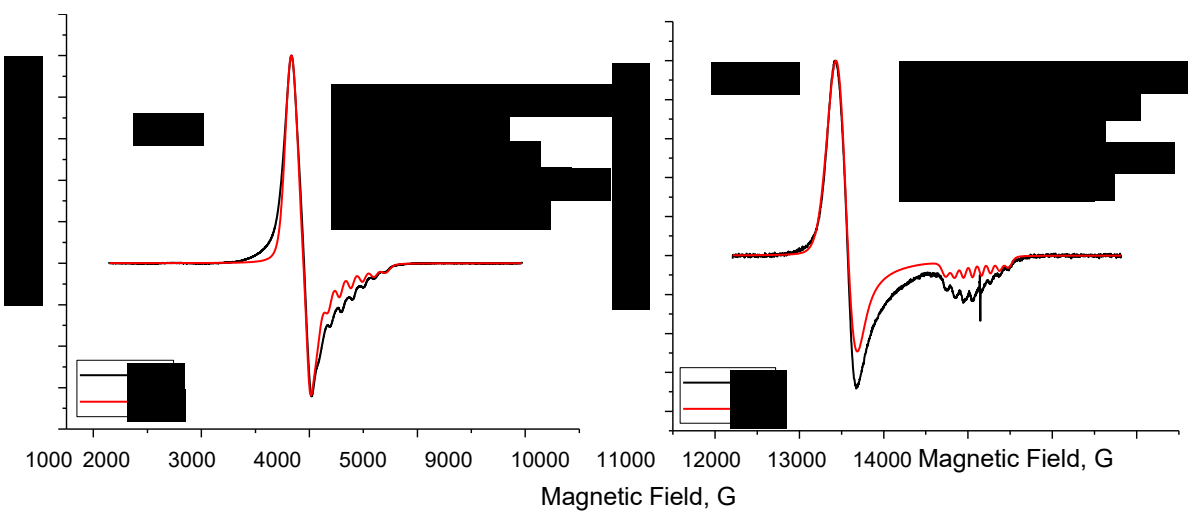

Figure 3.14. EPR powder spectrum of most shifted PNC[Co-*c*bipy-Co] in X and Q bands at room temperature.

For the spectrum obtained at 77 K, a strong isotropic superoxide radical with g-factor 2.0075 (**Figure 3.15A**) was observed due to the strong interaction of cobalt with radical electron. The

parameters found for g_{xy}, g_z, A_{xy} and A_z were 2.301, 2.007, 60 MHz and 300 MHz, respectively. Subsequently, the sample was degassed under vacuum using a Schlenk flask tube resulting in a reduced superoxide peak (**Figure 3.15B**). However, the parameters found at the degassed sample at 77 K were the same as those of the sample containing superoxide radical signal, as well as that of the freshly aerated sample (**Figure 3.15C**) confirming reversibility.

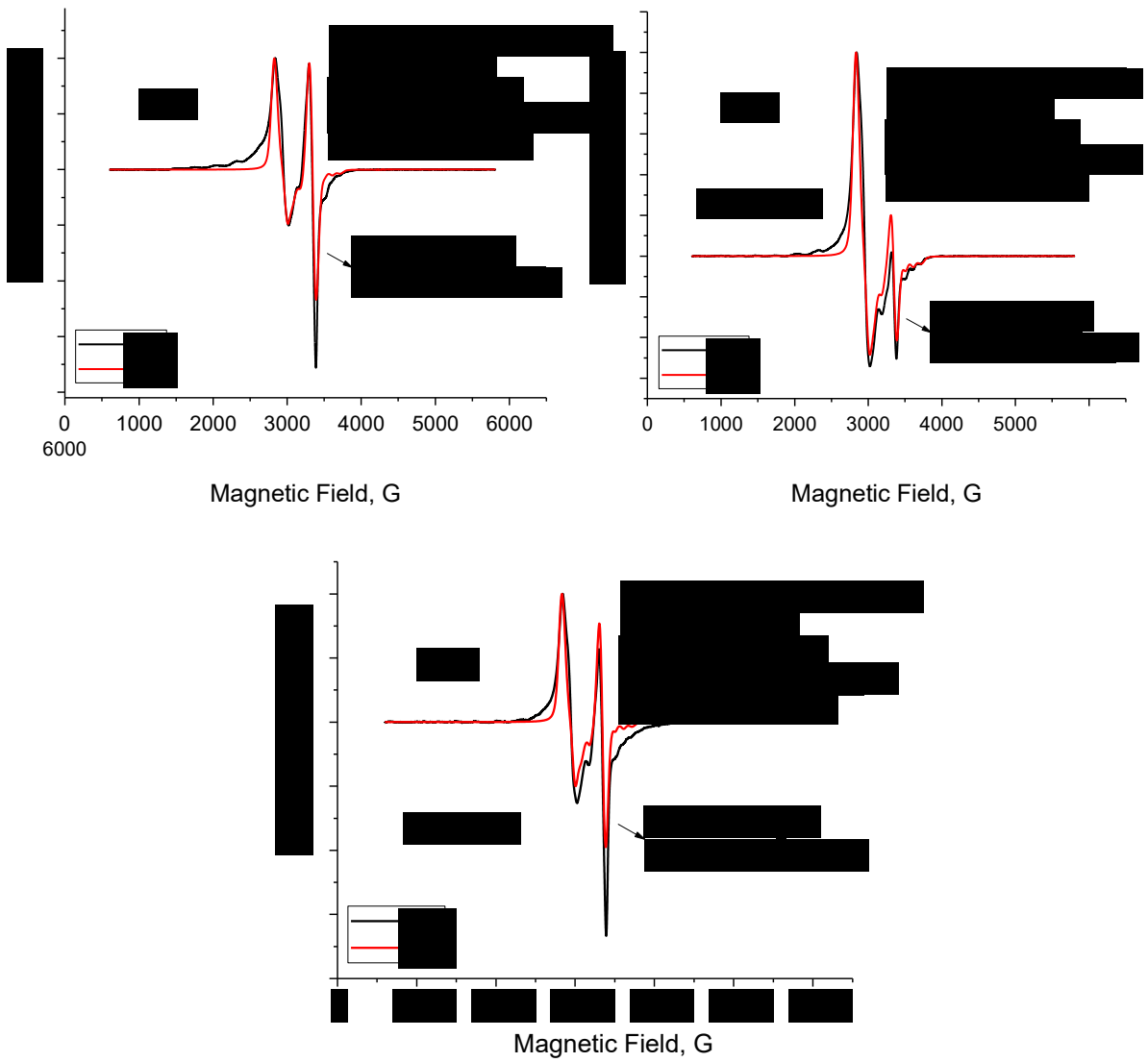

Figure 3.15. X-band powder EPR spectra of PNC[Co-*c*bipy-Co] at 77K.

The interesting conclusion of this investigation is that when the same experiments were carried out for the frozen solution at the stage of the degassing the superoxide radical disappears while in the powder spectrum still exists (**Figure 3.16**).

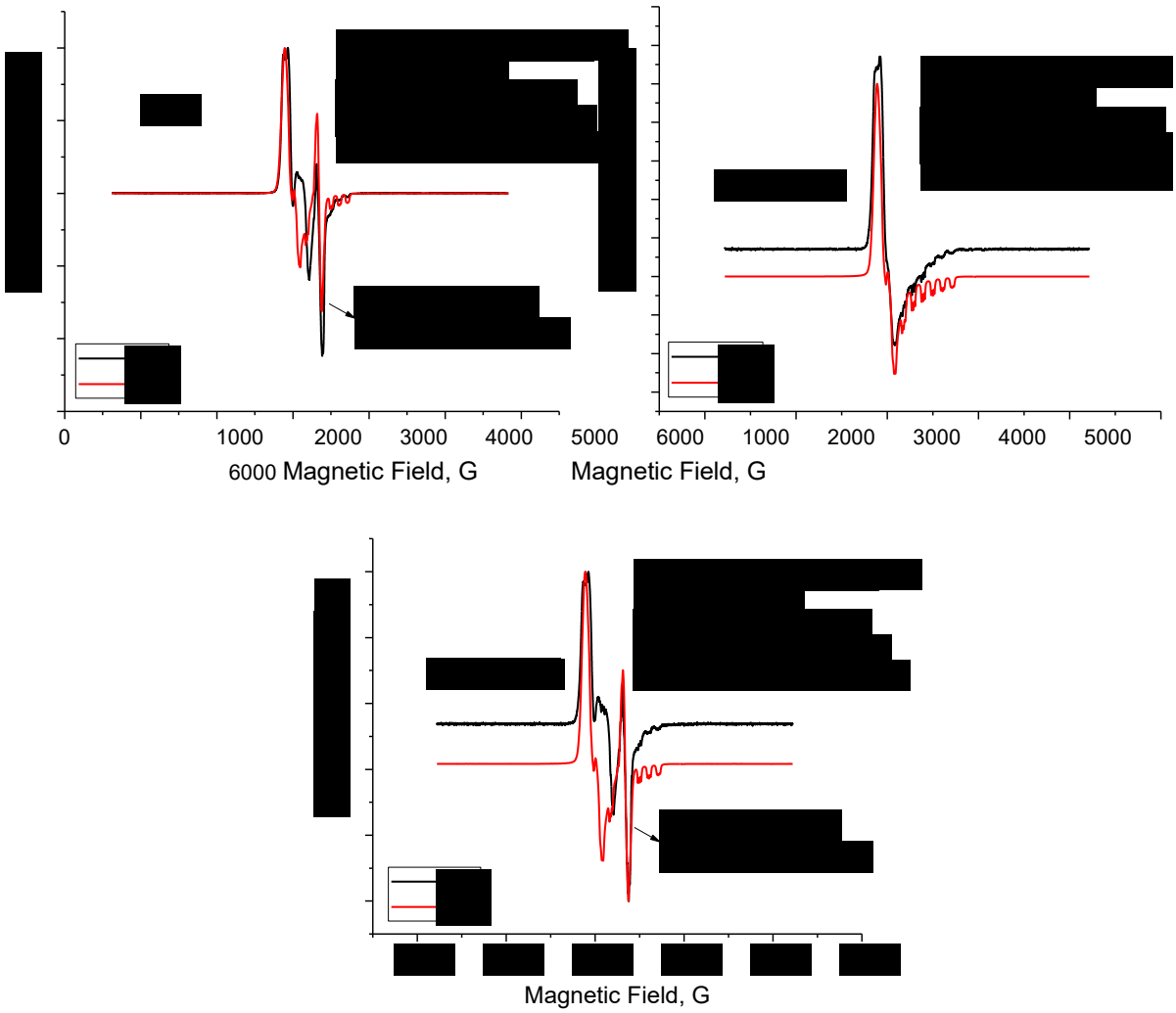

Figure 3.16. X-band frozen solution EPR spectra of PNC[Co-*c*bipy-Co] at 77K.

3.9 PNC[Co-*c*bpm-Co] and PNC[Co-*c*bipy-Co] comparison with cw-EPR experiment

There have been no previous reports on the EPR study of nanoporous phthalocyanine crystals or, indeed, studies of highly symmetric crystals made from phthalocyanines. The two complexes that were the focus of the study were the PNC[Co-*c*bpm-Co] and the PNC[Co-*c*bipy-Co] as powder samples. Powder X-band EPR spectroscopy was measured for PNC[Co-*c*bipy-Co] at 77 K and the spectrum (**Figure 3.17**) showed the signal of Co^{2+} (S = 1/2 and I = 7/2) with cobalt hyperfine coupling split at high field with $g_z > g_{xy}$. However, a second species may be observed at low field with $g_z < g_{xy}$. Additionally, this compound was interacting with air at low temperature resulting in the characteristic intense signal of a superoxide radical.

In order to clarify the hyperfine splitting at high field, the sample was degassed (**Figure 3.17 red**) and a decrease in the intensity of the superoxide radical was observed. On re-exposure to the ambient environment, the peak was restored to its original intensity (**Figure 3.17 blue**).

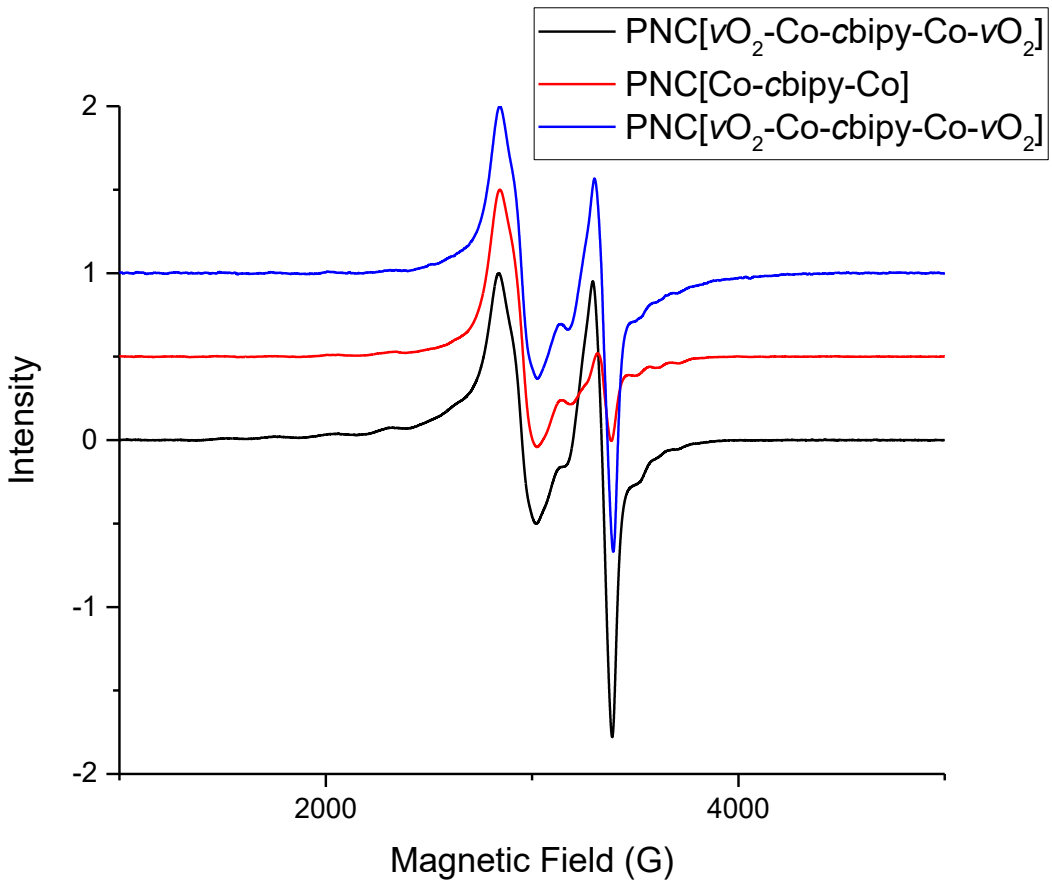

Figure 3.17. Powder cw-EPR spectrum of PNC[vO$_2$-Co-*c*bipy-Co-vO$_2$] in ambient environment (black), degassed with the diminished superoxide radical peak (red), and re-exposed to ambient environment (blue).

Similarly, powder X-band EPR spectroscopy was performed on PNC[Co-*c*bpm-Co] at 77 K and the spectrum (**Figure 3.18 black**) showed the signal of Co^{2+} (S = 1/2 and I = 7/2) similar to that of PNC[Co-*c*bipy-Co] , with strong evidence of the superoxide radical bound onto the metal centre.

However, upon degassing of the sample, the superoxide radical disappeared completely (**Figure 3.18 red**) but upon aeration of the sample the radical could be observed with the same intensity (**Figure 3.18 blue**).

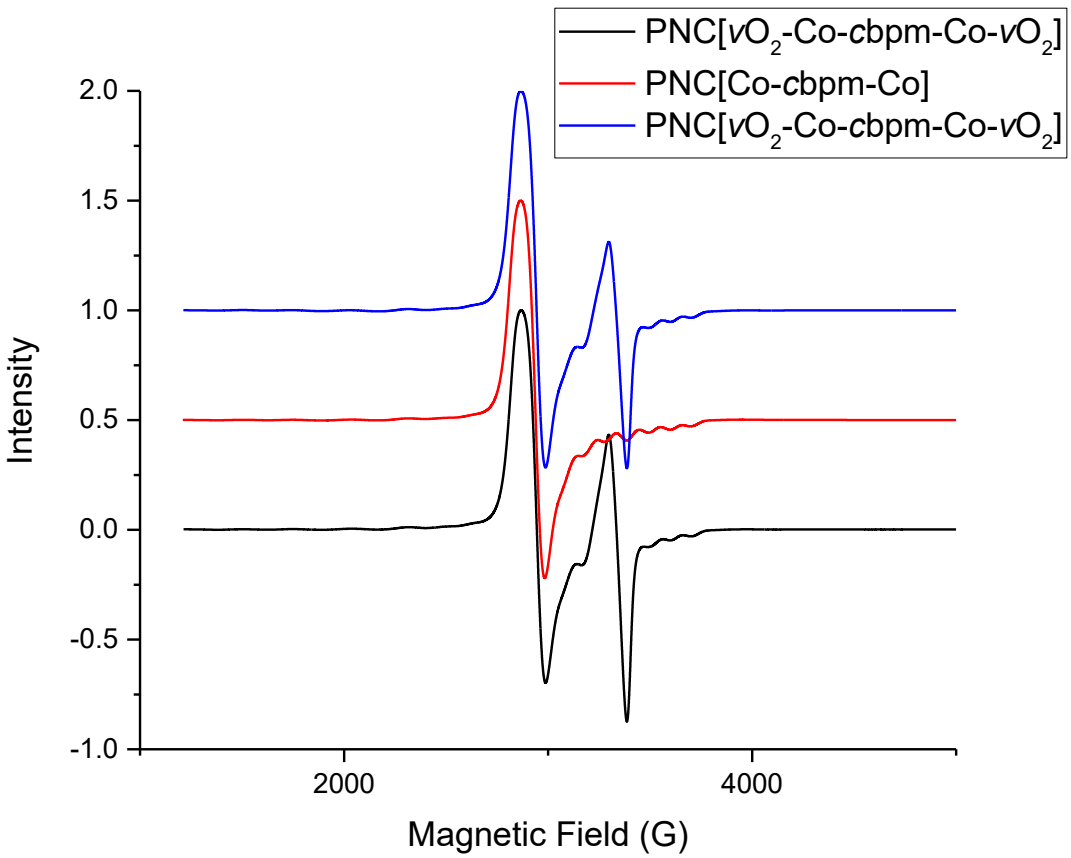

Figure 3.18. Powder cw-EPR spectrum of PNC[vO$_2$-Co-$c$bpm-Co-vO$_2$] in ambient environment (black), degassed with disappearance of the superoxide radical peak (red), and re-exposed to ambient environment (blue).

Comparing the **Figures 3.17** and **3.18**, it can be observed a clear difference between these two complexes is the strength of the physisorption of the oxygen forming the superoxide radical, which indicates a potential difference in reactivity due to the choice of wall-tie ligand for catalytic oxidation reactions. This conclusion is similar to that observed for the gas cell XRD experiments.

3.10 Co-crystallisations with TPP

Previously, the PNCs were obtained for some double decker lanthanide $(dipPhO)_8PcMPc$ complexes (M = Tb, Y, Dy, Pr, Yb) within which the smaller unsubstituted Pc ligands face into the voids (unpublished results, Luke Burt, PhD thesis). A similar result was obtained for the dimeric μ-nitrido complex $(dipPhO)_8PcFe$-N-Pc, PNC[*v*PcFe-N-Fe], (**Figure 3.19**). Therefore, it was of interest to synthesize an μ-nitrido bridge between $(dipPhO)_8PcFe$ and the commonly available iron tetraphenylporphyrin (FeTPP, **Figure 3.20**) following the procedure of C. Ercolani.[87] This porphyrin-phthalocyanine sandwich complex also crystallised in the desired nanoporous cubic crystal.

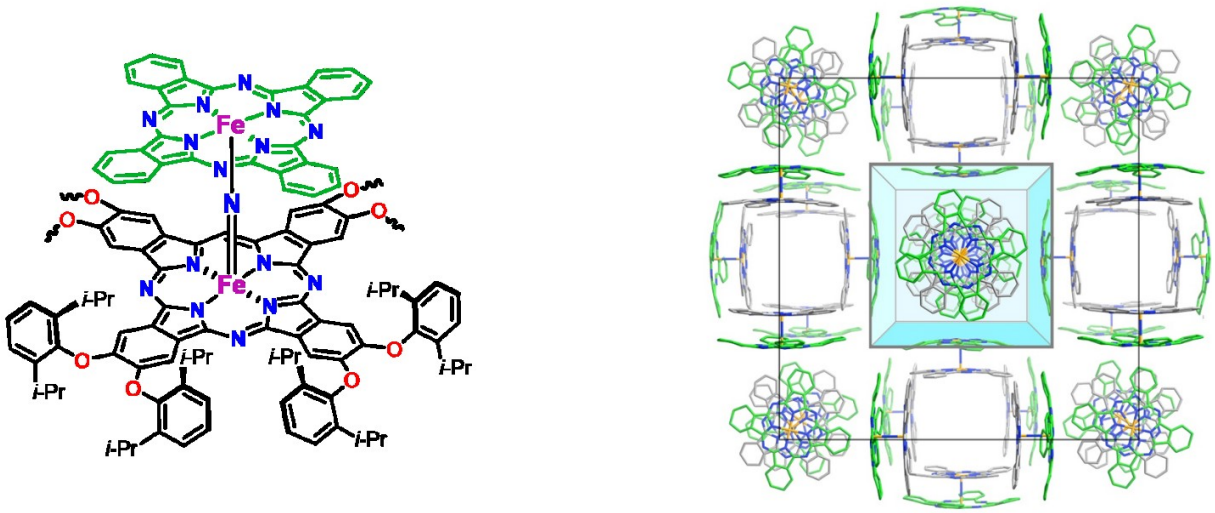

Figure 3.19. Molecular crystal structure of PNC[*v*PcFe-N-Fe].

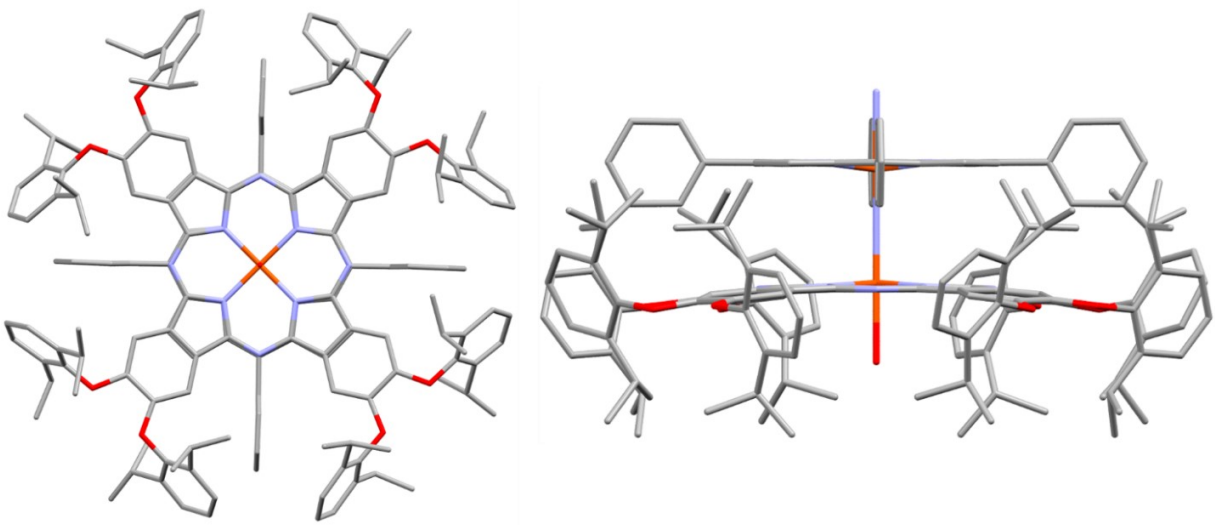

Figure 3.20. Molecular crystal structure of PNC[*v*TPPFe-N-Fe].

The clear symmetry-driven complementarity between the $(dipPhO)_8PcFe$ and TPPFe macrocycles within this complex prompted an investigation into the co-crystallisation of $(dipPhO)_8PcH_2$ and the $TPPH_2$. Co-crystals are solids that are crystalline materials composed of two or more molecules in the same crystal lattice.[88] The formation of such supramolecular adducts was also deemed viable by Spartan modelling with the phenyl groups of the TPP nestled within the gaps between the di-*iso*-propylphenyl units. The variables that were used for the modelling were the DFT B3LYP with a 6-31g* basis set, but since it was time consuming the semi empirical was used in the end providing the following model (**Figure 3.21**). The successful incorporation of $TPPH_2$ within the PNC structure derived from $(dipPhO)_8PcH_2$ is particularly pleasing because $(dipPhO)_8PcH_2$ does not normally crystallize in the nanoporous cubic space group, although PNC co-crystals with fullerenes have been successfully obtained.[50]

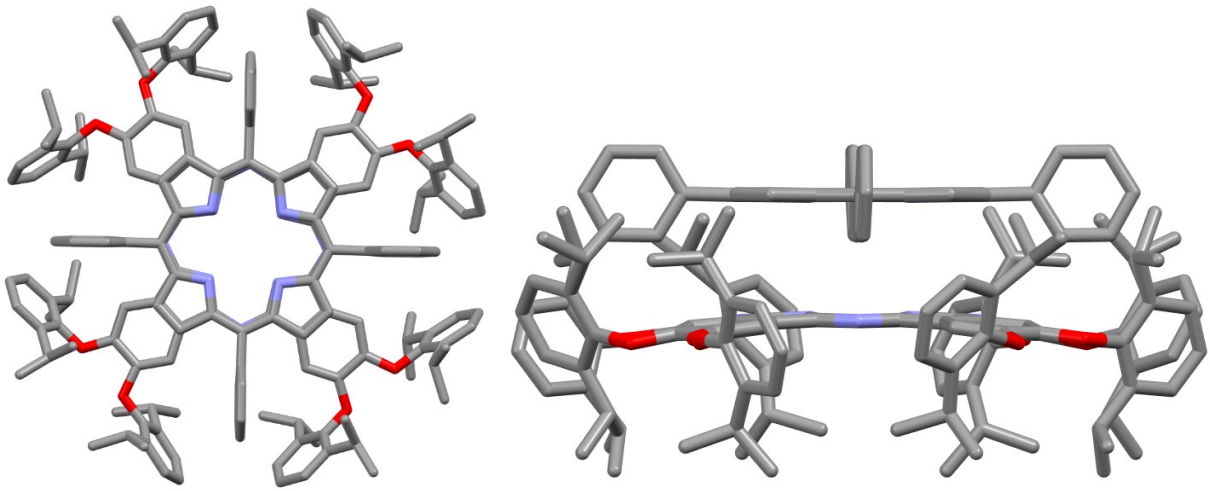

Figure 3.21. Spartan modelling of PNC[*v*TPPH_2/H_2].

Based on this encouraging result, the incorporation of TPP within crystals formed by a range of (dipPhO)8PcM complexes was investigated. In addition, a range of metal cations metals were incorporated within the TPP. The following denomination will be followed for describing the MTPP (dipPhO)$_8$PcM complex: PNC[vMTPP / M-cBidL-M / vMTPP] meaning that PNC is a phthalocyanine based nanoporous crystal, *v* denoting the void, *c* denoting the cavity, / denoting the floating of the TPP over the (dipPhO)$_8$Pc, and – denoting the bond between the metal with the BidL which is the bidentate ligand. (i.e. PNC[vH2TPP / Co-cbipy-Co / vH2TPP].

3.11 Co-crystallisation of PNC[*v*MTPP / M]

The co-crystallisation was tried with different ratios between the two compounds and in different solvent systems, but the most effective parameters were 1:1 ratio and co-crystallisation with slow diffusion of methanol in chloroform.

3.12 Characterisation of aggregates of (dipPhO)$_8$PcH$_2$ and H$_2$TPP

Initially, no obvious indication of aggregation of TPPH_2 with (dipPhO)$_8$PcH$_2$ was noted by UV-Vis spectroscopic characterisation of solutions containing the two macrocycles. However, by adding the non-solvent methanol (0.16 ml to 3.5 ml of DCM solution), which is used to induce co-crystallisation, changes in the UV-Vis spectra consistent with aggregation could be observed (**Figure 3.22**). The peaks at 525 to 575 nm correspond to those of H_2TPP and those at 675 to 700

nm are distinctive split Q-band of the $(dipPhO)_8PcH_2$. As more H_2TPP is added there is an increasing peak at 725 to 750 nm which corresponds to the dimeric aggregate.

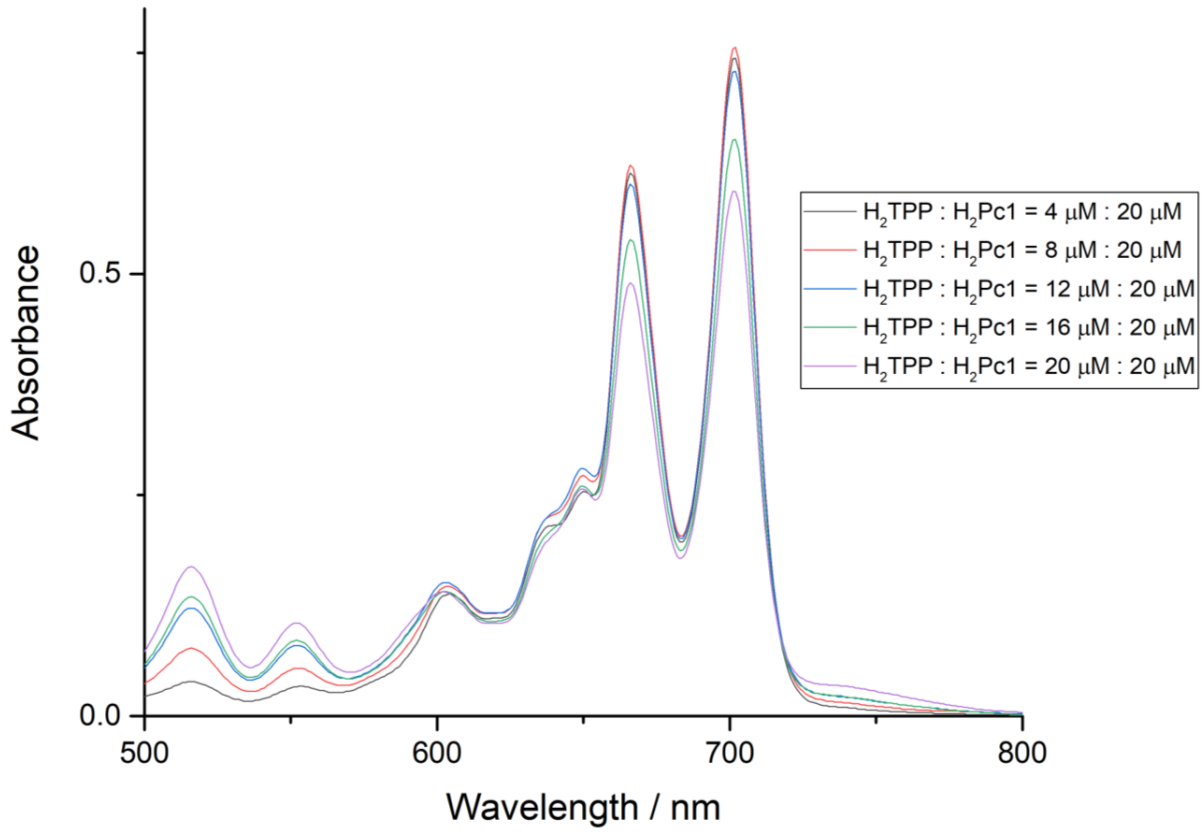

Figure 3.22. UV-Vis spectra differentiating the ratio of H_2TPP against $(dipPhO)_8PcH_2$ to obtain the maximum aggregation between the two compounds.

3.13 Analysis of the molecular structures of Pc/porphyrin dimers from single crystal XRD

Initially, the analysis was repeated following the methodology described in the previous chapter based on the distance of the metal extrusion from the plane of the four pyrrolic nitrogen atoms and the curvature of the macrocycle. Furthermore, the distance of the metal to metal centre between the two macrocycles and also the distance between the pyrrolic nitrogens of the PNC[*v*H_2/MTPP / H_2/M] (**Figure 3.23**) were compiled.

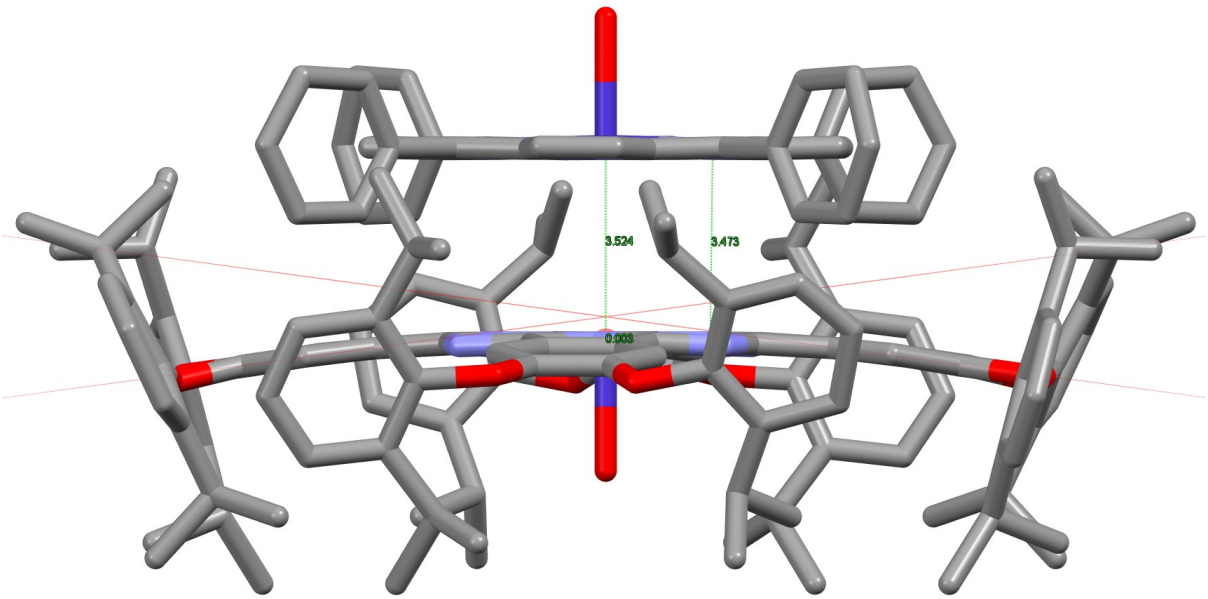

Figure 3.23. PNC[*v*H_2O-CoTPP/Co-*c*H_2O]. Distance of the metal to metal and nitrogen to nitrogen of the two macrocycles.

3.14 Analysis of cubic PNC from MTPP and (dipPhO)$_8$PcM

The first complex that was characterised by XRD was the PNC[*v*H_2TPP/H_2], where the results were interesting, for two main reasons. Firstly, normally the (dipPhO)$_8$PcH_2 when it crystallised by itself does not do so in the PNC cubic structure; with H_2TPP the porous crystal was obtained successfully. Secondly, the structure of the dimer formed by the two macrocycles was as predicted by modelling with close interactions between the *ortho* protons of the phenyls of the TPP with the nitrogen atoms at the *meso* position of the phthalocyanine (2.444 Å; **Figure 3.24**).

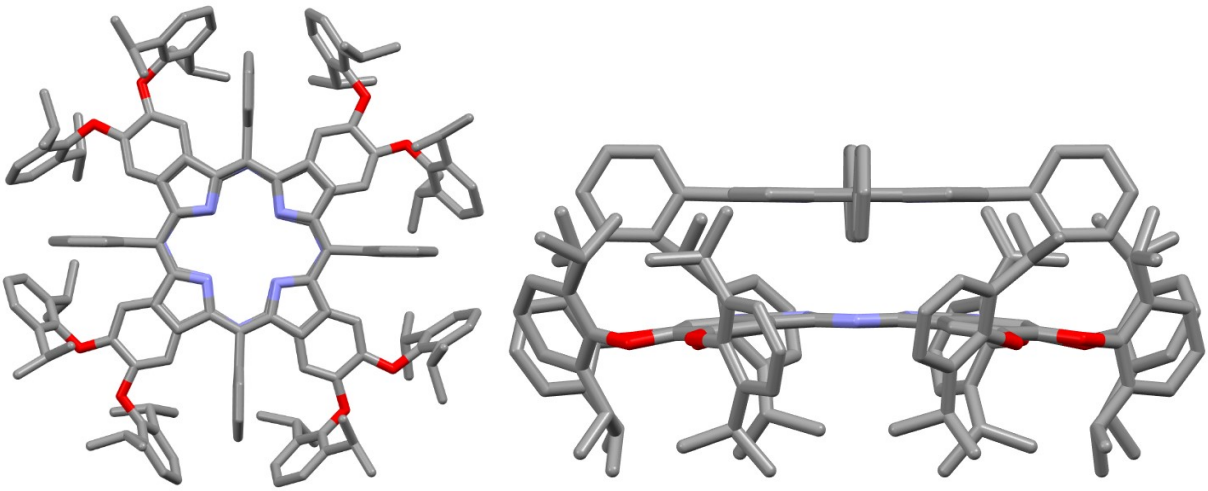

Figure 3.24. Molecular crystal structure of PNC[$v$$H_2$TPP/$H_2$].

Different $(dipPhO)_8PcM$ complexes were crystallised with the H_2TPP. The metals that were incorporated in the $(dipPhO)_8PcH_2$ are shown in **Figure 3.25** and in **Table 3.1**.

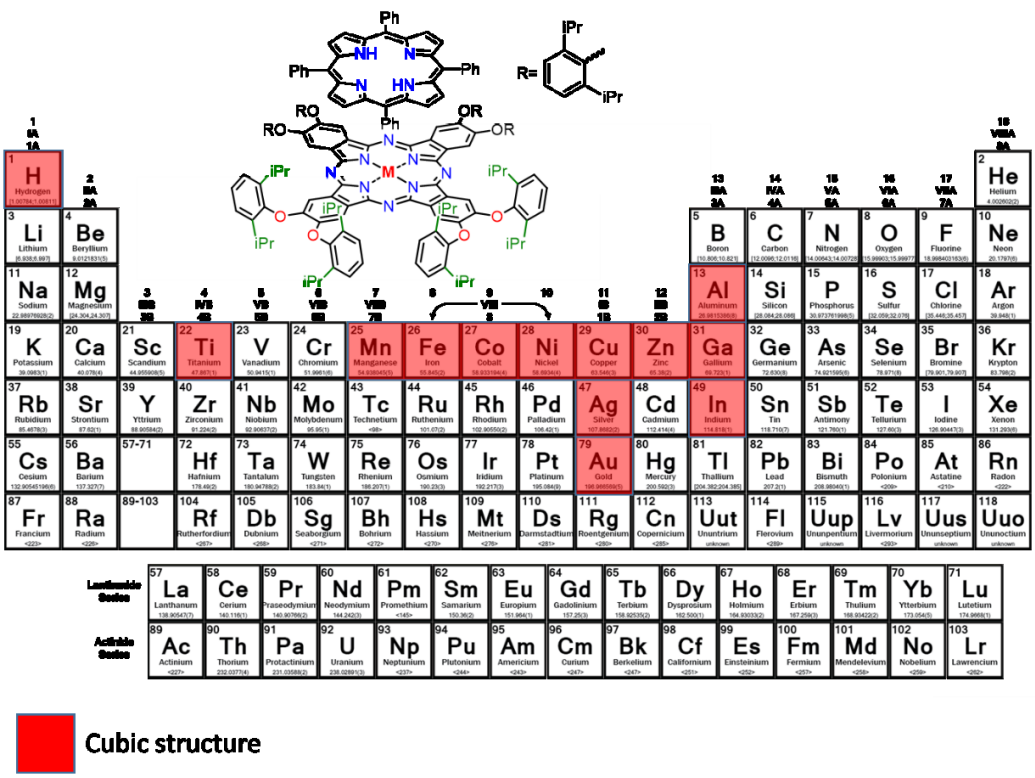

Figure 3.25. Periodic table depicting with red shading the elements M for which $(dipPhO)_8PcM$ co-crystallize in the PNC structure with H_2TPP.

An interesting result was that $(dipPhO)_8PcNi$ and $(dipPhO)_8PcCu$ had previously not crystallised in the PNC structure (although $(dipPhO)_8PcCu$ does form a PNC when co-crystallised with C_{60})[50] but by co-crystallisation with the $TPPH_2$ the PNC was obtained with the TPP incorporated into the void (**Table 3.1**).

In the case of PNC[*v*H_2TPP / Al], the percentage of H_2TPP deviates from 91 % up to 100 % occupancy, presumably due to the axial ligands that are bound onto the metal. More specifically, the metal has an 75 : 25 occupancy with the 75 % the metal located towards the cavity and 25 % located towards the void. In that 25 %, the TPP has co-crystallised with the metallated Pc 91 % while 9 % the TPP has not, but the interesting phenomenon is that the cubic structure is retained as well as the nanoporosity. The same applied for the PNC[*v*H_2TPP / Zn].

Furthermore, larger radius metals such as Ga, In, Ag and Au were used for the co-crystallisation experiments, and demonstrated that the metal can extrude out the plane of the macrocycle but pointing towards the cavity when the side of the Pc facing the void is blocked by the TPP (e.g. **Figure 3.43**). Similarly, the axial ligands are forced into the cavity (e.g. **Figure 3.34**).

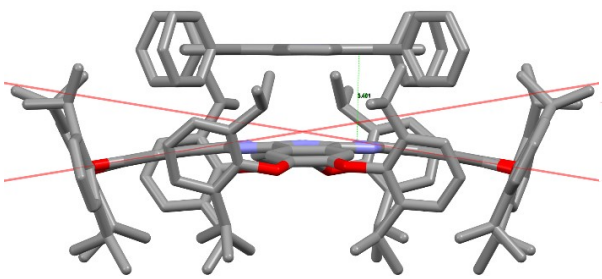

Figure 3.26. PNC[*v*H_2TPP/H_2], cubic, $Pn\bar{3}n$

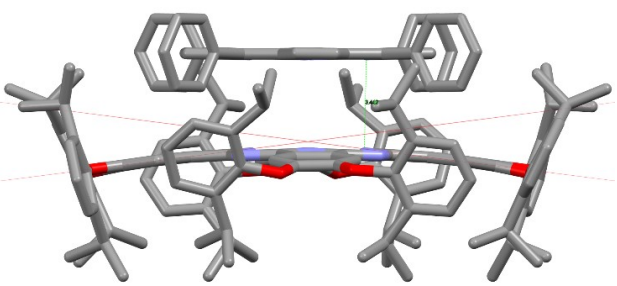

Figure 3.27. PNC[*v*H_2TPP/H_2] dried, cubic, $Pn\bar{3}n$

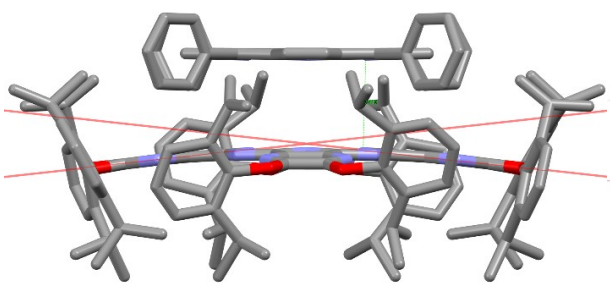

Figure 3.28. azaPNC[*v*H_2TPP/H_2], cubic, $Pn\bar{3}n$

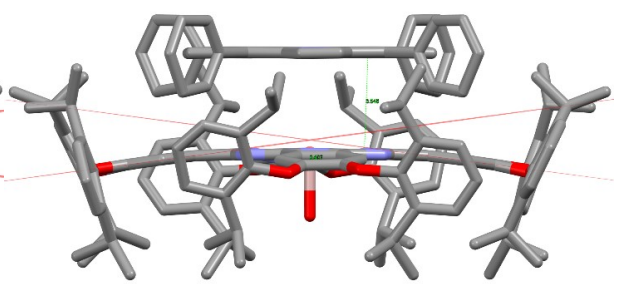

Figure 3.29. PNC[*v*H_2TPP/Al-*c*H_2O], cubic, $Pn\bar{3}n$ **(2A)**

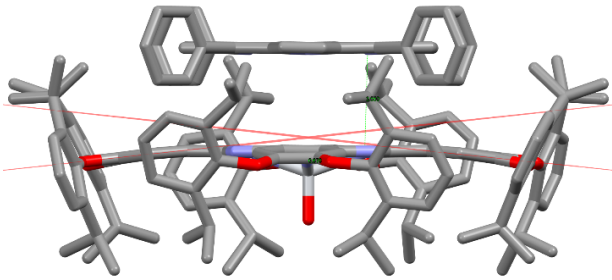

Figure 3.30. PNC[*v*H_2TPP/Ti-*c*H_2O], cubic, $Pn\bar{3}n$ **(2B)**

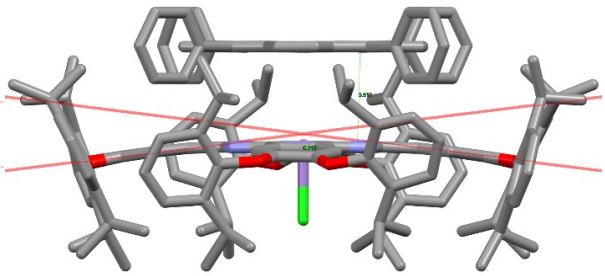

Figure 3.31. PNC[*v*H_2TPP/Mn-*c*Cl], cubic, $Pn\bar{3}n$ **(2C)**

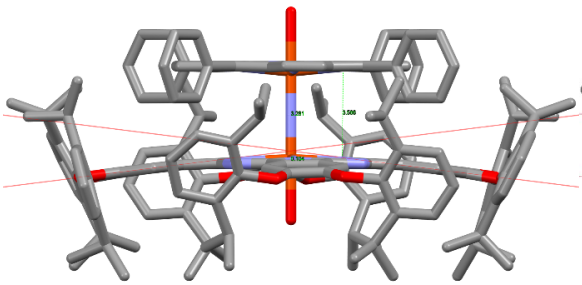

Figure 3.32. PNC[*v*H_2O-FeTPP-N-Fe-*c*H_2O], cubic, $Pn\bar{3}n$

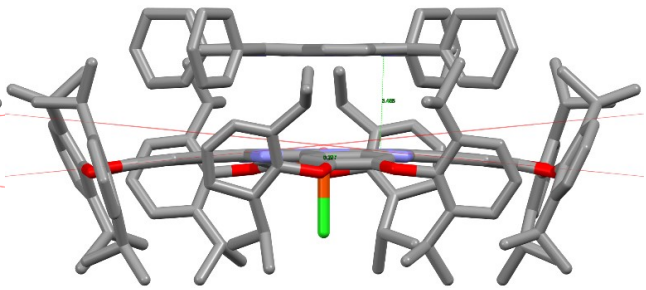

Figure 3.33 PNC[*v*H_2TPP/Fe-*c*Cl], cubic, $Pn\bar{3}n$ **(2D)**

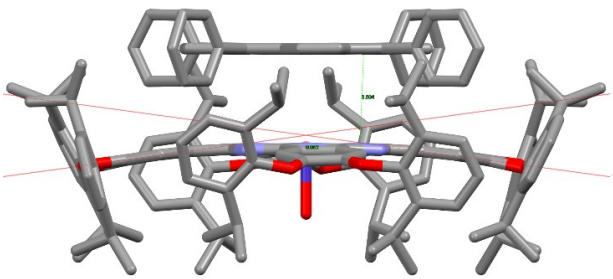

Figure 3.34. PNC[*v*H_2TPP/Co-*c*H_2O], cubic, $Pn\bar{3}n$ **(2E)**

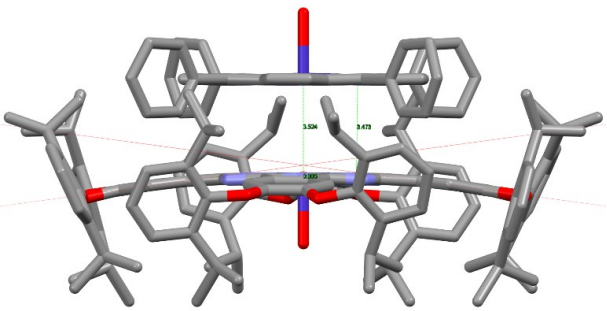

Figure 3.35. PNC[*v*H_2O-CoTPP/Co-*c*H_2O], cubic, $Pn\bar{3}n$

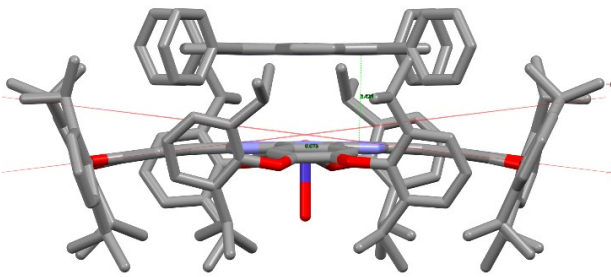

Figure 3.36. PNC[*v*CuTPP/Co-*c*H_2O], cubic, $Pn\bar{3}n$

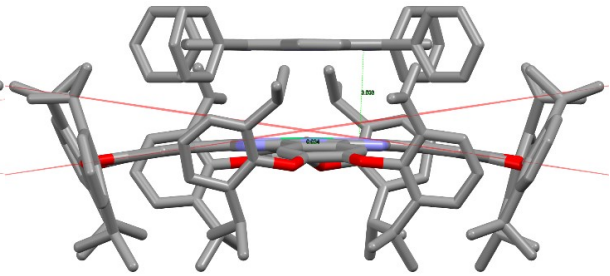

Figure 3.37. PNC[*v*H_2TPP/Ni], cubic, $Pn\bar{3}n$ **(2F)**

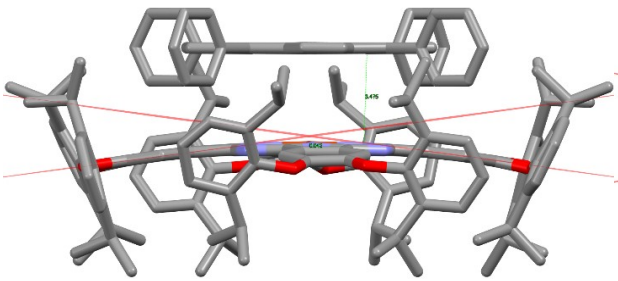

Figure 3.38. PNC[*v*H_2TPP/Cu], cubic, $Pn\bar{3}n$ **(2G)**

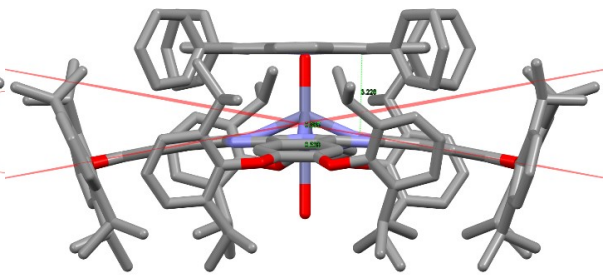

Figure 3.39. PNC[*v*H_2TPP/Zn-*c*H_2O], cubic, $Pn\bar{3}n$ **(2H)**

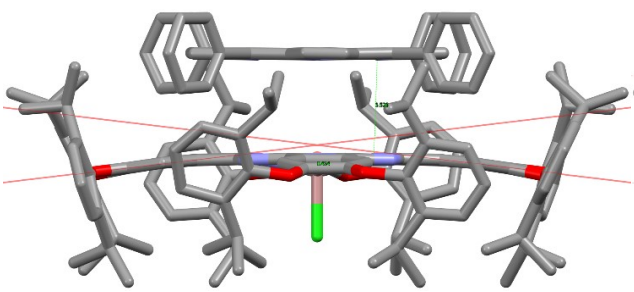

Figure 3.40. PNC[*v*H_2TPP/Ga-*c*Cl], cubic, $Pn\bar{3}n$ **(2I)**

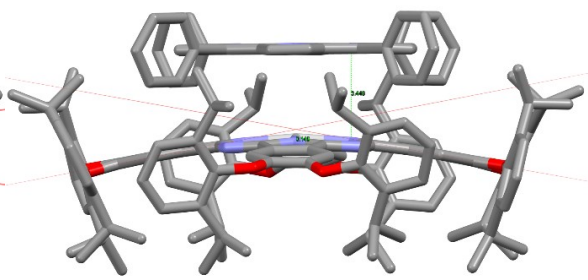

Figure 3.41. PNC[*v*H_2TPP/Ag], cubic, $Pn\bar{3}n$ **(2J)**

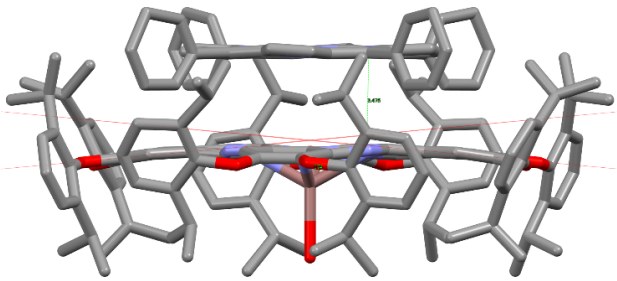

Figure 3.42. PNC[*v*H_2TPP/In-*c*H_2O], cubic, $Pn\bar{3}n$ **(2K)**

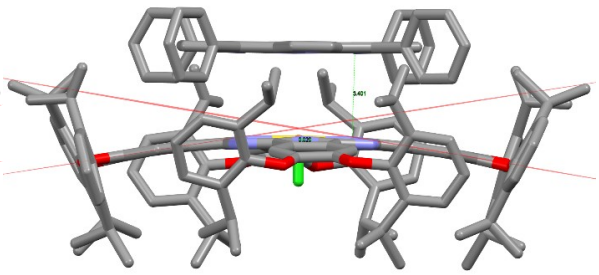

Figure 3.43. PNC[*v*H_2TPP/Au-*c*Cl], cubic, $Pn\bar{3}n$ **(2L)**

(Note that the legends shaded in red indicate structures obtained during the PhD programme.)

Phthalocyanine tetraphenylporphyrin complexes													
Acronym	Name	Chemical formula	M_r	Crystal system, space group	a (Å)	b (Å)	c (Å)	V (Å^3)	Z	Phthalocyanine curvature (degrees)	Metal to macrocycle distance (Å)	Macrocycle macrocycle distance (Å)	Metal to metal distance (Å)
PNC[*v* H_2TPP/H_2]	(dipPhO)$_8$PcH$_2$ + H_2TPP	$C_{128}H_{144}N_8O_8H_2$ $C_{44}H_{28}N_4H_2$	2539.319	cubic, $Pn\bar{3}n$	37.7730(2)	37.7730(2)	37.7730(2)	53894.5	12	18.6	N.A	3.461	N.A.
PNC[*v* H_2TPP/H_2] Dried	(dipPhO)$_8$PcH$_2$ + H_2TPP	$C_{128}H_{144}N_8O_8H_2$ $C_{44}H_{28}N_4H_2$	2539.319	cubic, $Pn\bar{3}n$	38.0858(3)	38.0858(3)	38.0858(3)	55244.5	12	14.59	N.A	3.442	N.A.
azaPNC[*v* H_2TPP/H_2]	(dipPhO)$_8$azaPcH$_2$ + H_2TPP	$C_{120}H_{136}N_{16}O_8H_2$ $C_{44}H_{28}N_4H_2$	2547.224	cubic, $Pn\bar{3}n$	37.5049(2)	37.5049(2)	37.5049(2)	52755	12	12.5	N.A	3.419	N.A.
PNC[*v* H_2TPP/Al]	(dipPhO)$_8$PcAl + H_2TPP	$C_{128}H_{144}N_8O_8Al$ $C_{44}H_{28}N_4H_2$	2564.285	cubic, $Pn\bar{3}n$	37.7939(3)	37.7939(3)	37.7939(3)	53984	12	15.17	-0.407	3.546	N.A.
PNC[*v* H_2TPP/Ti]	(dipPhO)$_8$PcTi + H_2TPP	$C_{128}H_{144}N_8O_8Ti$ $C_{44}H_{28}N_4H_2$	2585.170	cubic, $Pn\bar{3}n$	37.7674(2)	37.7674(2)	37.7674(2)	53870.5	12	12.3	-0.676	3.550	N.A.
PNC[*v* H_2TPP/Mn-*c* Cl]	(dipPhO)$_8$PcMn + H_2TPP	$C_{128}H_{144}N_8O_8Mn$ $C_{44}H_{28}N_4H_2$	2592.241	cubic, $Pn\bar{3}n$	37.7985(5)	37.7985(5)	37.7985(5)	54003.7	12	14.07	-0.248	3.518	N.A.
PNC[*v* H_2O-*v* FeTPP-N-Fe-*c* H_2O]	(dipPhO)$_8$PcFe + FeTPP	$C_{128}H_{144}N_8O_8Fe$ N $C_{44}H_{28}N_4Fe$	2660.985	cubic, $Pn\bar{3}n$	37.8683(6)	37.8683(6)	37.8683(6)	54303.5	12	14.27	0.104	3.566	3.281
PNC[*v* H_2TPP/Fe-*c* Cl]	(dipPhO)$_8$PcFe + H_2TPP	$C_{128}H_{144}N_8O_8Fe$ $C_{44}H_{28}N_4H_2$	2593.149	cubic, $Pn\bar{3}n$	37.8603(6)	37.8603(6)	37.8603(6)	54269	12	11.22	-0.297	3.485	N.A.
PNC[*v* H_2TPP/Co-*c* H_2O]	(dipPhO)$_8$PcCo + H_2TPP	$C_{128}H_{144}N_8O_8Co$ $C_{44}H_{28}N_4H_2$	2596.237	cubic, $Pn\bar{3}n$	37.8048(2)	37.8048(2)	37.8048(2)	54030.7	12	15.5	-0.052	3.504	N.A.
PNC[*v* H_2O-*v* CoTPP/Co-*c* H_2O]	(dipPhO)$_8$PcCo + CoTPP	$C_{128}H_{144}N_8O_8Co$ $C_{44}H_{28}N_4Co$	2653.154	cubic, $Pn\bar{3}n$	37.8225(4)	37.8225(4)	37.8225(4)	54106.7	12	15.35	-0.003	3.472	3.524
PNC[*v* CuTPP/Co-*c* H_2O]	(dipPhO)$_8$PcCo + CuTPP	$C_{128}H_{144}N_8O_8Co$ $C_{44}H_{28}N_4Cu$	2657.767	cubic, $Pn\bar{3}n$	37.85440(10)	37.85440(10)	37.85440(10)	54243.7	12	14.17	-0.073	3.424	3.530
PNC[*v* H_2TPP/Ni]	(dipPhO)$_8$PcNi + H_2TPP	$C_{128}H_{144}N_8O_8Ni$ $C_{44}H_{28}N_4H_2$	2595.997	cubic, $Pn\bar{3}n$	37.73920(10)	37.73920(10)	37.73920(10)	53750	12	16.71	-0.024	3.503	N.A.
PNC[*v* H_2TPP/Cu]	(dipPhO)$_8$PcCu + H_2TPP	$C_{128}H_{144}N_8O_8Cu$ $C_{44}H_{28}N_4H_2$	2600.849	cubic, $Pn\bar{3}n$	37.9675(2)	37.9675(2)	37.9675(2)	54731.3	12	15.15	-0.042	3.475	N.A.
PNC[*v* H_2TPP/Zn]	(dipPhO)$_8$PcZn + H_2TPP	$C_{128}H_{144}N_8O_8Zn$ $C_{44}H_{28}N_4H_2$	2602.712	cubic, $Pn\bar{3}n$	37.8110(2)	37.8110(2)	37.8110(2)	54057.3	12	20.46	-0.865	3.228	N.A.
PNC[*v* H_2TPP/Ga-*c* Cl]	(dipPhO)$_8$PcGa + H_2TPP	$C_{128}H_{144}N_8O_8Ga$ $C_{44}H_{28}N_4H_2$	2607.027	cubic, $Pn\bar{3}n$	37.8515(2)	37.8515(2)	37.8515(2)	54231.2	12	13.43	-0.444	3.523	N.A.
PNC[*v* H_2TPP/Ag]	(dipPhO)$_8$PcAg + H_2TPP	$C_{128}H_{144}N_8O_8Ag$ $C_{44}H_{28}N_4H_2$	2645.172	cubic, $Pn\bar{3}n$	37.8701(2)	37.8701(2)	37.8701(2)	54311.2	12	20.91	-0.149	3.448	N.A.
PNC[*v* H_2TPP/In-*c* Cl]	(dipPhO)$_8$PcIn + H_2TPP	$C_{128}H_{144}N_8O_8In$ $C_{44}H_{28}N_4H_2$	2652.122	cubic, $Pn\bar{3}n$	37.9239(2)	37.9239(2)	37.9239(2)	54543	12	10.6	-1.074	3.475	N.A.
PNC[*v* H_2TPP/Au-*v* Cl]	(dipPhO)$_8$PcAu + H_2TPP	$C_{128}H_{144}N_8O_8Au$ $C_{44}H_{28}N_4H_2$	2769.723	cubic, $Pn\bar{3}n$	37.7974(3)	37.7974(3)	37.7974(3)	53999	12	14.44	-0.020	3.416	N.A.

Table 3.1. PNC[vH_2/MTPP / H_2/M]

3.15 Comparison of the curvature and metal extrusion between PNCs derived from $(dipPhO)_8PcM$ and PNCs co-crystals from $(dipPhO)_8PcM$ and H_2TPP

The curvature and the metal extrusion within the PNCs derived from $(dipPhO)_8PcM$ and within the PNCs co-crystals from $(dipPhO)_8PcM$ and H_2TPP are compared (**Table 3.2**).

	Metal Phthalocyanines												
	Acronym	Name	Chemical formula	M_r	Crystal system, space group	*a* (Å)	*b* (Å)	*c* (Å)	*V* (Å^3)	*Z*	Phthalocyanine curvature (degrees)	Metal to macrocycle distance (Å)	CCDC
2a	PNC[Al]	$(dipPhO)_8PcAl$	$C_{128}H_{144}N_8O_8Al$	1949.548	cubic, $Pn\bar{3}n$	37.4064(4)	37.4064(4)	37.4064(4)	52340.5(10)	12	26.48	0.062	
2b	PNC[Ti]	$(dipPhO)_8PcTi$	$C_{128}H_{144}N_8O_8Ti$	1970.433	cubic, $Pn\bar{3}n$	37.5117(9)	37.5117(9)	37.5117(9)	52784(2)	12	25.90	0.745	
2c	PNC[Mn]	$(dipPhO)_8PcMn$	$C_{128}H_{144}N_8O_8Mn$	1977.504	cubic, $Pn\bar{3}n$	37.2511(5)	37.2511(5)	37.2511(5)	51691.3(12)	12	26.69	0.059	761412
2d	**PNC[Fe-*v* Cl]**	**$(dipPhO)_8PcFe$**	**$C_{128}H_{144}N_8O_8Fe$**	2013.385	cubic, $Pn\bar{3}n$	37.4365(2)	37.4365(2)	37.4365(2)	52466.9	12	24.90	0.056	
2e	PNC[*v* MeOH-Co-*c* H_2O]	$(dipPhO)_8PcCo$	$C_{128}H_{144}N_8O_8Co$	1981.499	cubic, $Pn\bar{3}n$	37.6395(3)	37.6395(3)	37.6395(3)	53325.1(7)	12	21.66	0.072	900375
2f	$(dipPhO)_8PcNi$	$(dipPhO)_8PcNi$	$C_{128}H_{144}N_8O_8Ni$	1981.259	monoclinic, $P2_1/c$	21.370(2)	16.88255(18)	18.726(2)	6098.7(11)	2	0	0	
2g	$(dipPhO)_8PcCu$	$(dipPhO)_8PcCu$	$C_{128}H_{144}N_8O_8Cu$	1986.112	monoclinic, $P2_1/c$	38.607(2)	16.8676(10)	18.4282(11)	11997	4	0	0	
2h	PNC[Zn]	$(dipPhO)_8PcZn$	$C_{128}H_{144}N_8O_8Zn$	1987.975	cubic, $Pn\bar{3}n$	37.6973(2)	37.6973(2)	37.6973(2)	53571.1	12	26.74	0.419	279644
2i	PNC[Ga]	$(dipPhO)_8PcGa$	$C_{128}H_{144}N_8O_8Ga$	1992.289	cubic, $Pn\bar{3}n$	37.6003(2)	37.6003(2)	37.6003(2)	53158.9(6)	12	28.30	0.119	
2j	PNC[Ag/*c* C_{60}/Ag]	$(dipPhO)_8PcAg + C_{60}$	$(C_{128}H_{144}N_8O_8Ag)_2\ C_{60}$	4781.513	cubic, $Pn\bar{3}n$	37.7144(2)	37.7144(2)	37.7144(2)	53644.1	12	28.08	0.148	1851746
2k	PNC[In]	$(dipPhO)_8PcIn$	$C_{128}H_{144}N_8O_8In$	2037.384	cubic, $Pn\bar{3}n$	37.4428(8)	37.4428(8)	37.4428(8)	52493.4(19)	12	33.92	0.995	
2l	PNC[Au]	$(dipPhO)_8PcAu$	$C_{128}H_{144}N_8O_8Au$	2119.533	cubic, $Pn\bar{3}n$	37.667(4)	37.667(4)	37.667(4)	53442	12	155.20	0.009	
2A	PNC[*v* H_2TPP/Al]	$(dipPhO)_8PcAl + H_2TPP$	$C_{128}H_{144}N_8O_8Al\ C_{44}H_{28}N_4H_2$	2564.285	cubic, $Pn\bar{3}n$	37.7939(3)	37.7939(3)	37.7939(3)	53984	12	15.17	-0.407	
2B	PNC[*v* H_2TPP/Ti]	$(dipPhO)_8PcTi + H_2TPP$	$C_{128}H_{144}N_8O_8Ti\ C_{44}H_{28}N_4H_2$	2585.170	cubic, $Pn\bar{3}n$	37.7674(2)	37.7674(2)	37.7674(2)	53870.5	12	12.3	-0.676	
2C	PNC[*v* H_2TPP/Mn-*c* Cl]	$(dipPhO)_8PcMn + H_2TPP$	$C_{128}H_{144}N_8O_8Mn\ C_{44}H_{28}N_4H_2$	2592.241	cubic, $Pn\bar{3}n$	37.7985(5)	37.7985(5)	37.7985(5)	54003.7	12	14.07	-0.248	
2D	PNC[*v* H_2TPP/Fe-*c* Cl]	$(dipPhO)_8PcFe + H_2TPP$	$C_{128}H_{144}N_8O_8Fe\ C_{44}H_{28}N_4H_2$	2593.149	cubic, $Pn\bar{3}n$	37.8603(6)	37.8603(6)	37.8603(6)	54269	12	11.22	-0.297	
2E	PNC[*v* H_2TPP/Co-*c* H_2O]	$(dipPhO)_8PcCo + H_2TPP$	$C_{128}H_{144}N_8O_8Co\ C_{44}H_{28}N_4H_2$	2596.237	cubic, $Pn\bar{3}n$	37.8048(2)	37.8048(2)	37.8048(2)	54030.7	12	15.5	-0.052	
2F	PNC[*v* H_2TPP/Ni]	$(dipPhO)_8PcNi + H_2TPP$	$C_{128}H_{144}N_8O_8Ni\ C_{44}H_{28}N_4H_2$	2595.997	cubic, $Pn\bar{3}n$	37.73920(10)	37.73920(10)	37.73920(10)	53750	12	16.71	-0.024	
2G	PNC[*v* H_2TPP/Cu]	$(dipPhO)_8PcCu + H_2TPP$	$C_{128}H_{144}N_8O_8Cu\ C_{44}H_{28}N_4H_2$	2600.849	cubic, $Pn\bar{3}n$	37.9675(2)	37.9675(2)	37.9675(2)	54731.3	12	15.15	-0.042	
2H	PNC[*v* H_2TPP/Zn]	$(dipPhO)_8PcZn + H_2TPP$	$C_{128}H_{144}N_8O_8Zn\ C_{44}H_{28}N_4H_2$	2602.712	cubic, $Pn\bar{3}n$	37.8110(2)	37.8110(2)	37.8110(2)	54057.3	12	20.46	-0.865	
2I	PNC[*v* H_2TPP/Ga-*c* Cl]	$(dipPhO)_8PcGa + H_2TPP$	$C_{128}H_{144}N_8O_8Ga\ C_{44}H_{28}N_4H_2$	2607.027	cubic, $Pn\bar{3}n$	37.8515(2)	37.8515(2)	37.8515(2)	54231.2	12	13.43	-0.444	
2J	PNC[*v* H_2TPP/Ag]	$(dipPhO)_8PcAg + H_2TPP$	$C_{128}H_{144}N_8O_8Ag\ C_{44}H_{28}N_4H_2$	2645.172	cubic, $Pn\bar{3}n$	37.8701(2)	37.8701(2)	37.8701(2)	54311.2	12	20.91	-0.149	
2K	PNC[*v* H_2TPP/In-*c* Cl]	$(dipPhO)_8PcIn + H_2TPP$	$C_{128}H_{144}N_8O_8In\ C_{44}H_{28}N_4H_2$	2652.122	cubic, $Pn\bar{3}n$	37.9239(2)	37.9239(2)	37.9239(2)	54543	12	10.6	-1.074	
2L	PNC[*v* H_2TPP/Au-*v* Cl]	$(dipPhO)_8PcAu + H_2TPP$	$C_{128}H_{144}N_8O_8Au\ C_{44}H_{28}N_4H_2$	2769.723	cubic, $Pn\bar{3}n$	37.7974(3)	37.7974(3)	37.7974(3)	53999	12	14.44	-0.020	

Table 3.2. Comparison of extrusion of the metals and of the phthalocyanine curvature between PNC[M] and PNC[*v* H_2TPP/M]

It is clear from **Figure 3.44** that when H_2TPP is incorporated into the PNC structure, all the values of curvature are much smaller (by around 10°). Hence the interaction with the planer TPP appears to flatten the $(dipPhO)_8PcM$. This effect is most obvious for $(dipPhO)_8PcIn$, which without TPP demonstrates a very large curvature (~35°) but with TPP is one of the least curved Pcs found in a PNC. This is due to the effect of the large metal being forced into the cavity by the TPP instead of protruding into the void (**Figure 3.45**).

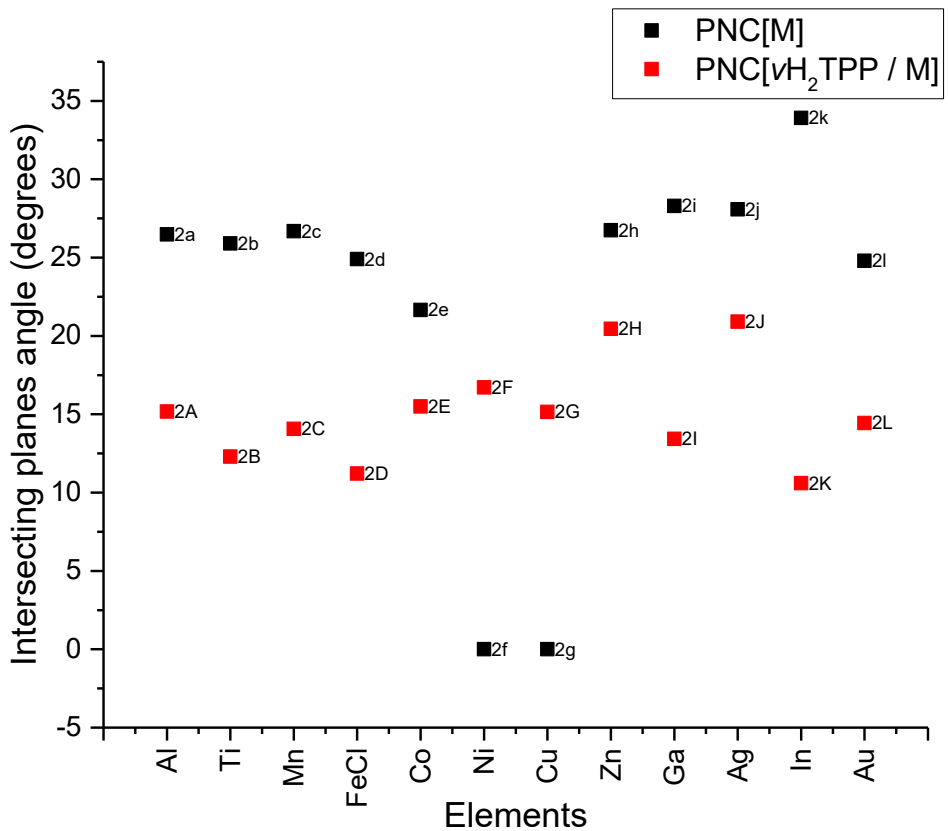

Figure 3.44. Comparing plot of different PNC[M] versus PNC[νH_2TPP / M] indicating the flexibility and rigidity of the two phthalocyanine systems.

The magnitude of the extrusion distance of the metal from the plane of the phthalocyanine is very similar for both PNCs with and without the TPP, however, when the TPP is incorporated the metal is forced into the cavity as the axial position facing the void is blocked by the TPP. Once again, this effect is most dramatic for $(dipPhO)_8PcIn$.

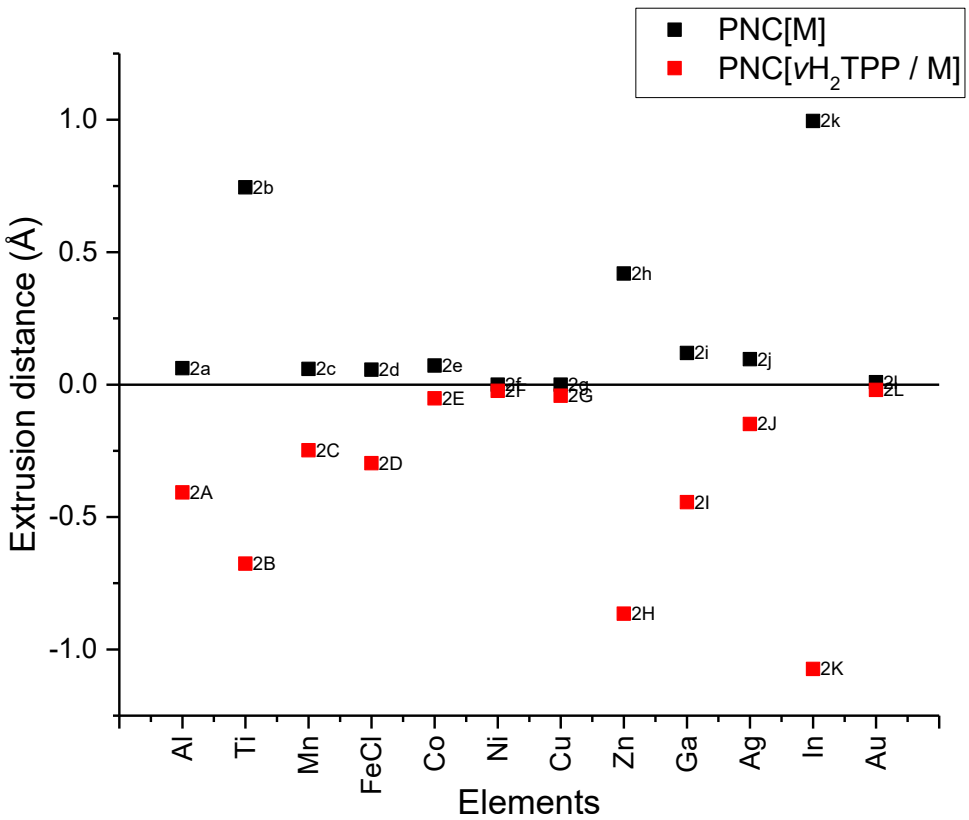

Figure 3.45. A comparison of the metal cation extrusion distances for different PNC[M] versus those for PNC[vH$_2$TPP/M].

3.16 SCSC transformations of PNC[vH$_2$/MTPP / H$_2$/M]

For the (dipPhO)$_8$PcH$_2$/H$_2$TPP co-crystals in the PNC structure, it was attempted to do single crystal to single metallations. The single-crystal to single-crystal transformations were performed within a single vial containing five crystals. One of these crystals was selected after the metalation was completed and was analysed with XRD. The same procedure was followed when the metalation and the bidentate ligand were inserted into the two macrocycles. There was no drop in data quality as the reflections could only reach a maximum of 1 Å, however after a number of data collections the crystal would no longer reflect. The experiment was performed by solubilising an excess of cobalt salt in MeOH and then adding this into the mother liquor in contact with the crystals. After three days, the crystals were analysed with XRD and the

experiment was successful, incorporating cobalt in both macrocycles with 100% occupancy (**Figure 3.46**).

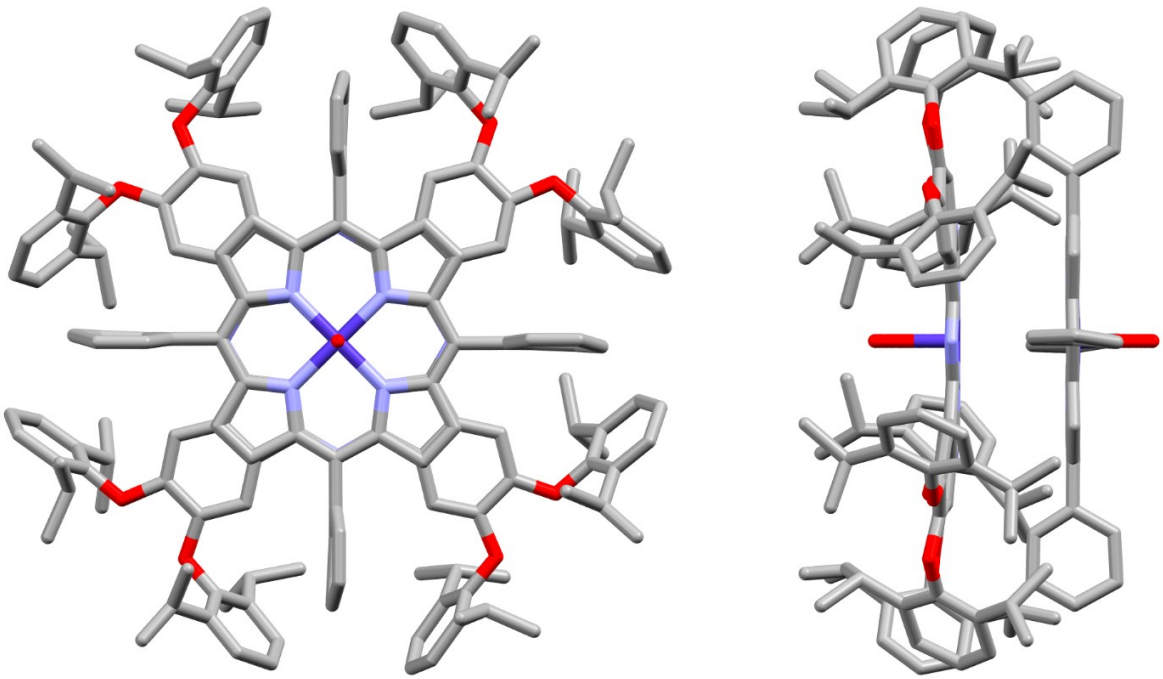

Figure 3.46. Molecular crystal structure of PNC[*v*H_2O-CoTPP / Co-*c*H_2O], cubic, $Pn\bar{3}n$.

Similarly for the co-crystal derived from $(dipPhO)_8PcCo$ and H_2TPP (PNC[*v*H_2TPP/Co] metalation of the TPP was attempted by adding an excess of $CuCl_2$ to the mother liquor that contained the crystals and after leaving for 3 days, the sample was analysed by XRD. Successful insertion of the copper in the TPP was observed with 100% occupancy to give PNC[*v*CuTPP /Co] (**Figure 3.47**).

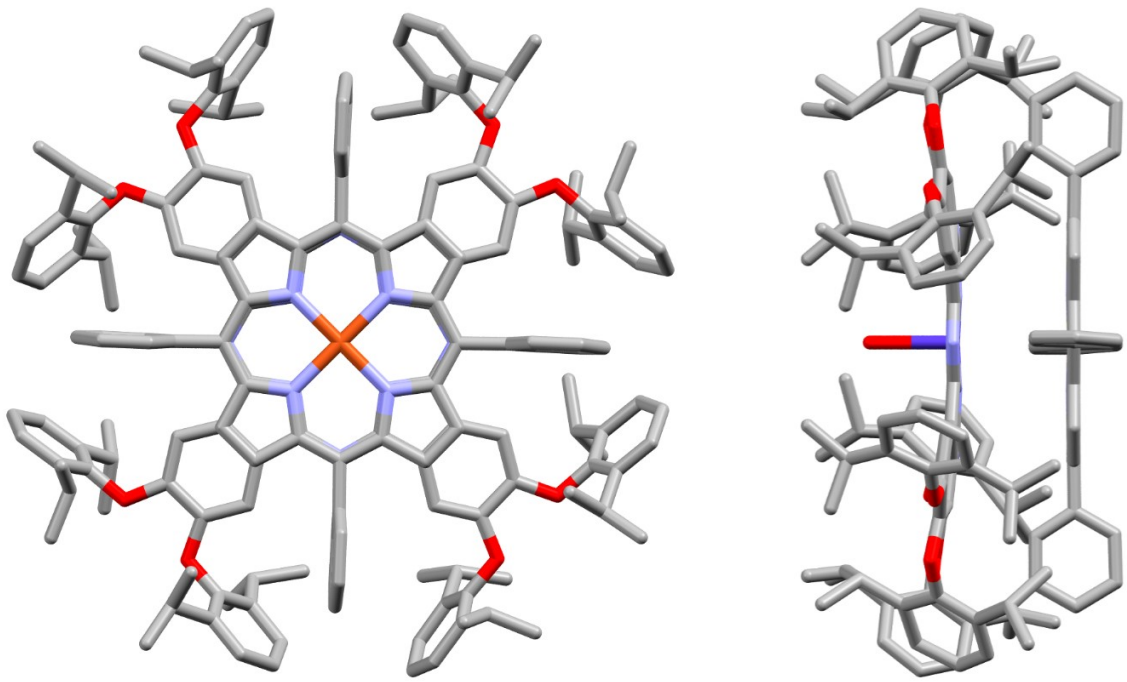

Figure 3.47. Molecular crystal structure of PNC[*v*CuTPP / Co-*c*H_2O], cubic, $Pn\bar{3}n$.

The next logical step was to do an *in-situ* incorporation of bipy and bpm, to act as a bidentate ligand to stabilise the crystal towards solvent removal. An excess of bipy was dissolved in MeOH and the solution was poured into the mother liquor in contact with the crystals. After three days the samples were analysed with XRD, and the insertion of the "wall-ties" was shown to be successful, binding across the cavity to the two cobalt cations of the phthalocyanines (**Table 3.3**).

Phthalocyanine tetraphenylporphyrin bidentate ligands complexes													
Acronym	Name	Chemical formula	M_r	Crystal system, space group	a (Å)	b (Å)	c (Å)	V (Å^3)	Z	Phthalocyanine curvature (degrees)	Metal to macrocycle distance (Å)	Macrocycle macrocycle distance (Å)	Metal to metal distance (Å)
PNC[*v* H_2O-*v* CoTPP/Co-*c* bipy-Co/*v* CoTPP-*v* H_2O]	$(dipPhO)_8PcCo$ + CoTPP + bipy	$(C_{128}H_{144}N_8O_8Co)_2$ $(C_{44}H_{28}N_4Co)_2$ $C_{10}H_8N_2$	5462.493	cubic, $Pn\bar{3}n$	37.8191(5)	37.8191(5)	37.8191(5)	54092.1	12	16.02	0.061	3.491	3.607
PNC[*v* CuTPP/Co-*c* bipy-Co/*v* CuTPP]	$(dipPhO)_8PcCo$ + CuTPP + bipy	$(C_{128}H_{144}N_8O_8Co)_2$ $(C_{44}H_{28}N_4Cu)_2$ $C_{10}H_8N_2$	5471.718	cubic, $Pn\bar{3}n$	37.91000(10)	37.91000(10)	37.91000(10)	54483	12	14.5	0.064	3.459	3.514
PNC[*v* CuTPP/Co-*c* bpm-Co/*v* CuTPP]	$(dipPhO)_8PcCo$ + CuTPP + bpm	$(C_{128}H_{144}N_8O_8Co)_2$ $(C_{44}H_{28}N_4Cu)_2$ $C_8H_6N_4$	5473.694	cubic, $Pn\bar{3}n$	37.80340(10)	37.80340(10)	37.80340(10)	54024.7	12	15.630	0.065	3.428	3.488
PNC[*v* H_2TPP/Co-*c* bipy-Co/*v* H_2TPP]	$(dipPhO)_8PcCo$ + H_2TPP + bipy	$(C_{128}H_{144}N_8O_8Co)_2$ $(C_{44}H_{28}N_4H_2)_2$ $C_{10}H_8N_2$	5348.658	cubic, $Pn\bar{3}n$	37.8503(2)	37.8503(2)	37.8503(2)	54226.1	12	15.58	0.053	3.480	N.A.
PNC[*v* H_2TPP/Co-*c* bpm-Co/*v* H_2TPP]	$(dipPhO)_8PcCo$ + H_2TPP + bpm	$(C_{128}H_{144}N_8O_8Co)_2$ $(C_{44}H_{28}N_4H_2)_2$ $C_8H_6N_4$	5350.634	cubic, $Pn\bar{3}n$	37.92800(10)	37.92800(10)	37.92800(10)	54560.7	12	14.26	0.072	3.482	N.A.

Table 3.3. PNC[*v* H_2/MTPP / M-*c* bipy/bpm-M / *v* H_2/MTPP]

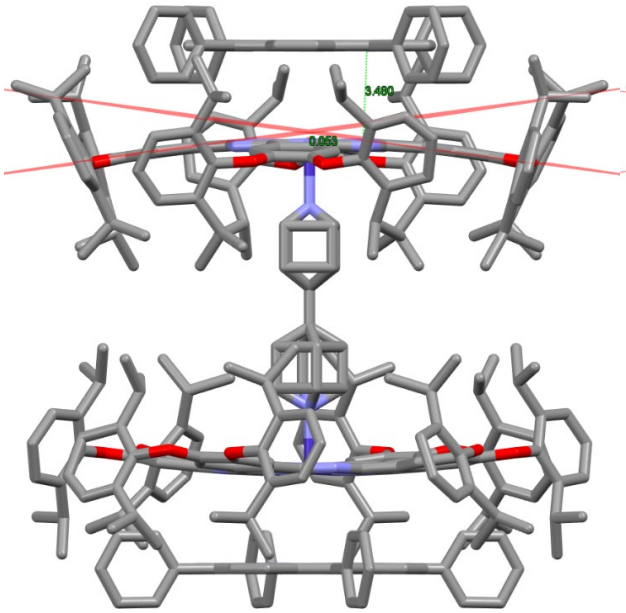

Figure 3.48. PNC[*v*H_2TPP/Co-*c*bipy-Co/*v*H_2TPP]

cubic, $Pn\bar{3}n$

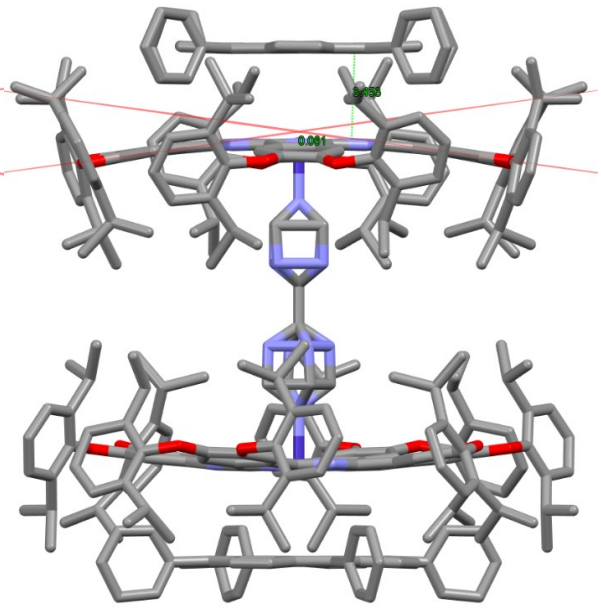

Figure 3.49. PNC[*v*H_2TPP/Co-*c*bpm-Co/*v*H_2TPP]

cubic, $Pn\bar{3}n$

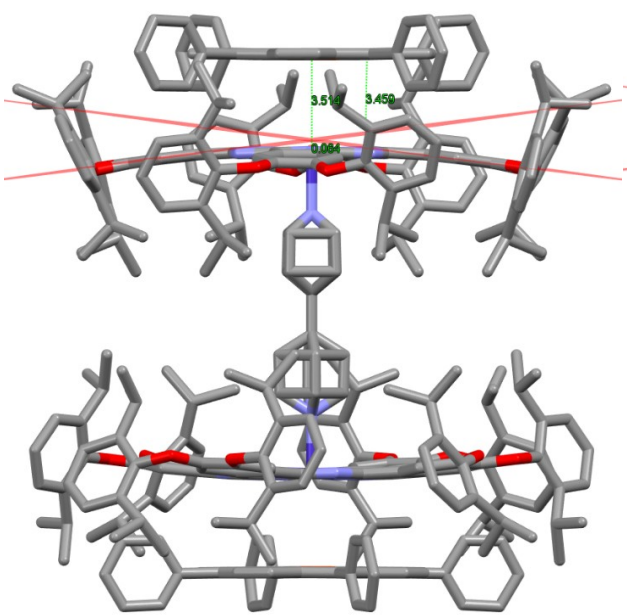

Figure 3.50. PNC[*v*CuTPP/Co-*c*bipy-Co / *v*CuTPP]

cubic, $Pn\bar{3}n$

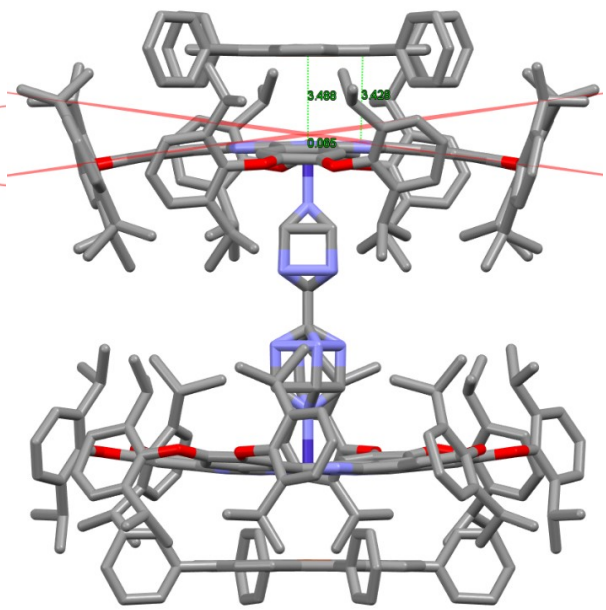

Figure 3.51. PNC[*v*CuTPP/Co-*c*bpm-Co/*v*CuTPP]

cubic, $Pn\bar{3}n$

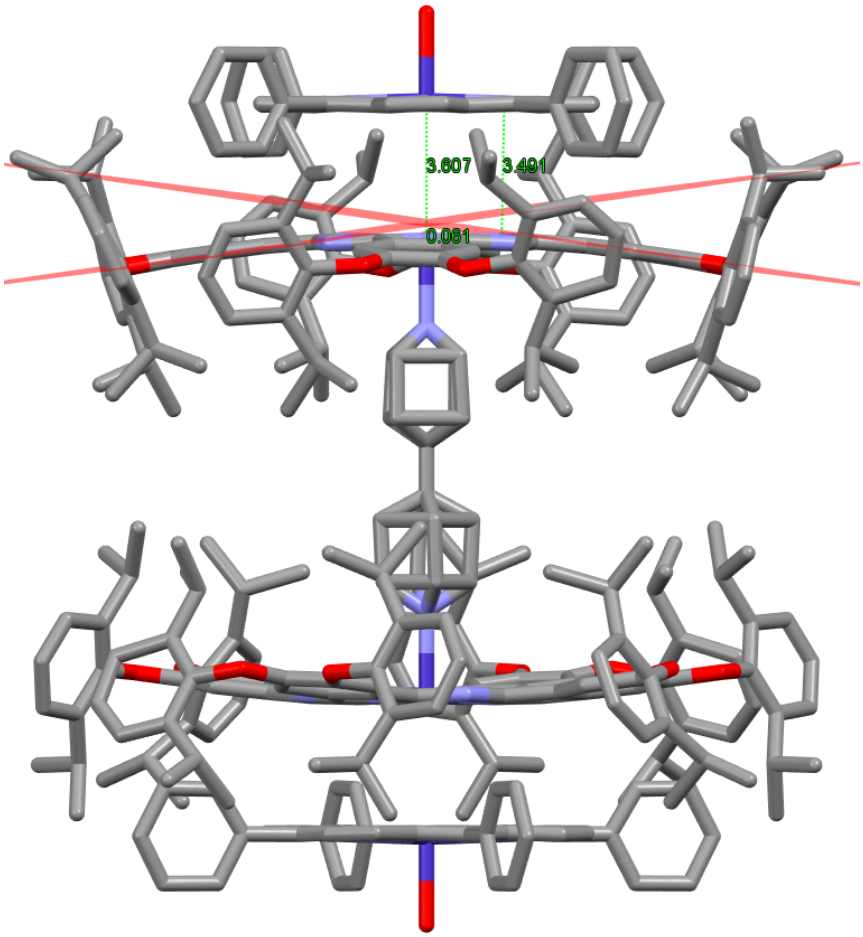

Figure 3.52. PNC[*v*H_2O-CoTPP/Co-*c*bipy-Co/*v*H_2O-CoTPP], cubic, $Pn\bar{3}n$

(Note that the legends shaded in red indicate structures obtained during the PhD programme.)

Sufficient sample of PNC[*v*H_2TPP/Co-*c*bipy-Co/*v*H_2TPP] was prepared in order to analyse using nitrogen adsorption at 77 K providing a value for the BET surface area of 450 $m^2\ g^{-1}$ with a pore volume of 0.22 ml g^{-1} (**Figure 3.53**). Both of these values are approximately half those obtained for PNC[Co-*c*bipy-Co] showing that the six TPP incorporated into each voids occupies around a half of the total porosity of the PNC structure.

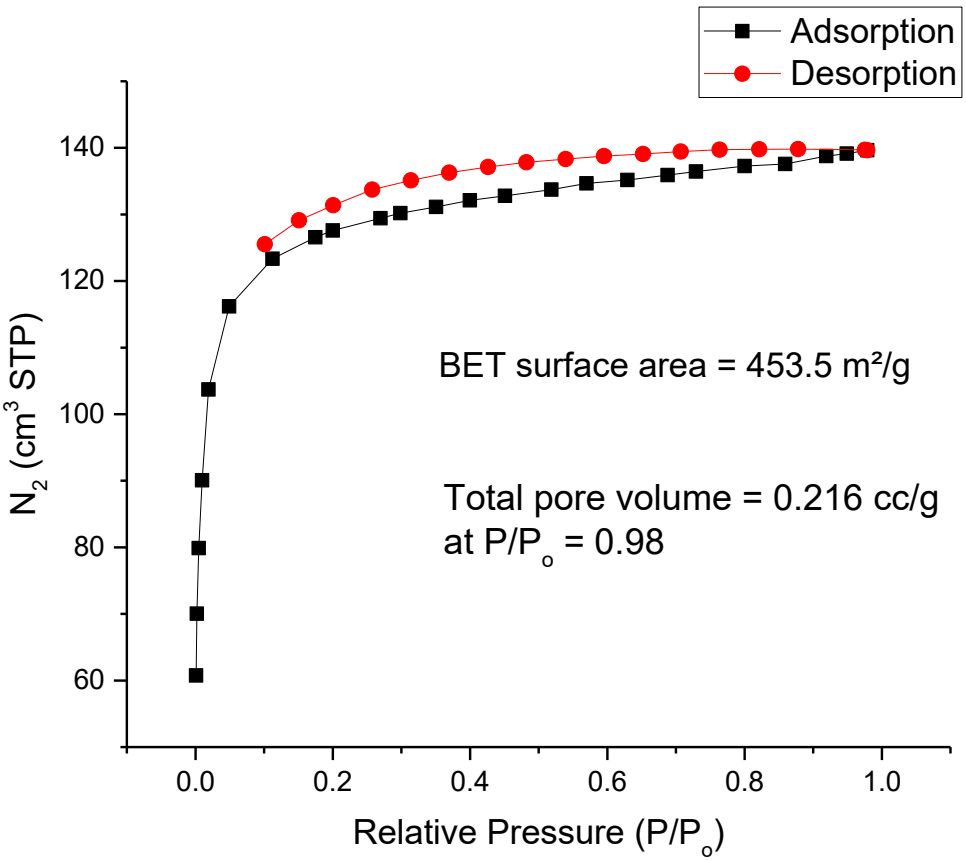

Figure 3.53. N_2 sorption isotherms of PNC[*v*H_2TPP/Co-*c*bipy-Co/*v*H_2TPP].

3.17 Cw-EPR of H_2/CuTPP (dipPhO)$_8$PcCo bipy

Cw-EPR experiments were performed on both powder samples and single crystals of PNC[*v*H_2CTPP/Co-*c*bipy-Co/*v*H_2TPP] and PNC[*v*CuTPP/Co-*c*bipy-Co/*v*CuTPP]. Firstly, the powder cw-EPR spectra of the compounds at diverse temperatures will be described. This will be followed by the results from single crystal cw-EPR spectroscopy.

For, PNC[*v*H_2TP /Co-*c*bipy-Co/*v*H_2TPP], spectra were recorded at room temperature (*ca.* 296 K) and at four other temperatures: 220 K, 120 K, 40 K and 5 K. As can be observed in **Figure 3.54**, the spectral line intensity increases when the temperature is lowered, and the overall shape of the spectrum also changes, displaying better resolved peaks. Characteristic ^{59}Co (I = 7/2)

hyperfine components are observed, along with a sharper signal at ca. 2000 G due to a Co(III)-O-O superoxo radical. The latter confirms the successful binding of oxygen to the metal.

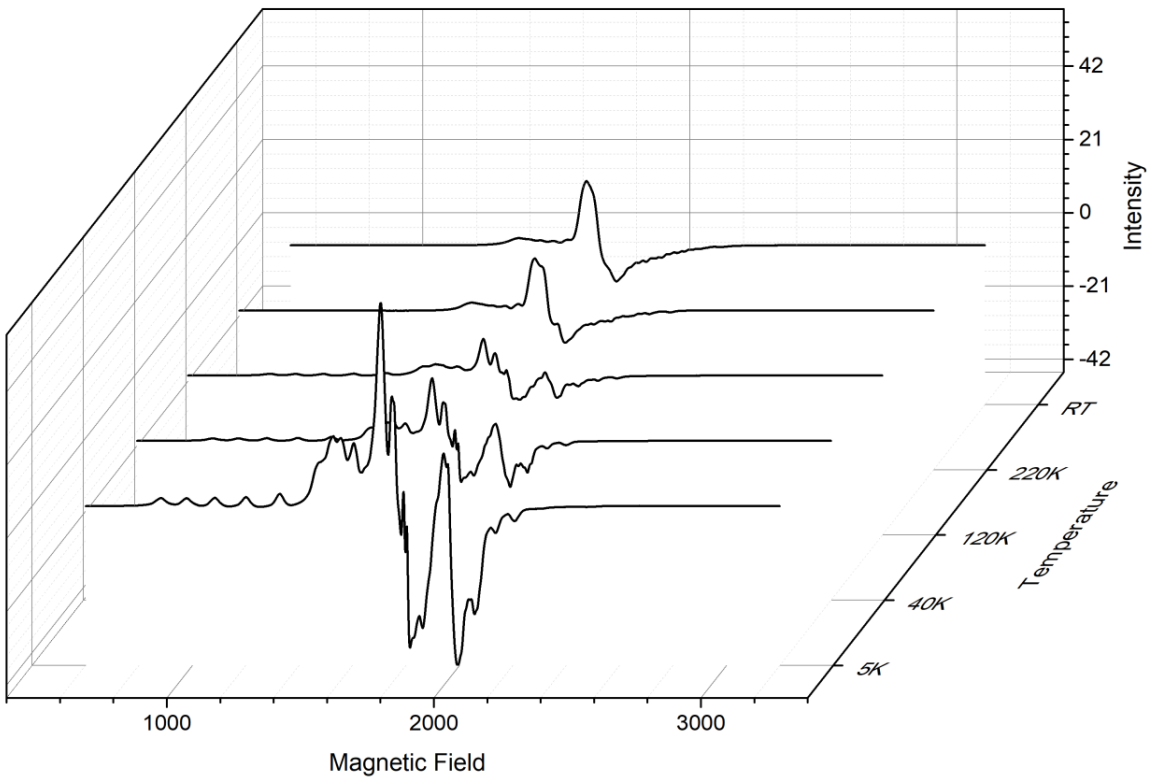

Figure 3.54. Powder cw-EPR spectra of PNC[*v*H_2TPP Co-*c*bipy-Co/*v*H_2TPP] at different temperatures.

For PNC[*v*CuTPP/Co-*c*bipy-Co/*v*CuTPP] spectra were acquired at room temperature (ca. 296 K) and at other four temperatures: 70 K, 40 K, 20 K and 5 K. On lowering the temperature, a clear quadruplet at 1200 to 1600 G is observed, which indicates the presence of Cu (I = 3/2), while at higher field the Co spectrum is observed (**Figure 3.55**). The super oxo radical signal is observed at ca. 3600 G (g = 2), confirming the successful binding of oxygen to the Co metal.

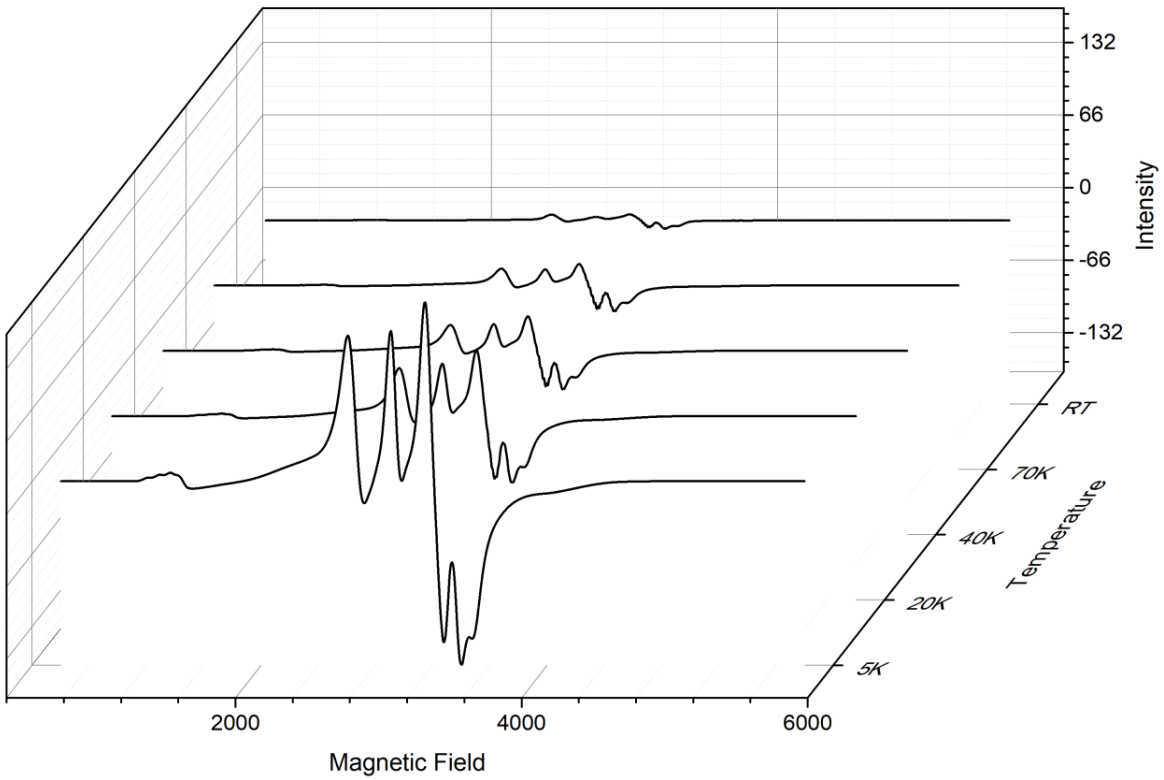

Figure 3.55. Powder cw-EPR spectra of PNC[*v*CuTPP/Co-*c*bipy-Co/*v*CuTPP] at different temperatures.

Single crystal EPR data for PNC[*v*H_2TPP/Co-*c*bipy-Co/*v*H_2TPP] were recorded at every 10 degrees of rotation at room temperature. Because of the high symmetry of the crystal, similar spectra at every 90 degrees are acquired (**Figures 3.56** and **3.57**).

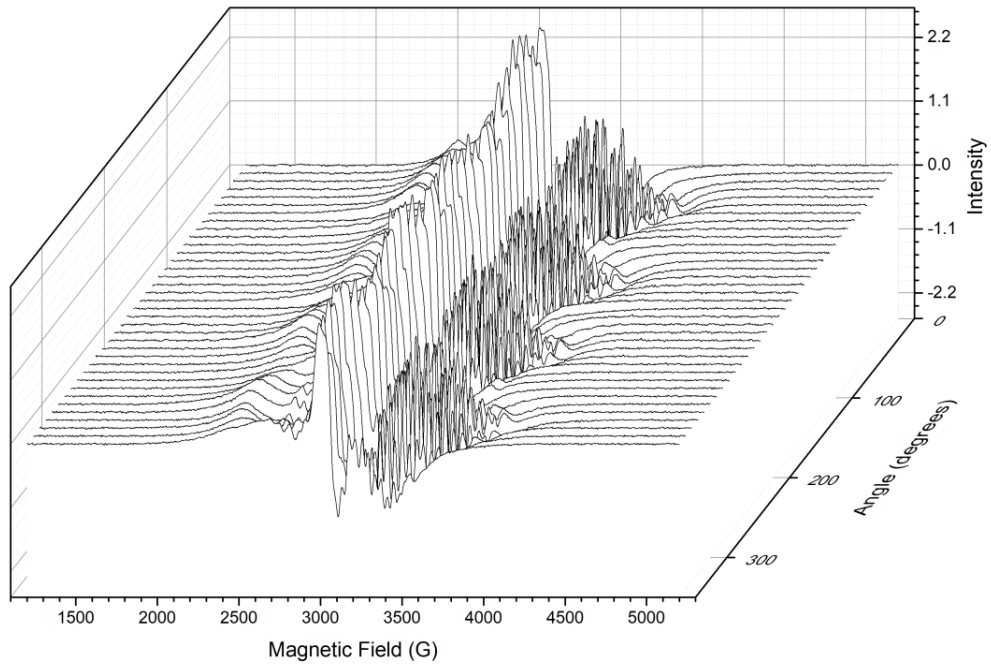

Figure 3.56. Waterfall representation of the X-band cw-EPR spectra of a single crystal of PNC[*v*H_2TPP/Co-*c*bipy-Co/*v*H_2TPP] that has followed rotation by 10 degrees around the z-axis of one of the dimers present in the structure.

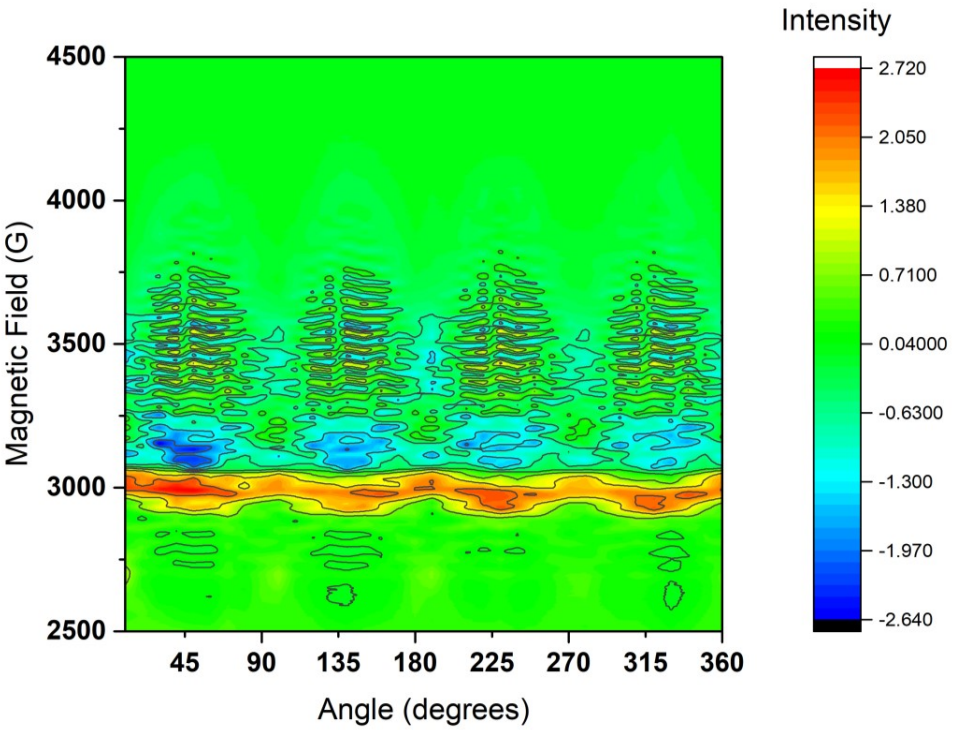

Figure 3.57. 2D representation of the X-band cw-EPR spectra of a single crystal of PNC[*v*H_2TPP/Co-*c*bipy-Co/*v*H_2TPP] that has undertaken rotation in similar conditions as in Figure 3.56.

3.18 Conclusions

Co-crystals of $(dipPhO)_8$PcM complexes with the novel wall-tie ligand bipyrimidine incorporated into the PNC structure were successfully prepared and found to resist structural collapse on removal of included solvent. The furthermore insertion of different metals on the nitrogen atoms on the bidentate ligand was unsuccessful but the chemisorption of small gases to the cobalt cation was investigated by single crystal XRD coupled to a gas cell (CO and NO) and by EPR (O_2). These studies revealed significant differences between the reactivity of the cobalt centre when bipyrimidine is used as wall-tie as compared to 4,4-bipyridyl.

Co-crystallisation of $(dipPhO)_8$PcM with metal free TPP produced a remarkable series of NPC structures in which the TPP was incorporated into the void of the crystals due to a symmetry dependent cofacial interaction between the phthalocyanine and porphyrin. Metals could be incorporated within the TPP via SCSC transformations, providing a system where two metals of

choice can be forced into close contact within a predictable crystal system. It was demonstrated that such metal-metal interactions can be probed using cw-EPR.

Chapter IV.

Conclusions and Future work

4.1 Conclusions

The work reported in this thesis further demonstrates the versatility of $(dipPhO)_8PcM$ complexes for the construction of porous molecular crystals. New metals have been incorporated into the macrocycle whilst retaining the cubic nanoporous structure. An analysis of the molecular structures within the PNCs shows that the structure tolerates large variations in phthalocyanine curvature and the extrusion distance of the metal cation from the macrocyclic plane.

Co-crystals which incorporate bidentate wall-ties stabilise the PNC structure but can also be used to modify the reactivity of the metal cation towards the chemisorption of small gases such as CO and NO, as probed by single crystal XRD combined with a gas cell, and O_2 as probed by EPR. The reversible binding of NO may have medical applications where the slow release of NO is beneficial for wound healing and as a disinfectant.

The co-crystallisation of TPP with $(dipPhO)_8PcM$ complexes has opened new possibilities for structural diversity with a large number of different combinations of metals within the PNC structure now possible. The close distance between the metals allows interactions, as demonstrated by EPR spin coupling, which may allow modifications of the reactivity of the accessible metalloporphyrin – one of the most studied class of molecular catalyst.

4.2 Future work:

4.2.1 Incorporation of the remaining elements in the phthalocyanine derivative

Most metallic elements have now been incorporated within the PNC structure as described in Chapter 2, especially if fullerene or TPP are used to make co-crystals, the latter being described in Chapter 3. However, some metals still remain unsuccessfully incorporated (e.g. B, K, Hf, Ge, Th) and may remain so and some are, as yet, unstudied (Li, Be, Na, Ca, Sr, Ba, As, Ta, Os, Hg, Tl, La, Ce, Nd, Pm, Sm, Gd, Ho, Er, Tm, Lu) (**Figure 4.1**). Due to their similar reactivities and ability to form Pc sandwich complexes the remaining lanthanide metals should be readily incorporated. In contrast, it is likely that the alkali metals will form similar non-PNC crystals as K. Radioactive elements (e.g. Tc and the Actinides) present difficulties for synthesis and would need to be investigated by a specialist research group. The other elements remain good cadicated for PNC inclusion.

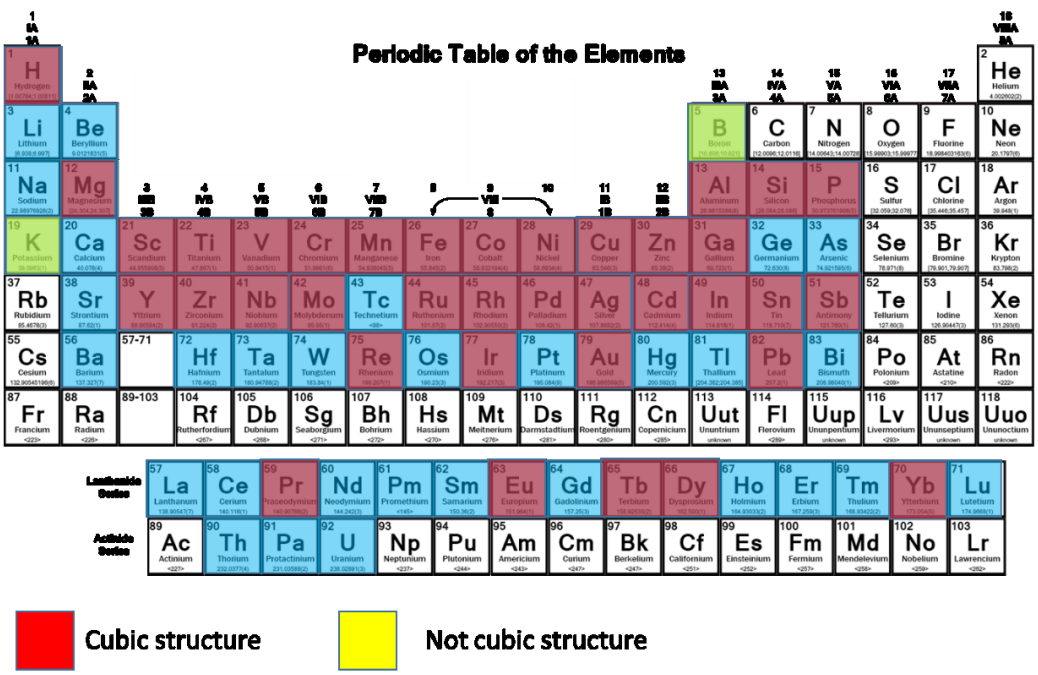

Figure 4.1. Periodic table depicting elements that form complexes with unsubstituted phthalocyanines shaded blue, red and yellow, with red the elements that form cubic nanoporous complexes with $(dipPhO)_8Pc$ and with yellow the elements that do not form cubic structure as characterised by sc-XRD analysis.

4.2.2 Incorporation of different metals in $(dipPhO)_8PcM$/TPP co-crystals.

As presented in Chapter 3, the co-crystallisation of $(dipPhO)_8PcM$ with TPP allows PNC formation with a range of metals in either the Pc or porphyrin macrocycles. As there are around 40 metals that can be incorporated within the central cavity of Pcs some 1600 combinations could be attempted. Those for which useful reactivity could be modified by the presence of a neighbouring metal, that show interesting metal-metal spin-coupling, or for which tandem catalysis could be performed should be prioritised. In addition, gas cell XRD could be used to investigate chemisorption and a sample of PNC[*v*CoTPP/Co-*c*bipy-Co/*v*CoTPP] and PNC[*v*CuTPP /Co-*c*bipy-Co/*v*CuTPP] have been submitted for study at the DLS.

4.2.3 The incorporation of substituted TPPs into PNCs

The investigation of $(dipPhO)_8PcM$ and the MTPP co-crystallisation has been made the topic of one of the Year 4 undergraduate mini-research projects within the School of Chemistry. Students are asked to prepare derivatives of TPP and study the aggregation with $(dipPhO)_8PcCo$ using UV-Vis, mass spectrometry, NMR, XRD. As an example, a non PNC co-crystal (space group = Pnma) was prepared from metal-free tetrakis(4-methylphenyl)porphyrin and $(dipPhO)_8PcM$ which indicates that substitution of the TPP at the *para* is not compatible with PNC formation, despite a neat 1:1 co-crystal being formed (**Figure 4.2**). This project will run regularly so that further data on this system will be acquired.

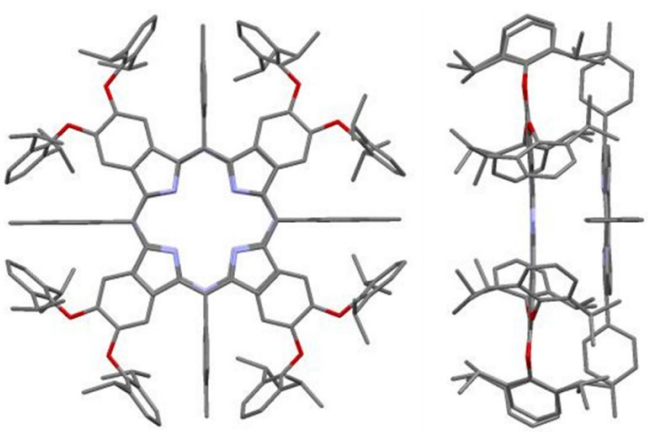

Figure 4.2. Molecular structure within the non-PNC $(dipPhO)_8PcH_2/H_2TPPMe_4$ co-crystal.

4.2.4 Incorporation of POMs as bidentate ligands or as axial ligands in the void.

Polyoxometalates (POMs) and phthalocyanines (Pc) are both widely studied as components of functional materials,[89,90] such as catalysts[91] and photonics, because each possesses enormous potential for structural variation and tuning of their electronic properties. In addition to POMs being good electron acceptors, in many ways the diverse photochemical, and coordination chemistry of phthalocyanines and POMs are complementary; therefore, robust complexes that photonically couple phthalocyanines and POMs should have unique properties. There are reports of materials wherein cationic phthalocyanines or porphyrins and POMs are mixed an axially bound POM counterion on Mo(V)Por,[92–95] and other porphyrin – POM structures,[96,97] but during the PhD programme it was attempted to prepare discrete ternary systems wherein a central metal ion is coordinated to both the PNC-forming $(dipPhO)_8PcM$ and a defect site in a lacunary POM. Following the previously reported procedure to prepare Zr(IV) and Hf(IV) porphyrins and phthalocyanines and the lacunary POM,[98,99] $H_3PW_{11}O_{39}^{4-}$ (**Figure 4.3**), the synthesis of the required $(dipPhO)_8PcHf$ with POM axial substituent was attempted.

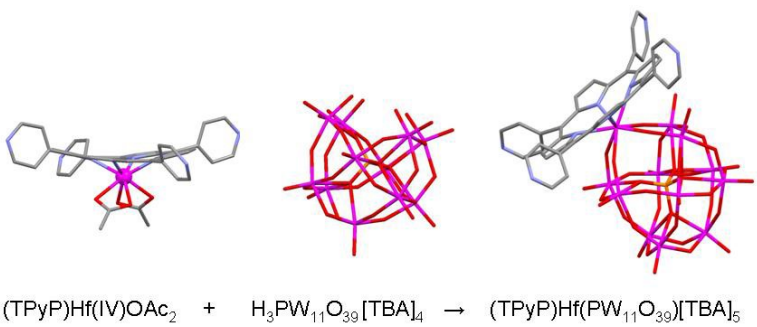

Figure 4.3. Molecular structures of the ternary complex TPP-Hf-POM.

The preparation of the lacunary polyoxometalate that was used for the synthesis of the ternary complexes of $(dipPhO)_8PcHf$-LPOM proved straightforward,[100] by using a slight modification of the synthesis by Ho and Klemperer and affords a product which can be used without any further purification (**Scheme 4.1**).

$$Na_2HPO_4 + Na_2WO_4 + TBABr \longrightarrow H_3PW_{11}O_{39}TBA_4$$

Scheme 4.1. Preparation of lacunary polyoxometalate.

The preparation of the complex of the lacunary polyoxometalate with the $(dipPhO)_8PcHf$ that following the procedure from Drain (**Scheme 4.2**),[98,99] where the $(dipPhO)_8PcHf$ was dissolved in a mixture of DCM/MeOH (1:1) and the LPOM was dissolved in MeCN as well as the counter ion TBA[Br] in MeCN. The resulting clear LPOM solution was added dropwise to the $(dipPhO)_8PcHf$ after which the counterion was added. The resulting mixture was stirred overnight, centrifuged, and then filtered through celite.

$$PcHfCl_2 + PW_{11}O_{39} + TBABr \longrightarrow PcHfPW_{11}O_{39}TBA_5$$

Scheme 4.2. Preparation of ternary complex $(dipPhO)_8PcHf$ – POM.

The complex was characterized by UV-Vis, mass spectrometry and XRD, which the first method did not show the anticipated shift of the $(dipPhO)_8PcHf$ peaks according to the publications.[98,99] When it was analysed with electron spray ionisation spectrometry (ESI – MALDI – TOF), the complex was formed and it was stable (**Figure 4.4**). Unfortunately, no crystals could be formed from this large complex.

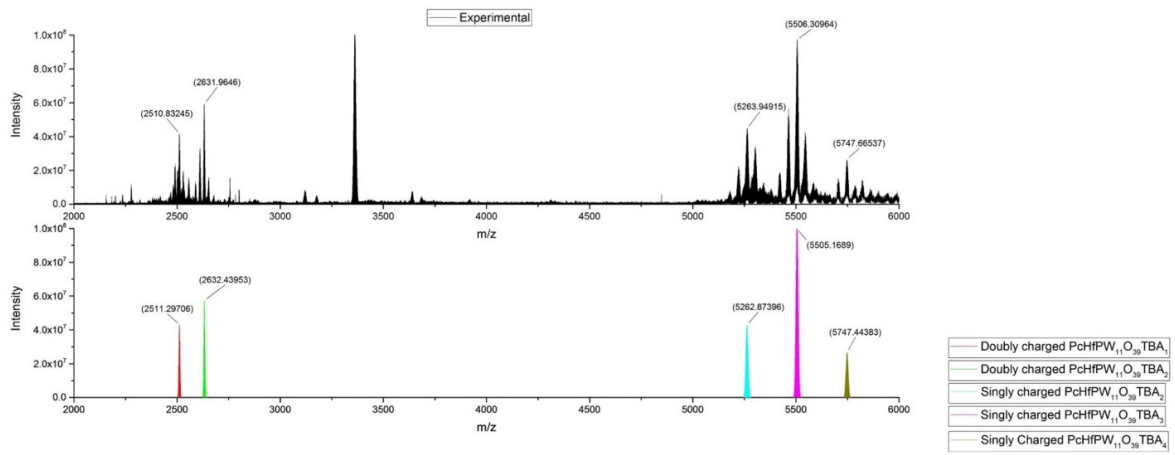

Figure 4.4. ESI spectrum of ternary complex $Pc1HfPW_{11}O_{39}$ with counter ion TBA and the simulation.

Chapter V:

Experimental

5.1 General

All reagents and solvents were purchased from Fisher Scientific, Alfa Aesar, Sigma-Aldrich or VWR and were used without further purification unless otherwise stated. Dry solvents were obtained were obtained from the lab solvent purification system where they are purified over activated alumina (diethyl ether, THF, toluene) of activated molecular sieves (hexane). All reactions using air/moisture sensitive reagents were conducted in oven-dried apparatus under a nitrogen atmosphere. Thin layer chromatography (TLC) analysis was carried out using aluminium- backed plates coated with Merck TLC silica gel 60 F254. Flash column chromatography was performed on silica gel from Sigma Aldrich (Particle size: 40 – 80 µm, pore size: 60 Å), or in cases where specified, neutral alumina from Sigma Aldrich (particle size: 50 – 150 µm).

5.2 Instrumentation

Microwave reactor

The reactions carried on a CEM Discover SP Microwave with ActiVent^{TM} technology apparatus to a maximum of 300 °C of temperature and 300 W of power.

Melting point analysis

Melting points were recorded on a Stuart SMP10 melting point apparatus to a maximum of 300 °C, and are uncorrected.

Thermogravimetric analysis

Thermogravimetric analysis (TGA) data were recorded on a TA SDT Q600 TGA system under N_2 atmosphere.

Infrared spectroscopy

Infra-red-spectra were recorded in the range of 4000 – 400 cm^{-1} using a Shimadzu IR Affinity-1S FTIR spectrophotometer as a solid powder.

UV-visible (UV-vis)

UV-visible absorption spectra were recorded in the range of 800 – 200 nm using a Shimadzu UV-1800 spectrophotometer.

Nuclear magnetic resonance (NMR)

^{1}H NMR spectra were recorded in a suitable deuterated solvent using an Advanced Bruker AVA400 (400 MHz) spectrometer, AVA500 (500 MHz) spectrometer equipped with a DCH cryo-probe, or PRO500 (500 MHz) spectrometer equipped with a Prodigy cryo-probe, with ^{13}C NMR recorded at 100 MHz, 125 MHz and 125 MHz respectively. Chemical shifts (δ_H and δ_C) are reported in parts per million relative to the traces of non-deuterated molecules in each corresponding deuterated solvent. The abbreviations s, d, t, q, m and br. refer to singlet, doublet, triplet, quartet, septuptlet, multiplet and broad resonances; all coupling constants were recorded in Hertz (Hz).

Mass spectrometry

MALDI-TOF-TOF mass spectroscopic analysis was performed on a Bruker Ultraflex Extreme spectrometer. Small molecule (< 1000 $gmol^{-1}$) low resolution mass spectrometry (LRMS) were performed using a Thermo Finnigan Sector instrument using electron ionisation (EI). Large molecule (> 3000 $gmol^{-1}$) high resolution mass spectrometry (HRMS) were performed with electron spray ionization using a Bruker MicrOTOF II UltrafleXreme with a MAT 900 sector which is internally calibrated using sodium formate.

5.3 General experimental procedure for metallated phthalocyanines

Preparation of metal phthalocyanines from phthalonitrile in bulk reaction with the use of microwave irradiation[101]

In a typical procedure, 4,5-di(2',6'-di-*iso*-propylphenoxy) phthalonitrile (**Pn1**) (0.20 mmol) and the appropriate metal salt (0.05 mmol) were heated by microwave irradiation at the required temperature and for the appropriate time depending on the metal. The product was then solubilised into DCM and precipitated with methanol.

5.4 Experimental procedures

4,5-Dichlorophthalonitrile[48]

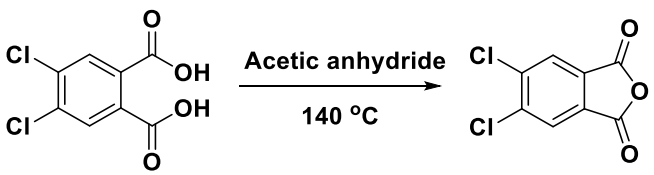

4,5-Dichlorophthalic acid (25.00 g, 106.00 mmol) and acetic anhydride (60.0 ml) were heated under gentle reflux for 5 h with slow distillation of solvent (15.0 ml). After cooling, the solid was filtered, washed with petroleum ether then dried under vacuum to obtain 5,6-dichlorobenzofuran-1,3-dione as a white powder (21.00 g, 96.77 mmol, 91%); m.p. 184 – 186 °C (lit[48] m.p. 184 – 186 °C); IR ($\tilde{\nu}$) 1830, 1786, 1378, 1310, 1248, 1094, 915, 733 cm^{-1}; ^{1}H NMR (400 MHz, $CDCl_3$) δ_H, ppm 8.44 (s, 2H, Ar*H*); ^{13}C NMR (100 MHz, $CDCl_3$) δ_C, ppm 161.1, 139.1, 131.1, 127.0; *m/z* (EI, LRMS) cluster of peaks centred at *m/z* = 216 g mol^{-1} (simulated for $C_8H_2O_3Cl_2$ formula cluster at 217.005 g mol^{-1}).

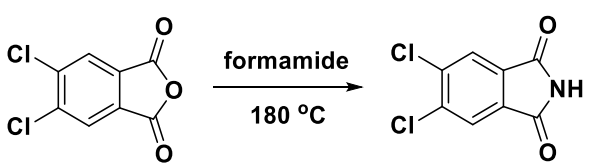

5,6-Dichlorobenzofuran-1,3-dione (21.00 g, 96.77 mmol) in formamide (40.0 ml) was heated at reflux for 3 h, under stirring. After cooling, the precipitate was filtered, washed with water and dried under vacuum to obtain 5,6-dichloroisoindoline-1,3-dione as an off-white powder (20.50 g,

94.91 mmol, 97%); m.p. 202 – 203 °C (lit[48] m.p. 193 – 195 °C); IR ($\tilde{\nu}$) 3225, 1711, 1345, 1059, 906, 742 cm^{-1}; ^{1}H NMR (400 MHz, $CDCl_3$) δ_H, ppm 8.05 (s, 2H, Ar*H*); ^{13}C NMR (100 MHz, $CDCl_3$) δ_C, ppm 167.0, 136.9, 132.4, 124.9; *m/z* (EI, LRMS) cluster of peaks centred at *m/z* = 215 g mol^{-1} (simulated for $C_8H_3O_2NCl_2$ formula cluster at 216.021 g mol^{-1}).

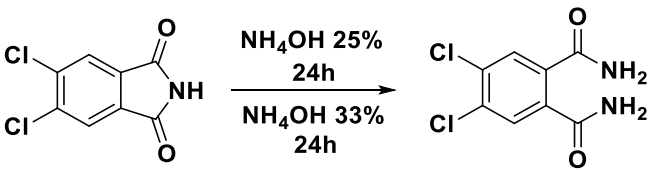

5,6-Dichloroisoindoline-1,3-dione (20.50 g, 94.91 mmol) was stirred for 24 h in 25% (w/v) NH_4OH (250.0 ml), then 33% (w/v) NH_4OH (100.0 ml) was added and stirring was continued for another 24 h. The precipitate was filtered, washed with water and dried under vacuum to obtain 4,5'-dichlorobenzene-1,2-diamide as a white powder (15.00 g, 64.38 mmol, 68%); m.p. 235 – 237 °C (lit[48] m.p. 245 – 247 °C); IR ($\tilde{\nu}$) 3426, 3296, 3131, 1667, 1608, 1173, 1121, 916, 897 cm^{-1}; ^{1}H NMR (400 MHz, $CDCl_3$) δ, ppm 7.84 (s, 2H, NH_2), 7.71 (s,2H, Ar*H*), 7.46 (s, 2H, NH_2); ^{13}C NMR (100 MHz, $CDCl_3$) δ, ppm 167.3, 136.2, 131.4, 129.3; *m/z* (EI, LRMS) cluster of peaks centred at *m/z* = 232 g mol^{-1} (simulated for $C_8H_6N_2O_2Cl_2$ formula cluster at 233.051 g mol^{-1}).

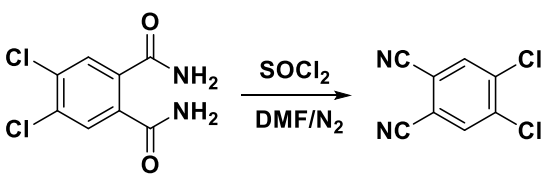

At 0 °C $SOCl_2$ (100.0 ml) was added under stirring and a N_2 atmosphere to anhydrous DMF (150.0 ml). After 2 h, 4,5'-dichlorobenzene-1,2-diamide (26.70 g, 114.60 mmol) was added and the mixture was stirred at 0 °C for 5 h, then at room temperature for 20 h. The mixture was slowly added to ice water to quench the excess of $SOCl_2$. The white product was collected by filtration and washed with water then recrystallised twice from methanol to obtain 4,5-dichlorophthalonitrile as an off-white crystalline material (17.50 g, 89.30 mmol, 78%); m.p. 180 – 183 °C (lit[48] m.p. 182 – 184 °C); IR ($\tilde{\nu}$) 2916, 2237, 1815, 1467, 1348, 1262, 1217, 1132, 917, 683 cm^{-1}; ^{1}H NMR (400 MHz, $CDCl_3$) δ_H, ppm 7.91 (s, 2H, Ar*H*); ^{13}C NMR (100 MHz, $CDCl_3$) δ_C, ppm

139.0, 134.9, 114.9, 113.6; *m/z* (EI, LRMS) cluster of peaks centred at *m/z* = 197 g mol^{-1} (simulated for $C_8H_2N_2Cl_2$ formula cluster at 197.021 g mol^{-1}).

4,5-Di(2',6'-di-*iso*-propylphenoxy)phthalonitrile (Pn1)[102]

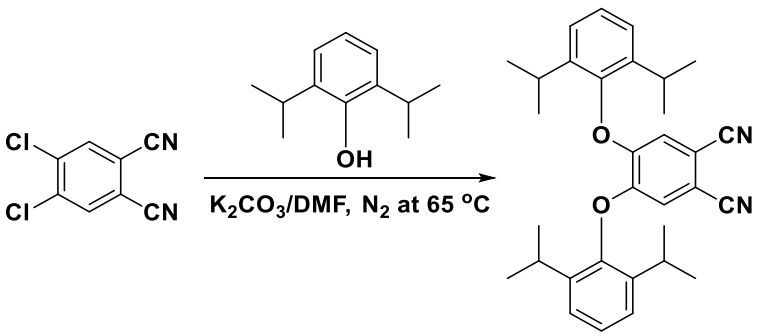

4,5-Dichlorophthalonitrile (7.00 g, 35.53 mmol) was dissolved into anhydrous dimethylformamide (105.0 ml), under N_2 atmosphere. Anhydrous potassium carbonate (19.00 g, 137.86 mmol) and then 2,6-di-*iso*-propylphenol (19.5 ml, 103.75 mmol) were added and stirred for 3 days at 65 °C. The mixture was cooled and was poured into H_2O (300.0 ml) and left stirring for 10 mins. The solid was filtered and washed with MeOH to remove the excess of the di-*iso*-propylphenol (purple colour) and dried under suction. The light blue product was purified by recrystallisation from MeOH (11.00 g, 60%); m.p. 161 – 163 °C; IR ($\tilde{\nu}$) 3080, 2228, 1589, 1503, 1332, 1096, 881, 795 cm^{-1}; ^{1}H NMR (400 MHz, $CDCl_3$) δ_H, ppm 7.26 (m, 6H, Ar*H*), 6.69 (s, 2H, Ar*H*), 2.87 (sept, 4H, *J* = 6.7 Hz, CH_3CHCH_3) 1.18 – 1.10 (d, 24H, *J* = 6.7 Hz, CH_3CHCH_3); ^{13}C NMR (100 MHz, $CDCl_3$) δ_C, ppm 151.4, 147.0, 140.6, 127.3, 125.1, 117.7, 115.3, 109.1, 27.4, 24.1, 22.4; *m/z* (EI, LRMS) $M^{\bullet+}$ 481 g mol^{-1} *m/z* (EI, LRMS) cluster of peaks centred at *m/z* = 481 g mol^{-1} (simulated for $C_8H_2N_2(OC_{12}H_{17})_2$ formula cluster at 480.641 g mol^{-1}).

2,3,9,10,16,17,23,24-Octa(2',6'di-*iso*-propylphenoxy)phthalocyanine [$(dipPhO)_8PcH_2$]

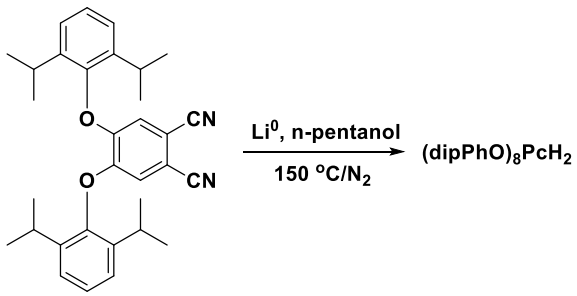

In a typical procedure lithium metal was added to a solution of 4,5-di(2',6'-di-*iso*-propylphenoxy) phthalonitrile (3.00 g, 2.10 mmol) in refluxing anhydrous *n*-pentanol (15.0 ml) under nitrogen and with stirring. The mixture of reaction was refluxed for 5 h and then cooled and acetic acid was added (3.0 ml, 0.1 M). The solvent was removed under reduced pressure to give the crude green product, which was purified by reprecipitation from chloroform solution with methanol to give $(dipPhO)_8PcH_2$ as a light green powder (1.41 g, 0.73 mmol, 35%); m.p. > 300 °C; IR ($\tilde{\nu}$) 3576, 2962, 1439, 1328, 1265, 1184, 1093, 1017, 877, 754 cm^{-1}; UV/Vis (DCM) λ 702.5, 667.5, 607, 420.5, 348.5, 297, 229.5 nm; ^1H NMR (500 MHz, $CDCl_3$) δ_H, ppm 8.13 (br, 8*H*), 7.50 (m, 24H, Ar*H*), 3.37 (sept, 16H, *J* = 6.5 Hz, CH_3CHCH_3), 1.28 (br m, 96H, CH_3CHCH_3), -0.84 (s, 2H, N*H*); ^{13}C NMR (125 MHz, $CDCl_3$) δ_C, ppm 152.6, 151.0, 149.1, 141.7, 139.8, 132.2, 126.4, 124.7, 107.4, 27.4, 23.8, 23.6; *m/z* (MALDI-TOF): cluster of peaks centred at *m/z* = 1925.710 g mol^{-1} (simulated for $C_{128}H_{146}N_8O_8$ formula 1924.585 g mol^{-1}); elemental analysis calc (%) for $C_{128}H_{146}N_8O_8$: C 79.88, H 7.65, N 5.82, found C 80.04, H 7.70, N 5.70; crystal data: first polymorph (DCM/MeOH) monoclinic, space group $P2_1/c$, *a* = 2.1293(7) nm, *b* = 1.6896(5) nm, *c* = 1.8283(6) nm, β = 114.657(4), *V* = 5.9778(7) nm^3, *Z* = 2, R_I = 0.0838. The asymmetric unit contains ½ of Pc1 with a solvent methanol molecule; second polymorph (EtOAc – DCM/MeOH) orthorhombic, space group *Pbca*, *a* = 1.94927(12) nm, *b* = 1.62918(10) nm, *c* = 3.8420(2) nm, *V* = 1.2201(1) nm^3, *Z* = 4, R_I = 0.0677. The asymmetric unit contains ½ of $(dipPhO)_8PcH_2$ with 2 solvent ethyl acetate molecules.

Cobalt(II)2,3,9,10,16,17,23,24-Octa(2',6'di-*iso*-propylphenoxy)phthalocyanine [(dipPhO)$_8$PcCo][39]

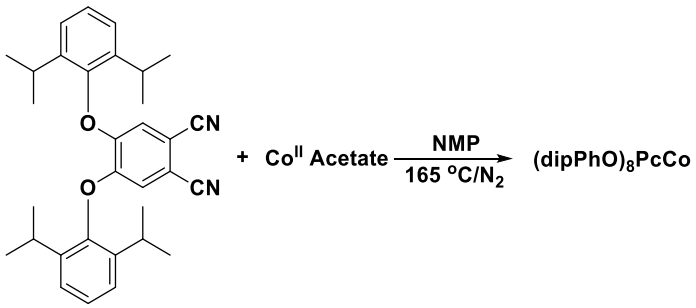

A stirred solution of 4,5-di(2',6'-di-*iso*-propylphenoxy) phthalonitrile (1.00 g, 2.10 mmol) and cobalt(II) acetate (0.130 g, 0.735 mmol) in anhydrous NMP (2.0 ml) was heated at 165 °C for 20 h under nitrogen. The reaction mixture was cooled to room temperature and poured into water (15.0 ml). The crude product was collected by filtration and then purified by reprecipitation from chloroform solution with methanol to give (dipPhO)$_8$PcCo as dark blue-green powder (0.60 g, 0.20 mmol, 60%); m.p. > 300 °C; IR ($\tilde{\nu}$) 2961, 1612, 1462, 1456, 1413, 1353, 1269, 1186, 1095, 1050, 904, 864, 799, 777, 755, 729 cm^{-1}; UV/Vis (DCM) λ 673, 608, 404, 331, 302, 229 nm; *m/z* (MALDI-TOF): cluster of peaks centred at *m/z* = 1982.055 g mol^{-1} (simulated for $C_{128}H_{144}N_8O_8Co$ formula 1982.935 g mol^{-1}); elemental analysis calc (%) for $C_{128}H_{146}N_8O_8Co$: C 77.59, H 7.32, N 5.66 found C 77.68, H 7.52, N 5.52; crystal data: first polymorph (DCM/acetone) monoclinic, space group $P2_1/c$, a = 3.8714(3) nm, b = 1.68469(12) nm, c = 1.82104(13), β = 90.7290(10), V = 11.8761(15) nm^3, Z = 4, R_I = 0.0792, the asymmetric unit contains 1 molecule of (dipPhO)$_8$PcCo with 2 disordered DCM solvent molecules; second polymorph (DCM/MeOH) cubic, $Pn\bar{3}n$, $a = b = c$ = 3.7391(3) nm, V = 52.2759 nm^3, Z = 12, R_I = 0.0983. The asymmetric unit contains ¼ of (dipPhO)$_8$PcCo molecule together with a solvent atom, assumed to be water at an occupancy of 50 %. In the axial sites there is a water/MeOH molecule.

Zinc(II)2,3,9,10,16,17,23,24-Octa(2',6'di-*iso*-propylphenoxy)phthalocyanine [(dipPhO)$_8$PcZn][39,40]

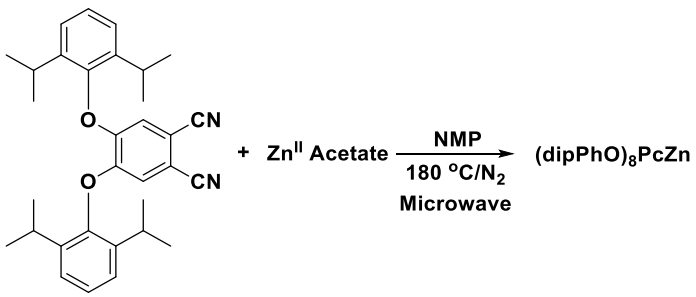

4,5-Di(2',6'-di-*iso*-propylphenoxy) phthalonitrile (0.30 g, 0.60 mmol) and zinc(II) acetate (0.11 g, 0.60 mmol) in anhydrous NMP (1.0 ml) were reacted as described in the general procedure for 1.5 h at 180 °C to give (dipPhO)$_8$PcZn as a dark green powder (0.20 g, 0.4 mmol, 60%); m.p. > 300 °C; IR ($\tilde{\nu}$) 2963, 1609, 1456, 1400, 1329, 1271, 1186, 1092, 1025, 894, 795 cm^{-1}; UV/Vis (DCM) λ 683, 653, 615, 347, 296, 229 nm; ^{1}H NMR (500 MHz, $CDCl_3$) δ_H, ppm 8.16 (s, 8H, Ar*H*), 7.50 (m, 24H, Ar*H*), 3.37 (sept, 16H, *J* = 6.5 Hz, CH_3CHCH_3), 1.28 (br m, 96H, CH_3CHCH_3); ^{13}C NMR (125 MHz, $CDCl_3$) δ_C, ppm 152.6, 150.7, 149.3, 141.8, 139.8, 132.2, 126.3, 124.7, 107.4, 27.5, 23.8, 23.6; *m/z* (MALDI-TOF): cluster of peaks centred at *m/z* = 1988.623 g mol^{-1} (simulated for $C_{128}H_{144}N_8O_8Zn$ formula 1989.012 g mol^{-1}); elemental analysis calc (%) for $C_{128}H_{146}N_8O_8Zn$: C 76.64, H 7.34, N 5.59 found C 76.95, H 7.53, N 5.58; crystal data (DCM/MeOH) cubic, space group $Pn\bar{3}n$, *a* = *b* = *c* = 3.7391(3) nm, *V* = 52.2759 nm^3, *Z* = 12, R_1 = 0.0983. The asymmetric unit contains ¼ of (dipPhO)$_8$PcZn molecule together with a solvent atom, assumed to be MeOH at an occupancy of 50 %.

Copper(II)2,3,9,10,16,17,23,24-Octa(2',6'di-*iso*-propylphenoxy)phthalocyanine [(dipPhO)$_8$PcCu][39,40]

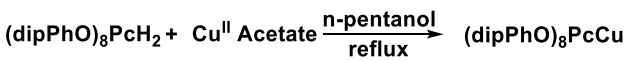

2,3,9,10,16,17,23,24-Octa(2',6'di-*iso*-propylphenoxy) phthalocyanine [(dipPhO)$_8$PcH$_2$] (0.10 g, 0.05 mmol) and copper(II) acetate (0.47 g, 2.50 mmol) in n-pentanol (5.0 ml) were heated at reflux for 4 h. After cooling, the slurry of reaction was dissolved in toluene and filtered to remove the excess of Cu^{II}acetate, and the solvent was evaporated under reduced pressure. The crude

product was purified by reprecipitation with methanol from its solution in DCM to give $(dipPhO)_8PcCu$ as dark green powder (0.08 g, 0.04 mmol, 80%); m.p. > 300 °C; IR ($\tilde{\nu}$) 2962, 1611, 1461, 1406, 1351, 1271, 1186, 1095, 1034, 899, 797, 775 cm^{-1}; UV/Vis (DCM) λ 682, 614, 405, 343, 295, 230 nm; *m/z* (MALDI-TOF): cluster of peaks centred at *m/z* = 1988.334 g mol^{-1} (simulated for $C_{128}H_{144}N_8O_8Cu$ formula cluster at 1987.842 g mol^{-1}); elemental analysis calc (%) for $C_{128}H_{144}N_8O_8Cu$: C 77.41, H 7.31, N 5.64 found C 77.97, H 7.52, N 5.36; crystal data (DCM/acetone) monoclinic, space group $P2_1/c$, a = 3.8607(2) nm, b = 1.68676(10) nm, c = 1.84282(11) nm, β = 91.3750, V = 11.997 nm^3, Z = 4, R_1 = 0.0747, the asymmetric unit contains 1 molecule of $(dipPhO)_8PcCu$ with a solvent acetone molecule and disordered solvent assumed to be DCM.

Nickel(II)2,3,9,10,16,17,23,24-Octa(2',6'di-*iso*-propylphenoxy)phthalocyanine [$(dipPhO)_8PcNi$][39,40]

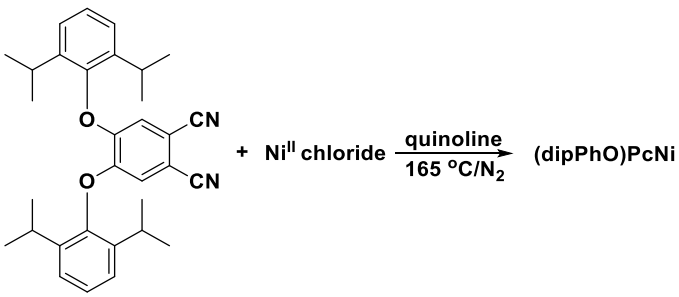

4,5-Di(2',6'-di-*iso*-propylphenoxy) phthalonitrile (0.50 g, 1.00 mmol) and nickel (II) chloride (0.10 g, 0.77 mmol) in anhydrous quinoline (1.0 ml) were heated at 165 °C for 30 h under nitrogen atmosphere. The reaction mixture was cooled to room temperature, poured into a mixture of methanol – water (20.0 ml, 1:1) then filtered off. The crude product was purified be reprecipitation with methanol from DCM solution to give $(dipPhO)_8PcNi$ as dark green powder (0.26 g, 0.50 mmol, 50%); m.p. > 300 °C; IR ($\tilde{\nu}$) 2962, 1464, 1417, 1359, 1272, 1189, 1095, 1051, 905 cm^{-1}; UV/Vis (DCM) λ 673, 608, 405, 309, 234 nm; ^{1}H NMR (500 MHz, $CDCl_3$) δ_H, ppm 8.03 (s, 8H, Ar*H*), 7.56 (m, 24H, Ar*H*), 7.45 (d, 16H, J = 7.7 Hz, Ar*H*) 3.42 (sept, 16H, J = 6.8 Hz, CH_3CHCH_3), 1.25 (br m, 96H, CH_3CHCH_3); ^{13}C NMR (125 MHz, $CDCl_3$) δ_C, ppm 152.4, 150.8, 149.1, 145.3, 141.7, 139.6, 131.4, 106.5, 132.4, 126.1, 125.2, 107.6, 27.4, 23.8, 23.6; *m/z* (MALDI-TOF): cluster of peaks centred at *m/z* = 1980.657 g mol^{-1} (simulated for $C_{128}H_{144}N_8O_8Ni$ formula 1979.012 g mol^{-}

[1]); Elemental analysis calc (%) for $C_{128}H_{146}N_8O_8Ni$: C 77.60, H 7.33, N 5.66 found C 77.67, H 7.22, N 5.27; crystal data (DCM/MeOH) monoclinic, space group $P2_1/c$, a = 2.1370(2) nm, b = 1.688255(18) nm, c = 1.8726(2) nm, β = 115.0680(10), V = 6.0987(11) nm^3, Z = 2, R_I = 0.0550, the asymmetric unit contains ½ molecule of $(dipPhO)_8PcNi$ with a fully occupied $CHCl_3$ molecule.

2,3,9,10,16,17,23,24-octa(2',6'di-*iso*-propylphenoxy) phthalocyanine metal derivatives

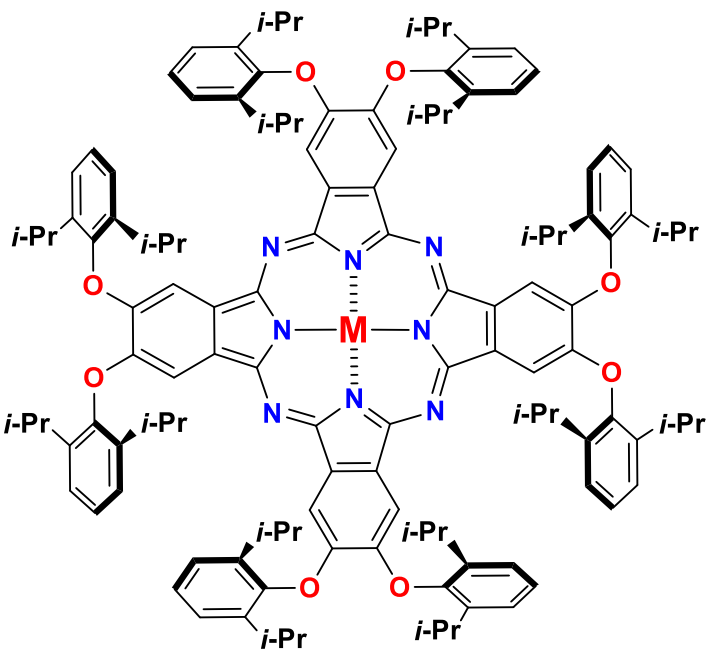

M = Fe^{3+}
M = P^{5+}
M = Ge^{3+}
M = Mo^{4+}
M = Cd^{2+}
M = Sb^{2+}
M = Hf^{4+}
M = W^{5+}
M = Re^{5+}
M = Ir^{3+}
M = Pt^{2+}
M = Pb^{2+}
M = Bi^{2+}

Molybdenum(IV)2,3,9,10,16,17,23,24-Octa(2',6'di-*iso*-propylphenoxy)phthalocyanine [$(dipPhO)_8PcMo$][103]

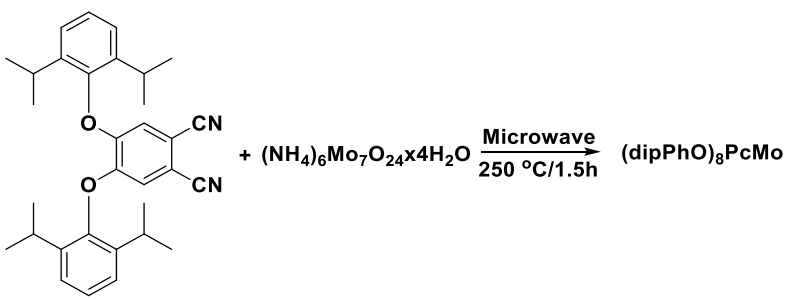

4,5-Di(2',6'-di-*iso*-propylphenoxy) phthalonitrile (0.20 g, 0.40 mmol) and ammonium heptamolybdate (0.12 g, 0.1 mmol) were reacted as described in the general procedure for 1.5 h at 250 °C. The crude product was purified be reprecipitation with methanol from DCM solution to give $(dipPhO)_8PcMo$ as dark green powder (0.10 g, 0.13 mmol, 35%); m.p. > 300 °C; IR ($\tilde{\nu}$) 3062,

2960, 2868, 2358, 1606, 1456, 1394, 1327, 1269, 1184, 1080, 1028, 902, 858, 792, 775, 748, 727 cm^{-1}; UV/Vis (DCM) λ 706, 667.8, 637, 601.8, 379 nm; ^{1}H NMR (500 MHZ, $CDCl_3$) δ_H, ppm 8.22 (s, 8H, Ar*H*), 7.62 (t, 8H, Ar*H*), 7.51 (d, 16H, Ar*H*), 3.45 – 3.39 (m, 16 H, C*H*$_3$CHC*H*$_3$), 1.44 – 1.08 (m, 96H, C*H*CH_3); ^{13}C NMR (125 MHZ, $CDCl_3$) δ_C, ppm 152, 151, 149, 142, 131, 127, 125, 107, 28, 27, 24, 23; *m/z* (MALDI-TOF): cluster of peaks centred at *m/z* = 2034.128 g mol^{-1} (simulated for $C_{128}H_{144}N_8O_8MoO$ formula 2035.014 g mol^{-1}); crystal data ($CHCl_3$/MeOH) cubic, space group $Pn\bar{3}n$, *a* = *b* = *c* = 3.75869 (5) nm, *V* = 53.1018 (2) nm^3, *Z* = 12, R_I = 0.1831, the asymmetric unit contains ¼ molecule of $(dipPhO)_8PcMo$ with a fully occupied $CHCl_3$ molecule and with 50% occupancy of the axial oxygen on either side.

Rhenium(V)2,3,9,10,16,17,23,24-Octa(2',6'di-*iso*-propylphenoxy)phthalocyanine [$(dipPhO)_8PcRe$][104]

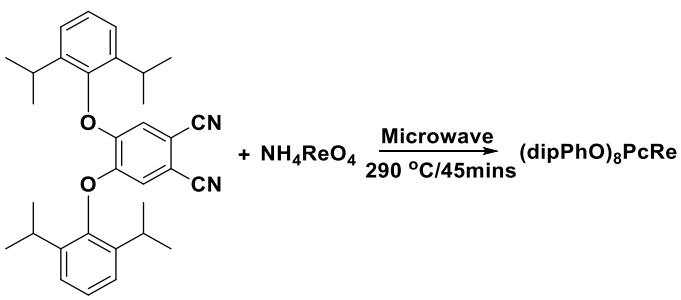

4,5-Di(2',6'-di-*iso*-propylphenoxy) phthalonitrile (0.40 g, 0.80 mmol) and ammonium perrhenate (0.06 g, 0.20 mmol) were reacted as described in general procedure for 45 mins at 290 °C. The crude product was purified be reprecipitation with methanol from DCM solution to give $(dipPhO)_8PcRe$ as dark green powder (0.06 g, 0.03 mmol, 10%); m.p. > 300 °C; IR ($\tilde{\nu}$) 3680, 3062, 3022, 3005, 2962, 2924, 2868, 2845, 1606, 1458, 1438, 1398, 1361, 1346, 1327, 1271, 1257, 1184, 1170, 1145, 1095, 1058, 1045, 1031, 904, 862, 796, 777, 754, 729 cm^{-1}; UV/Vis (DCM) λ 703, 671, 631.2, 433.8, 364.2, 344.2, 304.2, 282.2, 258.2 nm; ^{1}H NMR (500 MHz, $CDCl_3$) δ_H, ppm 8.22 (s, 8*H*), 7.61 (t, 8H, *J* = 8.5 Hz, Ar*H*), 7.50 (d, 16H, *J* = 6.5 Hz, Ar*H*) 3.44 (sept, 16H, *J* = 6.5 Hz, CH_3CHCH_3), 1.35 (br m, 96H, C*H*$_3$CHC*H*$_3$); ^{13}C NMR (125 MHz, $CDCl_3$) δ_C, ppm 151.7, 148.8, 147.9, 131.5 126.5, 124.8, 107.1, 27.4; *m/z* (MALDI-TOF): cluster of peaks centred at *m/z* = 2124.315 g mol^{-1} (simulated for $C_{128}H_{144}N_8O_8ReN$ formula cluster at 2123.073 g mol^{-1}); crystal data ($CHCl_3$/MeOH): Cubic, space group $Pn\bar{3}n$, *a* = *b* = *c* = 3.76052 (2) nm, *V* = 53.1794 nm^3, *Z* = 12, R_I = 0.1078, the asymmetric unit contains ¼ of the molecule of $(dipPhO)_8PcRe$ with one molecule of

nitrogen in the axial position, together with two molecules of chloroform that can be solved crystallographically. The calculated residual electron count per unit cell was 217, calculated by SQUEEZE relating to a possible 4 molecules of $CHCl_3$ per unit cell.

Bismuth(II)2,3,9,10,16,17,23,24-Octa(2',6'di-*iso*-propylphenoxy)phthalocyanine [$(dipPhO)_8PcBi$][105]

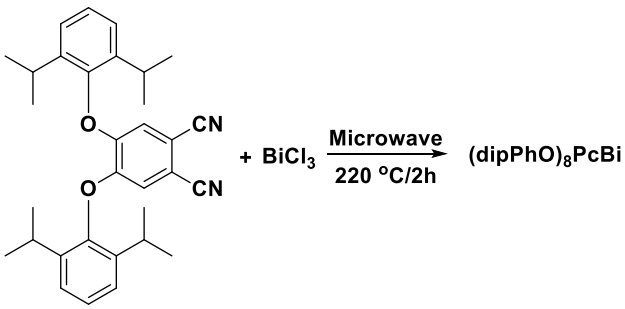

4,5-Bi(2',6'-di-*iso*-propylphenoxy) phthalonitrile (0.10 g, 0.20 mmol) and bismuth(III) chloride (0.02 g, 0.05 mmol) were irradiated by microwave for 2 h at 220 °C as described in general procedure. The product was purified by column chromatography on neutral alumina eluting with Hex/DCM (4/1) and then gradually increasing the polarity to give $(dipPhO)_8PcBi$ as dark green powder (0.02 g, 0.01 mmol, 10%); m.p. > 300 °C; IR ($\tilde{\nu}$) 2962, 2929, 1606, 1492, 1456, 1436, 1396, 1384, 1361, 1344, 1327, 1263, 1182, 1082, 1026, 935, 879, 792, 771, 744, 736, 719 cm^{-1}; UV/Vis (DCM) λ 737.8, 664.6, 480.6, 401.2, 293.6, 248.4 nm; ^1H NMR (500 MHZ, $CDCl_3$) δ_H, ppm 8.21 (s, 8H, Ar*H*), 7.65 – 7.61 (m, 8H, Ar*H*), 7.52 (d, 16H, Ar*H*), 3.41 (hept, 16H, CH_3CHCH_3), 1.33 (d, 96H, $CHCH_3$); *m/z* (MALDI-TOF): cluster of peaks centred at *m/z* = 2130.994 g mol^{-1} (simulated for $C_{128}H_{144}N_8O_8Bi$ formula cluster at 2131.094 g mol^{-1}).

Iridium(III)2,3,9,10,16,17,23,24-Octa(2',6'di-*iso*-propylphenoxy)phthalocyanine [(dipPhO)$_8$PcIr][106]

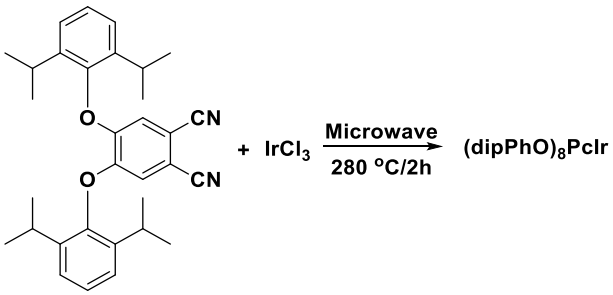

4,5-Di(2',6'-di-*iso*-propylphenoxy) phthalonitrile (0.10 g, 0.20 mmol) and iridium(III) chloride (0.03 g, 0.10 mmol) were irradiated by microwave for 2 h at 220 °C as described in general procedure. The crude product was purified be reprecipitation with methanol from DCM solution to give (dipPhO)$_8$PcIr as dark green powder (0.01 g, 0.02 mmol, 15%); m.p. > 300 °C; IR ($\tilde{\nu}$) 2964, 2868, 2229, 1595, 1579, 1568, 1500, 1438, 1400, 1384, 1327, 1282, 1251, 1203, 1174, 1145, 1093, 1074, 1058, 1031, 887, 848, 790, 756, 744, 530 cm^{-1}; UV/Vis (DCM) λ 701.8, 666.4, 653.8. 637.6, 605, 342 nm; *m/z* (MALDI-TOF): cluster of peaks centred at *m/z* = 2114.340 g mol^{-1} (simulated for $C_{128}H_{144}N_8O_8Ir$ formula cluster at 2115.077 g mol^{-1}); crystal data ($CHCl_3$/MeOH): Cubic, space group $Pn\bar{3}n$, *a* = *b* = *c* = 3.74658 (2) nm, *V* = 52.5902 nm^3, *Z* = 12, R_I = 0.1172, the asymmetric unit contains ¼ of (dipPhO)$_8$PcIr with one molecule of chloride in the axial positions with 50 % occupancy, together with one molecule of chloroform that can be solved crystallographically. The calculated residual electron count per unit cell was 1553, calculated by SQUEEZE relating to a possible 40 molecules of $CHCl_3$ and methanol per unit cell.

Hafnium(IV)2,3,9,10,16,17,23,24-Octa(2',6'di-*iso*-propylphenoxy)phthalocyanine [(dipPhO)$_8$PcHf][107]

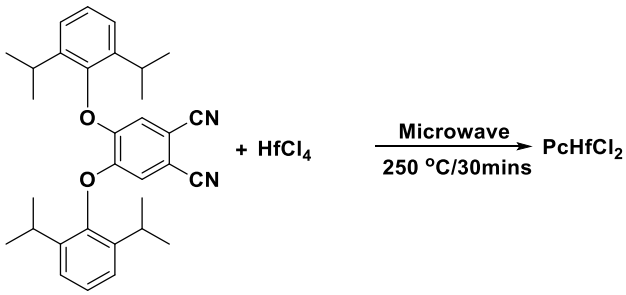

4,5-Di(2',6'-di-*iso*-propylphenoxy) phthalonitrile (**Pn1**) (0.20 g, 0.40 mmol) and hafnium(IV) chloride (0.13 g, 0.40 mmol) were reacted according to the general procedure for 30 mins at 250 °C. The crude product was purified be reprecipitation with methanol from DCM solution to give (dipPhO)$_8$PcHf as dark green powder (0.12 g, 0.25 mmol, 60%); m.p. > 300 °C; IR ($\tilde{\nu}$) 2964, 2929, 2870, 2229, 1720, 1595, 1500, 1438, 1400, 1327, 1282, 1251, 1203, 1172,1145, 1093, 1074, 848,790, 756, 530 cm^{-1}; UV/Vis (DCM) λ 764.6, 703.6, 668, 648.6, 638.2, 605.4, 577.8, 555, 401.4, 343 nm; *m/z* (MALDI-TOF): cluster of peaks centred at *m/z* = 2171.957 (simulated for $C_{128}H_{144}N_8O_8HfCl_2$ formula cluster at 2170.445).

Monolacunary polyoxometalate $H_3PW_{11}O_{39}TBA_4$[100]

$$Na_2HPO_4 + Na_2WO_4 + TBABr \longrightarrow H_3PW_{11}O_{39}TBA_4$$

Sodium phosphate dibasic heptahydrate (0.74 g, 2.75 mmol) was dissolved in water (20 ml) and sodium tungstate dihydrate (10.00 g, 30.30 mmol) was added. Concentrated HCl (2.0 ml, 12M) was then added with stirring over 15 mins. As the HCl was added, white flakes formed, which were allowed to dissolve before adding more acid. The solution was stirred for 1 h at room temperature during which a white precipitate formed. Hydrochloric acid (circa. 2.0 ml) was added until the pH reached 5.5. The white precipitate dissolved by the end of the addition. For another 30 mins, the pH of the solution was monitored continuously and dilute HCl was added as necessary to maintain the pH between 5.0 and 5.5. A solution of tetrabutylammonium bromide (4.00 g, 12.50 mmol) in water (30.0 ml) was added and the precipitation of the product began at once. The precipitation was completed by adding HCl (circa. 3.0 ml, 3 M) until the pH of the

solution remained between 1.1 for 5 mins. The product was filtered immediately on a coarse glass frit and washed with water and diethyl ether as well as it was dried in vacuo for 24 h at 60 °C (9.50 g, 28.80 mmol, 95%); m.p. > 300 °C; IR ($\tilde{\nu}$) 1107, 1054, 957, 886, 808, 754, 596, 519 cm^{-1}.

Ternary Hafnium(IV)2,3,9,10,16,17,23,24-Octa(2',6'di-*iso*-propylphenoxy)phthalocyanine [$(dipPhO)_8PcHf$] $H_3PW_{11}O_{39}TBA_4$ complex[98,99,107]

$$PcHfCl_2 + PW_{11}O_{39} + TBABr \longrightarrow PcHfPW_{11}O_{39}TBA_5$$

Hafnium phthalocyanine (0.10 g, 0.05 mmol) was dissolved in a 1 : 1 mixture of DCM : MeOH (10 ml). Monolacunary polyoxometalate (0.76 g, 0.02 mmol) and TBABr (0.05 g, 0.15 mmol) were dissolved separately in MeCN (5 ml) containing 1% v/v triethylamine. The resulting clear POM solution as well as the TBABr were added drop-wise over the course of 5 mins to the stirring hafnium phthalocyanine solution, and the reaction was left to run overnight, whereupon a small amount of precipitate was observed at the bottom of the test tube. The solvent was then removed under vacuum, and the residue was dissolved in a minimum amount of DCM and filtered to remove a small amount of insoluble salts (0.25 g, 0.04 mmol, 90%); m.p. > 300 °C; *m/z* (MALDI-ESI-TOF): cluster of peaks centred at *m/z* = 5746.6199 g mol^{-1} (simulated for the singly charged $(C_{128}H_{144}N_8O_8Hf)_1(PW_{11}O_{39})_1(C_{16}H_{36}N)_4$ formula cluster at 5748.4392 g mol^{-1} for the tetracoordinated TBA); cluster of peaks centred at *m/z* = 5505.3080 g mol^{-1} (simulated for singly charged $(C_{128}H_{144}N_8O_8Hf)_1(PW_{11}O_{39})_1(C_{16}H_{36}N)_3$ formula cluster at 5505.1525 g mol^{-1} for the tricoordinated TBA); cluster of peaks centred at *m/z* = 5262.8675 g mol^{-1} (simulated for singly charged $(C_{128}H_{144}N_8O_8Hf)_1(PW_{11}O_{39})_1(C_{16}H_{36}N)_2$ formula cluster at 5262.8675 g mol^{-1} for the dicoordinated TBA); cluster of peaks centred at *m/z* = 2629.9636 g mol^{-1} (simulated for doubly charged $(C_{128}H_{144}N_8O_8Hf)_1(PW_{11}O_{39})_1(C_{16}H_{36}N)_2$ formula cluster at 2632.4413 g mol^{-1} for the dicoordinated TBA); cluster of peaks centred at *m/z* = 2511.2987 g mol^{-1} (simulated for doubly charged $(C_{128}H_{144}N_8O_8Hf)_1(PW_{11}O_{39})_1(C_{16}H_{36}N)_1$ formula cluster at 2511.2987 g mol^{-1} for the monocoordinated TBA).

$[W(NO)_2Cl_2py_2]$[108]

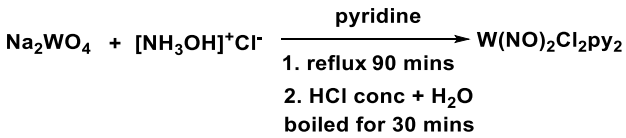

In a typical experiment, sodium tungstate (1.00 g, 4.00 mmol) and hydroxylamine hydrochloride (0.85 g, 12.00 mmol) were taken in pyridine (30.0 ml) and the mixture was refluxed for 90 mins. The starting colour was green which finally changed to brown. Then the mixture was acidified with concentrated hydrochloric acid (7.0 ml) and diluted with water (250.0 ml) and boiled for 30 mins and was kept at RT overnight. The green solid was filtered and washed with dilute hydrochloric acid, methanol and diethyl ether and dried. This crude was extracted with DCM, and the extracts were taken to dryness *in vacuo* to give the pure green product. (0.10 g, 0.4 mmol, 15%); IR ($\tilde{\nu}$) 1760, 1648, 310, 287 cm^{-1}.

$WNCl_3$[109]

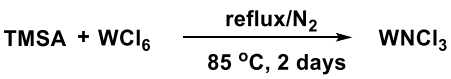

In a typical preparation, a solution of DCE (1.3 ml) and TMSA (0.04 ml, 0.30 mmol) was added dropwise to a refluxing solution of WCl_6 (0.12 g, 0.3 mmol) in DCE (1.3 ml). During the reaction, the colour of the solution remained purple but the colour of the particulate solid changed from purple to orange brown after 2 days. The reaction solution was refluxed for 3 days. Solid orange brown $WNCl_3$ was isolated by filtration and purified by a 2-day Soxhlet extraction with DCE to remove soluble silane compounds or WCl_6. The solid was then dried under vacuum for a period not less than 12 h under flow of N_2 atmosphere (0.09 g, 0.2 mmol, 65%); IR ($\tilde{\nu}$) 1086, 1082, 685, 400, 384, 371, 365, 358, 349, 343, 315 cm^{-1}.

Tungsten(V)2,3,9,10,16,17,23,24-Octa(2',6'di-*iso*-propylphenoxy)phthalocyanine [(dipPhO)$_8$PcW][110]

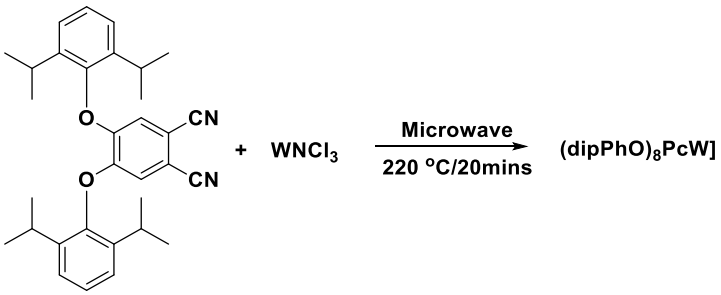

4,5-Di(2',6'-di-*iso*-propylphenoxy) phthalonitrile (0.10 g, 0.20 mmol) and $WNCl_3$ (0.03 g, 0.10 mmol) were irradiated by microwave for 20 mins at 220 °C as described in general procedure. The crude product was purified be reprecipitation with methanol from DCM solution to give (dipPhO)$_8$PcW as dark green powder (0.01 g, 0.02 mmol, 10%); m.p. > 300 °C; IR ($\tilde{\nu}$) 2964, 2929, 2870, 2229, 1720, 1595, 1500, 1438, 1400, 1327, 1282, 1251, 1203, 1172,1145, 1093, 1074, 848,790, 756, 530 cm^{-1}; UV/Vis (DCM) λ 764.6, 703.6, 668, 648.6, 638.2, 605.4, 577.8, 555, 401.4, 343 nm; *m/z* (MALDI-TOF): cluster of peaks centred at *m/z* = 2121.195 g mol^{-1} (simulated for $C_{128}H_{144}N_8O_8WN$ formula cluster at 2119.066 g mol^{-1}).

Platinum(II)2,3,9,10,16,17,23,24-Octa(2',6'di-*iso*-propylphenoxy)phthalocyanine [(dipPhO)$_8$PcPt][111]

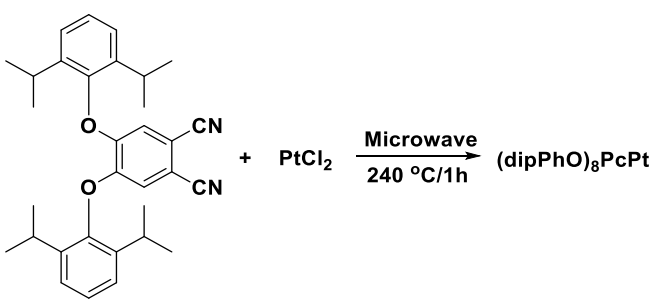

4,5-Di(2',6'-di-*iso*-propylphenoxy) phthalonitrile (0.10 g, 0.20 mmol) and platinum(II) chloride (0.03 g, 0.10 mmol) were irradiated by microwave for 1 h at 220 °C as described in general procedure. The crude product was purified be reprecipitation with methanol from DCM solution to give (dipPhO)$_8$PcPt as dark green powder (0.04 g, 0.04 mmol, 38%); m.p. > 300 °C; IR ($\tilde{\nu}$) 2962, 2929, 1595, 1504, 1462, 1456, 1435, 1409, 1384, 1361, 1325, 1278, 1255, 1190, 1168, 1145, 1093,

881, 866,794, 779, 752 cm^{-1}; UV/Vis (DCM) λ 655.8, 628.2, 591.4, 568.8, 549, 420.6, 370, 295.2 nm; ^{1}H NMR (500 MHz, $CDCl_3$) δ_H 8.04 (s, 8*H*), 7.58 (t, 8H, *J* = 9.0 Hz, Ar*H*), 7.48 (d, 16H, *J* = 7.7 Hz, Ar*H*) 3.47 (sept, 16H, *J* = 6.5 Hz, CH_3CHCH_3), 1.28 (br m, 96H, CH_3CHCH_3); ^{13}C NMR (125 MHz, $CDCl_3$) δ_C 151.7, 148.8, 147.9, 131.5 126.5, 124.8, 107.1, 27.4; *m/z* (MALDI-TOF): cluster of peaks centred at *m/z* = 2116.430 g mol^{-1} (simulated for $C_{128}H_{144}N_8O_8Pt$ formula cluster at 2117.078 g mol^{-1});

Germanium(III)2,3,9,10,16,17,23,24-Octa(2',6'di-*iso*-propylphenoxy)phthalocyanine [(dipPhO)$_8$PcGe][112]

$$(dipPhO)_8PcH_2 + GeCl_4 \xrightarrow[\text{Microwave}\ 240\ ^\circ C]{\text{Quinoline}} (dipPhO)_8PcGe$$

2,3,9,10,16,17,23,24-Octa(2',6'di-*iso*-propylphenoxy) phthalocyanine **[(dipPhO)$_8$PcH$_2$]** (0.10 g, 0.05 mmol) and germanium(IV) chloride (0.04 g, 0.15 mmol) in quinoline (1.0 ml) were heated at 240 °C by microwave irradiation for 4 h. The mixture was allowed to reach room temperature and poured into diluted HCl (2M) and then filtered under suction. The crude product was purified be reprecipitation with methanol from DCM solution to give (dipPhO)$_8$PcGe as dark green powder (0.06 g, 0.03 mmol, 60%); m.p. > 300 °C; IR ($\tilde{\nu}$) 2962, 2926, 2868, 1722, 1608, 1462, 1436, 1408, 1384, 1352, 1327, 1273, 1222, 1186, 1145, 1093, 1060, 1045, 1035, 902, 881, 862, 796, 775, 744, 731, 624, 520 cm^{-1}; UV/Vis (DCM) λ 695.6, 664.8, 624.8, 575.6, 445.6, 366.6, 346.8, 301.8, 281.6, 255 nm; *m/z* (MALDI-TOF): cluster of peaks centred at *m/z* = 2031.415 g mol^{-1} (simulated for $C_{128}H_{144}N_8O_8GeCl$ formula cluster at 2030.004 g mol^{-1}); crystal data (toluene/MeOH): Cubic, space group $Pn\bar{3}n$, *a* = *b* = *c* = 3.7650 (4) nm, *V* = 53.370 (9) nm^3, *Z* = 12, R_I = 0.0552, the asymmetric unit contains ¼ of (dipPhO)$_8$PcGe with one chloride in the axial position. The calculated residual electron count per unit cell was 1061, calculated by SQUEEZE relating to a possible 30 molecules of toluene and methanol per unit cell.

Cadmium(II)2,3,9,10,16,17,23,24-Octa(2',6'di-*iso*-propylphenoxy)phthalocyanine [(dipPhO)$_8$PcCd][113]

$$(dipPhO)_8PcH_2 + Cd(OAc)_2 \xrightarrow[140\ ^oC/N_2]{n\text{-pentanol}} (dipPhO)_8PcCd$$

A solution of 2,3,9,10,16,17,23,24-octa(2',6'di-*iso*-propylphenoxy) phthalocyanine **[(dipPhO)$_8$PcH$_2$]** (0.20 g, 0.10 mmol) in n-pentanol (1.00 ml) was brought to reflux and then cadmium(II) acetate (0.07 g, 0.30 mmol) was added. Reflux was continued for 45 mins. The hot mixture was added to excess cold MeOH (150.0 ml) and the flask left in the fridge overnight. The green solid was filtered and washed with MeOH. The crude product was purified be reprecipitation with methanol from DCM solution to give (dipPhO)$_8$PcCd as dark green powder (0.02 g, 0.01 mmol, 10%); m.p. > 300 °C; IR ($\tilde{\nu}$) 2962, 2927, 2870, 1598, 1435, 1384, 1361, 1327, 1255, 1197, 1172, 1095, 850, 771, 740, 617 cm^{-1}; UV/Vis (DCM) λ 687.4, 661.4, 619.6, 362.6 nm; *m/z* (MALDI-TOF): cluster of peaks centred at *m/z* = 2035.208 g mol^{-1} for the Cd and *m/z* = 2052.008 g mol^{-1} for the Cd with an axial ligand $^-$OH (simulated for $C_{128}H_{144}N_8O_8Cd$ and $C_{128}H_{144}N_8O_8CdOH$ formula cluster at 2035.018 g mol^{-1} and 2052.020 g mol^{-1} respectively); crystal data ($CHCl_3$/MeOH): Cubic, space group $Pn\bar{3}n$, *a* = *b* = *c* = 37.3224 (3) nm, *V* = 51.9887 nm^3, *Z* = 12, R_1 = 0.0552, the asymmetric unit contains ¼ of (dipPhO)$_8$PcCd, along with one molecule of methanol and one molecule of chloroform that can be solved crystallographically. The calculated residual electron count per unit cell was 959, calculated by SQUEEZE relating to a possible 25 molecules of chloroform and methanol per unit cell.

Lead(II)2,3,9,10,16,17,23,24-Octa(2',6'di-*iso*-propylphenoxy)phthalocyanine [(dipPhO)$_8$PcPb][114]

$$(dipPhO)_8PcH_2 + Pb(OAc)_2 \xrightarrow[140\ ^oC/N_2]{n\text{-pentanol}} (dipPhO)_8PcPb$$

A mixture of 2,3,9,10,16,17,23,24-octa(2',6'di-*iso*-propylphenoxy) phthalocyanine **[(dipPhO)$_8$PcH$_2$]** (0.10 g, 0.05 mmol) and lead(II) acetate (0.05 g, 0.15 mmol) in n-pentanol (4.0 ml) was heated at 140 °C under N_2 atmosphere for 8 h. The solvent was then removed in *vacuo* and the crude product was purified be reprecipitation with methanol from DCM solution to give (dipPhO)$_8$PcPb as dark green powder (0.04 g, 0.02 mmol, 40%); m.p. > 300 °C; IR ($\tilde{\nu}$) 2962, 2929,

2868, 1064, 1516, 1485, 1456, 1436, 1382, 1361, 1327, 1265, 1219, 1184, 1093, 1043, 1022, 999, 879, 792, 754, 746, 721, 667 cm^{-1}; UV/Vis (DCM) λ 718.4, 691.4, 644.2, 401.6, 364.2, 282.6; *m/z* (MALDI-TOF): cluster of peaks centred at *m/z* = 2129.009 g mol^{-1} (simulated for $C_{128}H_{144}N_8O_8Pb$ formula cluster at 2130.091 g mol^{-1}); Crystal data ($CHCl_3$/MeOH): Cubic, space group $Pn\bar{3}n$, *a* = *b* = *c* = 37.1115 (2) nm, *V* = 51.1123 nm^3, *Z* = 12, R_I = 0.0951, the asymmetric unit contains ¼ of $(dipPhO)_8PcPb$, along with one molecule of methanol and one molecule of chloroform that can be solved crystallographically. The calculated residual electron count per unit cell was 2750, calculated by SQUEEZE relating to a possible 72 molecules of chloroform and methanol per unit cell.

Iron(III)2,3,9,10,16,17,23,24-Octa(2',6'di-*iso*-propylphenoxy)phthalocyanine [$(dipPhO)_8PcFe$][115]

$$(dipPhO)_8PcH_2 + FeCl_3 \xrightarrow[180\ ^oC/N_2]{Quinoline} (dipPhO)_8PcFe$$

A mixture of 2,3,9,10,16,17,23,24-octa(2',6'di-*iso*-propylphenoxy) phthalocyanine **[$(dipPhO)_8PcH_2$]** (0.10 g, 0.05 mmol) and iron(III) chloride (0.04 g, 0.25 mmol) in quinoline were heated at 180 °C with stirring under nitrogen atmosphere for 4 h. After that HCl (1M) was added and the product precipitated. The crude product was purified be reprecipitation with methanol from DCM solution to give $(dipPhO)_8PcFe$ as dark green powder (0.05 g, 0.25 mmol, 50%); m.p. > 300°C; IR ($\tilde{\nu}$) 2961, 1612, 1456, 1462, 1413, 1353, 1269, 1168, 1095, 1050, 904, 864, 799, 777, 755, 729 cm^{-1}; UV/Vis (DCM) λ 672.6, 612.6, 589.2, 415.8, 348.2, 334.4, 312.2, 299.2, 286.8; *m/z* (MALDI-TOF): cluster of peaks centred at *m/z* = 2013.385 g mol^{-1} (simulated for $C_{128}H_{144}N_8O_8FeCl$ formula cluster at 2015.033 g mol^{-1}); crystal data ($CHCl_3$/MeOH): Cubic, space group $Pn\bar{3}n$, *a* = *b* = *c* = 3.74365 (2) nm, *V* = 52.4669 nm^3, *Z* = 12, R_I = 0.0893, the asymmetric unit contains ¼ of $(dipPhO)_8PcFe$ with one chloride in the axial position, along with one molecule of methanol and one molecule of chloroform that can be solved crystallographically. The calculated residual electron count per unit cell was 797, calculated by SQUEEZE relating to a possible 21 molecules of chloroform and methanol per unit cell.

Phosphorus(V)2,3,9,10,16,17,23,24-Octa(2',6'di-*iso*-propylphenoxy)phthalocyanine [(dipPhO)$_8$PcP][116]

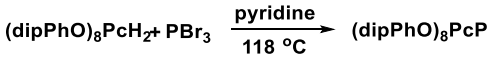

In a round bottom flask, 2,3,9,10,16,17,23,24-octa(2',6'di-*iso*-propylphenoxy) phthalocyanine **[(dipPhO)$_8$PcH$_2$]** (0.20 g, 0.1 mmol) in pyridine (1.0 ml) was heated to 118 °C and a large excess of phosphorus(III) bromide (1.35 g, 5.00 mmol) was added and the mixture stirred for 1 h. Then the volume was reduced and DCM/MeOH added and the solid filtered. The solid was dissolved in DCM and filtered again to remove the pyridinium bromide. The product was purified by column chromatography on silica eluting with 95/5 DCM/MeOH to give (dipPhO)$_8$PcP as dark green powder (0.100 g, 0.050 mmol, 50%); m.p. > 300 °C; IR ($\tilde{\nu}$) 2962, 2926, 2358, 2341, 1720, 1604, 1541, 1485, 1463, 1419, 1384, 1359, 1325, 1255, 1190, 1051, 935, 887, 866, 773, 748, 729 cm^{-1}; UV/Vis (DCM) λ 719.2, 696.8, 648.8, 622.4, 455, 341.8, 302.8; *m/z* (MALDI-TOF): cluster of peaks centred at *m/z* = 1968.858 g mol^{-1} for the P=O and *m/z* = 2014.902 g mol^{-1} for the P(OCH$_3$) (simulated for $C_{128}H_{144}N_8O_8PO$ and $C_{128}H_{144}N_8O_8PO_2C_2H_6$ formula cluster at 1969.082 g mol^{-1} and 2015.124 g mol^{-1} respectively); crystal data ($CHCl_3$/MeOH): Cubic, space group $Pn\bar{3}n$, *a* = *b* = *c* = 3.76935 (3) nm, *V* = 53.5549 nm^3, *Z* = 12, R_1 = 0.0857, the asymmetric unit contains ¼ of (dipPhO)$_8$PcP with one oxygen and one methoxy group in the axial positions, along with one molecule of methanol and one molecule of chloroform that can be solved crystallographically. The calculated residual electron count per unit cell was 3203, calculated by SQUEEZE relating to a possible 84 molecules of chloroform and methanol per unit cell.

Antimony(II)2,3,9,10,16,17,23,24-Octa(2',6'di-*iso*-propylphenoxy)phthalocyanine [(dipPhO)$_8$PcSb][117]

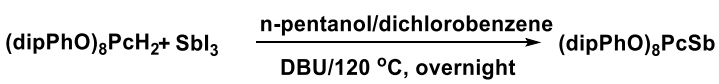

In a round bottom flask, DBU (0.5 ml) was added into a solution of 2,3,9,10,16,17,23,24-octa(2',6'di-*iso*-propylphenoxy) phthalocyanine **[(dipPhO)$_8$PcH$_2$]** (0.10 g, 0.05 mmol) in n-pentanol/dichlorobenzene 1:1 (0.5 ml) and left for 20 mins. A large excess of antimony(III) iodide

(0.25 g, 0.50 mmol) was added and stirred at 120 °C overnight. The solvent was removed under reduced pressure and the crude product was purified be reprecipitation with methanol from DCM solution to give $(dipPhO)_8PcSb$ as dark green powder (0.05 g, 0.03 mmol, 49%); m.p. > 300 °C; IR ($\tilde{\nu}$) 3116, 2960, 2927, 2868, 1645, 1608, 1581, 1436, 1398, 1382, 1361, 1323, 1263, 1145, 1091, 1014, 875, 848, 788, 769, 754, 705 cm^{-1}; UV/Vis (DCM) λ 764.6, 701.6, 666.4, 650.6, 636.8, 602.8; *m/z* (MALDI-TOF): cluster of peaks centred at *m/z* = 2044.146 g mol^{-1} (simulated for $C_{128}H_{144}N_8O_8Sb$ formula cluster at 2044.018 g mol^{-1}); crystal data ($CHCl_3$/MeOH): Cubic, space group $Pn\bar{3}n$, *a* = *b* = *c* = 3.73901 (4) nm, *V* = 52.2721 nm^3, *Z* = 12, R_I = 0.0948, the asymmetric unit contains ¼ of $(dipPhO)_8PcSb$, along with one molecule of methanol and one molecule of chloroform that can be solved crystallographically. The calculated residual electron count per unit cell was 882, calculated by SQUEEZE relating to a possible 23 molecules of chloroform and methanol per unit cell.

Potential bidentate ligands synthesis

4,4'-Bipyrimidine[75]

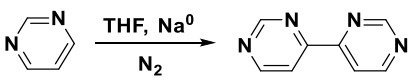

To a solution of pyrimidine (0.20 g, 2.50 mmol) in THF (5.0 ml) was added sodium metal (0.17 g, 7.50 mmol). The solution, which turned purple and then yellow, was stirred at room temperature overnight. The reaction was quenched with EtOH (4.0 ml) and trimethylamine (0.2 ml) and air was bubbled through for 1 h to promote oxidation. The reaction mixture was dissolved in DCM and washed three times with water. The bipyrimidine was purified by recrystallisation from MeOH (0.100 g, 0.63 mmol, 25%); IR ($\tilde{\nu}$) 1963, 1631, 1566, 1537, 1460, 1392, 1273, 1176, 1066, 985, 966, 839, 752, 692, 684, 634 cm^{-1}; ^1H NMR (400 MHz, $CDCl_3$) δ_H 9.36 (d, 2H, *J* = 1.30 Hz, NC*H*N), 8.97 (d, 2H, *J* = 5.17 Hz, NC*H*CH), 8.44 (dd, 2H, *J* = 5.13 Hz, *J* = 1.45 Hz, NCHC*H*); ^{13}C NMR (100 MHz, $CDCl_3$) δ_C 161.0, 159.4, 159.1, 118.2.

Octamethyl Polyhedral Oligomeric Silsesquioxane (POSS)[118]

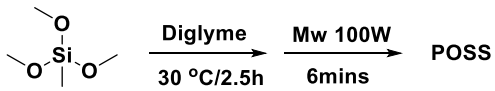

Diglyme (10.0 ml) then tetramethyl orthosilicate (0.6 ml, 3.50 mmol) and KOH 1M (0.3 ml) were added into a septum vial. The mixture was stirred at ambient temperature for 2 h for allowing the MeTMOS hydrolysis to occur. The solution was then placed in microwave reactor and the solution was irradiated at 100 W for 6 mins. After microwave irradiation, the reaction mixture changed to a suspension. The solid was filtered and washed with hexane (1.00 g, 1.86 mmol, 53%); IR ($\tilde{\nu}$) 2972, 1271, 1124, 773 cm^{-1}.

Lindqvist type polyoxometallate Mo_6O_{19}[119,120]

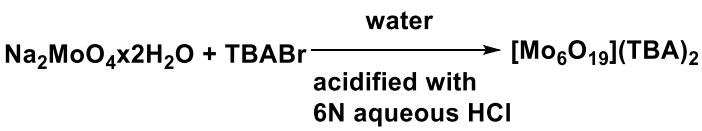

Sodium molybdate dihydrate (2.50 g, 10.30 mmol) in water (10.0 ml) was acidified with aqueous HCl (2.9 ml, 6 N, 17.40 mmol) while stirring. Tetrabutylammonium bromide (1.21 g, 3.75 mmol) in water (2.0 ml) was then added causing immediate formation of a white precipitate. The resulting slurry was heated to 80 °C with stirring for 45 mins. The white solid changed to yellow and the product was filtered on a sinter and washed with water. Crystallisation was accomplished by dissolving the product in hot acetone and cooling the solution to -20 °C. The pale yellow crystals were filtered and washed with diethyl ether (2.00 g, 1.45 mmol, 85%); IR ($\tilde{\nu}$) 988, 956, 890, 880, 800, 742 cm^{-1}.

Keggin type polyoxometallate $SiMo_{12}O_{40}$[121]

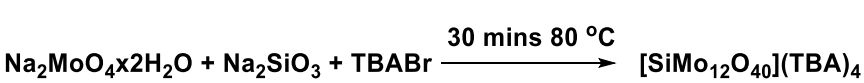

In a sodium molybdate dihydrate (2.40 g, 10.00 mmol) aquatic solution concentrated HNO_3 (3.0 ml, 13 M) was added. Then sodium silicate solution (5.0 ml) was added dropwise resulting in a yellow solution. After 30 mins at 80 °C during which the β to α isomerisation took place, the

precipitation was performed by adding tetrabutylammonium bromide (1.20 g, 3.70 mmol) in water (1.0 ml). The precipitate was filtered and washed with water, ethanol and diethyl ether. Recrystallisation was performed with acetone (1.50 g, 5.5 mmol, 55%); IR ($\tilde{\nu}$) 982, 945, 895, 857, 800, 737, 627, 537, 497, 415, 392, 377, 365, 340, 288 cm^{-1}.

Molecular cluster $Co_6Te_8(P^nBu_3)_6$[122]

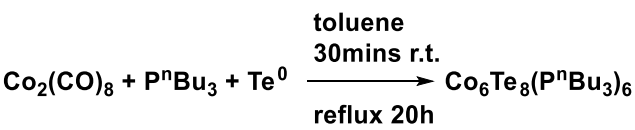

Dicobalt octacarbonyl (0.34 g, 1.00 mmol), tributyl phosphine (1.43 g, 7.00mmol) and elemental Te^0 (0.51 g, 4 mmol) were combined in toluene (6.0 ml), stirred at room temperature for 30 mins and then heated at reflux for 20 h. The resulting mixture was cooled to room temperature, filtered and concentrated in vacuo to approximately 2 ml. Pentane (5.0 ml) was added and the solution was cooled to -20 °C to initiate crystallisation. After 24 h the supernatant liquor was decanted and the crystalline solid was washed (3x5 ml pentane) and dried in vacuo to give $Co_6Te_8(P^nBu_3)_6$ as a very dark red – black crystalline solid (0.58 g, 0.23 mmol, 75%); UV/Vis (DCM) λ 538, 476, 400 nm.

Octaphenyl Polyhedral Oligomeric Silsesquioxane (POSS)[123]

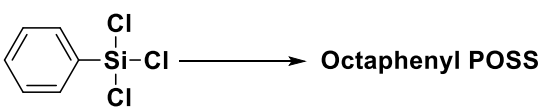

Phenyl trichlorosilane (8.0 ml, 50.00 mmol) was dissolved in toluene (50.0 ml). The solution was transferred to a separating funnel and shaken with water (20.0 ml, 1.12 mmol) until heat was produced. The aqueous layer was removed, and the organic layer washed thrice with water (3x20 ml). Methanolic benzyltrimethylammonium hydroxide 30% (1.6 ml, 3.00 mmol) was added and the mixture was heated under reflux for 16.5 h. The reaction was left to stand for 52 h, before being heated at reflux for further 24 h. Mixture was cooled to 0 °C. The white solid collected via vacuum filtration and washed thrice with ice cold toluene (3x20 ml) (1.00 g, 15.00 mmol, 30%).

Octahydroxy Polyhedral Oligomeric Silsesquioxane (POSS)[124]

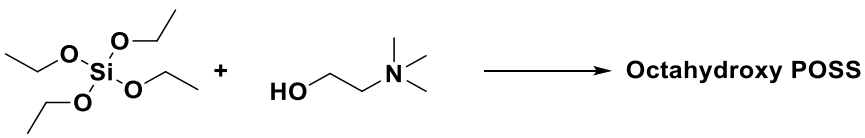

Tetraethoxysilane (25.0 ml, 111.96 mmol) and choline hydroxide solution (12.6 ml, 711.96 mmol) were stirred for 12 h at room temperature. After the completion of the stirring, 2-propanol (50 ml) was added to the solution. The solution was further stirred for 30 mins and then cooled to 3 °C, to precipitate a crude product out of the solution. The precipitated crude product was filtered out, washed with 2-propanol and dried (18.50 g, 24.00 mmol, 30%).

Octadimethyloxosilane Polyhedral Oligomeric Silsesquioxane (POSS)[124]

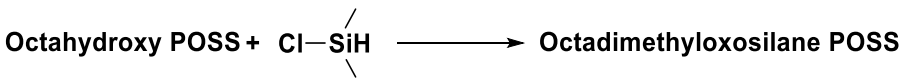

Dimethylchlorosilane (100 ml, 7.00 mmol), pyridine (20 ml) and 2-propanol (5 ml) were stirred and octahydroxy POSS (5.00 g, 3.61 mmol) was added into the flask. The resulting solution was stirred for 12 h at room temperature. After the completion of the stirring, the solution was reduced in volume. To the product toluene (50 ml) was added and washed thrice with water (3x150 ml). The organic layer was concentrated under reduced pressure to precipitate a crude product, which was washed with methanol and dried (4.00 g, 3.10 mmol, 80%).

2,7-Diazapyrene[125]

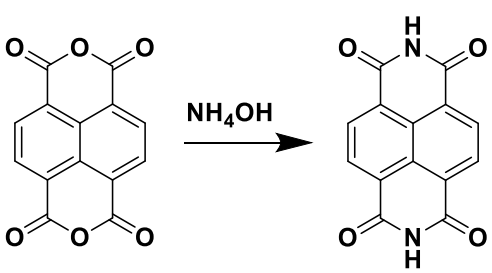

1,4,5,8-Naphthalenetetracarboxylic dianhydride (12.5 g, 46.6 mmol) was dissolved in concentrated ammonium hydroxide solution (625.0 ml, 29.5% w/w). The reaction mixture was stirred at room temperature for 6 hours under nitrogen. During that time, the diimide

precipitated as yellow product, which was filtered, washed with water, and dried under vacuum at 60 °C overnight (10.1 g, 37.65 mmol, 81%). M.P. > 300 °C. ^{1}H NMR (400 MHz, $CDCl_3$) δ_H 8.10 (s, 4H, Ar*H*). ^{13}C NMR (100 MHz, $CDCl_3$) δ_C 165.5, 134.9, 127.8, 125.4.

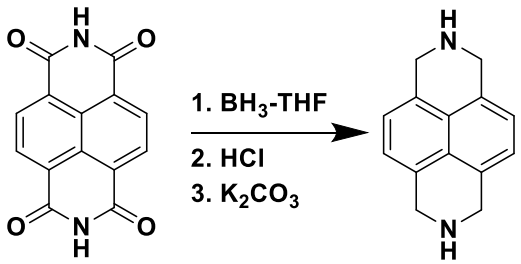

1,4,5,8-Napthalenetetracarboxylic diimide (2 g, 7.52 mmol) was dissolved in anhydrous THF (40.0 ml) and to this 1M solution of BH_3 – THF (80 ml) was added slowly, *via* dropping funnel, at room temperature. The reaction mixture was refluxed for 60 h. during that time there was hydrogen evolution and the colour of the reaction mixture turned to orange. After cooling to 0 °C, the reaction mixture was quenched by addition of MeOH (8.0 ml). after stirring for 30 mins at room temperature, HCl (10.0 ml, 6 M) was added and the mixture was refluxed for 3 h. The liquid was evaporated under reduced pressure. The residue was cooled to 0 °C and aqueous saturated potassium carbonate solution was added with stirring until the pH was basic. All of the liquid was evaporated under reduced pressure and the solid was dried completely under vacuum at 40 °C. The dry solid was extracted with refluxing benzene in a Soxhlet extractor for a week. The benzene was removed from the pale-yellow product, which can be recrystallised from benzene (1.00 g, 4.76 mmol, 63%); m.p. = 216 – 220 °C; ^{1}H NMR (400 MHz, $CDCl_3$) δ_H 7.17 (s, 4H, Ar*H*), 4.21 (s, 8H, CH_2); ^{13}C NMR (100 MHz, $CDCl_3$) δ_C 132.9, 127.9, 120.3, 48.9.

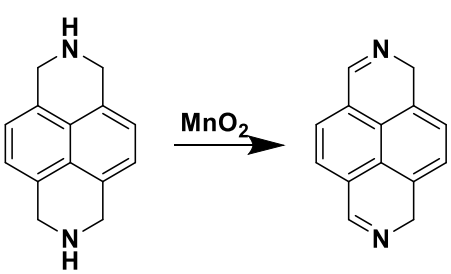

1,2,3,6,7,8-Hexahydro-2,7-diazapyrene (1.00 g, 4.76 mmol) in benzene (250.0 ml), activated MnO_2 (10.00 g, 115.02 mmol) was added. The solution was refluxed with a dean stark trap (for

water removal) for 24 h and the hot solution was filtered, and the benzene solution was kept. The filtered MnO_2 was dried under vacuum and subjected to a Soxhlet extraction with the benzene solution of the filtrate for 3 days. 2,7-diazapyrene was obtained after the removal of the benzene (0.50 g, 2.42 mmol, 51%); m.p. 280 – 285 °C; ^{1}H NMR (400 MHz, $CDCl_3$) δ_H 9.38 (s, 4H, Ar*H*) 8.06 (s, 4H, Ar*H*); ^{13}C NMR (100 MHz, $CDCl_3$) δ_C 144.3, 125.3, 125.2, 124.8.

Iron2,3,9,10,16,17,23,24-Octa(2',6'di-*iso*-propylphenoxy)phthalocyanine [(dipPhO)$_8$PcFe] iron5,10,15,20-Tetraphenylporphin [FeTPP] dimers PNC[Fe-N-*v*FeTPP]

Iron5,10,15,20-Tetraphenylporphin azide (N_3FeTPP)[87,126–130]

$$\mathbf{ClFeTPP + NaN_3 \longrightarrow N_3FeTPP}$$

Iron5,10,15,20-tetraphenylporphin (0.20 g, 0.28 mmol) was dissolved in $CHCl_3$ (100 ml). Sodium azide (1.40 g, 21.54 mmol) was dissolved in water (30 ml) and the solution was made acidic with concentrated sulfuric acid. The two solutions were stirred together for 18 h. The organic layer was dried over magnesium sulfate and the solvent was removed from the product under vacuum. The N_3FeTPP was recrystallised from either DCM or benzene by slow diffusion with pentane (0.07 g, 0.08 mmol, 30%).

Deactivation of sodium azide

The operation must be carried out in a chemical hood due to the formation of nitric oxide. An aqueous solution containing no more than 5% sodium azide is put into a three-necked flask equipped with a stirrer, a dropping funnel, and an outlet with plastic tubing to carry nitrogen oxides to the laboratory chemical hood flow. A 20% aqueous solution of sodium nitrite containing 1.5g (about 40% excess) of sodium nitrite per gram of sodium azide is added with stirring. A 20% aqueous solution of sulfuric acid is then added gradually until the reaction mixture is acidic to Ph paper.

Caution: This order of addition is essential. If the acid is added before the nitrite, poisonous volatile HN_3 will be evolved. When the evolution of nitrogen oxides is over, the acidic solution is tested with starch-iodide paper; if it turns blue, it means that excess nitrite is present, and decomposition is complete. The reaction mixture can safely be washed down the drain.

μ-nitrido bridge iron2,3,9,10,16,17,23,24-Octa(2',6'di-*iso*-propylphenoxy)phthalocyanine iron5,10,15,20-Tetraphenylporphin PNC[Fe-N-*v*FeTPP][87,126–130]

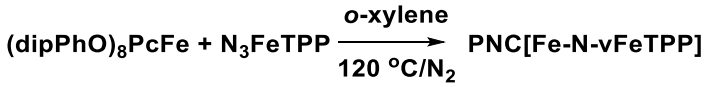

Iron2,3,9,10,16,17,23,24-Octa(2',6'di-*iso*-propylphenoxy) phthalocyanine (0.13 g, 0.07 mmol) was added to a suspension of finely ground iron nitride 5,10,15,20-tetraphenylporphin (0.07 g, 0.05 mmol) in *o*-xylene (20.0 ml). The mixture was refluxed at 120 °C under N_2 with constant stirring for 8 h. The reaction mixture was allowed to cool to room temperature and *o*-xylene was separated from the solid residue which was washed with *o*-xylene until the washings were light green colour and the excess of unreacted tetraphenylporphyrin complex was completely eliminated (0.10 g, 0.04 mmol, 60%); m.p. > 300 °C; *m/z* (MALDI-TOF): cluster of peaks centred at *m/z* = 2659.920 g mol^{-1} (simulated for $C_{128}H_{144}N_8O_8Fe$ – N – $C_{44}H_{30}N_4Fe$ formula cluster at 2661.230 g mol^{-1}).

4,5-di(2',6'-di-*iso*-propylphenoxy)azaphthalonitrile (azaPn1)[39]

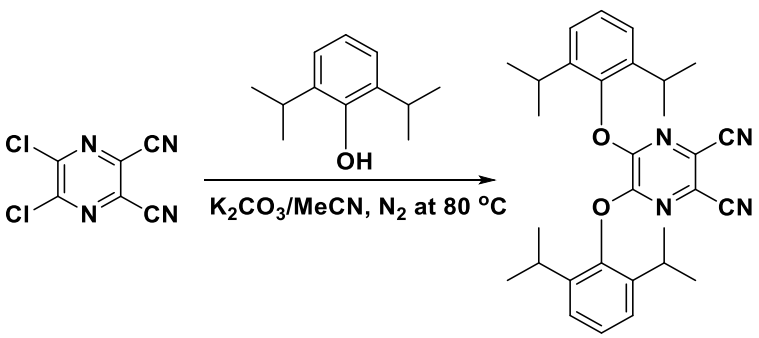

5,6-Dichloro-2,3-dicyanopyrazine (2.00 g, 10.00 mmol) was dissolved into MeCN (100 ml), under N_2. Anhydrous potassium carbonate (8.01 g, 58.00 mmol) and then 2,6-di-*iso*-propylphenol (4.16 ml, 22.50 mmol) were added and stirred for 1 day at 80 °C. After 1 day the mixture was cooled and was poured into H_2O (300.0 ml) and left stirring for 10 mins. The solid was filtered and washed with MeOH to remove the excess of the di-*iso*-propylphenol (purple color) and dried under suction. The product purified by recrystallisation from MeOH (1.93 g, 4.00 mmol, 40%).

2,3,9,10,16,17,23,24-Octa(2',6'di-*iso*-propylphenoxy)azaphthalocyanine [$(dipPhO)_8azaPcH_2$][39]

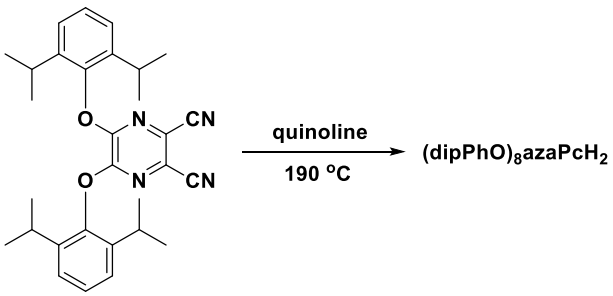

4,5-di(2',6'-di-*iso*-propylphenoxy) azaphthalonitrile (3.00 g, 2.10 mmol) was dissolved in quinoline and was heated at 190 °C for 2 hours. Then was cooled and water and HCl were added (3.0 ml) and the precipitate was filtered and recrystallised with DCM/MeOH (1.41 g, 0.73 mmol, 35%); m.p. > 300 °C.

5.5 General crystallisation procedures

(a) For crystallisation of metal-free or metallated phthalocyanines, co-crystallisation with metal-free tetraphenylporphyrin and bidentate ligands in bulk

In a typical procedure 2,3,9,10,16,17,23,24-octa(2',6'di-*iso*-propylphenoxy) phthalocyanine **[$(dipPhO)_8PcH_2$ / $(dipPhO)_8PcM$]** (0.10 g), 5,10,15,20-Tetraphenyl-21H,23H-porphine **(H_2TPP / MTPP)** (0.03 g) or both were solubilised in appropriate solvent in a petri dish with watch hour glass on top and through vapour diffusion with appropriate miscible anti-solvent in a container was crystallised.

(b) For crystallisation of metal-free or metallated phthalocyanines, co-crystallisation with metal-free tetraphenylporphyrin and bidentate ligands in bulk

In a typical procedure 2,3,9,10,16,17,23,24-octa(2',6'di-*iso*-propylphenoxy) phthalocyanine **[$(dipPhO)_8PcH_2$ / $(dipPhO)_8PcM$]** (0.10 g), 5,10,15,20-Tetraphenyl-21H,23H-porphine **(H_2TPP / MTPP)** (0.03 g) or both were solubilised in appropriate solvent and through slow evaporation was crystallised.

(c) For crystallisation of metal-free or metallated phthalocyanines, co-crystallisation with metal-free tetraphenylporphyrin and bidentate ligands in bulk

In a typical procedure 2,3,9,10,16,17,23,24-octa(2',6'di-*iso*-propylphenoxy) phthalocyanine **[$(dipPhO)_8PcH_2$ / $(dipPhO)_8PcM$]** (0.10 g), 5,10,15,20-Tetraphenyl-21H,23H-porphine **(H_2TPP / MTPP)** (0.03 g) or both were solubilised in appropriate solvent and through layering with appropriate miscible anti-solvent was crystallised.

(d) For single-crystal to single-crystal transformation of metallated and metal-free phthalocyanines, metallated tetraphenyl porphyrin by inserting bidentate ligands or metals in the macrocycles.

In a typical procedure in already formed nanoporous crystals of 2,3,9,10,16,17,23,24-octa(2',6'di-*iso*-propylphenoxy) phthalocyanine **[$(dipPhO)_8PcH_2$ / $(dipPhO)_8PcM$]** (0.10 g), 5,10,15,20-Tetraphenyl-21H,23H-porphine (**H_2TPP / MTPP**) (0.03 g) or both, a bidentate ligand or a metal was solubilised and was poured in the mother liquor with the crystals and left for 3 days.

5.6 Crystallisations

Crystallisation of $(dipPhO)_8PcH_2$ / $(dipPhO)_8PcM$

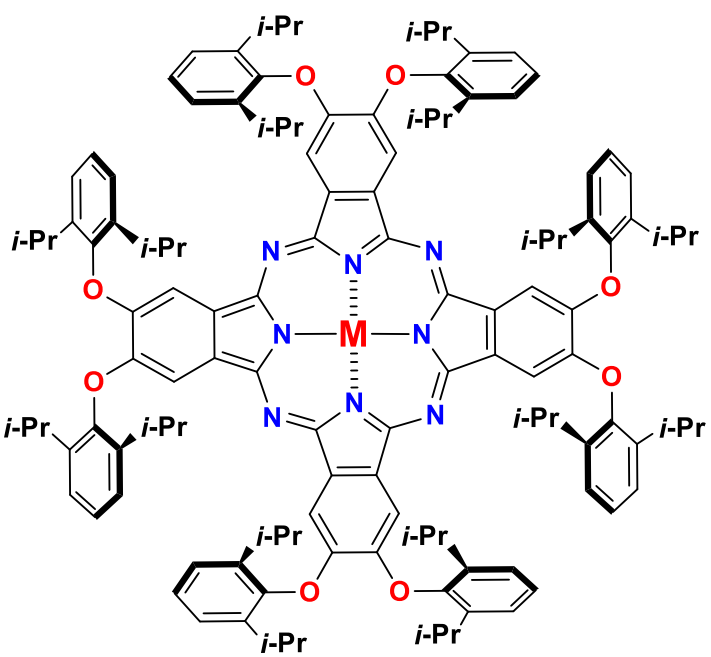

M = Fe^{3+}
M = P^{5+}
M = Ge^{3+}
M = Mo^{4+}
M = Cd^{2+}
M = Sb^{2+}
M = Hf^{4+}
M = W^{5+}
M = Re^{5+}
M = Ir^{3+}
M = Pt^{2+}
M = Pb^{2+}
M = Bi^{2+}

As described above in the general crystallisation procedures, there are mainly three ways that were used to grow crystals as will be shown in the next table.

No.	Name	Structure	Method	Data	Solvent	Anti-solvent
1	$(dipPhO)_8PcCo$	Cubic	a, b, c	a	DCM / $CHCl_3$	MeOH
2	$(dipPhO)_8PcCu$	Cubic	a, b, c	a	DCM / $CHCl_3$	MeOH
3	$(dipPhO)_8PcZn$	Cubic	a, b, c	a	DCM / $CHCl_3$	MeOH
4	$(dipPhO)_8PcNi$	Cubic	a, b, c	a	DCM / $CHCl_3$	MeOH
5	$(dipPhO)_8PcP$	Cubic	a, b, c	a	DCM / $CHCl_3$	MeOH
6	$(dipPhO)_8PcFe$	Cubic	a, b, c	a	DCM / $CHCl_3$	MeOH
7	$(dipPhO)_8PcGe$	Cubic	a, b, c	a	Toluene / Dichlorobenzene	MeOH
8	$(dipPhO)_8PcMo$	Cubic	a, b, c	a	DCM / $CHCl_3$	MeOH
9	$(dipPhO)_8PcCd$	Cubic	a, b, c	a	DCM / $CHCl_3$	MeOH
10	$(dipPhO)_8PcSb$	Cubic	a, b, c	a	DCM / $CHCl_3$	MeOH
11	$(dipPhO)_8PcW$	No	a, b, c	a	DCM / $CHCl_3$	MeOH
12	$(dipPhO)_8PcRe$	Cubic	a, b, c	a	DCM / $CHCl_3$	MeOH
13	$(dipPhO)_8PcIr$	Cubic	a, b, c	a	DCM / $CHCl_3$	MeOH
14	$(dipPhO)_8PcPt$	No	a, b, c	a	Toluene / Dichlorobenzene	MeOH
15	$(dipPhO)_8PcPb$	Cubic	a, b, c	a	DCM / $CHCl_3$	MeOH
16	$(dipPhO)_8PcBi$	No	a, b, c	a	Toluene / Dichlorobenzene	MeOH
17	$(dipPhO)_8PcHf$	No	a, b, c	a	Toluene / Dichlorobenzene	MeOH
18	$(dipPhO)_8PcHfPOM$	Pnma	a, b, c	a	DCM / $CHCl_3$	THF

Co-crystallisation of $(dipPhO)_8PcM$ with bidentate ligands PNC[M-*c*L-M]

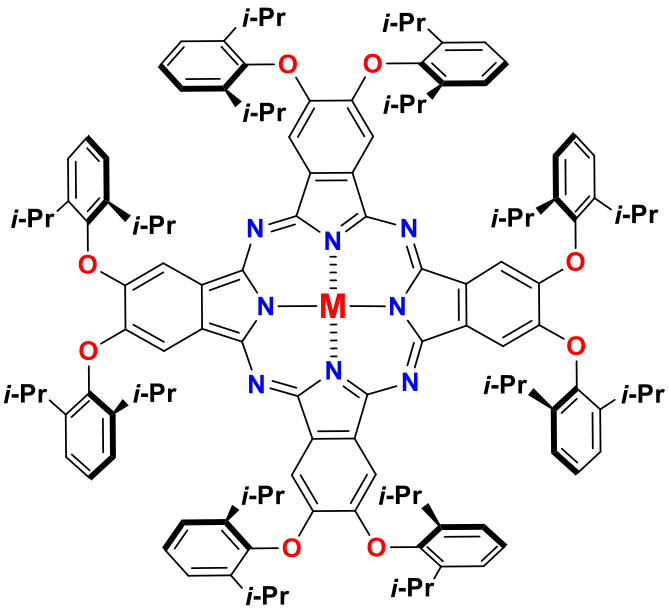

Bidentate ligands

M = Co^{3+}
M = Cu^{2+}
M = Zn^{2+}
M = Fe^{2+}
M = Fe^{3+}

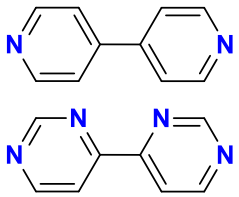

As described above in the general crystallisation procedures, there are mainly four ways that were used to co-crystallize or do single-crystal to single-crystal transformation of the phthalocyanine derivative with a bidentate ligand as shown in the following table.

No.	Name	Ligand	Structure	Method	Data	Solvent	Anti-solvent
1	$(dipPhO)_8PcCo$	Bpm	Cubic	a, b, c, d	a, d	DCM / $CHCl_3$	MeOH
2	$(dipPhO)_8PcCo$	Bipy	Cubic	a, b, c, d	a, d	DCM / $CHCl_3$	MeOH

Co-crystallisation of $(dipPhO)_8PcM$ with H_2TPP PNC[M/*v*H_2TPP]

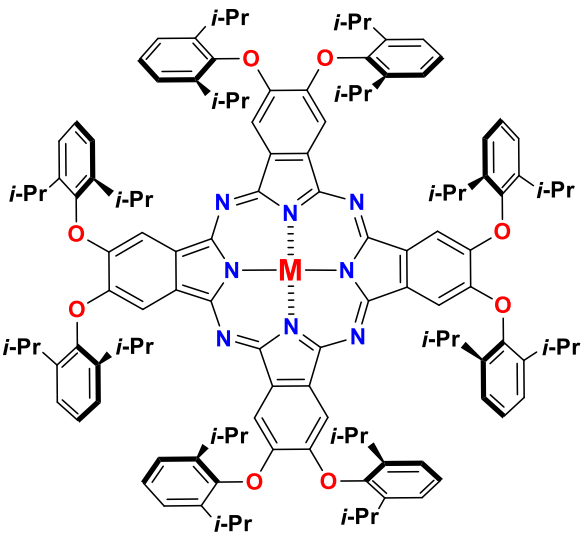

M = H_2
M = Sc^{2+}
M = Ti^{2+}
M = V^{4+}
M = Cr^{3+}
M = Mn^{2+}
M = Fe^{3+}
M = Co^{2+}
M = Ni^{2+}
M = Cu^{2+}
M = Zn^{2+}
M = Al^{3+}
M = Ga^{3+}
M = In^{3+}
M = Ag^{2+}
M = Pb^{2+}
M = Sn^{2+}
M = Au^{3+}
M = Fe^{2+}

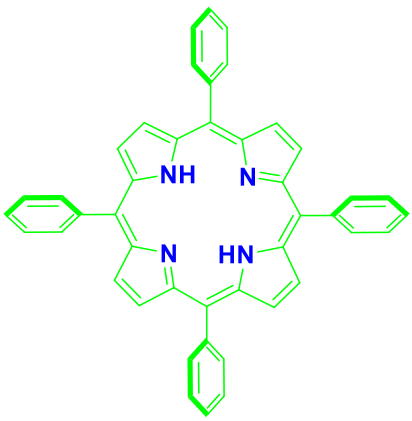

As described above in the general crystallisation procedures, there are mainly four ways that were used to co-crystallize or do single-crystal to single-crystal transformation of the phthalocyanine derivative with the metal-free tetraphenyl porphyrin as shown in the following table.

No.	Name	MPc	MTPP	Structure	Method	Data	Solvent	Anti-solvent
1	$(dipPhO)_8PcH_2 + H_2TPP$	H_2	H_2	Cubic	a, b, c	a	DCM / $CHCl_3$	MeOH
2	$(dipPhO)_8PcH_2 + H_2TPP$	Cu	Cu	Cubic	d	d	DCM / $CHCl_3$	MeOH
3	$(dipPhO)_8PcSc + H_2TPP$	Sc	H_2	No	a, b, c	a	DCM / $CHCl_3$	MeOH
4	$(dipPhO)_8PcTi + H_2TPP$	Ti	H_2	Cubic	a, b, c	a	DCM / $CHCl_3$	MeOH
5	$(dipPhO)_8PcV + H_2TPP$	V	H_2	No	a, b, c	a	DCM / $CHCl_3$	MeOH
6	$(dipPhO)_8PcCr + H_2TPP$	Cr	H_2	No	a, b, c	a	DCM / $CHCl_3$	MeOH
7	$(dipPhO)_8PcMn + H_2TPP$	Mn	H_2	Cubic	a, b, c	a	DCM / $CHCl_3$	MeOH
8	$(dipPhO)_8PcFe + H_2TPP$	Fe	H_2	Cubic	a, b, c	a	DCM / $CHCl_3$	MeOH
9	$(dipPhO)_8PcCo + H_2TPP$	Co	H_2	Cubic	a, b, c	a	DCM / $CHCl_3$	MeOH
10	$(dipPhO)_8PcCo + H_2TPP$	Co	Cu	Cubic	d	d	DCM / $CHCl_3$	MeOH
11	$(dipPhO)_8PcCo + H_2TPP$	Co	Co	Cubic	a, b, c	a	DCM / $CHCl_3$	MeOH
12	$(dipPhO)_8PcNi + H_2TPP$	Ni	H_2	Cubic	a, b, c	a	DCM / $CHCl_3$	MeOH
13	$(dipPhO)_8PcCu + H_2TPP$	Cu	H_2	Cubic	a, b, c	a	DCM / $CHCl_3$	MeOH
14	$(dipPhO)_8PcCu + H_2TPP$	Cu	Cu	Cubic	d	d	DCM / $CHCl_3$	MeOH
15	$(dipPhO)_8PcZn + H_2TPP$	Zn	H_2	Cubic	a, b, c	a	DCM / $CHCl_3$	MeOH
16	$(dipPhO)_8PcAl + H_2TPP$	Al	H_2	Cubic	a, b, c	a	DCM / $CHCl_3$	MeOH
17	$(dipPhO)_8PcGa + H_2TPP$	Ga	H_2	Cubic	a, b, c	a	DCM / $CHCl_3$	MeOH
18	$(dipPhO)_8PcIn + H_2TPP$	In	H_2	Cubic	a, b, c	a	DCM / $CHCl_3$	MeOH
19	$(dipPhO)_8PcAg + H_2TPP$	Ag	H_2	Cubic	a, b, c	a	DCM / $CHCl_3$	MeOH
20	$(dipPhO)_8PcPb + H_2TPP$	Pb	H_2	No	a, b, c	a	DCM / $CHCl_3$	MeOH
21	$(dipPhO)_8PcSn + H_2TPP$	Sn	H_2	No	a, b, c	a	DCM / $CHCl_3$	MeOH
22	$(dipPhO)_8PcAu + H_2TPP$	Au	H_2	Cubic	a, b, c	a	DCM / $CHCl_3$	MeOH
23	$(dipPhO)_8PcFe\text{-}N\text{-}FeTPP$	Fe	Fe	Cubic	a, b, c	a	DCM / $CHCl_3$	MeOH
24	$(dipPhO)_8azaPcH_2 + H_2TPP$	H_2	H_2	Cubic	a, b, c	a	DCM / $CHCl_3$	MeOH
25	$(dipPhO)_8azaPcCo + H_2TPP$	Co	H_2	No	a, b, c	a	DCM / $CHCl_3$	MeOH

Co-crystallisation of $(dipPhO)_8PcM$ with H_2/MTPP and bidentate ligands PNC[*v*H_2TPP/M-*c*L-M/*v*H_2TPP]

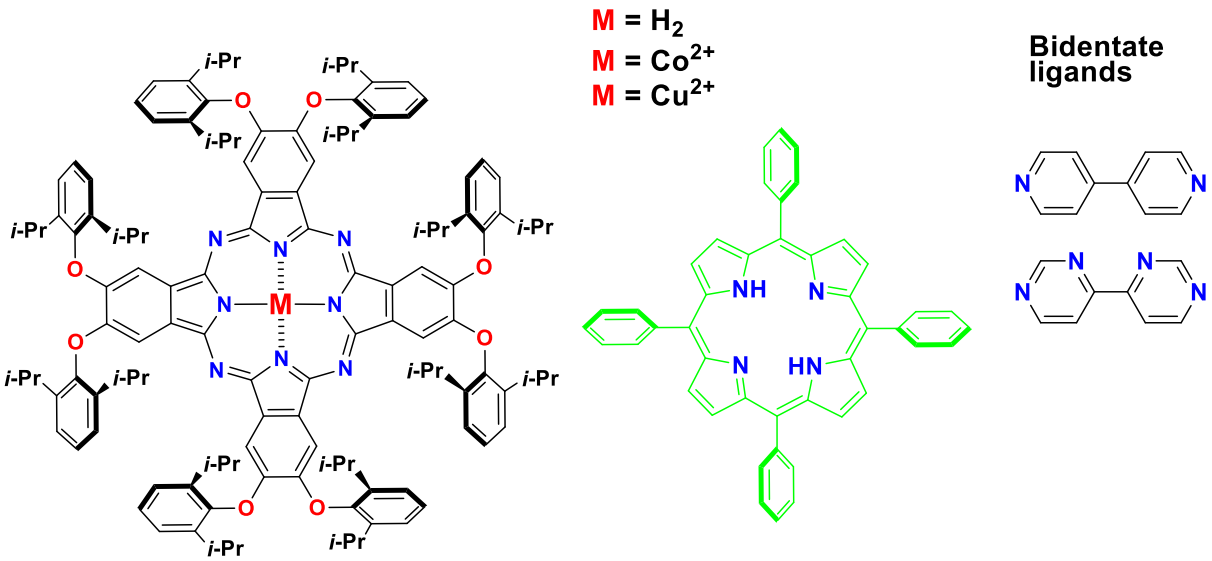

As described above in the general crystallisation procedures, there are mainly four ways that were used to co-crystallize and do single-crystal to single-crystal transformation of the phthalocyanine derivative with the metal-free tetraphenyl porphyrin and a bidentate ligand as shown in the following table.

No.	Name	MPc	MTPP	Ligand	Structure	Method	Data	Solvent	Anti-solvent
1	$(dipPhO)_8PcCo + H_2TPP + Bipy$	Co	H_2	Bipy	Cubic	a, b, c, d	d	DCM / $CHCl_3$	MeOH
2	$(dipPhO)_8PcCo + H_2TPP + Bipy$	Co	Cu	Bipy	Cubic	a, b, c, d	d	DCM / $CHCl_3$	MeOH
3	$(dipPhO)_8PcCo + H_2TPP + Bipy$	Co	Co	Bipy	Cubic	a, b, c, d	d	DCM / $CHCl_3$	MeOH
4	$(dipPhO)_8PcCu + CuTPP + Bipy$	Cu	Cu	Bpm	Cubic	a, b, c, d	d	DCM / $CHCl_3$	MeOH
5	$(dipPhO)_8PcCo + H_2TPP + Bpm$	Co	H_2	Bpm	Cubic	a, b, c, d	d	DCM / $CHCl_3$	MeOH
6	$(dipPhO)_8PcCo + H_2TPP + Bpm$	Co	Cu	Bpm	Cubic	a, b, c, d	d	DCM / $CHCl_3$	MeOH

5.7 Crystallography

Atlas and EH1

Single crystal X-ray analysis

X-ray crystal structure analysis was accomplished using a Bruker Smart Apex CCD diffractometer with $Mo_{K\alpha}$ radiation λ = 0.71073 Å at 150 K; Oxford Diffraction SuperNova diffractometer with $Cu_{K\alpha}$ radiation λ = 1.5405 Å at 120 K, or using synchrotron radiation at Diamond Light Source (Station I19-1) on a 3-circle diffractometer collecting data on a Pilatus 2M detector with $Zr_{K\alpha}$ radiation λ = 0.6889 Å at 100 K for the EH1 hutch.

Crystal data								
Name	$(dipPhO)_8PcH_2$	$(dipPhO)_8PcH_2$	$(dipPhO)_8PcCo$	$(dipPhO)_8PcCo$	$(dipPhO)_8PcZn$	$(dipPhO)_8PcCu$	$(dipPhO)_8PcNi$	$(dipPhO)_8PcMo$
Chemical formula	$C_{128}H_{144}N_8O_8H_2$	$C_{128}H_{144}N_8O_8H_2$	$C_{128}H_{144}N_8O_8Co$	$C_{128}H_{144}N_8O_8Co$	$C_{128}H_{144}N_8O_8Zn$	$C_{128}H_{144}N_8O_8Cu$	$C_{128}H_{144}N_8O_8Ni$	$C_{128}H_{144}N_8O_8Mo$
M_r	1925.710	1925.710	1980.499	1980.499	1988.623	1988.334	1980.657	2034.128
Crystal system, space group	monoclinic, $P2_1/c$	orthorhombic, *Pbca*	monoclinic, $P2_1/c$	cubic, $Pn\bar{3}n$	cubic, $Pn\bar{3}n$	monoclinic, $P2_1/c$	monoclinic, $P2_1/c$	cubic, $Pn\bar{3}n$
Temperature (K)	120	120	120	120	120	120	120	100
a (Å)	21.293(7)	19.4927(4)	38.714(3)	37.391(3)	37.391(3)	38.607(2)	21.370(2)	37.5869(5)
b (Å)	16.896(5)	16.2918(10)	16.8469(12)	37.391(3)	37.391(3)	16.8676(10)	16.88255(18)	37.5869(5)
c (Å)	18.283(6)	38.420(2)	18.2104(13)	37.391(3)	37.391(3)	18.4282(11)	18.726(2)	37.5869(5)
V (Å^3)	59778(7)	12201(1)	11876.1(15)	52275.9	52275.9	11997	6098.7(11)	53101.8(2)
Z	2	4	4	12	12	4	2	12
Radiation type	$Cu_{K\alpha}$, λ = 1.5405 Å	$Cu_{K\alpha}$, λ = 1.5405 Å	$Cu_{K\alpha}$, λ = 1.5405 Å	$Cu_{K\alpha}$, λ = 1.5405 Å	$Cu_{K\alpha}$, λ = 1.5405 Å	$Cu_{K\alpha}$, λ = 1.5405 Å	$Cu_{K\alpha}$, λ = 1.5405 Å	Synchrotron, λ = 0.6889 Å
Crystal size (mm)	0.10 x 0.05 x 0.05	0.05 x 0.05 x 0.10	0.10 x 0.05 x 0.05	0.10 x 0.10 x 0.10	0.10 x 0.10 x 0.10	0.10 x 0.05 x 0.05	0.10 x 0.05 x 0.05	0.10 x 0.10 x 0.10
R_{int}	0.0838	0.0677	0.0792	0.0983	0.0983	0.0747	0.0550	0.1831

Crystal data								
Name	$(dipPhO)_8PcRe$	$(dipPhO)_8PcIr$	$(dipPhO)_8PcGe$	$(dipPhO)_8PcCd$	$(dipPhO)_8PcPb$	$(dipPhO)_8PcFe$	$(dipPhO)_8PcP$	$(dipPhO)_8PcSb$
Chemical formula	$C_{128}H_{144}N_8O_8Re$	$C_{128}H_{144}N_8O_8Ir$	$C_{128}H_{144}N_8O_8Ge$	$C_{128}H_{144}N_8O_8Cd$	$C_{128}H_{144}N_8O_8Pb$	$C_{128}H_{144}N_8O_8Fe$	$C_{128}H_{144}N_8O_8P$	$C_{128}H_{144}N_8O_8Sb$
M_r	2124.315	2114.340	2031.415	2035.208	2129.009	2013.385	1968.858	2044.146
Crystal system, space group	cubic, $Pn\bar{3}n$	cubic, $Pn\bar{3}n$	cubic, $Pn\bar{3}n$	cubic, $Pn\bar{3}n$	cubic, $Pn\bar{3}n$	cubic, $Pn\bar{3}n$	cubic, $Pn\bar{3}n$	cubic, $Pn\bar{3}n$
Temperature (K)	120	120	120	120	120	100	100	120
a (Å)	37.9400(3)	37.6003(2)	37.650(4)	37.1526(2)	37.2220(12)	37.037(4)	37.3171(4)	37.2581(1)
b (Å)	37.9400(3)	37.6003(2)	37.650(4)	37.1526(2)	37.2220(12)	37.037(4)	37.3171(4)	37.2581(1)
c (Å)	37.9400(3)	37.6003(2)	37.650(4)	37.1526(2)	37.2220(12)	37.037(4)	37.3171(4)	37.2581(1)
V (Å^3)	54612.4(7)	53158.9(6)	53370	51282.6(6)	51570	50792	51966.4(7)	51720.4(7)
Z	12	12	12	12	12	12	12	12
Radiation type	$Cu_{K\alpha}$, λ = 1.5405 Å	$Cu_{K\alpha}$, λ = 1.5405 Å	$Cu_{K\alpha}$, λ = 1.5405 Å	$Cu_{K\alpha}$, λ = 1.5405 Å	$Cu_{K\alpha}$, λ = 1.5405 Å	Synchrotron, λ = 0.6889 Å	Synchrotron, λ = 0.6889 Å	$Cu_{K\alpha}$, λ = 1.5405 Å
Crystal size (mm)	0.10 x 0.10 x 0.10	0.10 x 0.10 x 0.10	0.10 x 0.10 x 0.10	0.10 x 0.10 x 0.10	0.10 x 0.10 x 0.10	0.10 x 0.10 x 0.10	0.10 x 0.10 x 0.10	0.10 x 0.10 x 0.10
R_{int}	0.1078	0.1172	0.0552	0.0552	0.0951	0.0893	0.0857	0.0948

Crystal data				
Acronym	PNC[H_2/*v* H_2TPP]	PNC[H_2/*v* H_2TPP] + $CuCl_2$	PNC[Ti/*v* H_2TPP]	PNC[Mn/*v* H_2TPP]
Name	$(dipPhO)_8PcH_2$ + H_2TPP	[$(dipPhO)_8PcH_2$ + H_2TPP] + $CuCl_2$	$(dipPhO)_8PcTi$ + H_2TPP	$(dipPhO)_8PcMn$ + H_2TPP
Chemical formula	$C_{128}H_{144}N_8O_8H_2$ + $C_{44}H_{28}N_4H_2$	$C_{128}H_{144}N_8O_8Cu$ + $C_{44}H_{28}N_4Cu$	$C_{128}H_{144}N_8O_8Ti$ + $C_{44}H_{28}N_4H_2$	$C_{128}H_{144}N_8O_8Mn$ + $C_{44}H_{28}N_4H_2$
M_r	2539.319	2662.380	2585.170	2592.241
Crystal system, space group	cubic, $Pn\bar{3}n$	cubic, $Pn\bar{3}n$	cubic, $Pn\bar{3}n$	cubic, $Pn\bar{3}n$
Temperature (K)	120	120	120	120
a (Å)	38.0858(3)	37.9100(10)	37.7674(2)	37.7985(5)
b (Å)	38.0858(3)	37.9100(10)	37.7674(2)	37.7985(5)
c (Å)	38.0858(3)	37.9100(10)	37.7674(2)	37.7985(5)
V (Å^3)	55244.5(13)	54483.0(4)	53870.5(9)	54004(2)
Z	12	12	12	12
Radiation type	Cu_{Ka}, λ = 1.5405 Å	Cu_{Ka}, λ = 1.5405 Å	Cu_{Ka}, λ = 1.5405 Å	Cu_{Ka}, λ = 1.5405 Å
Crystal size (mm)	0.10 x 0.10 x 0.10	0.10 x 0.10 x 0.10	0.10 x 0.10 x 0.10	0.10 x 0.10 x 0.10
R_{int}	0.0824	0.1170	0.1033	0.1139

Crystal data				
Acronym	PNC[Fe/*v* H_2TPP]	PNC[Co/*v* H_2TPP]	PNC[Co/*v* H_2TPP] + $CuCl_2$	PNC[Co/*v* CoTPP]
Name	$(dipPhO)_8PcFe$ + H_2TPP	$(dipPhO)_8PcCo$ + H_2TPP	[$(dipPhO)_8PcCo$ + H_2TPP] + $CuCl_2$	$(dipPhO)_8PcCo$ + CoTPP
Chemical formula	$C_{128}H_{144}N_8O_8FeCl$ + $C_{44}H_{28}N_4H_2$	$C_{128}H_{144}N_8O_8Co$ + $C_{44}H_{28}N_4H_2$	$C_{128}H_{144}N_8O_8Co$ + $C_{44}H_{28}N_4Cu$	$C_{128}H_{144}N_8O_8Co$ + $C_{44}H_{28}N_4Co$
M_r	2628.602	2596.237	2657.767	2653.154
Crystal system, space group	cubic, $Pn\bar{3}n$	cubic, $Pn\bar{3}n$	cubic, $Pn\bar{3}n$	cubic, $Pn\bar{3}n$
Temperature (K)	120	120	120	120
a (Å)	37.8603(6)	37.8048(2)	37.7924(3)	37.8225(4)
b (Å)	37.8603(6)	37.8048(2)	37.7924(3)	37.8225(4)
c (Å)	37.8603(6)	37.8048(2)	37.7924(3)	37.8225(4)
V (Å^3)	54269(3)	54030.7(9)	53977.6(13)	54106.6(17)
Z	12	12	12	12
Radiation type	Cu_{Ka}, λ = 1.5405 Å	Cu_{Ka}, λ = 1.5405 Å	Cu_{Ka}, λ = 1.5405 Å	Cu_{Ka}, λ = 1.5405 Å
Crystal size (mm)	0.10 x 0.10 x 0.10	0.10 x 0.10 x 0.10	0.10 x 0.10 x 0.10	0.10 x 0.10 x 0.10
R_{int}	0.1246	0.0863	0.0861	0.1727

Crystal data				
Acronym	PNC[Ni/*v* H_2TPP]	PNC[Cu/*v* H_2TPP]	PNC[Al/*v* H_2TPP]	PNC[Ga/*v* H_2TPP]
Name	$(dipPhO)_8PcNi + H_2TPP$	$(dipPhO)_8PcCu + H_2TPP$	$(dipPhO)_8PcAl + H_2TPP$	$(dipPhO)_8PcGa + H_2TPP$
Chemical formula	$C_{128}H_{144}N_8O_8Ni + C_{44}H_{28}N_4H_2$	$C_{128}H_{144}N_8O_8Cu + C_{44}H_{28}N_4H_2$	$C_{128}H_{144}N_8O_8Al + C_{44}H_{28}N_4H_2$	$C_{128}H_{144}N_8O_8Ga + C_{44}H_{28}N_4H_2$
M_r	2595.997	2600.849	2564.285	2607.027
Crystal system, space group	cubic, $Pn\bar{3}n$	cubic, $Pn\bar{3}n$	cubic, $Pn\bar{3}n$	cubic, $Pn\bar{3}n$
Temperature (K)	120	120	120	120
a (Å)	37.73920(10)	37.9675(2)	37.7939(3)	37.8515(2)
b (Å)	37.73920(10)	37.9675(2)	37.7939(3)	37.8515(2)
c (Å)	37.73920(10)	37.9675(2)	37.7939(3)	37.8515(2)
V (Å^3)	53749.9(4)	54731.3(9)	53984.0(13)	54231.2(9)
Z	12	12	12	12
Radiation type	$Cu_{K\alpha}$, λ = 1.5405 Å	$Cu_{K\alpha}$, λ = 1.5405 Å	$Cu_{K\alpha}$, λ = 1.5405 Å	$Cu_{K\alpha}$, λ = 1.5405 Å
Crystal size (mm)	0.10 x 0.10 x 0.10	0.10 x 0.10 x 0.10	0.10 x 0.10 x 0.10	0.10 x 0.10 x 0.10
R_{int}	0.0893	0.0768	0.1274	0.1049

Crystal data				
Acronym	PNC[In/*v* H_2TPP]	PNC[Ag/*v* H_2TPP]	PNC[Au/*v* H_2TPP]	PNC[Fe-*v* N-*v* FeTPP]
Name	$(dipPhO)_8PcIn + H_2TPP$	$(dipPhO)_8PcAg + H_2TPP$	$(dipPhO)_8PcAu + H_2TPP$	$(dipPhO)_8PcAu\text{-}N\text{-}FeTPP$
Chemical formula	$C_{128}H_{144}N_8O_8In + C_{44}H_{28}N_4H_2$	$C_{128}H_{144}N_8O_8Ag + C_{44}H_{28}N_4H_2$	$C_{128}H_{144}N_8O_8Au + C_{44}H_{28}N_4H_2$	$C_{128}H_{144}N_8O_8Fe + N + C_{44}H_{28}N_4Fe$
M_r	2652.122	2645.172	2734.270	2660.985
Crystal system, space group	cubic, $Pn\bar{3}n$	cubic, $Pn\bar{3}n$	cubic, $Pn\bar{3}n$	cubic, $Pn\bar{3}n$
Temperature (K)	120	120	120	120
a (Å)	37.9239(2)	37.8701(2)	37.7793(2)	37.8683(6)
b (Å)	37.9239(2)	37.8701(2)	37.7793(2)	37.8683(6)
c (Å)	37.9239(2)	37.8701(2)	37.7793(2)	37.8683(6)
V (Å^3)	54543.0(9)	54311.2(9)	53921.5(9)	54303(3)
Z	12	12	12	12
Radiation type	$Cu_{K\alpha}$, λ = 1.5405 Å	$Cu_{K\alpha}$, λ = 1.5405 Å	$Cu_{K\alpha}$, λ = 1.5405 Å	$Cu_{K\alpha}$, λ = 1.5405 Å
Crystal size (mm)	0.10 x 0.10 x 0.10	0.10 x 0.10 x 0.10	0.10 x 0.10 x 0.10	0.10 x 0.10 x 0.10
R_{int}	0.236	0.0867	0.0666	0.1213

Crystal data			
Acronym	azaPNC[H_2/*v* H_2TPP]	PNC[H_2/*v* H_2TPMeP]	PNC[Cu/*v* CuTPMeP]
Name	$(dipPhO)_8azaPcH_2$ + H_2TPP	$(dipPhO)_8PcH_2$ + H_2TPMeP	$(dipPhO)_8PcCu$ + CuTPMeP
Chemical formula	$C_{120}H_{144}N_{16}O_8H_2$ + $C_{44}H_{28}N_4H_2$	$C_{128}H_{144}N_8O_8H_2$ + $C_{44}H_{28}N_4(CH_3)_4H_2$	$C_{128}H_{144}N_8O_8Cu$ + $C_{44}H_{28}N_4(CH_3)_4Cu$
M_r	2555.287	2599.458	2722.518
Crystal system, space group	cubic, $Pn\bar{3}n$	orthorhombic, *Pnma*	orthorhombic, *Pnma*
Temperature (K)	120	120	120
a (Å)	37.5049(2)	20.2254(3)	20.3161(6)
b (Å)	37.5049(2)	39.3105(7)	39.2808(12)
c (Å)	37.5049(2)	20.5963(4)	20.6770(5)
V (Å^3)	52755.1(8)	16375.5(5)	16500.9(8)
Z	12	2	2
Radiation type	Cu_{Ka}, λ = 1.5405 Å	Cu_{Ka}, λ = 1.5405 Å	Cu_{Ka}, λ = 1.5405 Å
Crystal size (mm)	0.10 x 0.10 x 0.10	0.05 x 0.10 x 0.05	0.05 x 0.10 x 0.05
R_{int}	0.1304	0.1066	0.0993

Crystal data			
Acronym	PNC[*v* H_2TPP/Co-*c* bipy-Co/*v* H_2TPP]	PNC[*v* CoTPP/Co-*c* bipy-Co/*v* CoTPP]	PNC[*v* CuTPP/Co-*c* bipy-Co/*v* CuTPP]
Name	$(dipPhO)_8PcCo + H_2TPP + bipy$	$(dipPhO)_8PcCo + CoTPP + bipy$	$(dipPhO)_8PcCo + CuTPP + bipy$
Chemical formula	$(C_{128}H_{144}N_8O_8Co)_2 + (C_{44}H_{28}N_4H_2)_2 + C_{10}H_8N_2$	$(C_{128}H_{144}N_8O_8Co)_2 + (C_{44}H_{28}N_4Co)_2 + C_{10}H_8N_2$	$(C_{128}H_{144}N_8O_8Co)_2 + (C_{44}H_{28}N_4Cu)_2 + C_{10}H_8N_2$
M_r	5348.658	5462.493	5471.718
Crystal system, space group	cubic, $Pn\bar{3}n$	cubic, $Pn\bar{3}n$	cubic, $Pn\bar{3}n$
Temperature (K)	120	120	120
a (Å)	37.8503(2)	37.8191(5)	37.91000(10)
b (Å)	37.8503(2)	37.8191(5)	37.91000(10)
c (Å)	37.8503(2)	37.8191(5)	37.91000(10)
V (Å^3)	54226.0(9)	54092(2)	54483.0(4)
Z	12	12	12
Radiation type	Cu_{Ka}, λ = 1.5405 Å	Cu_{Ka}, λ = 1.5405 Å	Cu_{Ka}, λ = 1.5405 Å
Crystal size (mm)	0.10 x 0.10 x 0.10	0.10 x 0.10 x 0.10	0.10 x 0.10 x 0.10
R_{int}	0.0825	0.1459	0.1144

Crystal data			
Acronym	PNC[*v* CuTPP/Cu-*c* bipy-Cu/*v* CuTPP]	PNC[*v* H_2TPP/Co-*c* bpm-Co/*v* H_2TPP]	PNC[*v* CuTPP/Co-*c* bpm-Co/*v* CuTPP]
Name	$(dipPhO)_8PcCu + CuTPP + bipy$	$(dipPhO)_8PcCo + H_2TPP + bpm$	$(dipPhO)_8PcCo + CuTPP + bpm$
Chemical formula	$(C_{128}H_{144}N_8O_8Cu)_2 + (C_{44}H_{28}N_4Cu)_2 + C_{10}H_8N_2$	$(C_{128}H_{144}N_8O_8Co)_2 + (C_{44}H_{28}N_4H_2)_2 + C_8H_8N_4$	$(C_{128}H_{144}N_8O_8Co)_2 + (C_{44}H_{28}N_4Cu)_2 + C_8H_8N_4$
M_r	5480.944	5352.650	5475.710
Crystal system, space group	cubic, $Pn\bar{3}n$	cubic, $Pn\bar{3}n$	cubic, $Pn\bar{3}n$
Temperature (K)	120	120	120
a (Å)	37.7983(5)	37.8496(6)	37.80340(10)
b (Å)	37.7983(5)	37.8496(6)	37.80340(10)
c (Å)	37.7983(5)	37.8496(6)	37.80340(10)
V (Å^3)	54004(2)	54132.3(6)	54024.7(4)
Z	12	12	12
Radiation type	Cu_{Ka}, λ = 1.5405 Å	Cu_{Ka}, λ = 1.5405 Å	Cu_{Ka}, λ = 1.5405 Å
Crystal size (mm)	0.10 x 0.10 x 0.10	0.10 x 0.10 x 0.10	0.10 x 0.10 x 0.10
R_{int}	0.1139	0.0935	0.1264

I-19 Gas cell experimental procedure

Gas cell experiments

Gas cell experiments were carried out on station I19 using a quartz capillary static cell with a 5 mm outer diameter. The cell was attached to a goniometer head containing a standard Mitegen mount in which crystals of PNC[Co-*c*bipy-Co] and PNC[Co-*c*bpm-Co] were glued in order to avoid movement of the sample on application of pressure. The goniometer head was connected to a gas rig though stainless-steel capillary tubing (Swagelok SS-T1-S-014-6ME). Data were collected from high-vacuum (for at least 10 minutes, vacuum = 10^{-6} mbar) to 5 bar in CO and up to 28 bar in NO. The gas cell was used to collect evacuated crystals held under high-vacuum in order to remove as much solvent as possible. After exposing PNC[Co-*c*bipy-Co] and PNC[Co-*c*bpm-Co] to CO or NO, the crystal was then evacuated for at least 10 minutes to determine the reversibility of the gas uptake in the pores. Collections were carried out successively on a single crystal of either PNC[Co-cbipy-Co] or and PNC[Co-cbpm-Co].

Data collections were carried out using an exposure time and a step size of 1 second and 0.5 degrees respectively using a Pilatus 300K detector photon counting pixel array detector. For each data set, a full sphere of data was collected. Data processing were carried out using the program xia2,[131] while the adsorption correction was carried out using the program AIMLESS.[132]

Structure refinements were carried in Olex2.[133] All structures were refined against F^2 with an I/σ cut-off of 3. The aromatic rings in the organic linkers were restrained to hexagonal geometry and are rotationally disordered over two sites of equal occupancy. All other bond distances and angles were refined freely. Vibrational and thermal similarity restraints were applied to the phenyl rings and isopropyl groups on the phthalocyanine unit and to the CO and NO ligands, where applicable. The occupancy of the C and N-atoms in the CO and NO ligands were refined freely. All hydrogen atoms were placed geometrically and were constrained to ride on their host atoms. The pore volume and electron-count per unit cell was calculated using the SQUEEZE algorithm in Platon.[134] To determine if the ligands were bound at the open metal sites, structure models were refined both including and excluding the CO or NO ligand so that the integrity of the models could be compared.

Supplement Table 1. Experimental details for PNC[Co-*c*bipy-Co] during evacuation, and exposure to CO and NO.

Experimental gas cell conditions	Vacuum (10^{-6} mbar, 10 min, 298 K)	5 bar CO (180 K)	2.63 bar NO (180 K)	Vacuum (10^{-6} mbar, 10 min, 298 K)
Crystal data				
Chemical formula	$2(C_{128}H_{144}Co N_8O_8)$*c*bipy	$2(C_{128}H_{144}Co N_8O_8)$*c*bipy	$2(C_{128}H_{144}Co N_8O_8$-*v*NO)*c*bipy	$2(C_{128}H_{144}Co N_8O_8$-*v*NO)*c*bipy
M_r	4267.294	4267.294	4297.300	4297.300
Crystal system, space group	Cubic, $Pn\bar{3}n$	Cubic, $Pn\bar{3}n$	Cubic, $Pn\bar{3}n$	Cubic, $Pn\bar{3}n$
Temperature (K)	293	180	180	293
a (Å)	37.8156(2)	37.438(2)	37.9704(2)	37.785(2)
V (Å^3)	54077.0(5)	54628.9(5)	54743.9(5)	53946.7(5)
Z	6	6	6	6
Radiation type	Synchrotron, λ = 0.6889 Å	Synchrotron, λ = 0.6889 Å	Synchrotron, λ = 0.6889 Å	Synchrotron, λ = 0.6889 Å
μ (mm^{-1})	0.124	0.124	0.125	0.127
Crystal size (mm)	0.1 x 0.1 x 0.1	0.1 x 0.1 x 0.1	0.1 x 0.1 x 0.1	0.1 x 0.1 x 0.1
Data Collection				
Diffractometer	Pilatus 300K	Pilatus 300K	Pilatus 300K	Pilatus 300K
Absorption correction	Empirical (using intensity measurements) *CCP4* 7.0.027: AIMLESS, version 0.5.31 : 12/12/16 Scaling & analysis of unmerged intensities, absorption	Empirical (using intensity measurements) *CCP4* 7.0.027: AIMLESS, version 0.5.31 : 12/12/16 Scaling & analysis of unmerged intensities, absorption	Empirical (using intensity measurements) *CCP4* 7.0.027: AIMLESS, version 0.5.31 : 12/12/16 Scaling & analysis of unmerged intensities, absorption	Empirical (using intensity measurements) *CCP4* 7.0.027: AIMLESS, version 0.5.31 : 12/12/16 Scaling & analysis of unmerged intensities, absorption

	correction using spherical harmonics	correction using spherical harmonics	correction using spherical harmonics	correction using spherical harmonics
T_{min}, T_{max}	0.976, 1.000	0.977, 1.000	0.974, 1.000	0.984, 1.000
No. of measured, independent and observed [$I > 2.0\sigma(I)$] reflections	165909, 4737, 3481	268480, 4792, 3836	167841, 4761, 3956	198292, 6489, 4583
R_{int}	0.1019	0.0975	0.0820	0.0853
θ_{max} (°)	20.3	21.3	20.0	20.0
Refinement				
$R[F^2 > 2\sigma(F^2)]$, $wR(F^2)$, S	0.1030, 0.3441, 1.292	0.0931, 0.2752, 1.040	0.0872, 0.2641, 1.032	0.1015, 0.3326, 1.298
No. of reflections	6489	4761	4792	4737
No. of parameters	268	268	274	280
No. of restraints	45	45	45	45
H-atom treatment	H-atom parameters constrained	H-atom parameters constrained	H-atom parameters constrained	H-atom parameters constrained
$\Delta>_{max}$, $\Delta>_{min}$ (e Å^{-3})	0.6316, -0.4831	0.7731, -0.8052	0.9384, -0.6565	0.8865, -0.7303

Supplement Table 2. Experimental details for PNC[Co-*c*bpm-Co] during evacuation, and exposure to CO and NO.

Experimental gas cell conditions	Vacuum (10^{-6} mbar, 10 min, 298 K)	5 bar CO (180 K)	Vacuum (10^{-6} mbar, 38 min, 298 K)	4-28 bar NO (180 K)	Vacuum (10^{-6} mbar, 10 min, 298 K)
Crystal data					
Chemical formula	$2(C_{128}H_{144}Co N_8O_8)$cbpm	$2(C_{128}H_{144}Co N_8O_8)$*c*bpm	$2(C_{128}H_{144}Co N_8O_8)$*c*bpm	$2(C_{128}H_{144}Co N_8O_8)$*c*bpm*v*NO	$2(C_{128}H_{144}Co N_8O_8)$*c*bpm*v*NO
M_r	4279.310	4279.310	4279.310	4309.316	4309.316
Crystal system, space group	Cubic, $Pn\bar{3}n$	Cubic, $Pn\bar{3}n$	Cubic, $Pn\bar{3}n$	Cubic, $Pn\bar{3}n$	Cubic, $Pn\bar{3}n$
Temperature (K)	293	180	293	180	293
a (Å)	37.7457(3)	37.8873(2)	37.7086(3)	37.9112(2	37.6730(5)
V ($Å^3$)	53777.7(6)	54385.2(6)	53619.0(7)	54488.2(6)	53467.6(11)
Z	6	6	6	6	6
Radiation type	Synchrotron, λ = 0.6889 Å	Synchrotron, λ = 0.6889 Å	Synchrotron, λ = 0.6889 Å	Synchrotron, λ = 0.6889 Å	Synchrotron, λ = 0.6889 Å
μ (mm^{-1})	0.142	0.125	0.127	0.141	0.128
Crystal size (mm)	0.1 x 0.1 x 0.1	0.1 x 0.1 x 0.1	0.1 x 0.1 x 0.1	0.1 x 0.1 x 0.1	0.1 x 0.1 x 0.1
Data Collection					
Diffractometer	Pilatus 300K	Pilatus 300K	Pilatus 300K	Pilatus 300K	Pilatus 300K
Absorption correction	Empirical (using intensity measurements) *CCP4* 7.0.027: AIMLESS, version 0.5.31 : 12/12/16 Scaling & analysis of unmerged	Empirical (using intensity measurements) *CCP4* 7.0.027: AIMLESS, version 0.5.31 : 12/12/16 Scaling & analysis of unmerged	Empirical (using intensity measurements) *CCP4* 7.0.027: AIMLESS, version 0.5.31 : 12/12/16 Scaling & analysis of unmerged	Empirical (using intensity measurements) *CCP4* 7.0.027: AIMLESS, version 0.5.31 : 12/12/16 Scaling & analysis of unmerged	Empirical (using intensity measurements) *CCP4* 7.0.027: AIMLESS, version 0.5.31 : 12/12/16 Scaling & analysis of unmerged

	intensities, absorption correction using spherical harmonics	intensities, absorption correction using spherical harmonics	intensities, absorption correction using spherical harmonics	intensities, absorption correction using spherical harmonics	intensities, absorption correction using spherical harmonics
T_{min}, T_{max}	0.986, 1.000	0.985, 1.000	0.986, 1.000	0.985, 1.000	0.991, 1.000
No. of measured, independent and observed [$I > 2.0\sigma(I)$] reflections	162816, 4705, 3116	164708, 4746, 3615	161934, 4687, 4037	164732, 4741, 3616	160535, 4664, 2883
R_{int}	0.0814	0.0792	0.0833	0.0873	0.0985
θ_{max} (°)	20.1	19.0	18.9	19.0	20.1
Refinement					
$R[F^2 > 2\sigma(F^2)]$, $wR(F^2)$, S	0.1037, 0.3488, 1.267	0.1008, 0.3331, 1.304	0.1042, 0.3515, 1.249	0.1013, 0.3270, 1.298	0.1207, 0.3831, 1.296
No. of reflections	4705	4746	4687	4741	4665
No. of parameters	268	268	268	266	266
No. of restraints	45	45	45	45	45
H-atom treatment	H-atom parameters constrained	H-atom parameters constrained	H-atom parameters constrained	H-atom parameters constrained	H-atom parameters constrained
$\Delta>_{max}$, $\Delta>_{min}$ (e Å^{-3})	0.8321, -0.4481	0.8136, -0.6720	0.7594, -0.4068	0.7413, -0.4480	1.0190, -0.4202

Computer programs: DIALS 2theta refinement, DIALS 1.4.2-g92ff257-release, aimless (Evans, P. R. and Murshudov, G. N., 2013) CCP4 (Winn, M. D. et al., 2011) DIALS 1.4.2-g92ff257-release pointless (Evans, P., 2006) XIA2 0.5.170-g7abc92b-dials-1.4 (Winter, G., 2010), Olex2 1.2 (Dolmanov, L. J. et al, 2009)

Supplement Table 3. Structural refinement details for the evacuated pre-crystals of PNC[Co-*c*bipy-Co] and PNC[Co-*c*bpm-Co]. Electron-counts in the void were calculated using the SQUEEZE algorithm in Platon.[134] *q*1 is the nearest peak to the Co^{2+} binding site in the void, belonging to potentially adsorbed solvent.

PNC	PNC[Co-*c*bipy-Co]	PNC[Co-*c*bpm-Co]
Experimental gas cell conditons	Vacuum (10^{-6} mbar, 10 min, 298 K)	Vacuum (10^{-6} mbar, 10 min, 298 K)
Void *V* (Å^3)	18747	18517
Void electron-count	1417	4025
Cavity *V* (Å^3)	3783	3726
Cavity electron-count	654	570
*q*1 (e^-)	1.05	0.63
Co-*q*1 (Å)	0.873	2.435

Supplement Table 4. Structural refinement details Co-L (L = CO or NO) bond for PNC[Co-*c*bipy-Co] during evacuation, and exposure to CO and NO, modelled with the CO or NO ligand bound to Co (Co-*q*1-*q*2 where *q*1 is assigned as either C or N and *q*2 is assigned as O).

Experimental gas cell conditions	5 bar CO (180 K)	2.63 bar NO (180 K)	Vacuum (10^{-6} mbar, 10 min, 298 K)
*q*1 peak (e^-)	1.07	5.78	4.74
*q*2 peak (e^-)	1.10	1.55	1.93
Co-L (Å)	1.898	1.880	1.904
CoC/N-O (Å)	1.117	1.105	1.204
Co-C/N-O (°)	180.0	122.2	118.3
L Occupancy	0.44	1.00	1.00
R_1 (L in model)	0.0938	0.0872	0.1029
S (L in model)	1.040	1.032	1.298
R_1 (L not in model)	0.0910	0.1059	0.1307
S (L not in model)	1.040	1.535	1.635

Supplement Table 5. Structural refinement details Co-L (L = CO or NO) bond for PNC[Co-*c*bpm-Co] during evacuation, and exposure to CO and NO, modelled with the CO or NO ligand bound to Co (Co-*q*1-*q*2 where *q*1 is assigned as either C or N and *q*2 is assigned as O).

Experimental gas cell conditions	5 bar CO (180 K)	Vacuum (10^{-6} mbar, 38 min, 298 K)	4-28 bar NO (180 K)	Vacuum (10^{-6} mbar, 10 min, 298 K)
*q*1 peak (e^-)	1.71	0.93	4.68	3.40
*q*2 peak (e^-)	0.88	0.77	0.97	0.80
Co-L (Å)	1.644	1.193	1.859	1.936
CoC/N-O (Å)	1.424	1.114 (fixed)	1.097	1.124
Co-C/N-O (°)	180.0	180.0	120.4	116.2
L Occupancy	0.31	0.25 (fixed)	1.00	1.00
R_1 (L in model)	0.1042	0.1081	0.1013	0.1207
S (L in model)	1.315	0.262	1.298	1.296
R_1 (L not in model)	0.1042	0.1042	0.1144	0.1387
S (L not in model)	1.304	1.249	1.463	1.434

Supplement Table 6. Void volume and electron-count within the void for PNC[Co-*c*bipy-Co] during evacuation and exposure to CO and NO calculated using the SQUEEZE algorithm in Platon.[134]

Experimental gas cell conditions	Vacuum (10^{-6} mbar, 10 min, 298 K)	5 bar CO (180 K)	2.63 bar NO (180 K)	Vacuum (10^{-6} mbar, 10 min, 298 K)
Void (*x*, *y*, *z*)	0.000, 0.000, 0.000	0.000, -0.002, 0.000	-0.001, -0.002, -0.001	0.000, -0.001, 0.000
V (Å^3)	18747	19260	18953	18440
Electron-count	1417	2655	3137	1364
No. of L molecules*	N/A	190	209	91

*Assuming all electrons-density is associated with CO or NO.

Supplement Table 7. Void volume and electron-count within the void for PNC[Co-*c*bpm-Co] during evacuation and exposure to CO and NO calculated using the SQUEEZE algorithm in Platon.[134]

Experimental gas cell conditions	Vacuum (10^{-6} mbar, 10 min, 298 K)	5 bar CO (180 K)	Vacuum (10^{-6} mbar, 10 min, 298 K)	4-28 bar NO (180 K)	Vacuum (10^{-6} mbar, 10 min, 298 K)
Void (*x*, *y*, *z*)	0.000, -0.001, 0.000	-0.001, -0.002, -0.001	-0.001, -0.001, -0.001	-0.001, -0.002, -0.001	0.000, -0.001, 0.000
V (Å^3)	18517	19266	18518	18748	17989
Electron-count	4025	2535	1300	3144	1524
No. of L molecules*	N/A	181	93	210	102

*Assuming all electrons-density is associated with CO or NO.

Supplement Table 8. Structural *trans*-effect of axial NO on Co-N(bipy) and Co-N(bpm) bond lengths in PNC[Co-*c*bipy-Co] and PNC[Co-*c*bpm-Co].

PNC	PNC[Co-*c*bipy-Co]	PNC[Co-*c*bipy-Co-*v*NO]	PNC[Co-*c*bpm-Co]	PNC[Co-*c*bpm-Co-*v*NO]
Experimental gas cell conditions	Vacuum (10^{-6} mbar, 10 min, 298 K)	2.63 bar NO (180 K)	Vacuum (10^{-6} mbar, 10 min, 298 K)	4-28 bar NO (180 K)
Co-(bipy/bpm) (Å)	2.168	2.386	2.392	2.566

Bibliography

1. McKeown NB. *Phthalocyanine Materials: Synthesis, Structure, and Function*.; 1998. http://books.google.com/books?hl=en&lr=&id=iuDhWDW4FbcC&oi=fnd&pg=PR11&dq=Fibrous+Assemblies+Made+of+Amphiphilic+Metallophthalocyanines&ots=ZpuK2Wt32p&sig=IzgqmI-HdNrvhegxzIpa3W0h6aE%5Cnpapers://47c6313f-eeab-431b-a04b-78c121da8986/Paper/p2832.

2. McKeown NB. The Synthesis of Symmetrical Phthalocyanines. In: *The Porphyrin Handbook: Phthalocyanines: Synthesis*. Vol 15. ; 2012:61-124. doi:10.1016/B978-0-08-092389-5.50008-0

3. Dent E, Linstead RP, Lowe AR. Phthalocyanines. Part VI. The structure of the Phthalocyanines. *J Chem Soc*. 1934:1033-1039.

4. Linstead RP. Phthalocyanines Part I A new type of Synthetic Colouring Matters. *J Chem Soc*. 1934:1016-1017.

5. Linstead RP, Byrne GT, Lowe AR. Phthalocyanines. Part II. The Preparation of Phthalocyanine and Some Metallic Derivatives from o-Cyanobenzamide and Phthalimide. *J Chem Soc*. 1934:1017-1022.

6. Linstead RP, Dent CE. Phthalocyanines. Part IV. Copper Phthalocyanines. *J Chem Soc*. 1934:1027-1031.

7. Linstead RP, Lowe AR. Phthalocyanines. Part V. The molecular weight of magnesium Phthalocyanine. *J Chem Soc*. 1934:1031-1033.

8. Linstead RP, Lowe AR. Phthalocyanines. Part III. Preliminary Experiments on the Preparation of Phthalocyanines from Phthalonitrile. *J Chem Soc*. 1934:1022-1027.

9. Linstead RP, Robertson MJ. the stereochemistry of metallic phthalocyanines. *J Chem Soc*. 1936:1736-1738.

10. Robertson MJ. An X-Ray study of the structure of the phthalocyanines part I. *J Chem Soc*. 1934:615-621.

11. Robertson MJ. An X-Ray Study of the Phthulocyanines. Part 11. Quantitative Structure Determination of the Metal-free Compound. *J Chem Soc*. 1936:1195-1209.

12. Robertson MJ, Woodward I. An X-Ray Study of the Phthalocyanines. Part III. Quantitutive Structure Determination of Nickel Phthalocyanine. *J Chem Soc*. 1937:219-230.

13. Robertson MJ, Woodward I. An X-Ray study of the Phthalocyanines. Part IV. Direct Quantitative Analysis of the Platinum Compound. *J Chem Soc*. 1940:36-48.

14. Eastwood D, Edwards L, Gouterman M, Steinfeld J. vapor absorption and emission of phthalocyanines. *J Mol Spectrosc*. 1966;20:381-390.

15. Cook AH. Catalytic Properties of the Phthalocyanines. Part I. Catuluse Properties. *J Chem Soc*. 1938:1761-1768.

16. Rollmann LD, Iwamoto RT. Electrochemistry, Electron Paramagnetic Resonance, and Visible Spectra of Cobalt, Nickel, Copper, and Metal-Free Phthalocyanines in Dimethyl Sulfoxide. *J Am Chem Soc*. 1967;90(6):1455-1463.

17. Kadish K, Smith KM, Guilard R. *The Porphyrin Handbook*. Vol 11-20.; 2000.

18. Claessens CG, Blau WJ, Cook M, et al. Phthalocyanines and phthalocyanine analogues: The quest for applicable optical properties. *Monatshefte fur Chemie*. 2001;132(1):3-11. doi:10.1007/s007060170140

19. Claessens CG, Hahn U, Torres T. Phthalocyanines: From outstanding electronic properties to emerging applications. *Chem Rec*. 2008;8:75-97. doi:10.1002/tcr.20139

20. Leznoff CC, Lever ABP. *Phthalocyanines: Properties and Applications*. New York: Wiley-VCH; 1989.

21. Shirai R, Kobayashi N. *Phthalocyanines: Chemistry and Functions*. Tokyo: IPC; 1997.

22. McKeown NB, Chambrier I, Cook MJ. Synthesis and Characterisation of some 1,4,8,11 ,I 5,l 8,22,25-0cta-alkyl- and 1,4,8,11 ,I 5,18-Hexa-alkyl-22,25-bis(carboxypropyl)phthalocyanines. *J Chem Soc Perkin Trans*. 1990:1169-1177.

23. Brewis M, Clarkson GJ, Humberstone P, Makhseed S, McKeown NB. The synthesis of some phthalocyanines and napthalocyanines derived from sterically hindered phenols. *Chem - A Eur J*. 1998;4(9):1633-1640. doi:10.1002/(SICI)1521-3765(19980904)4:9<1633::AID-CHEM1633>3.0.CO;2-O

24. Thompson JA, Murata K, Miller D, et al. Synthesis of high-purity phthalocyanines (pc): high intrinsic conductivities in the molecular conductors H2 (pc) I and Ni (pc) I. *Inorg Chem*. 1993;32(8):3546-3553. doi:10.1021/ic00068a027

25. Poon K-W, Yan, Li X, Ng DKP. Synthesis and Electrochemistry of Ferrocenylphthalocyanines. *Organometallics*. 1999;18(17):3528-3533. doi:10.1021/om990208x

26. Mingos DMP. *Functional Phthalocyanine Molecular Materials*.; 2010. doi:10.1007/978-3-642-04752-7_1

27. de laTorre G, Vazquez P, Agullo-Lopez F, Torres T. Role of Structural Factors in the Nonlinear Optical Properties of Phthalocyanines and Related Compounds. *Chem Rev*. 2004;104(9):3723-3750. doi:10.1021/cr030206t

28. Morris RE, Wheatley PS. Gas storage in nanoporous materials. *Angew Chemie - Int Ed*. 2008;47:4966-4981. doi:10.1002/anie.200703934

29. Davis ME. Ordered porous materials for Emerging Applications. *Nature*. 2002;417:813-821. doi:10.1038/nnano.2015.251

30. Rouquerolt J, Avnir D, Fairbridge CW, et al. *Recommendations for the Characterisation of Porous Solids*. Vol 66.; 1994. doi:doi:10.1351/pac199466081739

31. Nassimbeni LR. Physicochemical aspects of host - Guest compounds. *Acc Chem Res*. 2003;36(8):631-637. doi:10.1021/ar0201153

32. Cooper AI. Molecular organic crystals: From barely porous to really porous. *Angew Chemie - Int Ed*. 2012;51:7892-7894. doi:10.1002/anie.201203117

33. Zhang G, Presly O, White F, Oppel IM, Mastalerz M. A shape-persistent quadruply

interlocked giant cage catenane with two distinct pores in the solid state. *Angew Chemie - Int Ed*. 2014;53:5126-5130. doi:10.1002/anie.201400285

34. Green HR, Lloyd GO. Porous Metal Organic Polygons and Polyhedra - Intrinsic vs. Extrinsic Porosity. In: *Monographs in Supramolecular Chemistry*. ; 2017:297-324. doi:10.1039/9781788010276-00297

35. McKeown NB. Nanoporous molecular crystals. *J Mater Chem*. 2010;20(47):10588-10597. doi:10.1039/c0jm01867h

36. Jones JTA, Hasell T, Wu X, et al. Modular and predictable assembly of porous organic molecular crystals. *Nature*. 2011;474:367-371. doi:10.1038/nature10125

37. Chen L, Reiss PS, Chong SY, et al. Separation of rare gases and chiral molecules by selective binding in porous organic cages. *Nat Mater*. 2014;13:954-960. doi:10.1038/nmat4035

38. Maekawa M, Konaka H, Minematsu T, Kuroda-Sowa T, Munakata M, Kitagawa S. Supplementary Material (ESI) for Bowl–shaped Cu(I) metallamacrocyclic ethylene and carbonyl adducts as structural analogues of organic calixarenes. *Chem Commun*. 2007;13:1-3. doi:10.1039/b000000x.For

39. McKeown NB, Makhseed S, Msayib KJ, Ooi LL, Helliwell M, Warren JE. A phthalocyanine clathrate of cubic symmetry containing interconnected solvent-filled voids of nanometer dimensions. *Angew Chemie - Int Ed*. 2005;44(46):7546-7549. doi:10.1002/anie.200502668

40. Bezzu CG, Helliwell M, Warren JE, Allan DR, McKeown NB. Heme-Like Coordination Chemistry Within Nanoporous Molecular Crystals. *Science (80-)*. 2010;327:1627-1630. doi:10.1126/science.1184228

41. Bezzu CG, Kariuki BM, Helliwell M, et al. In-situ coordination chemistry within cobalt-containing phthalocyanine nanoporous crystals. *Cryst Eng Commun*. 2013;15:1545-1550. doi:10.1039/C2CE26463C

42. Bench BA, Brennessel WW, Lee HJ, Gorun SM. Synthesis and structure of a biconcave cobalt perfluorophthalocyanine and its catalysis of novel oxidative carbon-phosphorus bonds formation by using air. *Angew Chemie - Int Ed*. 2002;41(5):750-754. doi:10.1002/1521-3773(20020301)41:5<750::AID-ANIE750>3.0.CO;2-6

43. Bench BA, Beveridge A, Sharman WM, Diebold GJ, Lier JE Van, Gorun SM. Introduction of Bulky Perfluoroalkyl Groups at the Peryphery of Zinc perfluorophthalocyanine. *Angew Chemie - Int Ed*. 2002;41(5):747-750. doi:10.1002/1521-3773(20020301)41:5<747::aid-anie747>3.0.co;2-j

44. Leng X, Choi C-F, Luo H-B, Cheng Y-K, Ng DKP. Host-guest interactions of 4-carboxyphenoxy phthalocyanines and beta-cyclodextrins in aqueous media. *Org Lett*. 2007;9(13):2497-2500. doi:10.1021/ol070888x

45. Tau P, Ogunsipe AO, Maree S, Maree MD, Nyokong T. Influence of cyclodextrins on the fluorescence, photostability and singlet oxygen quantum yields of zinc phthalocyanine and naphthalocyanine complexes. *J Porphyr Phthalocyanines*. 2003;07(06):439-446. doi:10.1142/S1088424603000562

46. Kryjewski M, Goslinski T, Mielcarek J. Functionality stored in the structures of cyclodextrin-porphyrinoid systems. *Coord Chem Rev*. 2015;300:101-120. doi:10.1016/j.ccr.2015.04.009

47. Basova T V., Parkhomenko RG, Polyakov M, et al. Effect of dispersion of gold nanoparticles on the properties and alignment of liquid crystalline copper phthalocyanine films. *Dye Pigment*. 2016;125:266-273. doi:10.1016/j.dyepig.2015.10.005

48. Woehrle D, Eskes M, Kiyotaka S, Yamada A. A simple synthesis of disubstituted dicyanobenzenes and octasubstituted phthalocyanines. *Synthesis (Stuttg)*. 1993:194-196. doi:10.1017/CBO9781107415324.004

49. Barbour LJ. Crystal porosity and the burden of proof. *Chem Commun*. 2006;(11):1163. doi:10.1039/b515612m

50. Bezzu CG, Burt LA, McMonagle CJ, et al. Highly stable fullerene-based porous molecular crystals with open metal sites. *Nat Mater*. 2019;18:740-745. doi:10.1038/s41563-019-0361-0

51. Hirakawa K, Umemoto H, Kikuchi R, et al. Determination of Singlet Oxygen and Electron Transfer Mediated Mechanisms of Photosensitized Protein Damage by Phosphorus(V)porphyrins. *Chem Res Toxicol*. 2015;28(2):262-267. doi:10.1021/tx500492w

52. Meshkov IN, Bulach V, Gorbunova YG, et al. Tuning photochemical properties of phosphorus(v) porphyrin photosensitizers. *Chem Commun*. 2017;53:9918-9921. doi:10.1039/c7cc06052a

53. Matsumoto J, Suzuki K, Yasuda M, et al. Photodynamic therapy of human biliary cancer cell line using combination of phosphorus porphyrins and light emitting diode. *Bioorganic Med Chem*. 2017;25:6536-6541. doi:10.1016/j.bmc.2017.10.031

54. Zhao JL, Guo SH, Qiu J, Gou XF, Hua CW, Chen B. Iron(III) phthalocyanine-chloride-catalyzed synthesis of sulfones from sulfonylhydrazones. *Tetrahedron Lett*. 2016;57:2375-2378. doi:10.1016/j.tetlet.2016.04.044

55. Sirotin S V., Tolbin AY, Moskovskaya IF, Abramchuk SS, Tomilova LG, Romanovsky B V. Heterogenized Fe(III) phthalocyanine: Synthesis, characterisation and application in liquid-phase oxidation of phenol. *J Mol Catal A Chem*. 2010;319(1-2):39-45. doi:10.1016/j.molcata.2009.11.017

56. Zhao J, Qiu J, Gou X, Hua C, Chen B. Iron(III) phthalocyanine chloride-catalyzed oxidation-aromatization of α, β-unsaturated ketones with hydrazine hydrate: Synthesis of 3, 5-disubstituted 1H-pyrazoles. *Cuihua Xuebao/Chinese J Catal*. 2016;37:571-578. doi:10.1016/S1872-2067(15)61043-9

57. Nandi G, Sarkar S. Solid-state synthesis of molybdenum and tungsten porphyrins and aerial oxidation of coordinated benzenethiolate to benzenesulfonate. *Inorg Chem*. 2012;51:6412-6420. doi:10.1021/ic3008377

58. Liu WS, Zhang R, Huang JS, Che CM, Peng SM. Synthesis and X-ray crystal structure of a chiral molybdenum porphyrin and its catalytic behaviour toward asymmetric epoxidation of aromatic alkenes. *J Organomet Chem*. 2001;634(1):34-38. doi:10.1016/S0022-328X(01)01075-0

59. Harada R, Matsuda Y, Okawa H, Kojima T. A porphyrin nanotube: Size-selective inclusion of tetranuclear molybdenum-oxo clusters. *Angew Chemie - Int Ed*. 2004;43(14):1825-1828. doi:10.1002/anie.200353325

60. Youming W. Iron molybdenum based catalyst. 2015:1-17.

61. Shiragami T, Matsumoto J, Inoue H, Yasuda M. Antimony porphyrin complexes as visible-light driven photocatalyst. *J Photochem Photobiol C Photochem Rev*. 2005;6(4):227-248. doi:10.1016/j.jphotochemrev.2005.12.001

62. Ertl M, Wöß E, Knör G. Antimony porphyrins as red-light powered photocatalysts for solar fuel production from halide solutions in the presence of air. *Photochem Photobiol Sci*. 2015;14:1826-1830. doi:10.1039/c5pp00238a

63. Murrer BA, Graetzel M, Nazeeruddin MK. Photosensitizers. 1998:1-23.

64. Bouwkamp-Wijnoltz AL, Palys BJ, Visscher W, Van Veen JAR. An in-situ Raman study of the effect of the support for adsorbed iridium-chelates in catalysing oxygen reduction. *J Electroanal Chem*. 1996;406(1-2):195-202. doi:10.1016/0022-0728(95)04420-5

65. Zhong X, Qin Y, Chen X, et al. PtPd alloy embedded in nitrogen-rich graphene nanopores: High-performance bifunctional electrocatalysts for hydrogen evolution and oxygen reduction. *Carbon N Y*. 2017;114:740-748. doi:10.1016/j.carbon.2016.12.004

66. Kogan I, Khomenko A. Electrochemically rechargeable metal-air cell with a replaceable metal anode. 2016:1-10.

67. Han JL, You J, Yonemura H, Yamada S, Wang SR, Li XG. Metallophthalocyanines as triplet sensitizers for highly efficient photon upconversion based on sensitized triplet-triplet annihilation. *Photochem Photobiol Sci*. 2016;15:1039-1045. doi:10.1039/c6pp00172f

68. Huang F, Li Y, Xu K, et al. Improved performance of lead phthalocyanine phototransistor by template inducing effect based on optimized-thickness copper phthalocyanine layers. *Synth Met*. 2017;234:100-105. doi:10.1016/j.synthmet.2017.09.013

69. Mendori D, Hiroya T, Ueda M, Sanyoushi M, Nagai K, Abe T. Novel photocatalytic material of organic p–n bilayer responsive to near-infrared energy. *Appl Catal B Environ*. 2017;205:514-518. doi:10.1016/j.apcatb.2016.12.071

70. Peng J, Geng Y, Yang HJ, et al. Efficient solvent-free fixation of CO2into cyclic carbonates catalyzed by Bi(III) porphyrin/TBAI at atmospheric pressure. *Mol Catal*. 2017;432:37-46. doi:10.1016/j.mcat.2017.01.019

71. Balasanthiran V, Chisholm MH, Durr CB. On the molecular structure and bonding in a lithium bismuth porphyrin complex: LiBi(TPP)2. *Angew Chemie - Int Ed*. 2014;53:1594-1597. doi:10.1002/anie.201308672

72. Halime Z, Lachkar M, Boitrel B. Coordination of bismuth and lead in porphyrins: Towards an in-situ generator for α-radiotherapy? *Biochimie*. 2009;91(10):1318-1320. doi:10.1016/j.biochi.2009.03.001

73. Burt LA, Bezzu CG, McMonagle CJ, Moggach SA, McKeown NB. A hindered subphthalocyanine that forms crystals with included aromatic solvent but will not play ball with C60. *J Porphyr Phthalocyanines*. 2016;20:1034-1040. doi:10.1142/S1088424616500528

74. http://abulafia.mt.ic.ac.uk/shannon/ptable.php.

75. Ioachim E, Medlycott EA, Polson MIJ, Hanan GS. Synthesis of a novel series of 6,6'-disubstituted 4,4'-bipyrimidines by radical anion coupling: New π-accepting ligands for coordination chemistry. *European J Org Chem*. 2005;(17):3775-3780. doi:10.1002/ejoc.200500335

76. Kadish KM, Ou Z, Tan X, et al. Synthesis and electrochemistry of cobalt b-halogenated meso- tetraphenylporphyrins containing a nitrosyl axial ligand. Crystal structure of

(TPPBr4 NO2)Co(NO). *Dalton Trans*. 1999:1595-1601.

77. Perry CB, Fernandes MA, Brown KL, Zou X, Valente EJ, Marques HM. Probing the nature of the COIII ion in cobalamins - Spectroscopic and structural investigations of the reactions of aquacobalamin (vitamin B12a) with ambident nucleophiles. *Eur J Inorg Chem*. 2003;11:2095-2107. doi:10.1002/ejic.200200600

78. Enemark JH, Feltham RD. Principles of structure, bonding, and reactivity for metal nitrosyl complexes. *Coord Chem Rev*. 1974;13(4):339-406. doi:10.1016/S0010-8545(00)80259-3

79. Miller SR, Alvarez E, Fradcourt L, et al. A rare example of a porous Ca-MOF for the controlled release of biologically active NO. *Chem Commun*. 2013;49:7773-7775. doi:10.1039/c3cc41987h

80. Bultitude J, Larkworthy LF, Mason J, Povey DC, Sandell B. Nitrogen-15 and cobalt-59 NMR study of the bent nitrosyl ligand in cobalt complexes. *Inorg Chem*. 1984;23(22):3629-3633. doi:10.1021/ic00190a040

81. Gallagher AT, Malliakas CD, Harris TD. CO Binding at a Four-Coordinate Cobaltous Porphyrin Site in a Metal-Organic Framework: Structural, EPR, and Gas Adsorption Analysis. *Inorg Chem*. 2017;56:4654-4661. doi:10.1021/acs.inorgchem.7b00292

82. Szalda DJ, Fujita E, Creutz C. Cobalt(I), -(II), and -(III) complexes of a tetraaza 14-membered macrocycle, 5,7,7,12,14,14-hexamethyl-1,4,8,11-tetraazacyclotetradeca-4,11-diene (L). Crystal and molecular structures of [CoL(CO)]ClO4, trans-CoLCl2, and cis-[CoL(CO3)]ClO4. *Inorg Chem*. 1989;28(8):1446-1450. doi:10.1021/ic00307a006

83. Keefer LK. Thwarting thrombus. *Nat Mater*. 2003;2:357-358.

84. Carrington EJ, Vitórica-Yrezábal IJ, Brammer L. Crystallographic studies of gas sorption in metal-organic frameworks. *Acta Crystallogr Sect B Struct Sci Cryst Eng Mater*. 2014;70:404-422. doi:10.1107/S2052520614009834

85. McDonald TM, Mason JA, Kong X, et al. Cooperative insertion of CO2in diamine-

appended metal-organic frameworks. *Nature*. 2015;519:303-308. doi:10.1038/nature14327

86. Schweiger A, Jeschke G. *Principles of Pulse Electron Paramagnetic Resonance*.; 2001.

87. Ercolani C, Hewage S, Heucher R, Rossi G. First Example of a Mixed-Ligand Bimetallic (Fe-Fe) N-Bridged Dimer: (μ-Nitrido)[((tetraphenylporphyrinato)iron)-(phthalocyaninato)iron]. *Inorg Chem*. 1993;32(13):2975-2977. doi:10.1021/ic00065a031

88. Aitipamula S, Banerjee R, Bansal AK, et al. Polymorphs, salts, and co-crystals: What's in a name? *Cryst Growth Des*. 2012;12:2147-2152. doi:10.1021/cg3002948

89. Carraro M, Gross S. Hybrid materials based on the embedding of organically modified transition metal oxoclusters or polyoxometalates into polymers for functional applications: A review. *Materials (Basel)*. 2014;7(5):3956-3989. doi:10.3390/ma7053956

90. Long D-L, Burkholder E, Cronin L. Polyoxometalate clusters, nanostructures and materials: from self assembly to designer materials and devices. *Chem Soc Rev*. 2007;36(1):105-121. doi:10.1039/b502666k

91. Patel A, Narkhede N, Singh S, Pathan S. Keggin-type lacunary and transition metal substituted polyoxometalates as heterogeneous catalysts: A recent progress. *Catal Rev*. 2016;58(3):337-370. doi:10.1080/01614940.2016.1171606

92. Yokoyama A, Kojima T, Ohkubo K, Fukuzumi S. A discrete conglomerate of a distorted Mo(v)-porphyrin with a directly coordinated Keggin-type polyoxometalate. *Chem Commun (Camb)*. 2007;39:3997-3999. doi:10.1039/b704994c

93. Yokoyama A, Kojima T, Ohkubo K, Fukuzumi S. Crystal structures and solution properties of discrete complexes composed of saddle-distorted molybdenum(V)-dodecaphenylporphyrins and Keggin-type heteropolyoxometalates linked by direct coordination. *Inorg Chem*. 2010;49(23):11190-11198. doi:10.1021/ic1019586

94. Yokoyama A, Kojima T, Fukuzumi S. Enclosure of a Keggin-type heteropolyoxometalate into a tubular π-space via hydrogen bonds with a nonplanar Mo(V)-porphyrin complex

forming a supramolecular assembly. *Dalt Trans*. 2011;40:6445-6450. doi:10.1039/c0dt01708f

95. Yokoyama A, Kojima T, Ohkubo K, Shiro M, Fukuzumi S. Formation of a hybrid compound composed of a saddle-distorted Tin(IV)-porphyrin and a keggin-type heteropolyoxometalate to undergo intramolecular photoinduced electron transfer. *J Phys Chem A*. 2011;115:986-997. doi:10.1021/jp109863d

96. Hagrman D, Hagrman PJ, Zubieta J. Solid-State Coordination Chemistry : The Self-Assembly of Microporous Organic ± Inorganic Hybrid Frameworks Constructed from Tetrapyridylporphyrin and Bimetallic Oxide Chains or Oxide Clusters **. *Angew Chemie - Int Ed*. 1999;38(21):3165-3168.

97. Tsuda A, Hirahara E, Kim YS, Tanaka H, Kawai T, Aida T. A molybdenum crown cluster forms discrete inorganic-organic nanocomposites with metalloporphyrins. *Angew Chemie - Int Ed*. 2004;43(46):6327-6331. doi:10.1002/anie.200460990

98. Falber A, Burton-Pye BP, Radivojevic I, et al. Ternary porphyrinato HfIV and ZrIV polyoxometalate complexes. *Eur J Inorg Chem*. 2009;5(17):2459-2466. doi:10.1002/ejic.200900284

99. Radivojevic I, Ithisuphalap K, Burton-Pye BP, Saleh R, Francesconi LC, Drain CM. Ternary phthalocyanato Hf(iv) and Zr(iv) polyoxometalate complexes. *RSC Adv*. 2013;3:2174-2177. doi:10.1039/c2ra22903j

100. Radkov E, Beer R. HIGH YIELD SYNTHESIS OF MIXED-METAL KEGGIN POLYOXOANIONS IN NON-AQUEOUS SOLVENTS: PREPARATION OF (n-Bu4N)4[PMWnO40] (M = V, Nb, Ta) EMIL. *Polyhedron*. 1995;14(15):2139-2143. doi:10.1097/00005650-196905000-00006

101. Safari N, Jamaat PR, Pirouzmand M, Shaabani A. Synthesis of metallophthalocyanines using microwave irradiation under solvent free and reflux conditions. *J Porphyr Phthalocyanines*. 2004;08(10):1209-1213. doi:10.1142/S1088424604000556

102. Jiang J, Pan H, Liu W, Wang C, Wang K. Phenanthro[4,5-fgh]quinoxaline-fused

Subphthalocyanines. Synthesis, Structure, and Spectroscopic Characterisation. *Chem - A Eur J*. 2016;22:9488-9492. doi:10.1002/chem.201601388

103. Edmondson S, Mitchell CH. Molybdenum Phthalocyanine. *Polyhedron*. 1986;5(1/2):315-317.

104. Ziener U, Hanack M. Synthesis and Characterisation of Nitrido(tetra-tert-butylphtha1ocyaninato)- rhenium(V) and Nitrido(phthalocyaninato)rhenium(V). *Chem Ber*. 1994;127:1681-1685.

105. Hahn F, Boucharat N, Benihya K, Mossoyan-de M, Terzian G. Synthesis , Crystal Structure and Spectral Characterisation , of a New Phase of Tris (phthalocyaninato) dibismuth (III), Bi 2 (Pc) 3. *Eur J Inorg Chem*. 2000:1771-1779.

106. Bouwkamp-Wijnoltz AL, Visscher W, van Veen JAR. Oxygen reduction catalysed by carbon supported iridium-chelates. *Electrochim Acta*. 1994;39(11-12):1641-1645. doi:10.1016/0013-4686(94)85148-4

107. Radivojevic I, Bazzan G, Burton-Pye BP, et al. Zirconium(IV) and hafnium(IV) porphyrin and phthalocyanine complexes as new dyes for solar cell devices. *J Phys Chem C*. 2012;116:15867-15877. doi:10.1021/jp301853d

108. Sarkar S, Mohammad I, Subramanian P. First report of the reductive nitrosylation of tungstate(VI) by hydroxylamine. Stereospecific synthesis of (W(NO)2Cl2(L)2). *Chem Lett*. 1985;(2):1633-1634.

109. Close MR, McCarley RE. Synthesis and Structure of WNCl3 and Evidence for Structural Modifications with Bound Chlorocarbon Solvents. *Inorg Chem*. 1994;33:4198-4201. doi:10.1021/ic00097a002

110. Frick K, Verma S, Sundermeyer J, Hanack M. Novel Nitrido- and Oxo(phthalocyaninato) Complexes of Molybdenum, Tungsten and Rhenium. *Eur J Inorg Chem*. 2000:1025-1030. doi:10.1002/(SICI)1099-0682(200005)2000:5<1025::AID-EJIC1025>3.0.CO;2-S

111. Keen IM, Malerbi BW. The preparation and infra-red spectra of phthalocyanine

derivatives of the platinum-group metals. *J Inorg Nucl Chem*. 1965;27(6):1311-1319. doi:10.1016/0022-1902(65)80095-1

112. Kenney ME, Joyner RD. Germanium Phthalocyanines. *J Am Chem Soc*. 1960;82:5790-5791.

113. Chambrier I, White GF, Cook MJ. Oligomeric cadmium-phthalocyanine complexes: Novel supramolecular free radical structures. *Chem Eur J*. 2007;13:7608-7618. doi:10.1002/chem.200700745

114. Bian Y, Li L, Dou J, et al. Synthesis, structure, spectroscopic properties, and electrochemistry of (1,8,15,22-tetrasubstituted phthalocyaninato)lead complexes. *Inorg Chem*. 2004;43(23):7539-7544. doi:10.1021/ic049080o

115. Rayner Canham GW, Myers J, Lever ABP. Higher Oxidation State Iron and Cobalt Phthalocyanine Derivatives . Phthalocyanine Radical Cation Complexes. *J Chem Soc Chem Commun*. 1973:483-484.

116. Fox JP, Goldberg DP. Octalkoxy-Substituted Phosphorus(V) Triazatetrabenzcorroles via Ring Contraction of Phthalocyanine Precursors. *Inorg Chem*. 2003;42(25):8181-8191. doi:10.1021/ic034792k

117. Modibane DK, Nyokong T. Synthesis, photophysical and photochemical properties of octa-substituted antimony phthalocyanines. *Polyhedron*. 2009;28(3):479-484. doi:10.1016/j.poly.2008.11.052

118. Iwamura T, Adachi K, Chujo Y. Simple and Rapid Eco-friendly Synthesis of Cubic Octamethylsilsesquioxane Using Microwave Irradiation. *Chem Lett*. 2010;39(4):354-355. doi:10.1246/cl.2010.354

119. Klemperer W. Tetrabutylammonium isopolyoxometalates. *Inorg Synth*. 1990;27:74-85. doi:10.1002/9780470132586.ch15

120. Maeda D, Aritome I, Shimakoshi H, Hisaeda Y. Bis[(2,3,6,7,12,13,16,17-octaethylporphycenato)oxomolybdenum(V)] hexamolybdate(VI). *Acta Crystallogr Sect E*

Struct Reports Online. 2006;62(6):1272-1274. doi:10.1107/S1600536806016461

121. Rocchiccioli-Deltcheff C, Fournier M, Franck R, Thouvenot R. Vibrational investigations of polyoxometalates. 2. Evidence for anion-anion Interactions in molybdenum(VI) and tungsten(VI) compounds related to the Keggin structure. *Inorg Chem*. 1983;22:207-216. doi:10.1021/ic00144a006

122. Stuczynski SM, Kwon YU, Steigerwald ML. The use of phosphine chalcogenides in the preparation of cobalt chalcogenides. *J Organomet Chem*. 1993;449(1-2):167-172. doi:10.1016/0022-328X(93)80120-Z

123. Kuroda K, Shimojima A, Kawahara K, et al. Utilization of alkoxysilyl groups for the creation of structurally controlled siloxane-based nanomaterials. *Chem Mater*. 2014;26:211-220. doi:10.1021/cm4023387

124. Honjo H, Ide T, Akamatsu Y, et al. Siloxane compound and cured product thereof. 2014. doi:10.1016/j.(73)

125. Sotiriou-Leventis C, Mao Z. A facile synthesis of 2,7 diazapyrene. *J Heterocycl Chem*. 2000;37:1665-1667.

126. Afanasiev P, Sorokin AB. μ-Nitrido Diiron Macrocyclic Platform: Particular Structure for Particular Catalysis. *Acc Chem Res*. 2016;49:583-593. doi:10.1021/acs.accounts.5b00458

127. Bottomley LA, Gorce JN, Goedken VL, Ercolani C. Spectroelectrochemistry of a μ-Nitrido-Bridged Iron Phthalocyanine Dimer. *Inorg Chem*. 1985;24(23):3733-3737. doi:10.1021/ic00217a008

128. Stuzhin PA, Ivanova SS, Dereven'kov I, Makarov S V., Silaghi-Dumitrescu R, Homborg H. First water-soluble μ-nitrido dimer of iron phthalocyanine. *Macroheterocycles*. 2012;5(2):175-177. doi:10.6060/mhc2012.120360s

129. Summerville DA, Cohen IA. Metal-Metal Interactions Involving Metalloporphyrins. III. Conversion of Tetraphenylporphinatoiron(III) Azide to an N-Bridged Hemin Dimer. *J Am Chem Soc*. 1976;98(7):1747-1752. doi:10.1021/ja00423a019

130. Kudrik E V., Afanasiev P, Alvarez LX, et al. An N-bridged high-valent diiron-oxo species on a porphyrin platform that can oxidize methane. *Nat Chem*. 2012;4:1024-1029. doi:10.1038/nchem.1471

131. Winter G. xia2: an expert system for macromolecular crystallography data reduction G. *J Appl Crystallogr*. 2009;43:186-190. doi:10.1107/S0021889809045701

132. Winn MD, Ballard CC, Cowtan KD, et al. Overview of the CCP4 suite and current developments. *Acta Crystallogr Sect D Biol Crystallogr*. 2011;67(4):235-242. doi:10.1107/S0907444910045749

133. Dolomanov O V., Bourhis LJ, Gildea RJ, Howard JAK, Puschmann H. OLEX2: A complete structure solution, refinement and analysis program. *J Appl Crystallogr*. 2009;42(2):339-341. doi:10.1107/S0021889808042726

134. Spek AL. Structure validation in chemical crystallography. *Acta Crystallogr Sect D Biol Crystallogr*. 2009;65:148-155. doi:10.1107/S090744490804362X